REGULATION OF GLOBAL METABOLISM BY PTS^{NTR}

IN *RHIZOBIUM LEGUMINOSARUM*

Olivia Tjahjono
Linacre College
University of Oxford

A thesis submitted for the degree of
Doctor of Philosophy
Trinity 2025

DECLARATION

I declare that this thesis is my own work and has not been submitted for a degree at any other university. I sincerely acknowledge the contributions of collaborators to the work presented in this thesis:

Chapter 3: Raman spectroscopy was performed by Jingkai Wang. The O_2 consumption assay and promoter activity studies for the *hprK* mutant were carried out by Evan Turner.

Chapter 4: The *ptsP* suppressor screening and *relA* mutant phenotypic characterisations were conducted by Carmen Sánchez Cañizares, Alicia Uceda Heras, Ramakrishnan Karunakaran, Francesco Pini, and Jürgen Prell. Single-nucleotide polymorphisms bioinformatic work was performed by Andrej Tkacz. PtsN and RelA protein-protein interaction results were obtained from Carmen Sánchez Cañizares, Denis Shutin, and Jani Reddy Bolla. (p)ppGpp quantification was conducted in collaboration with Ben Field and Sylvie Citerne. Microaerobic induction measurement was performed by Isidro Abreu and Maria Palomero-Gómez.

Olivia Tjahjono

ACKNOWLEDGEMENT

I would like to thank Professor Philip Poole for giving me the opportunity to work in such a wonderful lab and for the generous time he devotes to his students. One hour of science discussion with him would often resolve what might otherwise have been a month-long struggle for me. I am also deeply grateful to Dr Carmen Sánchez-Cañizares, my day-to-day supervisor, with whom I always felt I could talk about anything. Her temperament and flexibility in facing the uncertainties of research are qualities I have tried to learn from throughout my D.Phil., and I cannot emphasise enough how much she has shaped me during this journey. My thanks also go to Professor Antonis Papachristodoulou for always being so helpful, offering excellent advice, and engaging with my study; hearing his perspective on systems biology was always eye-opening. I am grateful to Dr Jani R. Bolla for generously agreeing to support me and for always keeping his door open for questions about protein work, to Professor Tim Barraclough for the opportunity to study in his supportive lab for my first rotation, Professor Gail Preston for DTP-related support, and to my college advisor, Dr Christine Kiire, for her warm encouragement and enjoyable conversations.

I owe much to the current and past members of the Rhizosphere Lab for their support and friendship. Special thanks to the postdocs for generously sharing their knowledge. Albert, thank you for always being open to discussion and for offering insightful ideas. Alison, thank you for managing the lab and noticing the small things; it always made me happy. Bea, thank you for being caring and dependable. Hayley, I always admire your organising skills. Isidro, thank you for the helpful advice and wonderful conversations. Raphael, our go-to troubleshooter, thank you. Special thanks to Helen and Lida for your steady support in running the lab. And to all the fellow bambinos — Anki, Bergthor, Clare, Jessie, Lea, Matt, Tom — I am so lucky to have gone through this degree with you. Conferences were especially fun because we could stay together and have long chats. The little things we did in and outside the lab were always a joy. I also appreciated visits from Andrea, Sandra, and Maria; those summer times when you were in the lab made my time there even more joyful, and I am so happy we have become friends. I am grateful to the admin and cleaning team in Plant Sciences for their friendly support.

I am also deeply thankful to the researchers, mentors, and teachers who have supported me along the way: Professor Sakakibara Hitoshi, my former group leader, for his kindness and understanding; Dr Fanny Bellegarde, who never cut corners and taught me how to think as a researcher; Professor Young-Jai You, whose support and guidance helped build my confidence; the late Professor Joyce Cartagena and Professor Jasmina Damnjanovic for creating a safe and welcoming environment for G30 Biology where I never felt alone in my early days in Nagoya; Professor Matsuda Tsukasa for giving me, an inexperienced student, the opportunity to learn in his lab; Professor Maria Vassileva, Professor Ji-Young Shin, and all lecturers in Nagoya G30 for their outstanding lectures, which remain foundational to how I learn and continue to serve as my greatest tool during graduate study; and all professors teaching the *gakusei jikken*, which gave me a strong foundation in experimental skills. My first experience of writing a dissertation at SMAK Dempo was invaluable, and I am deeply grateful to all the teachers who guided me.

My thanks to Dr Jason Terpolilli, Dr Ron Yates, and all members of the Legume Rhizobium Sciences for the opportunity to undertake a rewarding internship. That relatively short period in Perth helped clear my mind and renew my enthusiasm for rhizobia research.

I am also thankful to the Linacre College community for making this place feel like home – and most of all, thank you, Yun, Abir, and Siting. Our meals together were something I always looked forward to in the week. Countless hotpots, dinners, and laughs with you kept me going.

As a wise man once said, the first step in research (and education) is securing funding. I would therefore like to thank the Indonesia Endowment Fund for Education Agency (Beasiswa LPDP) for their generous stipends and continued support, BBSRC for research, travel, and training funds, and the Rhizosphere Lab for their support between positions.

Finally, to all the people I met during my time in Oxford, so many of you taught me so much that I cannot acknowledge everyone individually here, but I am forever grateful to each of you. How lucky I am to have been able to do research in this wonderful place!

Tesis ini kudedikasikan kepada Mama, Papa, dan Nelsen. Karena kalian selalu ada di sisiku, tidak ada yang terasa berat.

TABLE OF CONTENTS

ABSTRACT

Maintaining intracellular carbon-nitrogen balance is essential for rhizobial growth in the free-living state and for establishing effective symbiosis with host legumes. In these organisms, this balance is modulated post-translationally by the nitrogen-related phosphotransferase system (PTS^{Ntr}), which comprises the sensor protein PtsP (EI^{Ntr}), the phosphotransfer protein NPr, and the output regulators PtsN ($EIIA^{Ntr}$) and ManX ($EIIA^{Man}$). PtsP reacts to the intracellular nitrogen status of the cell. Under nitrogen-limiting conditions, PtsP autophosphorylates at a histidine residue and subsequently transfers the phosphate to NPr, which in turn phosphorylates the output proteins PtsN and ManX. In contrast, when the cell is nitrogen-sufficient, allosteric binding of glutamine inhibits the autophosphorylation of PtsP, resulting in nonphosphorylated NPr, PtsN and ManX. The bifunctional HPr kinase/phosphorylase (HPrK/P) adds an additional layer of control by phosphorylating a conserved serine on NPr, preventing histidine phosphorylation and blocking the phosphotransfer to the downstream effectors PtsN and ManX. In this thesis, I investigated the role of PTS^{Ntr} in the metabolism of *Rhizobium leguminosarum*. First, the components, signalling mechanisms, and known targets of the Alphaproteobacterial PTS^{Ntr} were reviewed. The involvement of ManX and HPrK/P in carbon metabolism was then examined; mutations in these proteins were found to perturb the TCA cycle, causing carbon to be redirected to storage compounds, a response also observed under nitrogen starvation. PTS^{Ntr} was also shown to sense nitrogen availability and signal to the RelA/SpoT homolog (RSH), which regulates amino-acid uptake through the AapJQMP transport system via modulation of the AbcR1/2 sRNAs. Finally, the rhizobial homolog of the *Escherichia coli* phosphohistidine phosphatase SixA was characterised and shown not to affect PTS^{Ntr} function under the conditions tested.

1. Introduction

1.1 Context and Aims

Rhizobia are a group of soil bacteria capable of establishing symbiotic associations with leguminous plants. Within root nodules, these bacteria fix atmospheric nitrogen (N_2) into ammonia (NH_3), which is assimilated by the plant as a readily available nitrogen source. In return, the host plant supplies rhizobia with carbon compounds derived from photosynthesis predominantly in the form of C4-dicarboxylates. This process of biological nitrogen fixation is ecologically significant and, in the context of modern agriculture, represents a promising sustainable alternative to synthetic nitrogen fertilisers, whose intensive use poses substantial environmental concerns (Ledermann et al., 2021; Poole et al., 2018; Reis Ely et al., 2025).

For rhizobia to form a successful symbiosis with the legume hosts, they must first persist within the complex and competitive soil microbiome before initiating host interactions, then rapidly colonise the roots, compete for nodulation, and differentiate into efficient, nitrogen-fixing bacteroids (Burghardt & diCenzo, 2023; Mendoza-Suárez et al., 2021). This challenge is amplified in agricultural systems, where high mineral-nitrogen inputs, physical disturbance, and frequent cultivar/genotype turnover reshape selection on rhizobia and favour soil-adapted competitors (Checcucci et al., 2017; Liu et al., 2020). Inoculant strains are effective only if they can both compete with indigenous populations for nodulation and subsequently reprogram central metabolism to differentiate into efficient, nitrogen-fixing bacteroids. Consequently, the regulation of carbon and nitrogen balance emerges as a critical determinant for selecting strains that combine ecological resilience with high nitrogen fixation efficiency in the field.

The nitrogen-related phosphotransferase (PTS^{Ntr}) system is a conserved central regulator of metabolism in Alphaproteobacteria that integrates carbon and nitrogen status (Dozot et al., 2010; Pflüger-Grau & Görke, 2010). This system comprises an initial sensor protein PtsP (EI^{Ntr}), a phosphotransfer protein NPr, and two output regulatory proteins, PtsN ($EIIA^{Ntr}$) and ManX ($EIIA^{Man}$). It functions as a rapid post-translational switch that coordinates nitrogen uptake, exopolysaccharide synthesis, ATP synthase-binding cassette (ABC) transporter activity, carbon metabolism, and potassium homeostasis (Prell et al., 2012; Sánchez-Cañizares et al., 2020). These traits are strongly linked to field persistence, stress tolerance, and competitive nodulation efficiency in rhizobia.

Although protein:protein interaction studies have established links between the core PTS^{Ntr} relay, the stringent response (Ronneau et al., 2016), and K^+ homeostasis (Feng et al., 2022; Prell et al., 2012), several mechanistic details remain unresolved. Its role in carbon metabolism is particularly underdefined: in *Rhizobium leguminosarum*, ManX has been implicated in carbon control, but downstream pathways remain to be mapped (Sánchez-Cañizares et al., 2020); in *Sinorhizobium meliloti*, the HPr kinase/phosphorylase (HPrK/P) branch influences succinate-mediated catabolite repression, though the mechanism is unclear (Pinedo & Gage, 2009); and SixA, a conserved histidine phosphatase known to modulate PTS^{Ntr} in *E. coli*, remains largely unexplored in rhizobia (Schulte et al., 2021). Similarly, while the PTS^{Ntr}-mediated regulation of ABC transporters involved in nitrogen uptake has been proposed based on physiological phenotypes, direct molecular interactions with specific transporters have not been demonstrated.

This work addresses these gaps by investigating the role of PTS^{Ntr} in carbon metabolism through the characterisation of *hprK*, *manX*, and *sixA* in rhizobia. We also propose a mechanism for how PTS^{Ntr} regulate ABC transporters. Under nitrogen starvation, the interaction between phosphorylated PtsN and RelA/Spot Homolog (RSH) induces the production of (p)ppGpp. This alarmone, in turn, controls the transcription of sRNAs AbcR1/2, which then post-transcriptionally regulate the transcripts of AapJQMP amino acid transporters and fine-tune their activity.

1.2 Thesis Outline

The main contents of this thesis are organised into three scientific manuscripts currently in preparation (Chapters 2–4), followed by an additional results chapter (Chapter 5).

Chapter 2 is written in a minireview format, providing a general overview of PTS^{Ntr} regulation in Alphaproteobacteria. The conserved structures, accessory components, phosphotransfer mechanisms, and downstream functions are discussed, along with their connections to other regulatory pathways. The review also highlights regulatory targets identified in other bacterial groups but not yet confirmed in Alphaproteobacteria and summarises all published functional insights to date.

Chapter 3 investigates the role of PTS^{Ntr} effectors ManX and HprK in regulating carbon metabolism. Using enzyme activity assays and polymer quantification, the impact of mutations in these genes on carbon flux and distribution was assessed. This study forms the basis of a manuscript currently in preparation.

Chapter 4 focuses on the crosstalk between PTS^{Ntr}, the RelA (RSH) stringent response, small RNAs AbcR1/2, and their downstream effects on amino acid transport in *Rhizobium leguminosarum*. Measurements of (p)ppGpp levels, amino acid transport

activity, and sRNA transcription in various PTS^{Ntr} mutants, coupled with interaction studies between PtsN and RSH using native mass spectrometry, provide insights into how PTS^{Ntr} senses nitrogen stress, signals to RelA, and regulates sRNA transcription to control amino acid uptake via the ABC transporter Aap. My main contributions were (p)ppGpp quantification, relative transcript quantification by RT-qPCR, and sRNA characterisation. This work is also in preparation for publication.

Chapter 5 presents the characterisation of SixA in *R. leguminosarum*. Mutant generation and phenotypic analysis were performed to assess PTS^{Ntr}-related functions.

Chapter 6 summarises the main findings of this thesis and provides perspectives for future research.

Beyond this thesis, my first D.Phil lab rotation also led to a manuscript:

Wong, E.L.Y., Lyu, J., Tjahjono, O., Alkemade, J., Buddie, A., Ryan, M.J. and Barraclough, T.G. 2026. Historical comparative genomics to track the evolution of fungal pathogens: a proof of concept. *BMC Genomics*. https://doi.org/10.1186/s12864-025-12472-2

2. Background

The nitrogen-related phosphotransferase system (PTS^{Ntr}) in Alphaproteobacteria: architecture, mechanisms, and functions

2.1 Abstract

The nitrogen-related phosphotransferase system (PTS^{Ntr}) is a conserved His-to-His phosphorelay consisting of EI^{Ntr} (PtsP), NPr (PtsO), and $EIIA^{Ntr}$ (PtsN). By integrating carbon and nitrogen status, this regulatory module reprograms bacterial physiology by controlling downstream effectors via phosphorylation-dependent protein:protein interactions. In Alphaproteobacteria, PTS^{Ntr} is broadly present, but downstream partners and outputs diverge across lineages. Inputs comprise the carbon flux via the [PEP]:[pyruvate] balance that sets PtsP autophosphorylation, and nitrogen status sensed by glutamine binding to the N-terminal GAF domain of PtsP. Downstream, PTS^{Ntr} regulates various cell functions, including K^+ uptake, stringent response, ABC transporter activity, and carbon metabolism. Here, we discuss the current understanding of the PTS^{Ntr} in Alphaproteobacteria, focusing on its component organisation, phosphotransfer mechanisms, and crosstalk with other regulatory pathways.

2.2 Introduction

Bacterial survival depends on their capacity to maintain the balance of intracellular metabolite pools. In Proteobacteria, the nitrogen-related phosphotransferase system (PTS^{Ntr}) functions as a conserved regulatory module that integrates carbon and nitrogen status to modulate diverse cellular processes (Dozot et al., 2010; Pflüger-Grau & Görke,

2010; Ronneau, Petit, et al., 2016; Sánchez-Cañizares, et al., 2020). Unlike the sugar-PTS, PTS^{Ntr} lacks the typical EIIB and EIIC, and instead of directly transporting sugars, it functions primarily as a regulatory system (Dozot et al., 2010; Pflüger-Grau & Görke, 2010).

The signalling pathway is driven by phosphoenolpyruvate (PEP) and involves a histidine-to-histidine phosphorelay: EI^{Ntr} (PtsP) autophosphorylates on a conserved histidine using PEP and transfers the phosphoryl group to NPr (PtsO) and then to $EIIA^{Ntr}$ (PtsN) (Dozot et al., 2010; Goodwin & Gage, 2014; Pflüger-Grau & Görke, 2010). In some species, the relay also branches to ManX, an EIIA-like output protein distinct from PtsN ($EIIA^{Ntr}$), creating a parallel regulatory arm (Sánchez-Cañizares, et al., 2020). In *Escherichia coli*, the GAF domain of PtsP senses the [glutamine]:[2-oxoglutarate] and [PEP]:[pyruvate] balance to relay specific physiological outputs (Dozot et al., 2010; Goodwin & Gage, 2014). Downstream, $EIIA^{Ntr}$ effector governs various cell functions, including the Rsh/SpoT (RSH) stringent response protein (Ronneau, Petit, et al., 2016; Ronneau et al., 2019a), ABC transporters (Prell et al., 2012; Untiet et al., 2013), KdpD/KdpE-dependent potassium (K+) uptake (Feng et al., 2022; Untiet et al., 2013), exopolysaccharide (EPS)/envelope-linked phenotype via ChvI/ChvG (Sánchez-Cañizares et al., 2020), and carbon metabolism (Dozot et al., 2010; Pinedo & Gage, 2009; Sánchez-Cañizares et al., 2020).

The relay protein, NPr, is tuned by lineage-specific auxiliary proteins. The histidine phosphatase SixA, which has been characterised in *E. coli*, dephosphorylates NPr and thus modulates the phosphorylation state of NPr and downstream EIIA proteins (Schulte et al., 2021; Schulte & Goulian, 2018). On the other hand, the homolog of HPr serine

kinase/phosphatase (HprK/P), originally identified in Firmicutes, can phosphorylate the PTS^{Ntr} carrier NPr on a conserved serine (Ser) residue in Alphaproteobacteria, and this Ser-phosphorylation antagonises PtsP-dependent phosphorylation of NPr on the histidine (His) residue (Dozot et al., 2010). Together, PTS^{Ntr} relays form a versatile hub that integrates carbon and nitrogen availability to regulatory outcomes.

In this review, we summarise recent mechanistic insights, evolutionary conservation, and functional interplay among the sensor, the relay, and the effector components of the PTS^{Ntr} system. We also investigate downstream regulatory targets, with particular emphasis on mechanisms operating in Alphaproteobacteria.

Foundational work

The phosphotransferase system (PTS) was first discovered in enteric bacteria as a PEP-dependent system that couples sugar import with concomitant phosphorylation (Fox et al., 1984; Kundig et al., 1964; Misset et al., 1983; Postma et al., 1993). The paralogs of EI, HPr, and EIIA were later identified and mapped to be genetically neighbouring the region of the sigma factor *rpoN*/σ^{54} circuitry (Powell et al., 1995). This distinct, non-transporting regulatory branch was designated as nitrogen-related PTS (PTS^{Ntr}), consisting of EI^{Ntr} (PtsP), NPr (PtsO), and $EIIA^{Ntr}$ (PtsN). EI^{Ntr} is distinguished from its sugar-transporting paralog by an N-terminal GAF domain, suggesting a role in metabolite-sensing within this pathway (Reizer et al., 1996). Biochemical and genetic evidence established that EI^{Ntr} phosphorylates NPr but not HPr, while EI (sugar) phosphorylates HPr but not NPr, thus maintaining a separation between the nitrogen and carbohydrate circuits (Rabus et al., 1999). Orthologs of PTS^{Ntr} have been identified beyond Enterobacteria, including *Pseudomonas* and *Brucella*, where regulatory roles for PtsN were later demonstrated

(Cases et al., 1999, 2001; Dozot et al., 2010). Comparative analyses indicate that PTS^{Ntr} is widespread across Proteobacteria (apart from ε-subdivision) and Firmicutes (Barabote & Saier, 2005), while occurrence outside these groups is inconsistent.

2.3 General phosphorelay mechanism in Alphaproteobacteria

The PTS^{Ntr} is a regulatory phosphorelay that routes phosphate from PEP to EI^{Ntr} (PtsP), then to the histidine phosphocarrier NPr (PtsO), and finally to $EIIA^{Ntr}$ (PtsN) (**Figure 1**). These proteins are paralogous to the canonical sugar-PTS components EI, HPr, and $EIIA^{Fru}$ identified in *E. coli* (Barabote & Saier, 2005; Reizer et al., 1996). In most Alphaproteobacteria, the PTS^{Ntr} functions without the sugar-PTS permeases and instead mediates exclusively regulatory roles rather than carbohydrate transport. Genome organisation and the structural relationships of these core proteins of the sugar-PTS are reviewed in more detail in (Barabote & Saier, 2005; Pflüger-Grau & Görke, 2010).

Sensor node: EI^{Ntr}/PtsP

EI^{Ntr} (PtsP) contains an N-terminal sensing GAF domain fused to an EI-like catalytic core, whereas the sugar-PTS EI lacks this GAF module (Rabus et al., 1999). Like the sugar-PTS, PTS^{Ntr} uses PEP as a phosphoryl donor to PtsP, releasing pyruvate (Begley & Jacobson, 1994; Dozot et al., 2010; Goodwin & Gage, 2014). This dependency on PEP makes the phosphotransfer flux sensitive to intracellular PEP levels, and positions PtsP as a sensor for the cellular energy state that monitors the [PEP]:[pyruvate] ratio. However, direct quantification of how the ratio of these two metabolites affects PtsP autophosphorylation remains limited.

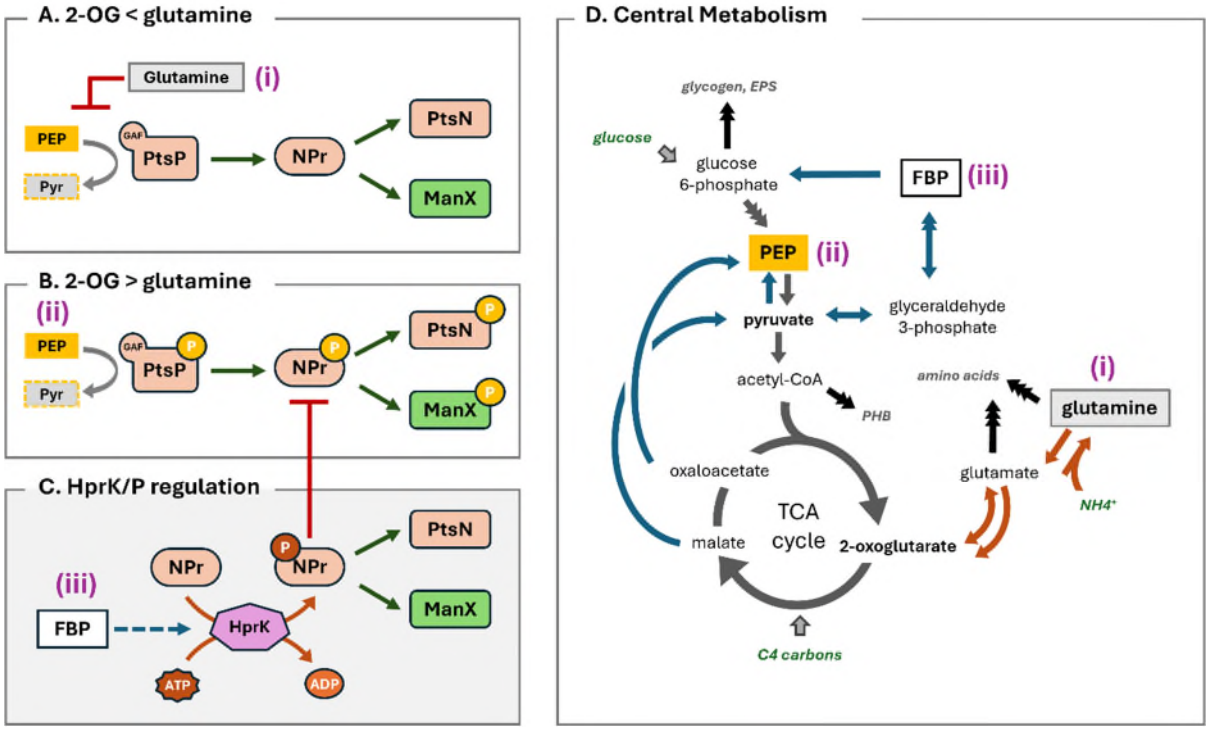

Figure 1. Phosphorylation cascades in PTS^{Ntr} under varying nutrient conditions: (A) 2-OG < glutamine; (B) 2-OG > glutamine; and (C) additional regulation by HprK/P. Points (i)–(iii) indicate key metabolic inputs: (i) glutamine; (ii) phosphoenolpyruvate (PEP), the phosphoryl donor that is converted into pyruvate (Pyr); and (iii) fructose-1,6-biphosphate (FBP). Yellow circles indicate histidine phosphorylation, while the red circles represent serine phosphorylation. (D) shows their position within central metabolism.

By contrast, the role of glutamine as a direct inhibitory ligand is well supported. While 2-OG, a precursor of glutamine, has been reported to stimulate PtsP in *E. coli* (Lee et al., 2013), evidence for this effect in Alphaproteobacteria is lacking. In *Sinorhizobium meliloti*, glutamine binds the N-terminal GAF domain of PtsP and suppresses its autophosphorylation, as demonstrated by *in vitro* kinetic assays at physiological glutamine concentrations (Goodwin & Gage, 2014). In *Caulobacter crescentus*, *in vivo* studies further show that glutamine deprivation elevates the PtsP→NPr→PtsN phosphorylation via the PtsP GAF domain (Ronneau, Petit, et al., 2016). 2-oxoglutarate (2-OG) was proposed as an alternative ligand for the PtsP GAF domain in *Brucella*

melitensis, but no direct binding was shown (Dozot et al., 2010). In *S. meliloti*, 2-OG binding to the PtsP GAF domain is not detected, nor competition with glutamine observed (Goodwin & Gage, 2014), suggesting that sensing and signal transduction mechanisms differ between Enterobacteria and Alphaproteobacteria.

Notably, the PtsP→NPr phosphotransfer of *S. meliloti* operates with lower catalytic efficiency than the classic sugar-PTS EI→HPr reaction measured in *E. coli,* which occurs near the diffusion limit, highlighting a slower kinetic regime for the PTS^{Ntr} branch (Goodwin & Gage, 2014; Hoving et al., 1981; Meadow et al., 2005).

Relay nodes: NPr, HprK/P and SixA

NPr

NPr is a structural and functional paralog of the sugar-PTS HPr. Despite the homology, NPr is not a productive substrate of EI-sugar and forms an insulated phosphorelay with PtsP (Rabus et al., 1999; Strickland et al., 2019). This specificity is enforced by the distinct stereospecific docking geometries at the PtsP:NPr and EI-sugar:HPr interfaces (Li et al., 2008; Strickland et al., 2016). While nuclear magnetic resonance (NMR) spectroscopy and other protein structural studies show that a transient, non-productive encounter can occur and bias partner search (e.g., between PtsP and Hpr), they did not lead to phosphotransfer (Strickland et al., 2019).

HprK/P

In many Firmicutes, HPr carries an additional regulatory serine (Ser46) that can be reversibly modified by the bifunctional HPr kinase/phosphorylase (HprK/P) (**Figure 2**) (Fieulaine et al., 2002; Mijakovic et al., 2002). The kinase reaction is ATP-dependent, while the reverse reaction proceeds via an unusual phosphorolysis mechanism, in which

inorganic phosphate (Pi) acts as the nucleophile to attack the phosphoryl group of HPr-Ser, resulting in the production of pyrophosphate (PPi).

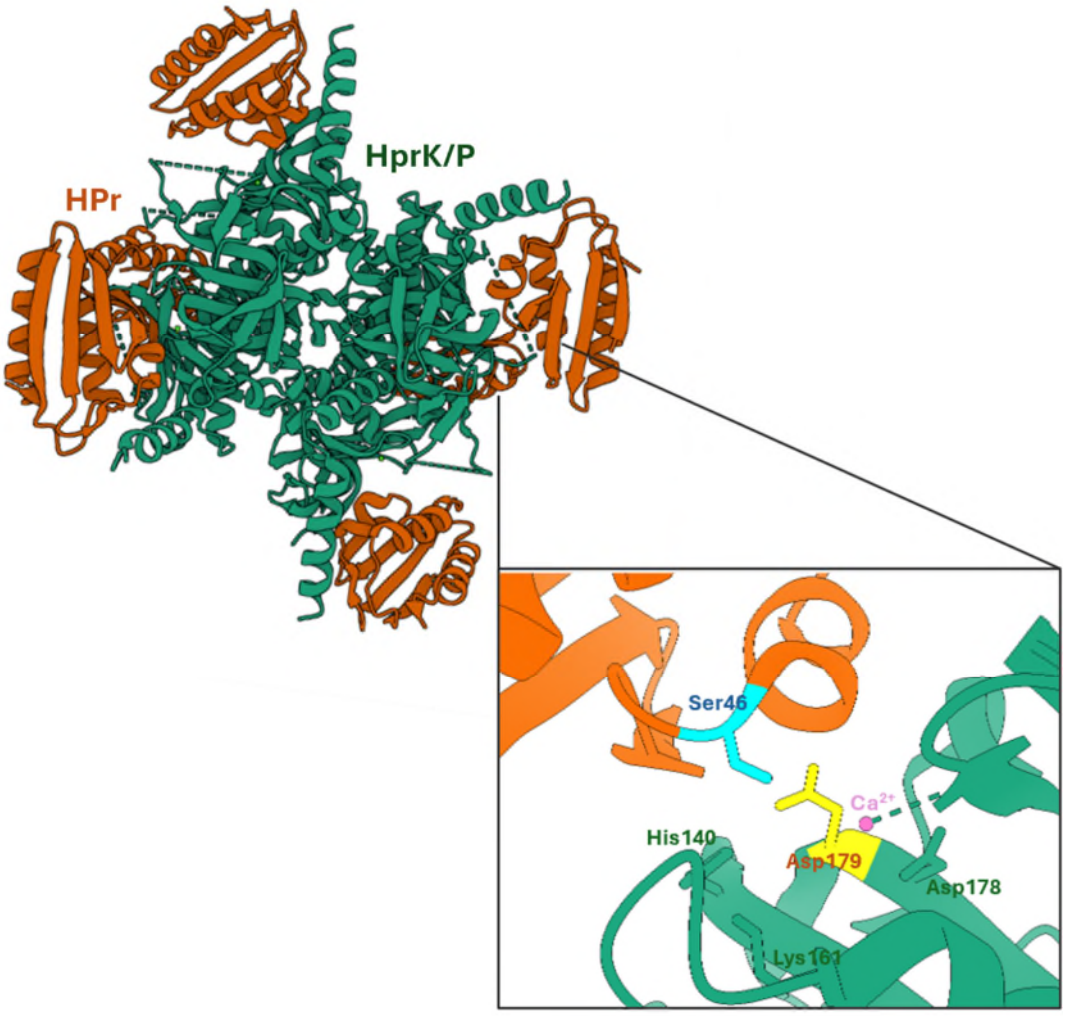

Figure 2. The X-ray crystal structure of HPr kinase/phosphorylase (HprK/P) hexamer from *Lactobacillus casei* (green) in complex with HPr from *Bacillus subtillis* (orange) (pdb_00001kkm) (Fieulaine et al., 2002). The core catalytic pocket at the HPr–HPrK/P interface is highlighted in the inset. Asp179 is proposed to function as the catalytic base, removing and donating a proton from Ser46-OH during phosphorylation and dephosphorylation, respectively. The crystal structure contains Ca^{2+} in the binding site; however, based on homology with other HPrK/P enzymes, Mg^{2+} is expected to occupy this site under physiological conditions. Structural superposition and rendering were performed using UCSF ChimeraX (Meng et al., 2023).

The HprK/P activity in firmicutes is directly linked to the glycolytic state, with fructose-1,6-bisphosphate (FBP) validated as an allosteric activator of HprK/P activity (Fieulaine et al., 2002; Nessler et al., 2003). Under conditions in which preferred carbon sources are abundant, FBP stimulates the ATP-dependent kinase activity, leading to phosphorylation of HPr at Ser46. The Ser46-phosphorylated HPr functions as a co-effector for the transcriptional regulator CcpA, forming CcpA-P~Ser-HPr/Crh complex, which induces carbon catabolite repression (CCR) (Chaptal et al., 2007; Galinier et al., 1998; Mijakovic et al., 2002). Conversely, when preferred carbon sources are limited (low FBP and ATP; high Pi), Pi serves as a substrate for the reverse reaction, dephosphorylating HPr Ser46. Loss of HPr-Ser~P disrupts the CcpA co-repressor complex, thereby relieving CCR and allowing the expression of genes required for the utilisation of alternative carbon sources.

HprK/P employs a single P-loop catalytic centre in its C-terminal domain for both kinase/phosphorolysis. The Walker A/P-loop (GxxxxGKS/T) binds the competing substrates ATP/Mg^{2+} (kinase mode) and Pi (phosphorolysis mode) (Deutscher et al., 2006; Nessler et al., 2003). In the kinase mode, ATP occupies the P-loop, and a conserved aspartate (Asp) residue serves as a general base to deprotonate HPr/NPr Ser, with FBP allosterically stabilising the kinase-active hexamer. In the reverse reaction, Pi binds in the same pocket and attacks the Ser-phosphate to release PPi; the same Asp then acts as a general acid to reprotonate the Ser (**Figure 3**).

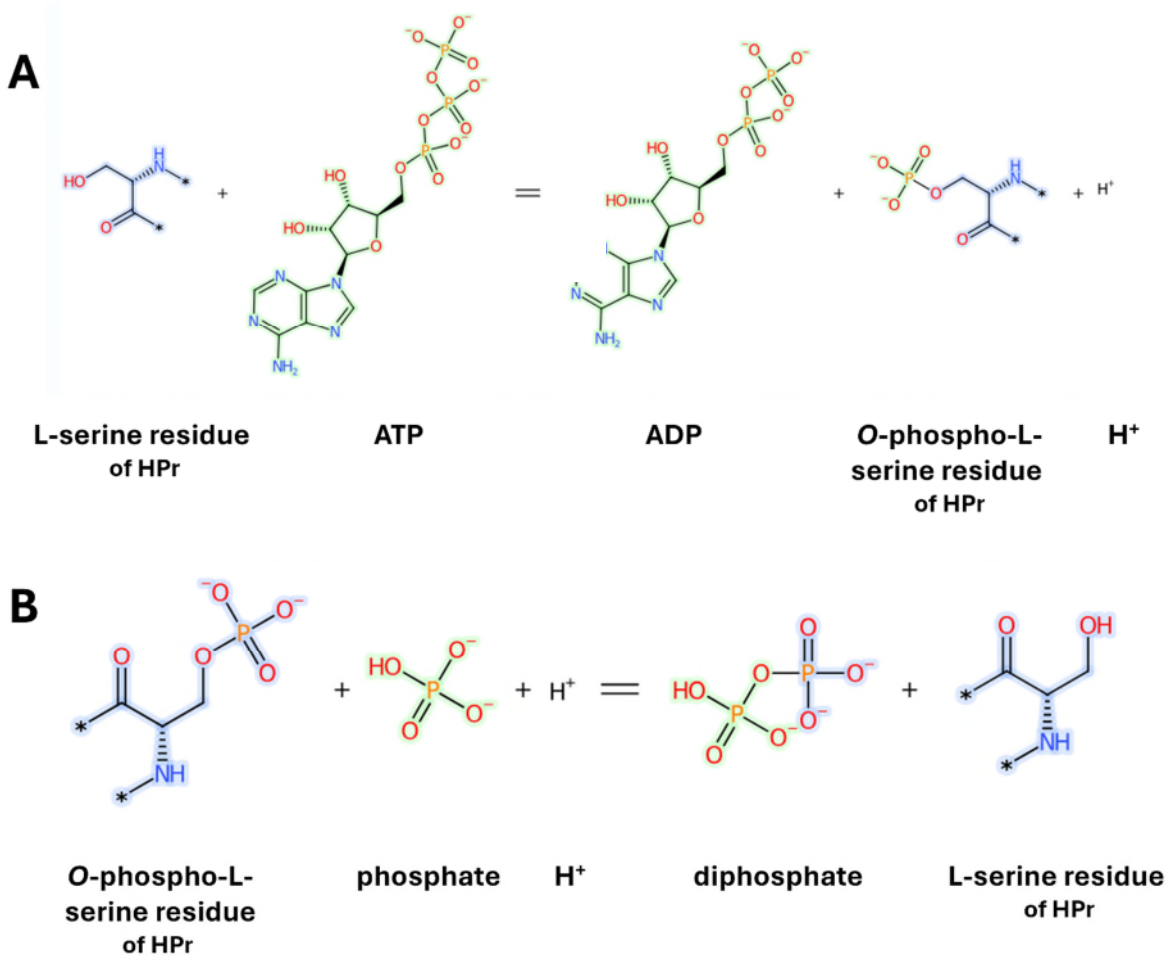

Figure 3. The catalytic activity of (A) phosphorylation and (B) phosphorolysis by HprK/P. Modified from the Uniprot database (Consortium, 2025).

Alphaproteobacteria generally lack the canonical sugar-PTS/CcpA system, and CcpA-dependent transcription via HPr(Ser~P) has not been demonstrated in this clade (Dozot et al., 2010; Pinedo & Gage, 2009). Regardless, the *hprK* gene is present in several Alphaproteobacteria, and typically resides upstream of the *npr* and *manX* genes (encoding NPr and $EIIA^{Man}$) (Hu & Saier, 2002; Pinedo & Gage, 2009). This HprK/P homolog is truncated in Alphaproteobacteria: the catalytic C-terminal P-loop domain is retained, whereas the N-terminal domain found in Firmicutes is absent (**Figure 4**) (Hu & Saier, 2002; Pinedo & Gage, 2009).

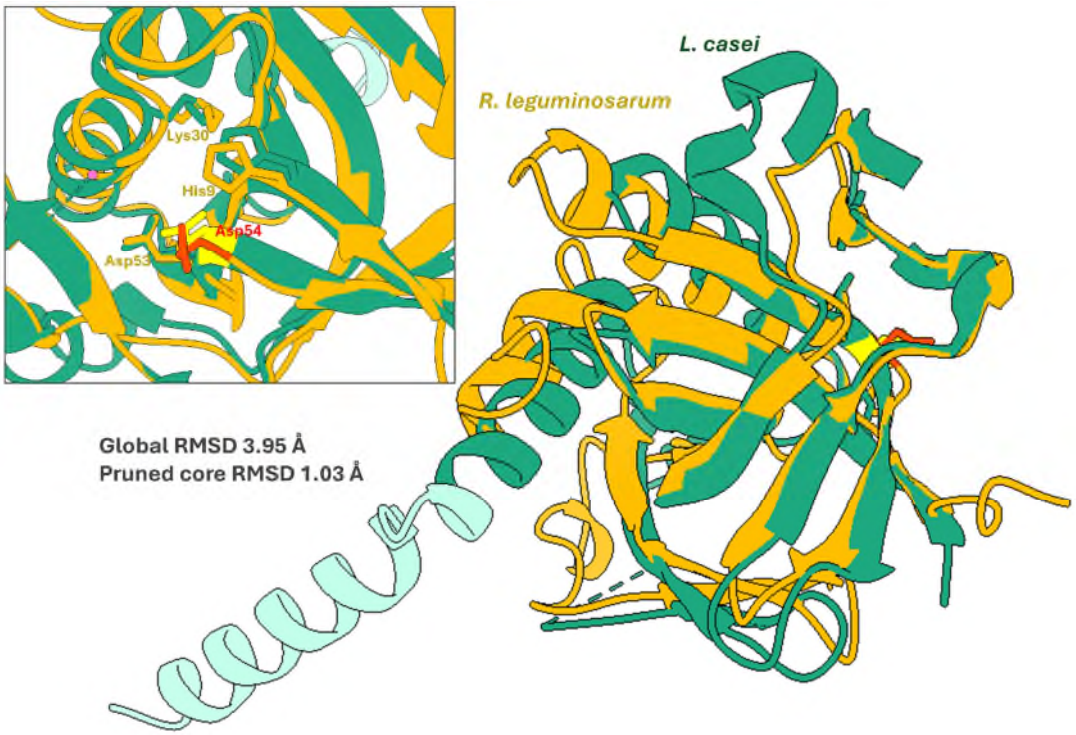

Figure 4. AlphaFold-predicted structure of HprK/P from *Rhizobium leguminosarum* bv. *viciae* 3841 (yellow) (Varadi et al., 2022, 2024) superimposed on the X-ray crystal structure of HprK/P from *Lactobacillus casei* (green, pdb_00001kkm) (Fieulaine et al., 2002). The light green region represents the N-terminal domain present in Firmicutes but missing in Alphaproteobacteria. Global backbone alignment gave an RMSD of 3.95 Å when all 131 aligned residues were included, but the pruned core of 82 residues superimposes with 1.03 Å RMSD, indicating that the two structures share a conserved core fold, while substantial differences occur in flexible loops or peripheral segments. The inset highlights the conservation of the catalytic site between the two species. Residue numbering corresponds to the *R. leguminosarum* sequence, and Asp54 is highlighted in red. Structural superposition and rendering were performed using UCSF ChimeraX (Meng et al., 2023).

Because the catalytic domain is present, Alphaproteobacterial HprK/Ps are expected to remain functional. Supporting this view, truncated HprK/P fragments without the N-terminal domain (resembling the Alphaproteobacteria version) are catalytically active in *Lactobacillus casei* (Fieulaine et al., 2001). Moreover, point mutations within the P-loop

of *L. casei* selectively reduce phosphorolysis activity (Monedero et al., 2001), suggesting that sequence differences in this loop could affect the enzyme function. Notably, Gram-negative Alphaproteobacteria such as *Rhizobium leguminosarum*, *Brucella* spp., and *Agrobacterium tumefaciens* exhibit few amino acid variations in the P-loop relative to Firmicutes, which may affect phosphorylase activity, although this remains to be tested experimentally.

Consistent with this, direct evidence from *Brucella melitensis* shows that HprK/P phosphorylates NPr on Ser61, with kinase activity stimulated by FBP and inhibited by inorganic phosphate (Dozot et al., 2010). Unlike in Firmicutes, *in vitro* tests show that Pi did not promote phosphorolysis of P~Ser-NPr by *Brucella* HprK/P, leaving the mechanism of dephosphorylation unresolved. These data indicate that metabolite signals (FBP, Pi) control the Ser-phosphorylation state of NPr and are expected to modulate the phosphotransfer through the PTS^{Ntr} relay from EI^{Ntr} to $EIIA^{Ntr}$.

While direct biochemistry was not presented, physiological characterisations in *S. meliloti* using *hprK* deletion mutant and a strain with NPr bearing single substitutions at Ser53 or His22 also support antagonism between the Ser and His residues (Pinedo & Gage, 2009). Phosphorylation at the Ser53 residue will prevent phosphorylation at His22, thereby reducing phosphotransfer to downstream PTS^{Ntr} components. HPrK/P also acts akin to a brake for CCR in *S. meliloti*: deletion of *hprK* produces a pronounced succinate-mediated catabolite repression (SMCR) phenotype due to accumulation of HPr-His22~P (Pinedo & Gage, 2009). Introducing *npr*(H22A) (non-His-phosphorylatable NPr) suppresses the *ΔhprK* SMCR phenotype, whereas *npr*(H22A) alone has an eased SMCR response.

SixA

In enteric γ-Proteobacteria, such as *E. coli* and *Salmonella*, HprK/P-Ser46 regulation is absent. *E. coli* HPr lacks the Ser46 regulatory loop, and NPr has no equivalent serine site (Nessler et al., 2003). In contrast, the dephosphorylation arm of the PTS^{Ntr} is provided by SixA (**Figure 5**), which was identified as the phosphohistidine phosphatase acting on the catalytic histidine of NPr via suppressor screening (Schulte & Goulian, 2018). Consistent with a role in PTS^{Ntr} signalling, the *sixA* mutant shows reduced intracellular potassium levels under the tested conditions, a phenotype also observed in *ptsN* mutants (Schulte & Goulian, 2018; Sharma et al., 2016). Other *E. coli* phenotypes of *ΔsixA* include a growth defect in minimal medium (Schulte & Goulian, 2018) and an NPr-dependent colonisation defect in the mouse intestine (Schulte et al., 2021).

Genetic evidence positions SixA at the NPr node, since loss of upstream phosphotransfer components such as *ptsP* suppresses the *ΔsixA* phenotype (Schulte & Goulian, 2018). The role of SixA is further supported by *in vivo* evidence showing an increased NPr~P fraction in *sixA* mutants, and by *in vitro* phosphotransfer assays demonstrating that SixA dephosphorylates NPr-His~P via phosphoryl transfer from NPr to a histidine residue on SixA, with strong selectivity for NPr over other PTS^{Ntr} components (PtsP and PtsN) (Schulte et al., 2021).

Beyond *E. coli*, *sixA* is conserved across Proteobacteria, Actinobacteria, and Cyanobacteria, and is typically not operon-linked to *ptsP/ptsO/ptsN* (Schulte & Goulian, 2018). To date, no definitive transcriptional, post-transcriptional, or allosteric regulators of SixA have been reported. Alternatively, SixA may provide a constant phosphatase capacity, while the metabolic inputs upstream of NPr (EI^{Ntr}) set the phosphate flux

through the standard histidine-mediated PTS^{Ntr} relay (Schulte et al., 2021; Schulte & Goulian, 2018).

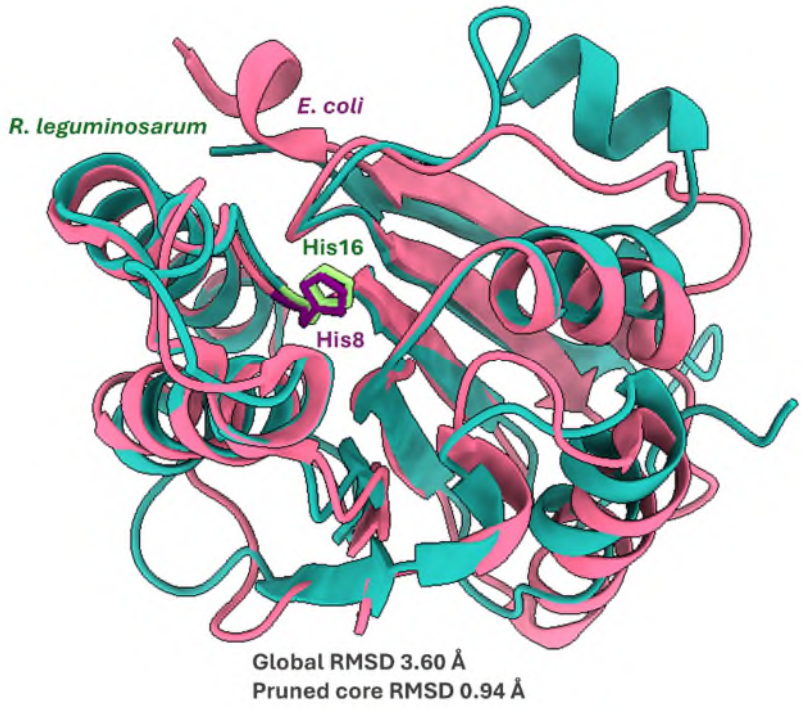

Figure 5. AlphaFold-predicted structure of SixA from *Rhizobium leguminosarum* bv. *viciae* 3841 (blue) (Varadi et al., 2022, 2024) superimposed on the X-ray crystal structure of *Escherichia coli* SixA (pink; pdb_00001ujb) (Hamada et al., 2005). The catalytic histidine is shown in green for *R. leguminosarum* (His16) and in purple for *E. coli* (His8). Global backbone alignment gave an RMSD of 3.60 Å when all 147 aligned residues were included, but the pruned core of 95 residues superimposes with 0.94 Å RMSD, indicating that the two structures share a very similar core fold, while most differences occur in flexible loops or peripheral segments. Structural superposition and rendering were performed using UCSF ChimeraX (Meng et al., 2023).

Effector nodes: PtsN (EIIA^{Ntr}) and ManX (EIIA^{Man})

PtsN

PtsN (EIIA^{Ntr}) is the terminal effector of the PTS^{Ntr} pathway, and in the canonical relay, phosphate flows PEP→PtsP (EI^{Ntr})→PtsO (NPr)→PtsN (EIIA^{Ntr}). A notable exception has

been reported in *Pseudomonas putida*, where cross-branch crosstalk allows FruB, a component of the fructose PTS, to phosphorylate PtsN *in vivo* during bacterial growth on fructose (Kremling et al., 2012; Pflüger & de Lorenzo, 2008).

The PtsN protein adopts the $EIIA^{Man}$ Rossmann-like fold with the conserved phospho-acceptor histidine positioned on the solvent-exposed loop (e.g., *E. coli* H73; *C. crescentus* H66; *P. putida* H68; *Brucella melitensis* H66; *R. leguminosarum* PtsN1 H66; *Azotobacter vinelandii* H68) (Dozot et al., 2010; Lee et al., 2007; Muriel-Millán et al., 2015; Noguez et al., 2008; Pflüger & de Lorenzo, 2008; Ronneau, Petit, et al., 2016; Sánchez-Cañizares et al., 2020). High-resolution structures and NMR data are available for *E. coli* PtsN (**Figure 6**) (Bordo et al., 1998; Wang et al., 2005). PtsN is active in its monomeric form in various species, including *E. coli* (Lee et al., 2007; Wang et al., 2005), *C. crescentus* (Ronneau, Petit, et al., 2016), and *S. meliloti* (Ronneau et al., 2019a). While most genomes encode a single *ptsN* copy, notable exceptions exist: *Sinorhizobium fredii* carries three $EIIA^{Ntr}$ paralogs (Feng et al., 2022), and *R. leguminosarum* harbours two PtsN copies (Sánchez-Cañizares et al., 2020). In both cases, the PtsN1 copy functions as the principal active paralog, since loss of this paralog produces strong phenotype defects.

The *ptsN* gene is frequently co-transcribed with *rpoN*, but it has been shown in *P. putida* that the PtsN-dependent regulation does not overlap with σ^{54} targets (Cases et al., 2001), as additional layers of control exist. The RNA-binding chaperone Hfq selectively targets *E. coli ptsN* transcripts without affecting *rpoN* (Sikora et al., 2024). In *Salmonella enterica*, post-translational control also tunes PtsN: excess nitrogen triggers PtsN

dephosphorylation followed by Lon-dependent degradation, and acidic pH lowers PtsN abundance in a PhoP- and Lon-dependent manner (Choi et al., 2019; Yoo et al., 2016).

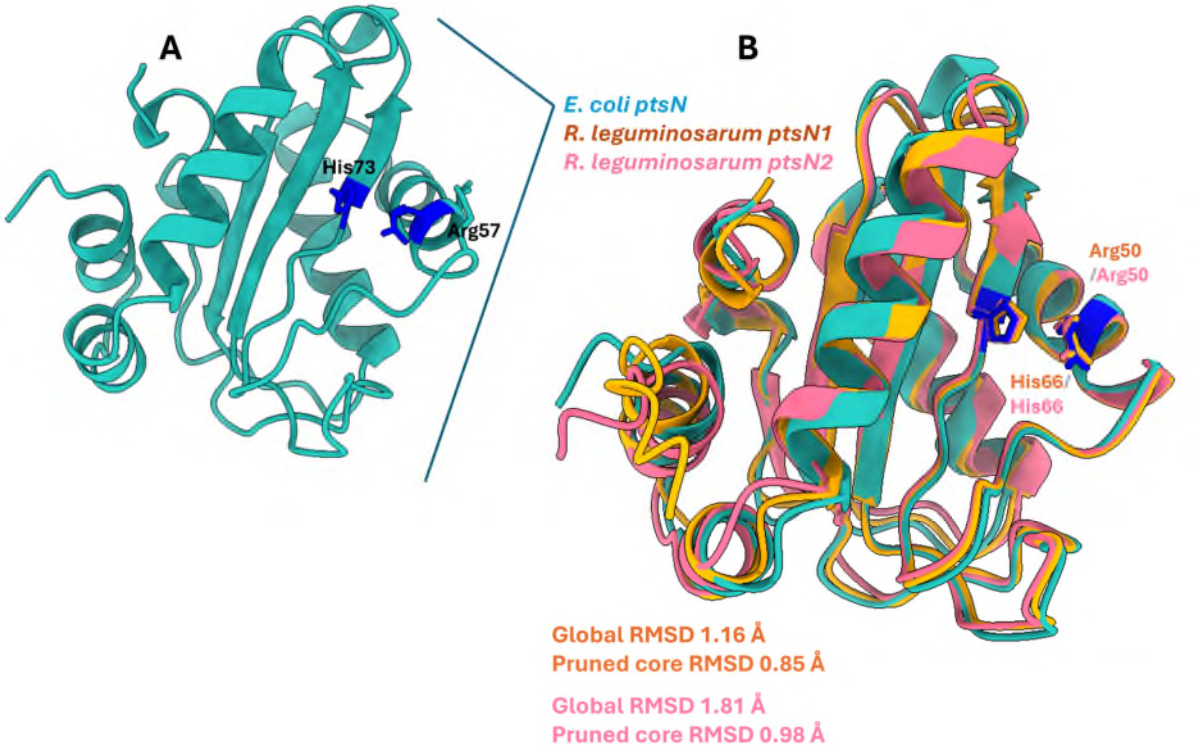

Figure 6. (A) The X-ray crystal structure of the PtsN of *E. coli* (blue; pdb_00001a6j) (Bordo et al., 1998). The conserved phosphate-acceptor histidine residue (His73) and adjacent catalytic arginine (Arg57) are highlighted in dark blue. (B) AlphaFold-predicted structure of PtsN1 (orange) and PtsN2 (pink) from *Rhizobium leguminosarum* bv. *viciae* 3841 (Varadi et al., 2022, 2024) superimposed on the X-ray crystal structure of *E. coli* (blue). The catalytic histidine for both PtsN1 and PtsN2 of *R. leguminosarum* is His50, and its catalytic arginine is Arg50. Global backbone alignment of *E. coli* PtsN to the two R. leguminosarum homologs, PtsN1 and PtsN2, yielded global RMSDs of 1.16 Å (148 residues) and 1.81 Å (147 residues), with pruned core RMSD of 0.85 Å (143 residues) and 0.98 Å (131 residues), respectively. These values indicate that both homologs closely preserve the *E. coli* PtsN core fold, with PtsN1 showing slightly higher overall structural similarity. Structural superposition and rendering were performed using UCSF ChimeraX (Meng et al., 2023).

ManX

In most Alphaproteobacteria, the sugar-PTS permeases EIIB/EIIC are absent, yet a homolog of the sugar-PTS system mannose-specific EIIA component (ManX) is present (Hu & Saier, 2002). This *manX* homolog, referred to as *ptsM* in some species, is typically encoded within a conserved locus along with *npr* and *hprK* (*ptsM-ptsO-hprK*). In *B. melitensis*, this locus lies near the two-component sensor kinase/response regulator pair *bvrR/bvrS* in (Sola-Landa et al., 1998), which is homologous to the *chvI/chvG* system in *R. leguminosarum* (Sánchez-Cañizares et al., 2020) and *Agrobacterium tumefaciens* (Charles & Nester, 1993), and to *chvI/exoS in S. meliloti* (Bélanger et al., 2009). Promoter fusion analysis in *R. leguminosarum* demonstrated that the *manX-npr* and *chvI-chvG-hprK* genes are transcribed together (Sánchez-Cañizares et al., 2020).

Structurally, Alphaproteobacterial ManX contains only the homolog of the N-terminal loop of the EIIA domain, while lacking the EIIB (**Figure 7**). The catalytic His (His10 in *E. coli*), which accepts phosphate from HPr-His in classical sugar-PTS relays, is retained (Erni et al., 1989; Gutknecht et al., 1999). In *E. coli*, $EIIA^{Man}$ donates the phosphate to $EIIB^{Man}$ at His175, which in turn passes it to the incoming sugar to mediate sugar transport. Therefore, because Alphaproteobacteria lack the EIIB and EIIC/D membrane domains, the remaining $EIIA^{Man}$ protein is best interpreted as a regulatory phosphate-accepting residue rather than part of a transport function. Consistent with this, *in vitro* experiments in *B. melitensis* showed that NPr efficiently phosphorylates $EIIA^{Man}$, integrating ManX as a functional EIIA partner within the PTS^{Ntr} system (Dozot et al., 2010). The same study also reported that, like PtsP and HprK, ManX interacts with itself to form oligomers, unlike PtsN.

The model Betaproteobacterium (β-proteobacteria) *Rastolnia eutropha* also possesses an incomplete mixed PTS system composed of EI (PtsH, without GAF-domain), HPr, $EIIA^{Ntr}$ (PtsN) and $EIIA^{Man}$ (PtsM) (Kraußе et al., 2009; Pries et al., 1991). *In vitro*, HPr~P transfers phosphates readily to PtsN and only extremely slowly to PtsM. However, these findings should not be generalised to Alphaproteobacteria, as they are evolutionarily distant from *Ralstonia* and possess a distinct genomic organisation of *ptsM, hprK, and hpr*.

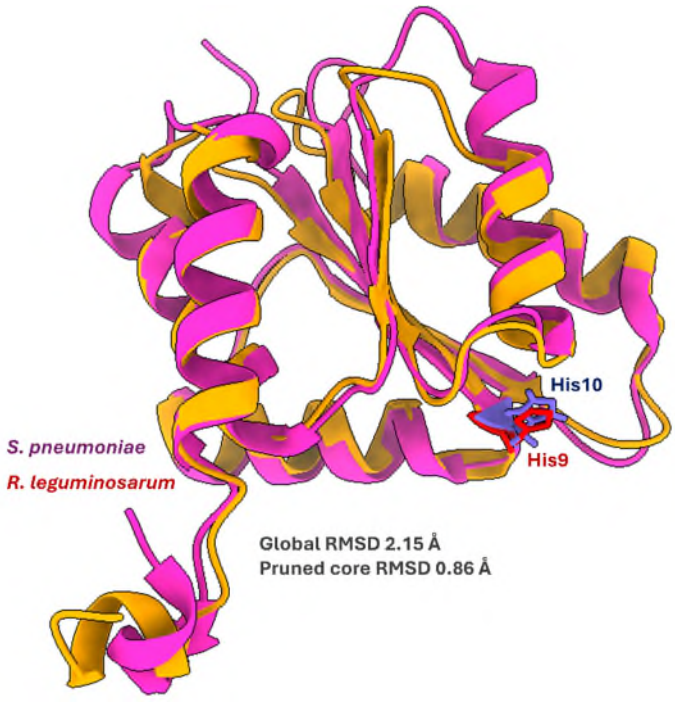

Figure 7. AlphaFold-predicted structure of ManX from *Rhizobium leguminosarum* bv. *viciae* 3841 (orange) (Varadi et al., 2022, 2024) superimposed on the X-ray crystal structure of EIIA-Man from *Streptococcus pneumoniae* (magenta; pdb_00006fmg) (Magoch et al., 2020). The catalytic histidine is shown in red for *R. leguminosarum* (His16) and in purple for *S. pneumoniae* (His11). Global backbone alignment gave an RMSD of 2.15 Å when all 132 aligned residues were included, but the pruned core of 107 residues superimposes with 0.86 Å RMSD, indicating that the two structures share a very similar core fold, while moderate differences occur in flexible loops or peripheral segments. Structural superposition and rendering were performed using UCSF ChimeraX (Meng et al., 2023).

Fate of the phosphoryl group in PTS^{Ntr}

In the sugar-PTS branch, the phosphoryl group is passed to the EIIB domain and then onto the imported sugar, yielding sugar-phosphate. By contrast, there is no EIIB/EIIC "sink" nor transfer of phosphate onto small metabolites in the regulatory PTS^{Ntr}. Instead, in the PtsP→NPr→PtsN or ManX cascade, phosphate is used as a regulatory signal that controls the binding of EIIAs to effectors rather than phosphorylating them. The phosphate of PtsN~P or ManX~P is dissipated as inorganic phosphate, either through spontaneous hydrolysis due to the intrinsic lability of His~P, or, as shown in *E. coli*, via a dedicated phosphohistidine phosphatase (SixA), which dephosphorylates NPr (Schulte et al., 2021; Schulte & Goulian, 2018). In other words, each signalling cycle spends PEP to set the phosphorylation state of the PTS^{Ntr} relay solely for its regulatory function.

2.4 Regulatory targets of PTS^{Ntr}

PTS^{Ntr} influences diverse cellular processes. Early comparative and genetic studies noted that *npr* (*ptsO*) frequently colocalises with *rpoN* (often in the same operon), and neighbour genes such as *hpf* (*yhbH*) and *rapZ* (*yhbJ*) in Enterobacteria or *hprK* in Alphaproteobacteria. These genomic contexts led to the hypothesis that PTS^{Ntr} integrates carbon and nitrogen metabolism (Barabote & Saier, 2005; Pflüger-Grau & Görke, 2010), and indeed, accumulating experimental evidence has since supported and refined this view. Below, we summarise confirmed PTS^{Ntr} targets in Alphaproteobacteria, along with additional examples from other bacterial lineages (**Table 1**).

Table 1. Physiologically confirmed PTS^{Ntr}-controlled processes in Alphaproteobacteria; ordered by year of discovery

Processes	Organisms	Component involved	Mechanism(s)	Reference(s)
Succinate-mediated catabolite response (SMCR)	*S. meliloti*	HprK/P	*ΔhprK* shows pronounced SMCR response and severe growth defect; direct mechanism remains unresolved.	(Pinedo et al., 2008; Pinedo & Gage, 2009)
Envelope & acid stress	*R. leguminosarum, S. meliloti*	PtsN	Phosphorylated PtsN correlates with increased EPS production; PtsN is shown to interact with ChvI sensor kinase of ChvI/ChvG system.	(Pinedo et al., 2008; Sánchez-Cañizares et al., 2020)
TCA cycle	*B. melitensis, R. leguminosarum*	ManX	Nonphosphorylated ManX interacts with SucA (component of 2-OG dehydrogenase complex); *ΔmanX* shows a growth defect and has impaired TCA cycle activity.	(Dozot et al., 2010; Sánchez-Cañizares et al., 2020)
Nutrient uptake via ABC transporters	*R. leguminosarum*	PtsN	PtsN~P is required for activation of various ABC transporters; molecular mechanisms remain to be fully defined.	(Prell et al., 2012; Untiet et al., 2013; Sánchez-Cañizares et al., 2020)
K+ Transport	*R. leguminosarum, S. fredii*	PtsN	The binding of unphosphorylated PtsN to the GAF domain of KdpD results in the induction of the *kdpFABC* operon for the high-affinity K^+ uptake system.	(Untiet et al., 2013; Feng et al., 2022)
Stringent response	*C. crescentus, S. meliloti*	PtsN, Npr	PtsN~P interacts with the ACT domain of RSH and inhibits its hydrolase activity, allowing (p)ppGpp to accumulate; NPr activates RelA/SpoT Homologs (RSH) synthase through an unknown mechanism.	(Ronneau, Petit, et al., 2016; Ronneau et al., 2019a)

Stringent response – RelA/SpoT (RSH)

RelA/Spot Homologs (RSH) control the synthesis and hydrolysis of the alarmone nucleotides ppGpp and pppGpp, collectively termed (p)ppGpp, which function as the central effectors of the stringent response (Dalebroux & Swanson, 2012). Most bacterial lineages encode at least one long, multi-domain RSH, whereas in many Gammaproteobacteria (γ-proteobacteria), these activities are partitioned between two proteins: RelA (a ribosome-activated synthetase) and SpoT (a bifunctional synthase-hydrolase).

Alphaproteobacteria typically encode a single "long" RSH (also termed Rel or SpoT/Rsh) that harbours both N-terminal synthase and hydrolase catalytic domains, followed by regulatory TGS (ThrRS–GTPase–SpoT), helical linker, ZFD (zinc-finger), and an ACT domain (**Figure 8**) (Atkinson et al., 2011; Brown et al., 2016). The ACT region is required for full hydrolase activity and for binding to PtsN (Ronneau, Petit, et al., 2016; Ronneau et al., 2019a).

The PtsN~P-ACT interaction inhibits hydrolase activity and promotes (p)ppGpp accumulation during nitrogen starvation. This PTS^{Ntr} and RSH crosstalk has been demonstrated in *C. crescentus* and *S. meliloti* (Ronneau, Petit, et al., 2016; Ronneau et al., 2019a; Ronneau & Hallez, 2019b), and PtsN-SpoT interaction has also been shown in the Betaproteobacteria *Ralstonia eutropha* (Karstens et al., 2014).

The regulatory cascade is as follows: nitrogen starvation lowers intracellular glutamine, alleviating inhibition of PtsP autophosphorylation. This drives the phosphate flow PEP→PtsP→NPr→PtsN, and results in PtsN~P. Once bound to the C-terminal ACT domain of the long RSH, PtsN~P inhibits its hydrolase activity, thereby elevating

(p)ppGpp. The elevated (p)ppGpp will then orchestrate the canonical stringent response, which includes reduction of ribosome biogenesis, global reduction in protein synthesis, and transcription and metabolism to enhance survival under nitrogen limitation (Ronneau & Hallez, 2019b). Relief of the stringent state occurs when nitrogen is replenished, and RSH hydrolase activity resumes.

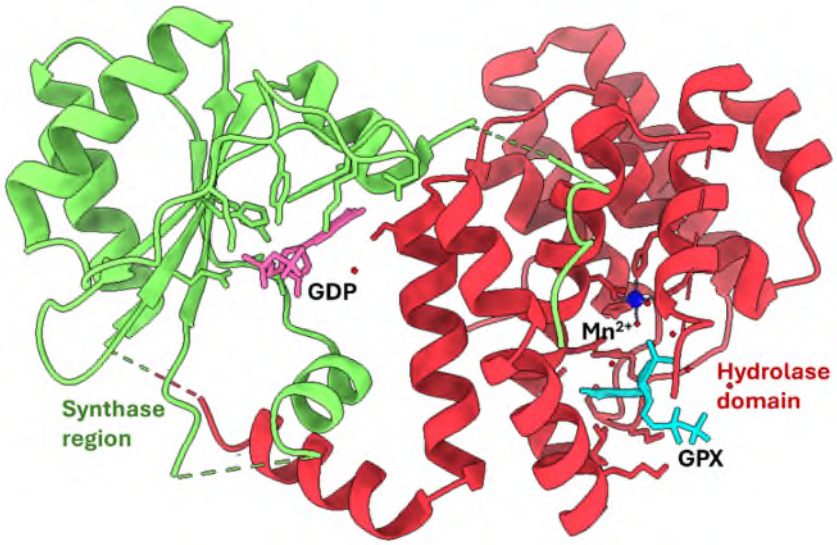

Figure 8. The X-ray structure of the bifunctional RelA/SpoT homolog (RSH) from *Streptococcus equisimilis* (pdb_00001vj7) (Hogg et al., 2004). The synthase region is shown in green, and the hydrolase domain in red. Ligands are depicted as follows: guanosine-5'-diphosphate (GDP), pink; Guanosine 5'-diphosphate 2'-3'-cyclic monophosphate (GPX), blue; manganese (II) ion, dark blue. Structural superposition and rendering were performed using UCSF ChimeraX (Meng et al., 2023).

Notably, under N-starvation (p)ppGpp accumulation can still occur in *ΔptsN* or a strain carrying a non-phosphorylatable PtsN (*ptsN H66A*) background, but not in *ΔptsP* or *Δnpr*. This indicates that RSH is controlled by PTS^{Ntr} by at least two mechanisms: one PtsN~P-dependent, and another PtsN~P-independent route whose mechanism remains unresolved (Ronneau, Petit, et al., 2016; Ronneau & Hallez, 2019).

By contrast, direct PtsN–SpoT interaction has not been established in Gammaproteobacteria such as *E. coli*. Instead, SpoT integrates other signals: it binds acyl carrier protein (ACP) via its C-terminal regulatory region (Battesti & Bouveret, 2006) and is controlled by the ribosome-associated GTPase CgtA (Jiang et al., 2007; Raskin et al., 2007). The sugar-PTS component, HPr, can also influence SpoT indirectly via the anti-σ factor Rsd (Lee et al., 2018).

Nutrient uptake – ABC transporters

ABC transporters (ATP synthase-binding cassette transporters) are high-affinity, widely spread ATP-dependent transporters present in all kingdoms of life. Rhizobia, representative soil-dwelling bacteria, encode many ABC transporters, several of which remain poorly characterised (Mauchline et al., 2006; Ramachandran et al., 2011). In *R. leguminosarum*, uptake of diverse ABC transporter substrates, including γ-amino butyric acid (GABA), ALA, glucose and myo-inositol, has been examined (Prell et al., 2012). For their relevance to symbiosis, an emphasis has been placed on the study of Aap and Bra branched-chain amino acid transporters, where the uptake of non-metabolizable amino-acid analogue AIB (2-Aminoisobutyric acid) provides a quantitative readout for ABC transporter capacity (Prell et al., 2012; Sánchez-Cañizares et al., 2020; Untiet et al., 2013).

Transport through ABC uptake systems in *R. leguminosarum* requires the PTS^{Ntr} phosphorelay. Phosphorylation of PtsP and NPr is required for full transporter activity (Untiet et al., 2013), and genetic as well as physiological evidence on *ptsN* mutant (*ΔptsN*), non-phosphorylatable PtsN (PtsN H66A), and phosphomimetic PtsN strains (PtsN H66E) implicates phosphorylated PtsN as the key activator (Sánchez-Cañizares et

al., 2020). Notably, the intracellular potassium levels determine the regulatory mode of PtsN (Untiet et al., 2013). Under strong K^+ limitation, unphosphorylated PtsN contributes to the inactivation of ABC systems, while its phosphorylation favours activation. This PtsN regulation occurs post-translationally, as observed in the transporter activity level, with a minimum change observed in the transcript abundance of the Aap transporter (Prell et al., 2012). However, no direct protein:protein interaction between PtsN and any component of the ABC transporter has been shown yet. Thus, while the evidence ties ABC transporter activity to the PTS^{Ntr} phosphorelay and positions PtsN as the most probable regulatory node, the causal mechanism remains to be proven.

Potassium homeostasis – KdpD/KdpE

Bacteria use four main K^+ uptake systems: Trk, Ktr, Kup, and Kdp, for adaptations to different environments (Diskowski et al., 2015). KdpFABC is a high-affinity K+ uptake system, whose expression is controlled by the two-component regulatory system KdpD (a membrane-bound sensor histidine kinase) and KdpE (a cytosolic response regulator). Direct protein:protein interaction between PtsN and KdpD is well established in non-Alphaproteobacterial models. In *E. coli*, the dephosphorylated form of PtsN binds the DHp/HisKA part of the KdpD transmitter region to stimulate signalling (Lüttmann et al., 2015; Mörk-Mörkenstein et al., 2017). A similar cross-talk has also been reported in *P. putida* (Deuschle et al., 2015).

In Alphaproteobacteria, *R. leguminosarum* requires PtsN for the induction of the *kdpABC* operon under K^+ limitation (Prell et al., 2012; Untiet et al., 2013). A mechanistic breakthrough came in *Sinorhizobium fredii*, where unphosphorylated PtsN1 binds the N-terminal GAF domain of KdpD, unlike the interaction described for *E. coli* PtsN (Feng et

al., 2022). Indeed, the non-phosphorylatable PtsN (H66A), but not the phosphomimetic PtsN (H66E), binds to KdpD. KdpD then uses its HisKA–HATPase region to engage response regulator KdpE, which induces the *kdpFABC* operon encoding the high-affinity K^+ uptake system. While PtsN–KdpD coupling occurs via the GAF domain in *S. fredii*, not all Alphaproteobacteria (e.g. *C. crescentus*) encode a KdpD with a cytoplasmic GAF domain, suggesting a lineage-specific wiring of the K^+ response (Quintero-Yanes et al., 2024).

Beyond Kdp activation, K^+ limitation also correlates with inactivation of several ATP-dependent ABC transporters in *R. leguminosarum*, indicating coordinated control of K^+ and nutrient uptake under potassium stress (Untiet et al., 2013). Because PtsP autophosphorylation integrates carbon and nitrogen cues (e.g., glutamine), the phosphate flux through PTS^{Ntr} can indirectly tune Kdp output via PtsN, supporting the broader view that K^+ homeostasis is integrated with central metabolism rather than being a purely ionic/osmotic reflex.

Envelope and acid stress – ChvG/ChvI

Across Alphaproteobacteria, ChvG/ChvI (also known as ExoS/ChvI, BvrS/BvrR, or ChvIG) functions as a two-component system responsive to envelope and acid stress (Greenwich et al., 2023). In *Agrobacterium* and many rhizobia, its activation is gated by a third periplasmic regulatory protein, ExoR, which enables ChvG/ChvI to upregulate succinoglycan (EPS-I) biosynthesis, export, and processing while repressing motility (Bouchier et al., 2025; Greenwich et al., 2023; Williams et al., 2022). By contrast, ExoR-lacking lineages such as *Brucella* and *Caulobacter* rely on the periplasmic sensing domain of ChvG to directly monitor acid and envelope perturbations, leading to lineage-

specific outputs (Greenwich et al., 2023). Additionally, ChvG/ChvI is also activated by ExoR-independent cell wall/envelope stress; in *Agrobacterium*, this induction occurs without detectable ExoR cleavage and contributes to intrinsic β-lactam tolerance (Bouchier et al., 2025; Williams et al., 2022). The molecular features of envelope stress sensed by ChvG remain to be defined.

Previous work in *R. leguminosarum* links PTS^{Ntr} signalling to ChvI/ChvG regulation. Bacterial two-hybrid assays show that PtsN physically interacts with the ChvI sensor kinase (Sánchez-Cañizares et al., 2020), and phosphorylation of PtsN correlates with increased EPS polymerase gene *pssA*, supporting a model in which PtsN~P promotes EPS production via ChvI. Prior work in *S. meliloti* places PtsN signalling upstream of EPS control, consistent with potential crosstalk between the PTS^{Ntr} pathway and ExoS/ChvI signalling (Pinedo et al., 2008).

Carbon metabolism

ManX and HprK act as carbon-response nodes in Alphaproteobacteria, with the strongest direct protein:protein interaction evidence coming from *B. melitensis*. Yeast 2-hybrid (Y2H) assays show that $EIIA^{Man}$ (ManX) interacts with SucA (Enzyme 1 subunit of 2-OG dehydrogenase complex), and their intracellular interaction is supported by DivIVA-based polar recruitment localisation experiments in *E. coli* (Dozot et al., 2010). Because budding yeast lacks the PTS phosphorelay, these Y2H experiments report dephosphorylated ManX binding SucA. However, several attempts to delete *manX* (*ptsM*) in this work failed, and thus the phenotypes of a *ΔmanX* strain were not reported.

Phenotypical studies of the *manX* and *hprK* mutants in *S. meliloti* indeed suggest a relation to carbon-mediated regulation. The *manX* and *hprK* mutant show slower growth

on several single carbon sources, and additionally, the *hprK* mutant displays pronounced succinate-mediated catabolite response (SMCR) phenotypes on mixed carbon sources. *ΔhprK* displays prolonged diauxic lag when grown on succinate plus lactose or raffinose, along with minimal lactose utilisation compared to the wild-type. Additionally, both *ΔmanX* and *ΔhprK* accumulate succinoglycan, while showing reduced expression of sugar-utilisation operons *melA-agp* (α-galactoside) and *lac* (β-galactoside) (Pinedo et al., 2008; Pinedo & Gage, 2009).

In *R. leguminosarum*, the *manX* mutant grows more slowly than the wild-type, exhibiting reduced oxygen consumption across different carbon and nitrogen conditions, consistent with impaired tricarboxylic acid (TCA) cycle flux (Sánchez-Cañizares et al., 2020). Activities of two TCA cycle enzymes, malate dehydrogenase (MDH) and 2-OG dehydrogenase (α-KGDH), are decreased in *ΔmanX*, but the expression levels of *mdh-lacZ* and *sucA-lacZ* transcriptional fusions are unchanged relative to wild-type, indicating a primarily post-transcriptional effect. Polarity effects on the adjacent *npr* gene were excluded, confirming that the observed phenotypes were exclusively due to loss of *manX*.

Regulatory targets in non-Alphaproteobacteria

K^+ transporters – Trk system

In *E. coli*, unphosphorylated PtsN binds to TrkA to inhibit Trk-mediated K^+ uptake (Lee et al., 2007). Concomitantly, PtsN activates KdpD/KdpE signalling to induce *kdpFABC*, thereby favouring high-affinity Kdp uptake over Trk under appropriate conditions (discussed in more detail in the earlier section: *Potassium Transport – KdpD/KdpE*). Across Alphaproteobacteria, Trk components are inconsistently distributed; for

example, they are clearly present in *S. meliloti* but absent from *R. leguminosarum (Domínguez-Ferreras et al., 2009)*. Regardless, a direct interaction between PtsN and TrkA has not been reported outside of *E. coli*.

Phosphate stress response - PhoR/PhoB

In *E. coli*, PtsN directly interacts with the histidine kinase PhoR and modulates the PhoR/PhoB two-component system that activates the phosphate-starvation *pho* regulon (Hsieh & Wanner, 2010; Lüttmann et al., 2012). This interaction is reported to depend on the phosphorylation state of PtsN, with the dephosphorylated form leading to increased PhoB~P and elevated expression of *pho* genes. PhoR/PhoB is well conserved in Alphaproteobacteria and is functional in Alphaproteobacteria (Al-Niemi et al., 1997; Hagberg et al., 2016), although interaction with PtsN has not been reported.

Virulence regulatory system - PhoP/PhoQ

Another two-component system functionally linked to PtsN is the PhoP response regulator and PhoQ sensor kinase (PhoP/PhoQ), which regulates a broad set of virulence genes in response to environmental cues, including low Mg^{2+}, acidic pH, and antimicrobial peptides (Groisman et al., 2021). In *Salmonella enterica*, acidic pH induces a Lon- and PhoP-dependent reduction of PtsN protein levels. The PhoP/Q system, via Lon protease, indirectly controls the degradation of PtsN. At the same time, because PtsN inhibits DNA binding by PhoP, its initial presence suppresses PhoP activity, and subsequent PtsN degradation removes this inhibition, creating a programmed delay in PhoP activation (Choi et al., 2019). Some Alphaproteobacteria (e.g. *Agrobacterium spp.* and *R. leguminosarum*) appear to encode *phoP/phoQ* orthologs, but experimental characterisation is lacking (Groisman et al., 2021). Instead, the acid/envelope-stress-

responsive ChvG/ChvI system is conserved and functionally central across many Alphaproteobacteria (Greenwich et al., 2023). Regulation of ChvG/ChvII has been discussed in greater detail in the previous section: *Envelope and acid stress: ChvG/ChvI*.

Pathogenicity – SsrA/SsrB

The SsrA/SsrB two-component system is located within *Salmonella* pathogenicity island 2 (SPI-2), which encodes the type III secretion system and many of its effectors required for intracellular survival and virulence. PtsN forms a complex with the response regulator SsrB and inhibits its DNA binding, thereby lowering the expression of SPI-2 target genes. Deletion of *ptsN* increases SPI-2 expression, but the original study did not determine which phosphorylation state of PtsN is active (Choi et al., 2010). Subsequent work in *Salmonella* indicates that PtsN phosphorylation state and abundance are condition-dependent. Excess nitrogen promotes PtsN dephosphorylation and Lon-dependent degradation, and acidic pH decreases PtsN levels via a PhoP- and Lon-dependent mechanism. By inference, conditions that lower PtsN abundance would relieve inhibition and favour SsrB promoter binding (Choi et al., 2019; Yoo et al., 2016).

Non-EIIA-mediated outputs of the PTS^{Ntr}

Beyond Alphaproteobacteria, there is stronger evidence that the components of the PTS^{Ntr} relay can function outside phosphate transfer to EIIA. In *E. coli*, dephosphorylated NPr directly binds LpxD to down-regulate lipid A biosynthesis (Kim et al., 2011). In *P. aeruginosa*, recent work indicates that NPr and PtsN can regulate overlapping but distinct sets of quorum-sensing-controlled genes, with NPr-dependent effects detectable even in the absence of PtsN. This supports the model in which NPr

contributes to regulatory outputs that are at least partly independent of EIIA (Banerjee et al., 2025).

In Alphaproteobacteria, most established outputs of the PTS^{Ntr} relay run through EIIA-type effectors: primarily through PtsN (EIIA), with some species also encoding a parallel EIIA-Man/ManX branch. Robust evidence for Alphaproteobacterial NPr acting as a direct effector independent of EIIA is currently lacking. That said, in *C. crescentus*, NPr~P contributes to activation of the Rsh/SpoT synthetase activity under glutamine starvation, increasing (p)ppGpp. However, the underlying mechanism is not fully resolved, and direct binding of NPr to RSH has not been demonstrated (Ronneau, Petit, et al., 2016).

2.5 Regulators of carbon-nitrogen metabolism beyond PTS^{Ntr}

In addition to the PTS^{Ntr} system, Alphaproteobacteria possess additional central regulators integrating carbon and nitrogen metabolism. This section highlights two regulators that are proposed to sense the [glutamine]:[2-oxoglutarate] ratio and modulate downstream nitrogen-responsive pathways.

PII signaling

PII proteins (GlnB/GlnK family) are ubiquitous trimeric sensor-integrators of cellular nitrogen and energy status present in nearly all bacteria, including Alphaproteobacteria (Huergo et al., 2013; Shapiro, 1969). PII senses the cellular status through competitive ATP/ADP binding and through 2-OG, which binds only as part of a ternary Mg–ATP–2-OG complex. A second control layer is the GlnD-mediated post-translational modification: when glutamine levels are low, GlnD uridylylates Tyr51 in the T-loop (a flexible loop structure that mediates interaction between PII and many of their target proteins); when glutamine is high, GlnD removes the uridylyl (UMP) group, shifting partner affinities

accordingly (Merrick, 2015; Yurgel et al., 2010). Downstream regulation by PII reflects the combination of these two modulatory layers.

In Alphaproteobacteria, confirmed PII targets include the AmtB ammonium channel, the NtrB/NtrC two-component system, and GlnE, which controls glutamine synthetase (GS) (Arcondéguy et al., 1997; Michel-Reydellet & Kaminski, 1999; Yurgel et al., 2010). Activation of N-acetylglutamate kinase (NAGK) by PII is conserved across bacteria, but it is inferred rather than directly demonstrated in rhizobia (Huergo et al., 2013; Merrick, 2015). Under nitrogen limitation (high 2-OG, low glutamine), PII is uridylylated and, together with Mg–ATP–2-OG binding, it disengages from AmtB, allowing NH_4^+ influx. Urydylated PII is also released from NtrB, resulting in NtrC~P accumulation, which drives transcription of σ54-dependent nitrogen stress-regulated genes. Uridylylated PII also biases GlnE toward deadenylylation, thereby activating GS. The converse holds under nitrogen sufficiency. Reviews by Huergo et al. (2013) and Merrick (2015) provide detailed descriptions of PII mechanisms and their downstream effectors.

There is no established direct mechanistic coupling between the PII and PTS^{Ntr} systems, and their primary targets are largely distinct. Nonetheless, both systems sense the same metabolic signal, the glutamine and 2-OG ratio, and each includes fast post-translational responses (within minutes) alongside slower transcriptional programs, suggesting coordinated actions.

Hfq/sRNAs

Hfq is a central RNA chaperone in rhizobia that stabilises trans-acting sRNAs and accelerates their base-pairing to mRNAs, mostly those mRNAs related to nutrient uptake systems and metabolic enzymes (Gao et al., 2010; Torres-Quesada et al., 2014).

Hfq-sRNA interactions fine-tune translation initiation and mRNA stability, enabling fast, concentration-sensitive regulation (Hussein & Lim, 2011; Torres-Quesada et al., 2014). In rhizobia, deletion of Hfq globally derepresses many ABC importers, shifts the metabolism of nitrogen compounds, and impairs symbiosis (Gao et al., 2010; Sobrero et al., 2012; Torres-Quesada et al., 2013). Additionally, in *C. crescentus*, loss of Hfq disrupts 2-OG homeostasis, consistent with reduced 2-OG dehydrogenase enzyme (α-KGDH) activity due to Coenzyme A (CoA) limitation, leading to 2-OG accumulation. This imbalance impairs peptidoglycan biosynthesis, demonstrating how Hfq-dependent post-transcriptional control can influence cell wall biogenesis through metabolite-level effects (Irnov et al., 2017). The direct post-transcriptional routes by which Hfq affects the TCA cycle remain unknown.

The dominant, validated axis that links Hfq to carbon and nitrogen metabolism in Alphaproteobacteria is via the AbcR-family of sRNAs (AbcR1/AbcR2), which use conserved anti-Shine–Dalgarno motifs to repress translation of mRNAs encoding periplasmic binding proteins (PBPs) and permease subunits of ABC importers for amino acids, peptides, and polyamines (García-Tomsig et al., 2022; Sheehan & Caswell, 2018; Torres-Quesada et al., 2013). Their action dampens inappropriate uptake, aligns import with physiological state, and, together with broader Hfq effects, reshapes flux through TCA/gluconeogenic nodes. Direct validations show that AbcR1 represses GABA-binding PBP Atu2422 in *A. tumefaciens* (Wilms et al., 2012), while in *S. meliloti*, AbcR1/AbcR2 directly repress *livK, prbA, aapQ*, and SMa0495 (García-Tomsig et al., 2022; Torres-Quesada et al., 2013). In *B. abortus*, AbcR1/2 act redundantly to silence multiple amino-acid and polyamine transporter mRNAs (Caswell et al., 2012). Generally, AbcR1

predominates during exponential growth/early infection, while AbcR2 accumulates during stationary or stress conditions.

Additionally, another Hfq-dependent trans-encoded sRNA, MmgR, has been shown to be a negative regulator of polyhydroxybutyrate (PHB) storage under nitrogen limitation (carbon surplus). Its expression responds to the carbon/nitrogen balance, where activation under nitrogen limitation requires NtrC, and repression under carbon limitation requires AniA (also known as PhaR, a transcriptional regulator linked to PHB metabolism) (Ceizel Borella et al., 2018; Lagares et al., 2017, 2025).

2.6 Conclusions

In Alphaproteobacteria, PTS^{Ntr} senses the intracellular nitrogen status through glutamine binding to the PtsP GAF domain, which inhibits PtsP autophosphorylation. In lineages encoding HprK/P, a carbon/energy layer is added: high FBP levels induce HprK/P to phosphorylate a serine residue on NPr, antagonising the PtsP-dependent His phosphorylation. These integrated inputs at the NPr node will then shape the phosphorylation state of the output EIIAs (PtsN and ManX). As proposed in *R. leguminosarum*, nitrogen-rich/carbon-limiting conditions bias ManX and PtsN toward the dephosphorylated state, whereas nitrogen-limiting/carbon-rich conditions bias them toward the phosphorylated state (Sánchez-Cañizares et al., 2020). This reciprocally regulated PtsN-ManX module thus allows continuous balancing of carbon-skeleton supply based on nitrogen availability.

The nitrogen response mediated by the PtsN regulatory branch is particularly evident, with the phosphorylation state of PtsN coherent with the initiating signal. When the cell is nitrogen starved and glutamine is low, PtsP autophosphorylates and transfers

phosphate via NPr to yield phosphorylated PtsN. Phosphorylated PtsN then induces the Rsh/SpoT-mediated stringent response, which supports survival under N-starvation (Ronneau & Hallez, 2019b).

The carbon arm, likely mediated by ManX, is less well defined mechanistically but supported functionally. HprK/P, whose kinase activity is stimulated by FBP and inhibited by Pi, can serine-phosphorylate NPr and counteract EIIA His-phosphorylation (Dozot et al., 2010), resulting in unphosphorylated EIIAs downstream. Unphosphorylated ManX has indeed been shown to be functional in *R. leguminosarum*, where it tunes the TCA/central carbon flux (Sánchez-Cañizares et al., 2020).

The conservation of FBP as the activator of HprK in Alphaproteobacteria suggests an interesting functional divergence of this protein. In Firmicutes, FBP is a glycolytic intermediate which directly gates CCR via the HPrK/CcpA system. Many Alphaproteobacteria lack phosphofructokinase (PFK), and consequently, FBP is predominantly made during gluconeogenesis, including during growth on C4 organic acids (Hottes et al., 2004; Zhang et al., 2016). In this clade, a high FBP level does not necessarily result in high glycolytic activity. Instead, HprK may primarily function during growth on organic acids, where its kinase activity promotes NPr-Ser phosphorylation, lowering PtsN~P and ManX~P, and therefore stimulating the TCA cycle.

While the core PTS^{Ntr} relay and at least one key regulatory target, the PtsN~P interaction with the ACT domain of the RSH enzyme, appear to be conserved across Alpharoteobacteria, downstream targets and physiological outputs vary between clades and even among species. For instance, in *S. fredii*, unphosphorylated PtsN1 interacts with the GAF domain of KdpD to drive the activation of the high-affinity K^+ uptake pathway

(Feng et al., 2022), whereas *C. crescentus* KdpD has been reported to lack a GAF domain, making a similar PtsN–KdpD-GAF interface unlikely in this organism (Quintero-Yanes et al., 2024). Additionally, since *sixA* orthologs are present in Alphaproteobacteria genomes, a potential hypothesis is that SixA could dephosphorylate NPr on the conserved His residue and thereby tune PTS^{Ntr} outputs; this remains untested in the Alphaproteobacterial systems covered here. Accordingly, cross-clade results should be treated as mechanistic guidance rather than general rules. Experimental validation within the Alphaproteobacteria lineage is needed before extrapolating PTS^{Ntr} outputs.

The downstream targets and regulatory mechanisms by which PTS^{Ntr} influences central carbon metabolism in Alphaproteobacteria are incompletely mapped. *R. leguminosarum* provides evidence in which PTS^{Ntr} signals bifurcate to ManX (controlling TCA flux) and to PtsN (controlling nitrogen uptake, EPS, and K^+ homeostasis), but broader conservation and molecular details remain to be defined. HprK/P has also been tied to the SMCR response, but the mechanism behind its regulation remains unclear. Additionally, the interplay between PTS^{Ntr} and other major carbon and nitrogen regulatory circuits, such as the PII and Ntr systems, remains unexplored.

Alphaproteobacteria are a diverse taxonomic group that occupy niches ranging from oceanic oligotrophs to plant symbionts and obligate intracellular pathogens. Among them, members of the Rhizobiales (Hyphomicrobiales) are particularly well studied because of their ability to establish symbioses with legumes and provide nitrogen for the host (*Rhizobium, Sinorhizobium*), as well as their biotechnology significance (*Agrobacterium*) (Hördt et al., 2020; Hwang et al., 2017; Udvardi & Poole, 2013). Perturbing PTS^{Ntr} components alters nitrogen-fixation efficiency as well as traits tied to

soil resilience and competitive nodulation, suggesting that a better understanding of its regulation could inform strategies to develop improved rhizobial inoculants (Greenwich et al., 2023; Sánchez-Cañizares et al., 2020). Beyond symbiosis, PTS^{Ntr} circuits also intertwine metabolic state and environmental cues in related pathogenic Rhizobiales (e.g. *Brucella and Agrobacterium*), regulating their ability to infect and interact with their hosts (Dozot et al., 2010; Hwang et al., 2017; Ronneau, Moussa, et al., 2014). Therefore, investigating this global PTS^{Ntr} regulatory network is strategically important, as these systems act as rapid post-translational switches that rebalance carbon oxidation, nitrogen uptake, potassium homeostasis, and other related processes in response to intracellular nutrient status.

2.7 References

Al-Niemi, T. S., Summers, M. L., Elkins, J. G., Kahn, M. L., & McDermott, T. R. (1997). Regulation of the phosphate stress response in *Rhizobium meliloti* by PhoB. *Applied and Environmental Microbiology, 63*(12), 4978–4981. https://doi.org/10.1128/aem.63.12.4978-4981.1997

Arcondéguy, T., Huez, I., Tillard, P., Gangneux, C., de Billy, F., Gojon, A., Truchet, G., & Kahn, D. (1997). The *Rhizobium meliloti* PII protein, which controls bacterial nitrogen metabolism, affects alfalfa nodule development. *Genes & Development, 11*(9), 1194–1206. https://doi.org/10.1101/gad.11.9.1194

Atkinson, G. C., Tenson, T., & Hauryliuk, V. (2011). The RelA/SpoT homolog (RSH) superfamily: Distribution and functional evolution of ppGpp synthetases and hydrolases across the tree of life. *PLOS ONE, 6*(8), e23479. https://doi.org/10.1371/journal.pone.0023479

Banerjee, S., Smalley, N. E., Saenjamsai, P., Fehr, A. R., Dandekar, A. A., Cabeen, M. T., & Chandler, J. R. (2025). Quorum sensing regulation by the nitrogen phosphotransferase system in *Pseudomonas aeruginosa*. *Journal of Bacteriology, 207*(8), e00048-25. https://doi.org/10.1128/jb.00048-25

Barabote, R. D., & Saier, M. H. (2005). Comparative genomic analyses of the bacterial phosphotransferase system. *Microbiology and Molecular Biology Reviews, 69*(4), 608–634. https://doi.org/10.1128/MMBR.69.4.608-634.2005

Battesti, A., & Bouveret, E. (2006). Acyl carrier protein/SpoT interaction, the switch linking SpoT-dependent stress response to fatty acid metabolism. *Molecular Microbiology, 62*(4), 1048–1063. https://doi.org/10.1111/j.1365-2958.2006.05442.x

Begley, G. S., & Jacobson, G. R. (1994). Overexpression, phosphorylation, and growth effects of ORF162, a *Klebsiella pneumoniae* protein encoded by a gene linked to *rpoN*, the gene encoding σ54. *FEMS Microbiology Letters, 119*(3), 389–394. https://doi.org/10.1111/j.1574-6968.1994.tb06918.x

Bélanger, L., Dimmick, K. A., Fleming, J. S., & Charles, T. C. (2009). Null mutations in *Sinorhizobium meliloti exoS* and *chvI* demonstrate the importance of this two-component regulatory system for symbiosis. *Molecular Microbiology, 74*(5), 1223–1237. https://doi.org/10.1111/j.1365-2958.2009.06931.x

Bordo, D., van Monfort, R. L. M., Pijning, T., Kalk, K. H., Reizer, J., Saier, M. H., & Dijkstra, B. W. (1998). The three-dimensional structure of the nitrogen regulatory protein IIA^{Ntr} from *Escherichia coli*. *Journal of Molecular Biology*, *279*(1), 245–255. https://doi.org/10.1006/jmbi.1998.1753

Bouchier, J. M., Knebel, E., Amstutz, J., Torrens, G., Santiago-Collazo, G., McCurry, C., Weisberg, A. J., Cava, F., & Brown, P. J. B. (2025). Activation of the ChvG–ChvI pathway promotes survival during cell wall stress in *Agrobacterium tumefaciens*. *Molecular Biology of the Cell, 36*(7). https://doi.org/10.1091/mbc.E24-12-0546

Brown, A., Fernández, I. S., Gordiyenko, Y., & Ramakrishnan, V. (2016). Ribosome-dependent activation of stringent control. *Nature, 534*(7606), 277–280. https://doi.org/10.1038/nature17675

Cases, I., Pérez-Martín, J., & de Lorenzo, V. (1999). The IIA^{Ntr} (PtsN) protein of *Pseudomonas putida* mediates the C source inhibition of the σ^{54}-dependent *Pu* promoter of the TOL plasmid. *Journal of Biological Chemistry, 274*(22), 15562–15568. https://doi.org/10.1074/jbc.274.22.15562

Cases, I., Lopez, J.-A., Albar, J.-P., & De Lorenzo, V. (2001). Evidence of multiple regulatory functions for the PtsN (IIA^{Ntr}) protein of *Pseudomonas putida*. *Journal of Bacteriology, 183*(3), 1032–1037. https://doi.org/10.1128/JB.183.3.1032-1037.2001

Caswell, C. C., Gaines, J. M., Ciborowski, P., Smith, D., Borchers, C. H., Roux, C. M., Sayood, K., Dunman, P. M., & Roop, R. M., II. (2012). Identification of two small regulatory RNAs linked to virulence in *Brucella abortus* 2308. *Molecular Microbiology, 85*(2), 345–360. https://doi.org/10.1111/j.1365-2958.2012.08117.x

Ceizel Borella, G., Lagares, A., Jr., & Valverde, C. (2018). Expression of the small regulatory RNA gene *mmgR* is regulated negatively by AniA and positively by NtrC in *Sinorhizobium meliloti* 2011. *Microbiology, 164*(1), 88–98. https://doi.org/10.1099/mic.0.000586

Chaptal, V., Vincent, F., Gueguen-Chaignon, V., Monedero, V., Poncet, S., Deutscher, J., Nessler, S., & Morera, S. (2007). Structural analysis of the bacterial HPr kinase/phosphorylase V267F mutant gives insights into the allosteric regulation mechanism of this bifunctional enzyme. *Journal of Biological Chemistry, 282*(48), 34952–34957. https://doi.org/10.1074/jbc.M705979200

Charles, T. C., & Nester, E. W. (1993). A chromosomally encoded two-component sensory transduction system is required for virulence of *Agrobacterium tumefaciens*. *Journal of Bacteriology, 175*(20), 6614–6625. https://doi.org/10.1128/jb.175.20.6614-6625.1993

Choi, J., Kim, H., Chang, Y., Yoo, W., Kim, D., & Ryu, S. (2019). Programmed delay of a virulence circuit promotes *Salmonella* pathogenicity. *mBio, 10*(2), e00291-19. https://doi.org/10.1128/mBio.00291-19

Choi, J., Shin, D., Yoon, H., Kim, J., Lee, C.-R., Kim, M., Seok, Y.-J., & Ryu, S. (2010). *Salmonella* pathogenicity island 2 expression negatively controlled by $EIIA^{Ntr}$–SsrB interaction is required for *Salmonella* virulence. *Proceedings of the National Academy of Sciences of the United States of America, 107*(47), 20506–20511. https://doi.org/10.1073/pnas.1000759107

Consortium, T. U. (2025). UniProt: the Universal Protein Knowledgebase in 2025. *Nucleic Acids Research*, *53*(D1), D609–D617. https://doi.org/10.1093/nar/gkae1010

Dalebroux, Z. D., & Swanson, M. S. (2012). ppGpp: Magic beyond RNA polymerase. *Nature Reviews Microbiology, 10*(3), 203–212. https://doi.org/10.1038/nrmicro2720

Deuschle, M., Limbrunner, S., Rother, D., Heermann, R., Jung, K., & Görke, B. (2015). Interplay of the PtsN (EIIA^{Ntr}) protein of *Pseudomonas putida* with its target sensor kinase KdpD. *Environmental Microbiology Reports, 7*(6), 899–907. https://doi.org/10.1111/1758-2229.12323

Deutscher, J., Francke, C., & Postma, P. W. (2006). How phosphotransferase system-related protein phosphorylation regulates carbohydrate metabolism in bacteria. *Microbiology and Molecular Biology Reviews, 70*(4), 939–1031. https://doi.org/10.1128/MMBR.00024-06

Diskowski, M., Mikusevic, V., Stock, C., & Hänelt, I. (2015). Functional diversity of the superfamily of K^+ transporters to meet various requirements. *Biological Chemistry, 396*(9–10), 1003–1014. https://doi.org/10.1515/hsz-2015-0123

Domínguez-Ferreras, A., Muñoz, S., Olivares, J., Soto, M. J., & Sanjuán, J. (2009). Role of potassium uptake systems in *Sinorhizobium meliloti* osmoadaptation and symbiotic performance. *Journal of Bacteriology, 191*(7), 2133–2143. https://doi.org/10.1128/JB.01567-08

Dozot, M., Poncet, S., Nicolas, C., Copin, R., Bouraoui, H., Mazé, A., Deutscher, J., De Bolle, X., & Letesson, J.-J. (2010). Functional characterization of the incomplete phosphotransferase system (PTS) of the intracellular pathogen *Brucella melitensis*. *PLOS ONE, 5*(9), e12679. https://doi.org/10.1371/journal.pone.0012679

Erni, B., Zanolari, B., Graff, P., & Kocher, H. P. (1989). Mannose permease of *Escherichia coli*. *Journal of Biological Chemistry, 264*(31), 18733–18741. https://doi.org/10.1016/S0021-9258(18)51529-5

Feng, X. Y., Tian, Y., Cui, W. J., Li, Y. Z., Wang, D., Liu, Y., Jiao, J., Zhang, L., & Yuan, Z. (2022). The PTS^{Ntr}–KdpDE–KdpFABC pathway contributes to low-potassium stress adaptation and competitive nodulation of *Sinorhizobium fredii*. *mBio, 13*(1), e03721-21. https://doi.org/10.1128/mbio.03721-21

Fieulaine, S., Morera, S., Poncet, S., Monedero, V., Gueguen-Chaignon, V., Galinier, A., Janin, J., Deutscher, J., & Nessler, S. (2001). X-ray structure of HPr kinase: A bacterial protein kinase with a P-loop nucleotide-binding domain. *The EMBO Journal, 20*(15), 3917–3927. https://doi.org/10.1093/emboj/20.15.3917

Fieulaine, S., Morera, S., Poncet, S., Mijakovic, I., Galinier, A., Janin, J., Deutscher, J., & Nessler, S. (2002). X-ray structure of a bifunctional protein kinase in complex with its protein substrate HPr. *Proceedings of the National Academy of Sciences of the United States of America, 99*(21), 13437–13441. https://doi.org/10.1073/pnas.192368699

Fox, D., Kukuruzinska, M., Liu, K. D.-F., Meadow, N. D., Saffen, D., & Roseman, S. (1984). Regulation of sugar transport by the bacterial phosphoenolpyruvate:glucose phosphotransferase system. *Biochemical Society Transactions, 12*(2), 155–157. https://doi.org/10.1042/bst0120155

Galinier, A., Kravanja, M., Engelmann, R., Hengstenberg, W., Kilhoffer, M.-C., Deutscher, J., & Haiech, J. (1998). New protein kinase and protein phosphatase families mediate signal transduction in bacterial catabolite repression. *Proceedings of the National Academy of Sciences of the United States of America, 95*(4), 1823–1828. https://doi.org/10.1073/pnas.95.4.1823

Gao, M., Barnett, M. J., Long, S. R., & Teplitski, M. (2010). Role of the *Sinorhizobium meliloti* global regulator Hfq in gene regulation and symbiosis. *Molecular Plant-Microbe Interactions, 23*(4), 355–365. https://doi.org/10.1094/MPMI-23-4-0355

García-Tomsig, N. I., Robledo, M., diCenzo, G. C., Mengoni, A., Millán, V., Peregrina, A., Uceta, A., & Jiménez-Zurdo, J. I. (2022). Pervasive RNA regulation of metabolism enhances the root colonization ability of nitrogen-fixing symbiotic α-rhizobia. *mBio, 13*(1), e03576-21. https://doi.org/10.1128/mbio.03576-21 (ASM Journals)

Goodwin, R. A., & Gage, D. J. (2014). Biochemical characterization of a nitrogen-type phosphotransferase system reveals that enzyme EI^{Ntr} integrates carbon and nitrogen signaling in *Sinorhizobium meliloti*. *Journal of Bacteriology, 196*(10), 1901–1907. https://doi.org/10.1128/JB.01489-14

Greenwich, J. L., Heckel, B. C., Alakavuklar, M. A., & Fuqua, C. (2023). The ChvG–ChvI regulatory network: A conserved global regulatory circuit among the Alphaproteobacteria with pervasive impacts on host interactions and diverse cellular processes. *Annual Review of Microbiology, 77*(1), 131–148. https://doi.org/10.1146/annurev-micro-120822-102714

Groisman, E. A., Duprey, A., & Choi, J. (2021). How the PhoP/PhoQ system controls virulence and Mg^{2+} homeostasis: Lessons in signal transduction, pathogenesis, physiology, and evolution. *Microbiology and Molecular Biology Reviews, 85*(3), e00176-20. https://doi.org/10.1128/MMBR.00176-20

Gutknecht, R., Flükiger, K., Lanz, R., & Erni, B. (1999). Mechanism of phosphoryl transfer in the dimeric $IIAB^{Man}$ subunit of the *Escherichia coli* mannose transporter. *Journal of Biological Chemistry, 274*(10), 6091–6096. https://doi.org/10.1074/jbc.274.10.6091

Hagberg, K. L., Yurgel, S. N., Mulder, M., & Kahn, M. L. (2016). Interaction between nitrogen and phosphate stress responses in *Sinorhizobium meliloti*. *Frontiers in Microbiology, 7*, 1928. https://doi.org/10.3389/fmicb.2016.01928

Hamada, K., Kato, M., Shimizu, T., Ihara, K., Mizuno, T., & Hakoshima, T. (2005). Crystal structure of the protein histidine phosphatase SixA in the multistep His-Asp phosphorelay. *Genes to Cells*, *10*(1), 1–11.

Hogg, T., Mechold, U., Malke, H., Cashel, M., & Hilgenfeld, R. (2004). Conformational Antagonism between Opposing Active Sites in a Bifunctional RelA/SpoT Homolog Modulates (p)ppGpp Metabolism during the Stringent Response. *Cell*, *117*(1), 57–68. https://doi.org/10.1016/S0092-8674(04)00260-0

Hördt, A., López, M. G., Meier-Kolthoff, J. P., Schleuning, M., Weinhold, L.-M., Tindall, B. J., Gronow, S., Kyrpides, N. C., Woyke, T., & Göker, M. (2020). Analysis of 1,000+ type-strain genomes substantially improves taxonomic classification of Alphaproteobacteria. *Frontiers in Microbiology, 11*, 468. https://doi.org/10.3389/fmicb.2020.00468

Hottes, A. K., Meewan, M., Yang, D., Arana, N., Romero, P., McAdams, H. H., & Stephens, C. (2004). Transcriptional profiling of *Caulobacter crescentus* during growth on complex and minimal media. *Journal of Bacteriology, 186*(5), 1448–1461. https://doi.org/10.1128/JB.186.5.1448-1461.2004

Hoving, H., Lolkema, J. S., & Robillard, G. T. (1981). *Escherichia coli* phosphoenolpyruvate-dependent phosphotransferase system: Equilibrium kinetics and mechanism of enzyme I phosphorylation. *Biochemistry, 20*(1), 87–93. https://doi.org/10.1021/bi00504a015

Hsieh, Y.-J., & Wanner, B. L. (2010). Global regulation by the seven-component Pi signaling system. *Current Opinion in Microbiology, 13*(2), 198–203. https://doi.org/10.1016/j.mib.2010.01.014

Hu, K.-Y., & Saier, M. H. (2002). Phylogeny of phosphoryl transfer proteins of the phosphoenolpyruvate-dependent sugar-transporting phosphotransferase system. *Research in Microbiology, 153*(7), 405–415. https://doi.org/10.1016/S0923-2508(02)01339-6

Huergo, L. F., Chandra, G., & Merrick, M. (2013). PII signal transduction proteins: Nitrogen regulation and beyond. *FEMS Microbiology Reviews, 37*(2), 251–283. https://doi.org/10.1111/j.1574-6976.2012.00351.x

Hussein, R., & Lim, H. N. (2011). Disruption of small RNA signaling caused by competition for Hfq. *Proceedings of the National Academy of Sciences of the United States of America, 108*(3), 1110–1115. https://doi.org/10.1073/pnas.1010082108

Hwang, H.-H., Yu, M., & Lai, E.-M. (2017). *Agrobacterium*-mediated plant transformation: Biology and applications. *The Arabidopsis Book, 15*, e0186. https://doi.org/10.1199/tab.0186

Irnov, I., Wang, Z., Jannetty, N. D., Bustamante, J. A., Rhee, K. Y., & Jacobs-Wagner, C. (2017). Crosstalk between the tricarboxylic acid cycle and peptidoglycan synthesis in *Caulobacter crescentus* through the homeostatic control of α-ketoglutarate. *PLOS Genetics, 13*(8), e1006978. https://doi.org/10.1371/journal.pgen.1006978

Jiang, M., Sullivan, S. M., Wout, P. K., & Maddock, J. R. (2007). G-protein control of the ribosome-associated stress response protein SpoT. *Journal of Bacteriology, 189*(17), 6140–6147. https://doi.org/10.1128/JB.00315-07

Karstens, K., Zschiedrich, C. P., Bowien, B., Stülke, J., & Görke, B. (2014). Phosphotransferase protein EIIA^{Ntr} interacts with SpoT, a key enzyme of the stringent response, in *Ralstonia eutropha* H16. *Microbiology, 160*(4), 711–722. https://doi.org/10.1099/mic.0.075226-0

Kim, H.-J., Lee, C.-R., Kim, M., Peterkofsky, A., & Seok, Y.-J. (2011). Dephosphorylated NPr of the nitrogen PTS regulates lipid A biosynthesis by direct interaction with LpxD. *Biochemical and Biophysical Research Communications, 409*(3), 556–561. https://doi.org/10.1016/j.bbrc.2011.05.044

Krauße, D., Hunold, K., Kusian, B., Lenz, O., Stülke, J., Bowien, B., & Deutscher, J. (2009). Essential role of the *hprK* gene in *Ralstonia eutropha* H16. *Journal of Molecular Microbiology and Biotechnology, 17*(3), 146–152. https://doi.org/10.1159/000233505

Kremling, A., Pflüger-Grau, K., Chavarría, M., Puchalka, J., Martins, V., Santos, D., & de Lorenzo, V. (2012). Modeling and analysis of flux distributions in the two branches of the phosphotransferase system in *Pseudomonas putida*. *BMC Systems Biology, 6*, 149. https://doi.org/10.1186/1752-0509-6-149

Kundig, W., Ghosh, S., & Roseman, S. (1964). Phosphate-bound to histidine in a protein as an intermediate in a novel phospho-transferase system. *Proceedings of the National Academy of Sciences of the United States of America, 52*(4), 1067–1074. https://doi.org/10.1073/pnas.52.4.1067

Lagares, A., Borella, G. C., Linne, U., Becker, A., & Valverde, C. (2017). Regulation of polyhydroxybutyrate accumulation in *Sinorhizobium meliloti* by the trans-encoded small RNA MmgR. *Journal of Bacteriology, 199*(8), e00776-16. https://doi.org/10.1128/JB.00776-16

Lagares, A., Krol, E., Müller, T., Glatter, T., & Becker, A. (2025). A systems-level insight into PHB-driven metabolic adaptation orchestrated by the PHB-binding transcriptional regulator AniA (PhaR). *bioRxiv*. https://doi.org/10.1101/2025.02.17.638283

Lee, C. R., Park, Y. H., Kim, M., Kim, Y. R., Park, S., Peterkofsky, A., & Seok, Y. J. (2013). Reciprocal regulation of the autophosphorylation of enzyme I^{Ntr} by glutamine and α-ketoglutarate in *Escherichia coli*. *Molecular microbiology, 88(3),* 473–485. https://doi.org/10.1111/mmi.12196

Lee, C.-R., Cho, S.-H., Yoon, M.-J., Peterkofsky, A., & Seok, Y.-J. (2007). *Escherichia coli* enzyme IIA^{Ntr} regulates the K^+ transporter TrkA. *Proceedings of the National Academy of Sciences of the United States of America, 104*(10), 4124–4129. https://doi.org/10.1073/pnas.0609897104

Lee, J.-W., Park, Y.-H., & Seok, Y.-J. (2018). Rsd balances (p)ppGpp level by stimulating the hydrolase activity of SpoT during carbon source downshift in *Escherichia coli*. *Proceedings of the National Academy of Sciences of the United States of America, 115*(29), E6845–E6854. https://doi.org/10.1073/pnas.1722514115

Li, X., Peterkofsky, A., & Wang, G. (2008). Solution structure of NPr, a bacterial signal-transducing protein that controls the phosphorylation state of the potassium transporter-regulating protein IIA^{Ntr}. *Amino Acids, 35*(3), 531–539. https://doi.org/10.1007/s00726-008-0079-9

Lüttmann, D., Göpel, Y., & Görke, B. (2012). The phosphotransferase protein EIIA^{Ntr} modulates the phosphate starvation response through interaction with histidine kinase PhoR in *Escherichia coli*. *Molecular Microbiology, 86*(1), 96–110. https://doi.org/10.1111/j.1365-2958.2012.08176.x

Lüttmann, D., Göpel, Y., & Görke, B. (2015). Cross-talk between the canonical and the nitrogen-related phosphotransferase systems modulates synthesis of the KdpFABC potassium transporter in *Escherichia coli*. *Journal of Molecular Microbiology and Biotechnology, 25*(2–3), 168–177. https://doi.org/10.1159/000381548

Magoch, M., Nogly, P., Grudnik, P., Ma, P., Boczkus, B., Neves, A. R., Archer, M., & Dubin, G. (2020). Crystal Structure of Mannose Specific IIA Subunit of Phosphotransferase System from Streptococcus pneumoniae. *Molecules*, *25*(20).

Mauchline, T. H., Fowler, J. E., East, A. K., Sartor, A. L., Zaheer, R., Hosie, A. H. F., Poole, P. S., & Finan, T. M. (2006). Mapping the *Sinorhizobium meliloti* 1021 solute-binding protein-dependent transportome. *Proceedings of the National Academy of Sciences of the United States of America, 103*(47), 17933–17938. https://doi.org/10.1073/pnas.0606673103

Meadow, N. D., Mattoo, R. L., Savtchenko, R. S., & Roseman, S. (2005). Transient-state kinetics of enzyme I of the phosphoenolpyruvate:glucose phosphotransferase system of *Escherichia coli*: Equilibrium and second-order rate constants for the phosphotransfer reactions with phosphoenolpyruvate and HPr. *Biochemistry, 44*(38), 12790–12796. https://doi.org/10.1021/bi0502846

Meng, E. C., Goddard, T. D., Pettersen, E. F., Couch, G. S., Pearson, Z. J., Morris, J. H., & Ferrin, T. E. (2023). UCSF ChimeraX: Tools for structure building and analysis. *Protein Science*, *32*(11), e4792. https://doi.org/https://doi.org/10.1002/pro.4792

Merrick, M. (2014). Post-translational modification of PII signal transduction proteins. *Frontiers in Microbiology, 5*, 763. https://doi.org/10.3389/fmicb.2014.00763

Michel-Reydellet, N., & Kaminski, P. A. (1999). *Azorhizobium caulinodans* PII and GlnK proteins control nitrogen fixation and ammonia assimilation. *Journal of Bacteriology, 181*(8), 2655–2658. https://doi.org/10.1128/JB.181.8.2655-2658.1999

Mijakovic, I., Poncet, S., Galinier, A., Monedero, V., Fieulaine, S., Janin, J., Nessler, S., Marquez, J. A., Scheffzek, K., Hasenbein, S., Hengstenberg, W., & Deutscher, J. (2002). Pyrophosphate-producing protein dephosphorylation by HPr kinase/phosphorylase: A relic of early life? *Proceedings of the National Academy of Sciences of the United States of America, 99*(21), 13442–13447. https://doi.org/10.1073/pnas.212410399

Misset, O., Blaauw, M., & Robillard, G. T. (1983). Bacterial phosphoenolpyruvate-dependent phosphotransferase system: Mechanism of the transmembrane sugar translocation and phosphorylation. *Biochemistry, 22*(26), 6163–6170. https://doi.org/10.1021/bi00295a019

Monedero, V., Poncet, S., Mijakovic, I., Fieulaine, S., Dossonnet, V., Martin-Verstraete, I., Nessler, S., & Deutscher, J. (2001). Mutations lowering the phosphatase activity of HPr kinase/phosphatase switch off carbon metabolism. *The EMBO Journal, 20*(15), 3928–3937. https://doi.org/10.1093/emboj/20.15.3928

Mörk-Mörkenstein, M., Heermann, R., Jung, K., Görke, B., & Görke, C. (2017). Non-canonical activation of histidine kinase KdpD by phosphotransferase protein PtsN through interaction with the transmitter domain. *Molecular Microbiology, 106*(1), 54–73. https://doi.org/10.1111/mmi.13751

Muriel-Millán, L. F., Moreno, S., Romero, Y., Bedoya-Pérez, L. P., Castañeda, M., Segura, D., & Espín, G. (2015). The unphosphorylated $EIIA^{Ntr}$ protein represses the synthesis of alkylresorcinols in *Azotobacter vinelandii*. *PLOS ONE, 10*(2), e0117184. https://doi.org/10.1371/journal.pone.0117184

Nessler, S., Fieulaine, S., Poncet, S., Galinier, A., Deutscher, J., & Janin, J. (2003). HPr kinase/phosphorylase, the sensor enzyme of catabolite repression in Gram-positive bacteria: Structural aspects of the enzyme and the complex with its protein substrate. *Journal of Bacteriology, 185*(14), 4003–4010. https://doi.org/10.1128/JB.185.14.4003-4010.2003

Noguez, R., Segura, D., Moreno, S., Hernandez, A., Juarez, K., & Espín, G. (2008). Enzyme I^{Ntr}, NPr and IIA^{Ntr} are involved in regulation of the poly-β-hydroxybutyrate biosynthetic genes in *Azotobacter vinelandii*. *Journal of Molecular Microbiology and Biotechnology, 15*(4), 244–254. https://doi.org/10.1159/000108658

Pflüger-Grau, K., & de Lorenzo, V. (2008). Evidence of in vivo cross talk between the nitrogen-related and fructose-related branches of the carbohydrate phosphotransferase system of *Pseudomonas putida*. *Journal of Bacteriology, 190*(9), 3374–3380. https://doi.org/10.1128/JB.02002-07

Pflüger-Grau, K., & Görke, B. (2010). Regulatory roles of the bacterial nitrogen-related phosphotransferase system. *Trends in Microbiology, 18*(5), 205–214. https://doi.org/10.1016/j.tim.2010.03.005

Pinedo, C. A., Bringhurst, R. M., & Gage, D. J. (2008). *Sinorhizobium meliloti* mutants lacking phosphotransferase system enzyme HPr or EIIA are altered in diverse processes, including carbon metabolism, cobalt requirements, and succinoglycan production. *Journal of Bacteriology, 190*(8), 2947–2956. https://doi.org/10.1128/JB.01917-07

Pinedo, C. A., & Gage, D. J. (2009). HPrK regulates succinate-mediated catabolite repression in the Gram-negative symbiont *Sinorhizobium meliloti*. *Journal of Bacteriology, 191*(1), 298–309. https://doi.org/10.1128/JB.01115-08

Postma, P. W., Lengeler, J. W., & Jacobson, G. R. (1993). Phosphoenolpyruvate:carbohydrate phosphotransferase systems of bacteria. *Microbiological Reviews, 57*(3), 543–594. https://doi.org/10.1128/mr.57.3.543-594.1993

Powell, B. S., Court, D. L., Inada, T., Nakamura, Y., Michotey, V., Cui, X., Reizer, A., Saier, M. H., & Reizer, J. (1995). Novel proteins of the phosphotransferase system encoded within the *rpoN* operon of *Escherichia coli*. *Journal of Biological Chemistry, 270*(9), 4822–4839. https://doi.org/10.1074/jbc.270.9.4822

Prell, J., Mulley, G., Haufe, F., White, J. P., Karunakaran, R., Downie, J. A., & Poole, P. S. (2012). The PTS^{Ntr} system globally regulates ATP-dependent transporters in *Rhizobium leguminosarum*. *Molecular Microbiology, 84*(1), 117–129. https://doi.org/10.1111/j.1365-2958.2012.08014.x

Pries, A., Priefert, H., Krüger, N., & Steinbüchel, A. (1991). Identification and characterization of two *Alcaligenes eutrophus* gene loci relevant to the poly(β-hydroxybutyric acid)-leaky phenotype which exhibit homology to *ptsH* and *ptsI* of *Escherichia coli*. *Journal of Bacteriology, 173*(18), 5843–5853. https://doi.org/10.1128/jb.173.18.5843-5853.1991

Quintero-Yanes, A., Léger, L., Collignon, M., Mignon, J., Mayard, A., Michaux, C., & Hallez, R. (2024). Regulation of potassium uptake in *Caulobacter crescentus*. *Journal of Bacteriology, 206*(9), e00107-24. https://doi.org/10.1128/jb.00107-24

Rabus, R., Reizer, J., Paulsen, I., & Saier, M. H. (1999). Enzyme I^{Ntr} from *Escherichia coli*. *Journal of Biological Chemistry, 274*(37), 26185–26191. https://doi.org/10.1074/jbc.274.37.26185

Ramachandran, V. K., East, A. K., Karunakaran, R., Downie, J. A., & Poole, P. S. (2011). Adaptation of *Rhizobium leguminosarum* to pea, alfalfa and sugar beet rhizospheres investigated by comparative transcriptomics. *Genome Biology, 12*(10), R106. https://doi.org/10.1186/gb-2011-12-10-r106

Raskin, D. M., Judson, N., & Mekalanos, J. J. (2007). Regulation of the stringent response is the essential function of the conserved bacterial G protein CgtA in *Vibrio cholerae*. *Proceedings of the National Academy of Sciences of the United States of America, 104*(11), 4636–4641. https://doi.org/10.1073/pnas.0611650104

Reizer, J., Reizer, A., Merrick, M. J., Plunkett, G., Rose, D. J., & Saier, M. H. (1996). Novel phosphotransferase-encoding genes revealed by analysis of the *Escherichia coli* genome: A chimeric gene encoding an enzyme I homologue that possesses a putative sensory transduction domain. *Gene, 181*(1–2), 103–108. https://doi.org/10.1016/S0378-1119(96)00481-7

Ronneau, S., Moussa, S., Barbier, T., Conde-Álvarez, R., Zúñiga-Ripa, A., Moriyón, I., & Letesson, J.-J. (2014). *Brucella*, nitrogen and virulence. *Critical Reviews in Microbiology, 42*(5), 507–525. https://doi.org/10.3109/1040841X.2014.962480

Ronneau, S., Petit, K., De Bolle, X., & Hallez, R. (2016). Phosphotransferase-dependent accumulation of (p)ppGpp in response to glutamine deprivation in *Caulobacter crescentus*. *Nature Communications, 7*(1), 11423. https://doi.org/10.1038/ncomms11423

Ronneau, S., Caballero-Montes, J., Mayard, A., Garcia-Pino, A., & Hallez, R. (2019a). Regulation of (p)ppGpp hydrolysis by a conserved archetypal regulatory domain. *Nucleic Acids Research, 47*(2), 843–854. https://doi.org/10.1093/nar/gky1210

Ronneau, S., & Hallez, R. (2019b). Make and break the alarmone: Regulation of (p)ppGpp synthetase/hydrolase enzymes in bacteria. *FEMS Microbiology Reviews, 43*(4), 389–400. https://doi.org/10.1093/femsre/fuz009

Sánchez-Cañizares, C., Prell, J., Pini, F., Rutten, P., Kraxner, K., Wynands, B., Karunakaran, R., & Poole, P. S. (2020). Global control of bacterial nitrogen and carbon metabolism by a PTS^{Ntr}-regulated switch. *Proceedings of the National Academy of Sciences of the United States of America, 117*(19), 10234–10245. https://doi.org/10.1073/pnas.1917471117

Schulte, J. E., & Goulian, M. (2018). The phosphohistidine phosphatase SixA targets a phosphotransferase system. *mBio, 9*(6), e01666-18. https://doi.org/10.1128/mBio.01666-18

Schulte, J. E., Roggiani, M., Shi, H., Zhu, J., & Goulian, M. (2021). The phosphohistidine phosphatase SixA dephosphorylates the phosphocarrier NPr. *Journal of Biological Chemistry, 296*, 100090. https://doi.org/10.1074/jbc.RA120.015121

Shapiro, B. M. (1969). Glutamine synthetase deadenylylating enzyme system from *Escherichia coli*: Resolution into two components, specific nucleotide stimulation, and cofactor requirements. *Biochemistry, 8*(2), 659–670. https://doi.org/10.1021/bi00830a030

Sharma, R., Shimada, T., Mishra, V. K., Upreti, S., & Sardesai, A. A. (2016). Growth inhibition by external potassium of *Escherichia coli* lacking PtsN (IIA^{Ntr}) is caused by potassium limitation mediated by YcgO. *Journal of Bacteriology, 198*(13), 1868–1882. https://doi.org/10.1128/JB.01029-15

Sheehan, L. M., & Caswell, C. C. (2018). An account of evolutionary specialization: The AbcR small RNAs in the Rhizobiales. *Molecular Microbiology, 107*(1), 24–33. https://doi.org/10.1111/mmi.13869

Sikora, F., Budja, L. V. P., Milojevic, O., Ziemniewicz, A., Dudys, P., & Görke, B. (2024). Multiple regulatory inputs including cell envelope stress orchestrate expression of the *Escherichia coli rpoN* operon. *Molecular Microbiology, 122*(1), 11–28. https://doi.org/10.1111/mmi.15280

Sobrero, P., Schlüter, J.-P., Lanner, U., Schlosser, A., Becker, A., & Valverde, C. (2012). Quantitative proteomic analysis of the Hfq-regulon in *Sinorhizobium meliloti* 2011. *PLOS ONE, 7*(10), e48494. https://doi.org/10.1371/journal.pone.0048494

Sola-Landa, A., Pizarro-Cerdá, J., Grilló, M., Moreno, E., Moriyón, I., Blasco, J., Gorvel, J.-P., & López-Goñi, I. (1998). A two-component regulatory system playing a critical role in plant pathogens and endosymbionts is present in *Brucella abortus* and controls cell invasion and virulence. *Molecular Microbiology, 29*(1), 125–138. https://doi.org/10.1046/j.1365-2958.1998.00913.x

Strickland, M., Stanley, A. M., Wang, G., Botos, I., Schwieters, C. D., Buchanan, S. K., Peterkofsky, A., & Tjandra, N. (2016). Structure of the NPr:EIN^{Ntr} complex: Mechanism for specificity in paralogous phosphotransferase systems. *Structure, 24*(12), 2127–2137. https://doi.org/10.1016/j.str.2016.10.007

Strickland, M., Kale, S., Strub, M.-P., Schwieters, C. D., Liu, J., Peterkofsky, A., & Tjandra, N. (2019). Potential regulatory role of competitive encounter complexes in paralogous phosphotransferase systems. *Journal of Molecular Biology, 431*(12), 2331–2342. https://doi.org/10.1016/j.jmb.2019.04.040

Torres-Quesada, O., Millán, V., Nisa-Martínez, R., Bardou, F., Crespi, M., Toro, N., & Jiménez-Zurdo, J. I. (2013). Independent activity of the homologous small regulatory RNAs AbcR1 and AbcR2 in the legume symbiont *Sinorhizobium meliloti*. *PLOS ONE, 8*(7), e68147. https://doi.org/10.1371/journal.pone.0068147

Torres-Quesada, O., Reinkensmeier, J., Schlüter, J.-P., Robledo, M., Peregrina, A., Giegerich, R., Toro, N., Becker, A., & Jiménez-Zurdo, J. I. (2014). Genome-wide profiling of Hfq-binding RNAs uncovers extensive post-transcriptional rewiring of major stress response and symbiotic regulons in *Sinorhizobium meliloti*. *RNA Biology, 11*(5), 563–579. https://doi.org/10.4161/rna.28239

Udvardi, M., & Poole, P. S. (2013). Transport and metabolism in legume-rhizobia symbioses. *Annual Review of Plant Biology, 64*, 781–805. https://doi.org/10.1146/annurev-arplant-050312-120235

Untiet, V., Karunakaran, R., Krämer, M., Poole, P., Priefer, U., & Prell, J. (2013). ABC transport is inactivated by the PTS^{Ntr} under potassium limitation in *Rhizobium leguminosarum* 3841. *PLOS ONE, 8*(5), e64682. https://doi.org/10.1371/journal.pone.0064682

Varadi, M., Anyango, S., Deshpande, M., Nair, S., Natassia, C., Yordanova, G., Yuan, D., Stroe, O., Wood, G., Laydon, A., Žídek, A., Green, T., Tunyasuvunakool, K., Petersen, S., Jumper, J., Clancy, E., Green, R., Vora, A., Lutfi, M., … Velankar, S. (2022). AlphaFold Protein Structure Database: massively expanding the structural coverage of protein-sequence space with high-accuracy models. *Nucleic Acids Research*, *50*(D1), D439–D444. https://doi.org/10.1093/nar/gkab1061

Varadi, M., Bertoni, D., Magana, P., Paramval, U., Pidruchna, I., Radhakrishnan, M., Tsenkov, M., Nair, S., Mirdita, M., Yeo, J., Kovalevskiy, O., Tunyasuvunakool, K., Laydon, A., Žídek, A., Tomlinson, H., Hariharan, D., Abrahamson, J., Green, T., Jumper, J., … Velankar, S. (2024). AlphaFold Protein Structure Database in 2024: providing structure coverage for over 214 million protein sequences. *Nucleic Acids Research*, *52*(D1), D368–D375. https://doi.org/10.1093/nar/gkad1011

Wang, G., Peterkofsky, A., Keifer, P. A., & Li, X. (2005). NMR characterization of the *Escherichia coli* nitrogen regulatory protein IIA^{Ntr} in solution and interaction with its partner protein, NPr. *Protein Science, 14*(4), 1082–1090. https://doi.org/10.1110/ps.041232805

Williams, M. A., Bouchier, J. M., Mason, A. K., & Brown, P. J. B. (2022). Activation of ChvG–ChvI regulon by cell wall stress confers resistance to β-lactam antibiotics and initiates surface spreading in *Agrobacterium tumefaciens*. *PLOS Genetics, 18*(12), e1010274. https://doi.org/10.1371/journal.pgen.1010274

Yoo, W., Yoon, H., Seok, Y.-J., Lee, C.-R., Lee, H. H., & Ryu, S. (2016). Fine-tuning of amino sugar homeostasis by IIA^{Ntr} in *Salmonella Typhimurium*. *Scientific Reports, 6*, 33055. https://doi.org/10.1038/srep33055

Yurgel, S. N., Rice, J., Mulder, M., & Kahn, M. L. (2010). GlnB/GlnK PII proteins and regulation of the *Sinorhizobium meliloti* Rm1021 nitrogen stress response and symbiotic function. *Journal of Bacteriology, 192*(10), 2473–2481. https://doi.org/10.1128/JB.01657-09

Zhang, Y., Smallbone, L. A., diCenzo, G. C., Morton, R., & Finan, T. M. (2016). Loss of malic enzymes leads to metabolic imbalance and altered levels of trehalose and putrescine in the bacterium *Sinorhizobium meliloti*. *BMC Microbiology, 16*, 163. https://doi.org/10.1186/s12866-016-0780-x

CHAPTER 3

Regulation of central carbon metabolism and storage polymers by PTS^{Ntr} in *Rhizobium leguminosarum*

Olivia Tjahjono[1], Jingkai Wang[2], Evan Turner[1], Jürgen Prell[1], Wei E. Huang[2], Philip Poole[1]#*, Carmen Sánchez-Cañizares[1]#*

[1]Department of Biology, University of Oxford, Oxford, UK

[2]Department of Engineering Science, University of Oxford, UK

Running title: Regulation of carbon metabolism and storage polymers in *Rhizobium leguminosarum*

jointly led this project

* correspondence to philip.poole@biology.ox.ac.uk and carmen.sanchez-canizares@biology.ox.ac.uk

ABSTRACT

Coordination of intracellular carbon and nitrogen levels is essential for optimal bacterial growth, and in rhizobia, for their survival in the soil, root colonisation, and symbiotic interactions with their host plants. Here, we show that the phosphoransferase system PTS^{Ntr}, a global regulator of carbon and nitrogen metabolism, influences the tricarboxylic acid (TCA) cycle and the accumulation of three important carbon storage polymers: glycogen, polyhydroxybutyrate, and exopolysaccharide in *R. leguminosarum*. The unphosphorylated form of the effector protein ManX is essential for the full activation of the TCA cycle dehydrogenase enzymes. Loss of *manX* leads to reduced dehydrogenase activity and overflow carbon to storage polymers. This accumulation of key carbon polymers mimics the phenotype of wild-type cells grown under nitrogen starvation. Furthermore, we demonstrate that tight regulation of carbon metabolism in *R. leguminosarum* is also mediated by the HPr kinase/phosphorylase (HprK) protein. In an *hprK* mutant, loss of NPr Ser48 phosphorylation favours phosphorylation through the histidyl arm and is predicted to increase phosphorylation of downstream PTS^{Ntr} components. When grown on glucose, the *hprK* mutant shows elevated intracellular pyrimidine levels and increased malate dehydrogenase and TCA cycle activity, indicating a shift toward gluconeogenesis. It also overproduces EPS, an effect potentially mediated by crosstalk between phosphorylated PtsN and the ChvI/ChvG system. These data suggest that HprK exerts pleiotropic regulatory effects on processes regulated by PTS^{Ntr}, influencing central metabolism while also repressing EPS production, likely by promoting the unphosphorylated state of PtsN.

Word count: 237

INTRODUCTION

Biological nitrogen fixation (BNF) is essential for sustainable agriculture by supplying bioavailable nitrogen, thereby reducing the reliance on synthetic fertilisers (1, 2). The symbiotic bacteria that carry out this process must persist as free-living cells in the soil and as intracellular growth-arrested bacteroids within their legume hosts (3, 4). Each stage of this complex lifecycle is intricately linked to cellular energy homeostasis, as well as carbon and nitrogen metabolism (5, 6). A tight regulation of bacterial carbon and nitrogen metabolism is necessary to adapt to diverse environments while meeting energy demands and supporting growth across different lifestyles.

Among the major systems coordinating nitrogen and carbon metabolisms in Alphaproteobacteria (α-proteobacteria) are the Ntr/PII pathway and the nitrogen-related phosphotransferase system (PTS^{Ntr}). The Ntr/PII system mediates both post-translational and transcriptional effects in response to nitrogen availability, which is sensed by PII proteins through the [glutamine]:[α-ketoglutarate] ratio (7–11). As a key tricarboxylic acid (TCA) cycle intermediate, α-ketoglutarate is converted to glutamine through the GS-GOGAT pathway (11). This ratio therefore signals the relative state of both carbon and nitrogen metabolism. A low [glutamine]:[α-ketoglutarate] ratio, signalling for nitrogen deficiency, leads to upregulation of nitrogen and amino acid uptake in the free-living state (12, 13). In contrast, a high [glutamine]:[α-ketoglutarate] ratio is indicative of nitrogen sufficiency.

Another regulatory system important in sensing carbon and nitrogen balance, the nitrogen-related phosphotransferase system (PTS^{Ntr}), is primarily a post-translational signalling system that regulates various cell functions via protein-protein interactions

(14–17). It is a three-step phosphorelay cascade in which PtsP (EI^{Ntr}) autophosphorylates using phosphoenolpyruvate (PEP) as the phosphate donor, transfers the phosphate to Npr (PtsO), and ultimately to output regulators PtsN ($EIIA^{Ntr}$) and ManX ($EIIA^{Man}$), whose phosphorylation states regulate downstream targets. PtsP has a GAF sensing domain that detects changes in internal nitrogen availability, with autophosphorylation being inhibited by glutamine-binding in Alphaproteobacteria (17). The function of output regulators, PtsN and ManX, depends on their phosphorylation states: unphosphorylated ManX has been shown to be necessary for full activation of the tricarboxylic acid (TCA) cycle (17–19), while phosphorylated PtsN activates ATP-binding cassette (ABC) transporters and interacts with the two-component regulatory system ChvI/ChvG controlling exopolysaccharide (EPS) secretion (17, 20, 21).

In Alphaproteobacteria, PTS^{Ntr} is additionally regulated by a bifunctional HPr kinase/phosphorylase (HprK/P) (19, 22). This enzyme phosphorylates Npr at a conserved serine (Ser) residue, which in turn reduces subsequent histidine phosphorylation of Npr by PtsP. Although homologous to the Firmicutes HprK/P, which phosphorylates HPr at Ser46 rather than NPr, the Alphaproteobacterial HprK/P lacks the N-terminal phosphate-binding domain characteristic of the Firmicutes protein (22–24). Direct evidence for HprK/P activity in Alphaproteobacteria comes from *Brucella melitensis*, where this enzyme phosphorylates NPr on Ser61 in an ATP-dependent reaction. The kinase is inhibited by inorganic phosphate and stimulated by fructose-1,6-bisphosphate (FBP) (19). In *Sinorhizobium meliloti*, deletion of *hprK* causes a severe growth defect and significantly enhances succinate-mediated catabolite repression (22). Similarly, our previous work in *R. leguminosarum* has shown that *hprK* mutants display severe growth

86 defects, suggesting that HprK/P is a potential PTS^{Ntr} component involved in carbon
87 regulation (17).

88 Besides the *hprK* mutant, PTS^{Ntr} mutants such as *ptsP, npr*, and *manX* mutants exhibited
89 growth defects. For reference, the mean generation times of the PTS^{Ntr} mutant strains, as
90 well as several phosphomimetic and nonphosphorylatable variants of *R. leguminosarum*
91 described in our previous study (17), are included in **Table S1** with newly plotted growth
92 curves shown in **Figure S1**. The PTS^{Ntr} regulatory interactions and associated cellular
93 functions in *R. leguminosarum* bv *viciae* 3841 (Rlv3841) are summarised in **Figure 1.A**,
94 while an overview of carbon metabolism in this bacterium, highlighting features relevant
95 to this study, is shown in **Figure 1.B**.

96 Although PTS^{Ntr} has been implicated in coordinating carbon metabolism relative to
97 nitrogen availability in Alphaproteobacteria, the physiological roles and regulatory logic
98 of its individual components remain incompletely understood. Nevertheless, direct
99 interaction of ManX with key enzymes has been previously demonstrated. In *B.*
100 *melitensis,* Yeast 2-hybrid (Y2H) assays showed interaction of ManX and SucA, a
101 component of the 2-oxoglutarate dehydrogenase (α-KGDH) complex (19). In
102 *Pseudomonas putida*, the sole EIIA component of PTS^{Ntr} (PtsN) binds to pyruvate
103 dehydrogenase (PDH), shown by co-immunoprecipitation and mass-spectrometry (18).
104 However, similar interactions with central metabolic enzymes have not been shown in
105 other species, including *R. leguminosarum*.

106 A link between PTS^{Ntr} and internal carbon storage has been proposed through
107 mechanisms that are not yet understood (17, 20–22, 27–30). In *S. meliloti*, the promoter
108 region of *manX* contains putative consensus binding sites for PhaR

(polyhydroxybutyrate, PHB-binding transcriptional regulator), and its expression increased under PHB-producing conditions (30). Polyhydroxyalkanoates (PHA) accumulate in the *ptsN* mutant of *P. putida* (28), while phosphorylated PtsN (PtsN~P) of *R. leguminosarum* is shown to interact with the ChvI/ChvG two-component system to regulate the synthesis of the extracellular carbon-polymer exopolysaccharide (EPS) (17). This function is conserved in *S. meliloti*, where PtsN interacts with the homologous system ChvI/ExoS to modulate the production of the surface polymers galactoglucan and succinoglycan (20, 21). Additionally, as shown in *S. meliloti* (22, 29) and more recently in *R. leguminosarum* (17), the *hprK* mutant also accumulates EPS when grown on nitrogen-excess media.

Thus, in this work, we investigate how PTS^{Ntr} contributes to the allocation of carbon between central metabolism and storage in *R. leguminosarum*. Using biochemical assays complemented with Raman spectroscopy, we characterise patterns of polymer accumulation in the wild-type under contrasting nitrogen conditions. We then assess the physiological consequences of disrupting the PTS^{Ntr} components ManX, PtsN, and HprK, by integrating data on central metabolic enzyme activities and polymer accumulation with previously characterised growth phenotypes.

A

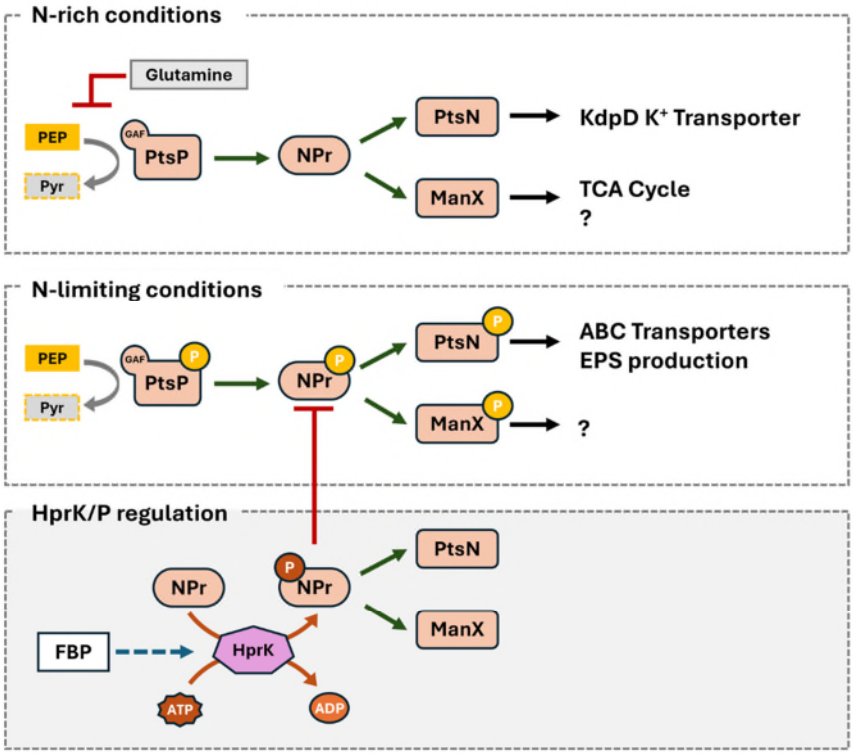
N-rich conditions
Glutamine
PEP
Pyr
GAF
PtsP
NPr
PtsN
KdpD K⁺ Transporter
ManX
TCA Cycle
?
N-limiting conditions
PEP
Pyr
GAF
PtsP
P
NPr
PtsN
ABC Transporters
EPS production
ManX
?
HprK/P regulation
NPr
NPr
PtsN
ManX
FBP
HprK
ATP
ADP

B

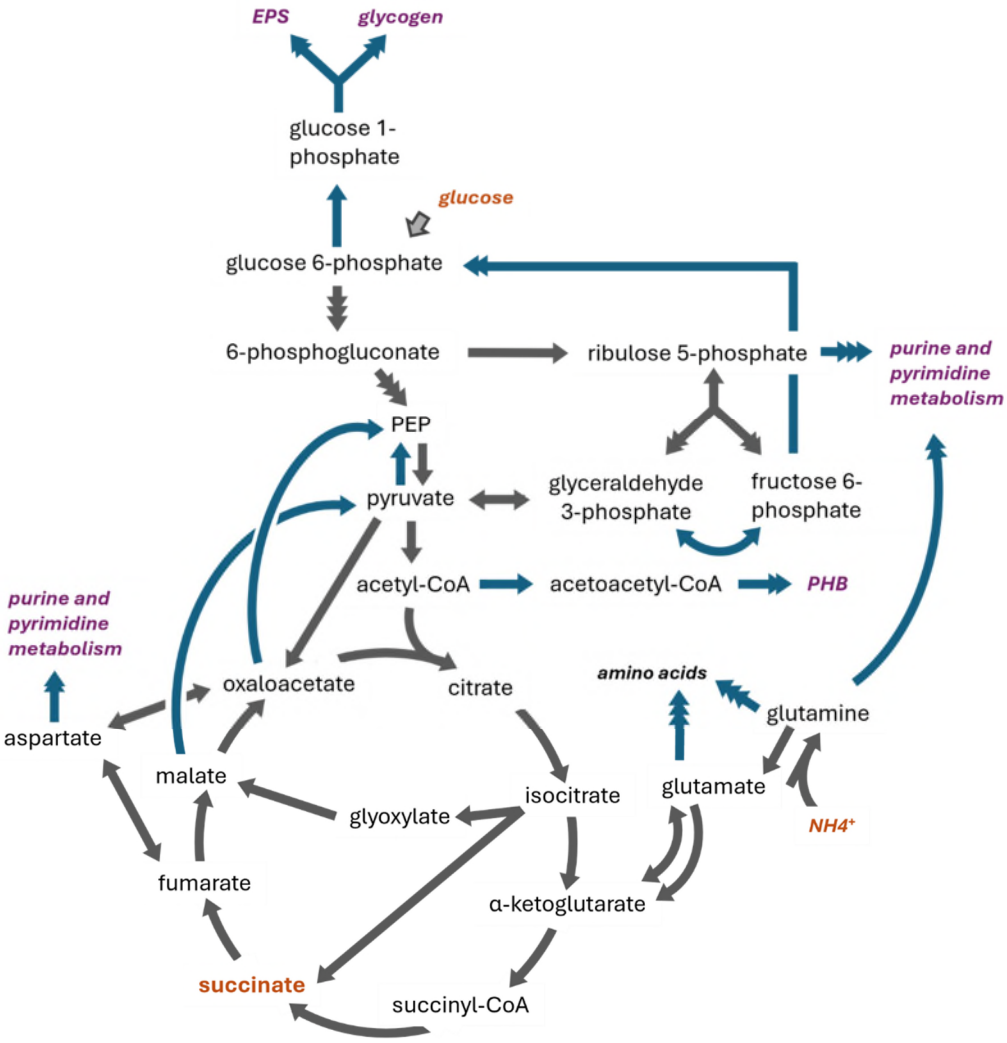
EPS
glycogen
glucose 1-phosphate
glucose
glucose 6-phosphate
6-phosphogluconate
ribulose 5-phosphate
purine and pyrimidine metabolism
PEP
pyruvate
glyceraldehyde 3-phosphate
fructose 6-phosphate
acetyl-CoA
acetoacetyl-CoA
PHB
purine and pyrimidine metabolism
oxaloacetate
citrate
amino acids
glutamine
aspartate
malate
isocitrate
glutamate
glyoxylate
NH4+
fumarate
α-ketoglutarate
succinate
succinyl-CoA

Figure 1. PTS^{Ntr} regulatory system and carbon metabolism in *R. leguminosarum*. (A) Schematic diagram of the current understanding of PTS^{Ntr} regulation. Under N-rich conditions, glutamine inhibits PtsP autophosphorylation. In contrast, under N-limiting conditions, autophosphorylated PtsP transfers its phosphate to NPr on His17 and downstream effectors PtsN and ManX. The phosphorylation state of NPr is additionally modulated by an alternative serine phosphorylation (Ser48) by HprK. Yellow circles indicate histidine phosphorylation, while red circles indicate serine phosphorylation. (B) Overview of the carbon metabolism pathways in Rlv3841. Blue arrows indicate anabolic metabolic pathways. Orange labels are key carbon sources (glucose and succinate) and the nitrogen source (ammonia) used in this study, while purple labels indicate polymers (EPS, glycogen, and PHB) and other compounds (pyrimidines) quantified in this work. Only selected reactions are shown, based on information from (25, 26).

RESULTS

ManX modulates the activity of TCA cycle dehydrogenases

Reduced malate dehydrogenase (MDH) and 2-oxoglutarate dehydrogenase (α-KDH) activities shown previously in the Rlv3841 *manX* mutant background indicate that ManX is essential for the complete activation of the TCA cycle (17). To further elucidate the role of ManX in TCA cycle activity, we measured activities of TCA cycle enzymes (**Figure 2.A**). In addition to confirming reduced activity of MDH and α-KDH, we examined additional enzymes: fumarase hydratase (FH), citrate synthase (CS), isocitrate dehydrogenase (IDH), as well as pyruvate dehydrogenase (PDH) that catalyses the intermediate reaction linking glycolysis to the TCA cycle (**Figure 2.B)**. Enzyme activity assays were performed on crude extracts of Rlv3841 wild-type and *manX* mutant strains. The reaction kinetics were assessed by monitoring substrate consumption over time. All bacterial strains were grown in UMS minimal medium supplemented with 10 mM glucose and 10 mM NH_4Cl, which corresponds to nitrogen (N)-excess conditions.

The specific activities of CS and fumarase (**Figure 2.B.b and 2.B.h**) were not affected in the *manX* mutant. However, the activity of MDH decreased by ~40%, α-KDH by ~54%, IDH by ~17%, and PDH by ~40% (**Figure 2.B.i, 2.B.e, 2.B.c, and 2.B.a,** respectively). The *manX**H9A mutant (strain OPS1012), which mimics the non-phosphorylated state of ManX (His9 replaced by an alanine residue), exhibited wild-type growth across diverse carbon sources and wild-type levels of oxygen (O_2) consumption rates (17). We therefore assayed MDH activity and found that it remains unchanged in the *manX**H9A mutant relative to wild-type (**Figure 2.B.i**). Collectively, our results suggest that ManX modulates the dehydrogenase enzymes of the TCA cycle, and its non-phosphorylated state is

sufficient for activation of the TCA cycle's dehydrogenases. In the absence of ManX regulation, TCA dehydrogenase enzymes exhibit reduced activity.

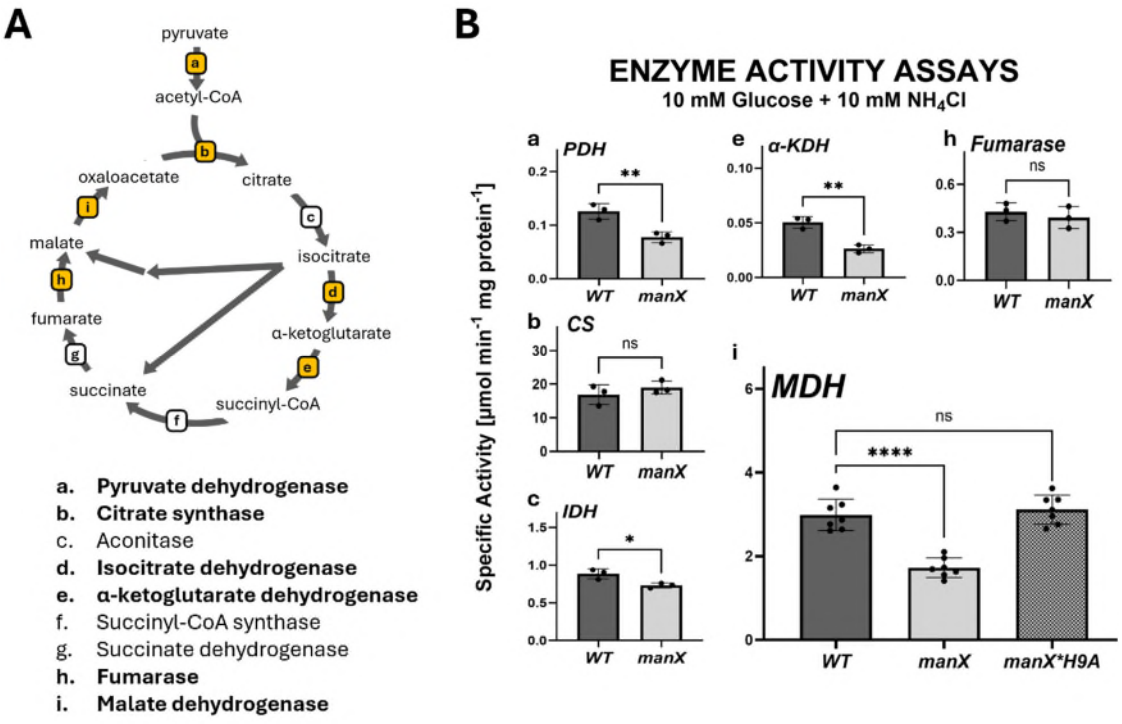

Figure 2. Loss of ManX is associated with reduced activity of TCA cycle dehydrogenase enzymes. (A) Diagram of the TCA cycle and its enzymes, with the assayed enzymes being highlighted in yellow boxes: (A.a) pyruvate dehydrogenase, (A.b) citrate synthase (CS), (A.d) isocitrate dehydrogenase (IDH), (A.e) α-ketoglutarate dehydrogenase (α-KDH), (A.h) fumarase, and (A.i) malate dehydrogenase (MDH). (B) Enzyme activity assays of those six TCA cycle enzymes were performed using cell lysates of wild-type, *manX* mutant, and *manX**H9A strain. Assays were normalised to total protein content. The *manX* mutant showed significantly reduced activity of dehydrogenase enzymes (PDH, MDH, α-KDH, IDH), but not fumarase and CS. (B.i) The MDH activity of the *manX**H9A strain recovers to wild-type level, suggesting that the non-phosphorylated state of ManX is required for activation of the TCA cycle dehydrogenase enzymes to wild-type level. Data are averages (±SEM) from at least three independent cultures. Statistical significances were assessed by one-way ANOVA (for MDH) or Student's t-test (other enzymes), with asterisks indicating the following level of significance: **** $P \leq 0.0001$, ** $P \leq 0.01$, * $P \leq 0.05$, and ns, not significant.

The *hprK* mutant shows reduced oxidative metabolism

As an aerobe, *R. leguminosarum* oxidises TCA cycle intermediates to facilitate growth (31). Therefore, O_2 consumption can serve as a proxy of aerobic respiratory activity and oxidative metabolism in free-living liquid cultures. Building from the previous observation that the Rlv3841 *hprK* mutant exhibits lower growth rates in various carbon sources (17), we now show that this growth defect is accompanied by reduced O_2 consumption rate when the *hprK* mutant is grown under N-excess conditions (10 mM NH_4Cl), supplemented with either 10 mM glucose or 20 mM succinate as carbon sources (**Figure 3.A)**. As seen in the wild-type, the O_2 consumption rate for the *hprK* mutant is higher when succinate is used as the sole carbon source. This can be explained by the fact that, unlike glucose, which is catabolised via the Entner-Doudoroff (ED) pathway, succinate feeds directly into the TCA cycle. Previous studies have also confirmed that supplying succinate or other dicarboxylates leads to increased O_2 demand and a highly reduced redox state (5, 32). Under N-limiting conditions (**Figure S2**), the O_2 consumption is low in the wild-type and *hprK* mutant.

MDH activity is increased in the *hprK* mutant

To determine whether the reduced O_2 consumption observed in the *hprK* mutant could be associated with downregulated TCA cycle activity, we measured the *in vitro* enzyme activity of MDH and α-KDH (**Figure 3.B**). Paradoxically, despite the overall slowdown of the TCA cycle, MDH activities were significantly upregulated in the *hprK* mutant, while α-KDH activity was at the same rate as that of wild-type. This regulation exerted by HprK on the TCA cycle appears to occur at the post-translational level, potentially by modulating the PTS^{Ntr} activity and consequent changes in the accumulation of phosphorylated ManX,

or via other direct regulation of carbon metabolic processes. This is supported by the absence of changes in the promoter activities of *mdh* and *sucA* (coding for Enzyme 1 component of α-KDH) in the *hprK* mutant (**Figure 3.C**). The promoter activities of both genes remain unchanged and comparable to those of the wild-type, indicating once again that PTS^{Ntr} regulation occurs at the post-translational level.

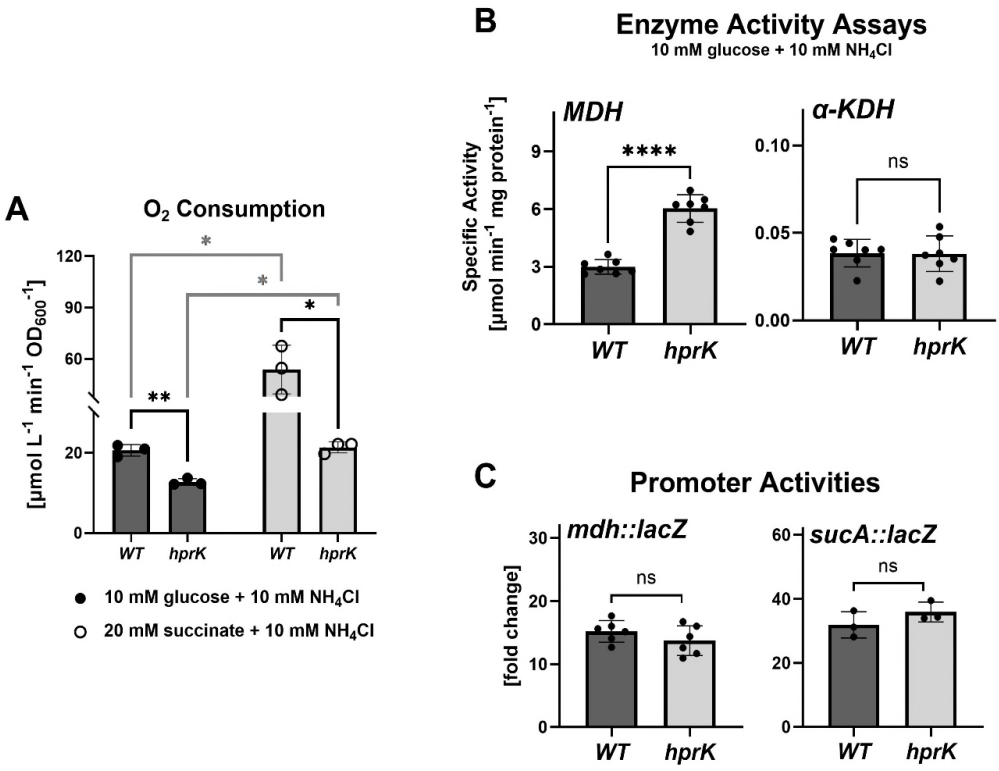

Figure 3. The TCA cycle is altered in the *hprK* mutant despite upregulation of MDH activity at the post-transcriptional level. (A) The TCA cycle activity of the *hprK* mutant, assessed indirectly by O_2 consumption rates, is reduced relative to wild-type. The strains were grown in liquid UMS cultures supplemented with 10 mM NH_4Cl as nitrogen source and either 10 mM glucose (dark grey bars) or 20 mM succinate as carbon source (light grey bars). (B) Enzyme activity assays of malate dehydrogenase (MDH) and α-KDH were performed in cell lysates of wild-type and *hprK* mutant grown in UMS cultures with 10 mM glucose and 10 mM NH_4Cl and normalised to total protein contents. Despite reduced O_2 consumption, *hprK* showed an increase in the activity of MDH. (C) Promoter activities for the genes encoding *mdh* and *sucA* were measured using the *lacZ* reporter assay on

cultures grown on UMS with 10 mM glucose and 10 mM NH_4Cl. Values are shown as the fold change relative to the strain-specific background rate of the promoter-less *lacZ* plasmid. Data are averages (±SEM) from at least three independent cultures. Statistical significances were assessed by Student's t-test, with asterisks indicating the following level of significance: **** $P \leq 0.0001$, ** $P \leq 0.01$, * $P \leq 0.05$, and ns, not significant. In panel A, black asterisks are comparisons between strains grown in the same conditions, whereas grey asterisks indicate comparisons of the same strain grown under different carbon sources, done as a separate T-test.

The accumulation of extracellular and intracellular polymers is affected by PTS^{Ntr} regulation

As PTS^{Ntr} influences TCA cycle enzymes, the disruption of PTS^{Ntr} regulation could lead to either overaccumulation or depletion of carbon storage polymers, depending on nutrient availability. Indeed, previous evidence indicated that PTS^{Ntr} regulates carbon storage in various gram-negative bacterial species (17, 20–22, 28, 29). Given the essential role of ManX in sustaining the activity of TCA cycle dehydrogenases, PTS^{Ntr} kinases, particularly ManX, PtsN, and HprK, together may function as a regulatory node linking central carbon metabolism and carbon storage. To investigate this possibility, we performed chemical assays to quantify and compare the accumulation pattern of carbon polymers in wild-type and PTS^{Ntr} mutant strains. EPS and two important internal carbon storage polymers in rhizobia, PHB and glycogen (**Figure 4.A-C**), were measured on cultures grown in UMS supplemented with 10 mM glucose under two different nitrogen regimes: N-excess (10 mM NH_4Cl) and N-limiting (0.5 mM NH_4Cl). Additionally, the PHB content was also quantified in cultures grown in UMS with 10 mM succinate as a carbon source, as we reasoned that PHB storage might be different when the cells are grown on sugars or on an organic acid that feeds directly into the TCA cycle (**Figure 4.D**).

Our results show that when carbon (glucose) was in surplus due to N-limitation (0.5 mM NH_4Cl), Rlv3841 wild-type cells allocated carbon into internal storage polymers (PHB and glycogen) and extracellular polymers (EPS) (**Figure 4.A-C**). Unlike wild-type, the *manX* mutant constitutively accumulates a significant amount of PHB, glycogen, and EPS regardless of nitrogen availability (**Figure 4.A-C**). This accumulation was not observed in *manX**H9A, which retains a functional TCA cycle in contrast to the *manX* mutant and restores carbon storage patterns to wild-type levels (**Figure 4.A-C**), indicating that it is the non-phosphorylated version of ManX that acts on central metabolism. Intracellular polymer concentrations were not altered in the *ptsN1N2* mutant, with PHB (**Figure 4.C**) and glycogen (**Figure 4.B**) levels comparable to those of wild-type. As previously reported, *ptsN1N2* produces less EPS compared to wild-type (**Figure 4.A**) (17). The *ptsN**H66D mutant (strain OPS1104), which is a phosphomimetic version of PtsN (His66 replaced by a glutamate residue), enhances EPS production beyond wild-type levels, whereas *ptsN**H66A (strain OPS1102), a permanently non-phosphorylated PtsN, exhibited reduced EPS comparable to the original *ptsN1N2* mutant (**Figure 4.A**). These results suggest that PtsN primarily influences EPS synthesis, and its phosphorylated form (PtsN~P) induces the production.

This was further supported by complementation assays of an *npr* mutant with NPr variants containing amino acid substitutions at the phosphorylation sites (His17 and Ser48). The original *npr* mutant showed dry colony morphology when grown on agar plates, indicative of reduced EPS production (**Figure S5.B**) (17). The same phenotype was observed when the *npr* mutant was complemented with an NPr version carrying His17-to-alanine (H17A) (**Figure S5.D, H**) or the double mutation NPr His17A and Ser48-to-

alanine (S48A) (**Figure S5. F, J**). In contrast, complementation with Npr carrying a S48A mutation, which mimics phosphorylation by HprK, resulted in a very wet colony morphology (**Figure S5. E, I**), in agreement with the *hprK* mutant EPS phenotype (**Figure 4.A**). Together, these results suggest that HprK-mediated Ser phosphorylation of NPr inhibits EPS production, whereas His-dependent phosphotransfer via NPr is required for EPS induction. These findings also indicate that His17 is the Npr dominant phosphorylation site and are therefore consistent with a model in which EPS production is modulated by the activity of phosphorylated PtsN.

We also observed a different PHB accumulation pattern when succinate was used as the carbon source. Wild-type cells grown in succinate accumulated less PHB when nitrogen was limited, compared to when glucose was the carbon source. The *manX* mutant still accumulates PHB regardless of the carbon sources and nitrogen status. Strikingly, the *hprK* mutant, which did not accumulate PHB when grown in glucose as the sole carbon source (**Figure 4.C**), built up PHB when grown on succinate under N-limiting conditions (**Figure 4.D**).

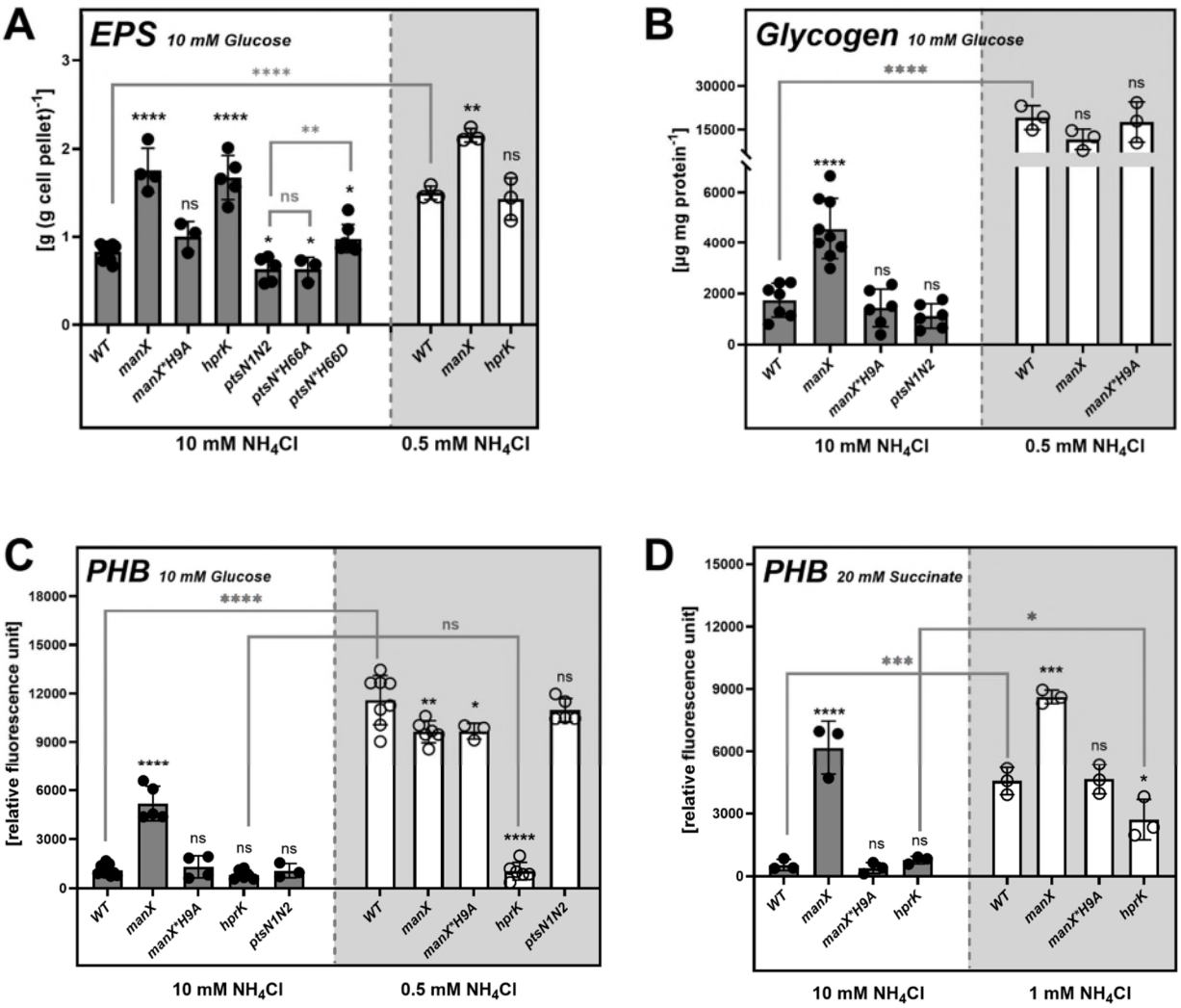

Figure 4. The accumulation patterns of storage polymers are impacted in PTS^{Ntr} mutants under differing nitrogen availability and carbon sources. Quantification of three main carbon storage compounds in *R. leguminosarum*: (A) exopolysaccharide, (B) glycogen, (C) and (D) polyhydroxybutyrate. The strains were grown in liquid UMS cultures supplemented with either 10 mM glucose (A-C) or 20 mM succinate (D), and with 10 mM NH_4Cl (dark grey bars) or 0.5 mM NH_4Cl (white bars). Data are averages (±SEM) from at least three independent cultures. Statistical significances were assessed by two independent one-way ANOVAs (for N-rich condition and for N-poor condition separately), with asterisks indicating the following level of significance: **** $P \leq 0.0001$, *** $P \leq 0.001$, ** $P \leq 0.01$, * $P \leq 0.05$, and ns, not significant. Black asterisks are comparisons between strains grown in the same conditions, whereas grey asterisks indicate Student's t-test comparisons between the specific strains being compared, as indicated by the connecting lines.

Raman spectral analysis reveals altered biomolecule accumulation in PTS^{Ntr} mutant strains

The results from chemical assays were further validated using single-cell Raman spectroscopy (SCRS), a non-invasive technique to monitor intracellular metabolites in their native cellular context based on their vibrational fingerprints (33). To do that, we first applied different principal component analysis (PCA) combinations to the obtained spectra, classified the spectra based on the loadings of individual Raman shifts, and then spotted several biologically meaningful Raman bands. Previous work in Rlv3841 had previously identified a peak at 1735 cm^{-1} as a biomarker for PHB, while peaks at 850 cm^{-1} and 1050 cm^{-1} for glycogen (34). Calculation of the Raman spectra intensities of selected biomolecules provided further insights into the allocation of macromolecules under different mutants. In addition to quantifying peaks corresponding to glycogen and PHB as discussed in the previous section, we also assessed spectral regions associated with pyrimidine (765-795 cm^{-1}) (35, 36) and amides (1645-1676 cm^{-1}) (35–37). 10 mM glucose was used as the carbon source for growing all cultures, and 10 mM NH_4Cl as the nitrogen source for wild-type control, *manX* and *hprK* mutants. Additionally, wild-type was also grown under N-limiting conditions in UMS with 0.5 mM of NH_4Cl for comparison across different nitrogen regimes. As expected, Rlv3841 wild-type cells grown under N-limiting conditions accumulated internal polymers (PHB and glycogen), reflecting an imbalance of the ability of cells to metabolise available carbon sources (**Figure 5.A-F**). This was accompanied by reduced amides and pyrimidines, as nitrogen scarcity limits the synthesis of amino acids and nucleotides (38). Even when nitrogen was available, the *manX* mutant built up glycogen and PHB, while also having reduced levels of amides and DNAs that mimicked wild-type grown under N-limitation. In contrast to the *manX* mutant,

the *hprK* mutant accumulated nucleotides, while its levels of PHB, glycogen, and amides were those of wild-type grown under N-excess conditions (**Figure 5.A-F**).

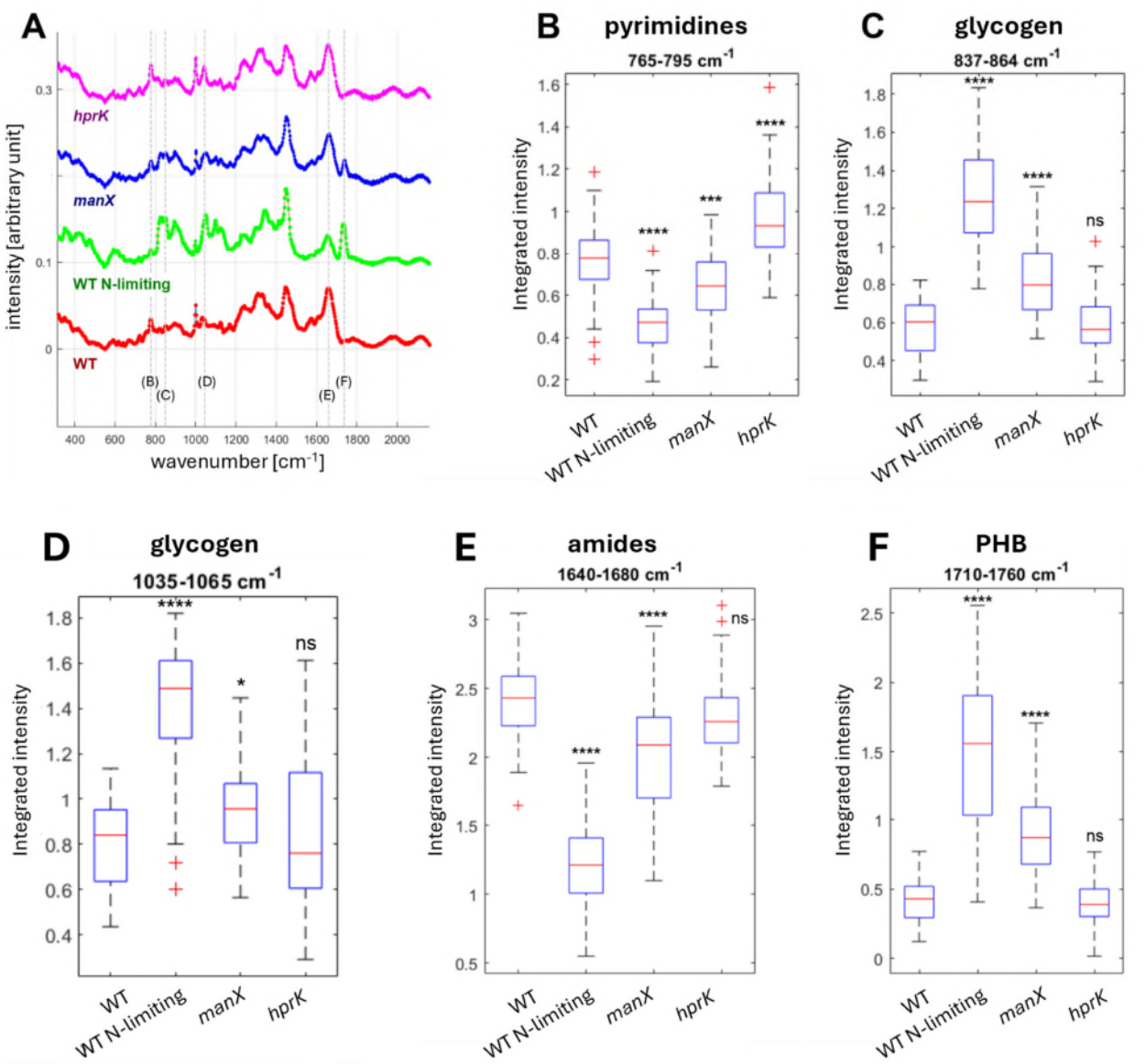

Figure 5. Quantification of biomolecular features using integrated band intensities of Single-cell Raman Spectra. (A) Averaged single-cell Raman spectra of wild-type (red), *manX* (blue), and *hprK* (magenta) grown under N-excess conditions (10 mM glucose + 10 mM NH_4Cl), and wild-type under N-limiting conditions (green; 10 mM glucose +0.5 mM NH_4Cl). (B-F) Box plots of integrated areas under selected Raman bands for quantitative analysis. Integrated intensity of each band was calculated after baseline correction, with bands' identity as such: 765-795 cm^{-1} (pyrimidine ring breathing), 837-864 cm^{-1}

(glycogen), 1035-1065 cm^{-1} (glycogen), 1640-1680 cm^{-1} (amides), and 1710-1760 cm^{-1} (PHB). Data are averages (±SEM) from at least 60 replicates, and red crosses are outliers. Statistical significances were assessed by one-way ANOVA, with asterisks indicating the following level of significance: **** $P \leq 0.0001$, *** $P \leq 0.001$, * $P \leq 0.05$, and ns, not significant.

Differential expression of *pckR* and its target genes in the *hprK* mutant is consistent with gluconeogenic bias under glycolytic conditions

The combined phenotypes of growth defects on both glucose and succinate, elevated MDH activity, and abnormal accumulation of EPS and PHB in the *hprK* mutant suggested a shift in the balance between the Entner-Doudoroff (ED)/glycolytic pathways and the TCA cycle/gluconeogenesis towards gluconeogenesis. Because the LacI-type transcriptional regulator PckR (PEP carboxykinase regulator) is implicated in this metabolic control in rhizobia (39, 40), we measured *pckR* and selected PckR target genes during growth on glucose and succinate to assess whether the *hprK* mutant phenotypes were consistent with altered *pckR* expression. The PckR target genes analysed included *pckA* and *fbaB* (encoding phosphoenolpyruvate carboxykinase and fructose-bisphosphate aldolase, respectively) on the gluconeogenic side and *zwf* and *pgl* (encoding glucose-6-phosphate dehydrogenase and 6-phosphogluconolactonase) on the ED side.

When grown on glucose, the *hprK* mutant showed increased expression of gluconeogenic genes, with *pckA* at approximately 3.7-fold and *fbaB* at approximately 2-fold relative to wild-type. In contrast, expression of the ED pathway gene *zwf* was slightly reduced, while no significant difference was observed for *pgl*. During growth on succinate, the expression levels of *pckA*, *fbaB*, *zwf* and *pgl* of the *hprK* mutant were

comparable to those of wild-type, where *pckA* and *fbaB* were induced approximately 19-fold and 120-fold, respectively. The transcript level of *pckR* was approximately twofold lower in the *hprK* mutant during growth on glucose and was similar to wild-type during growth on succinate.

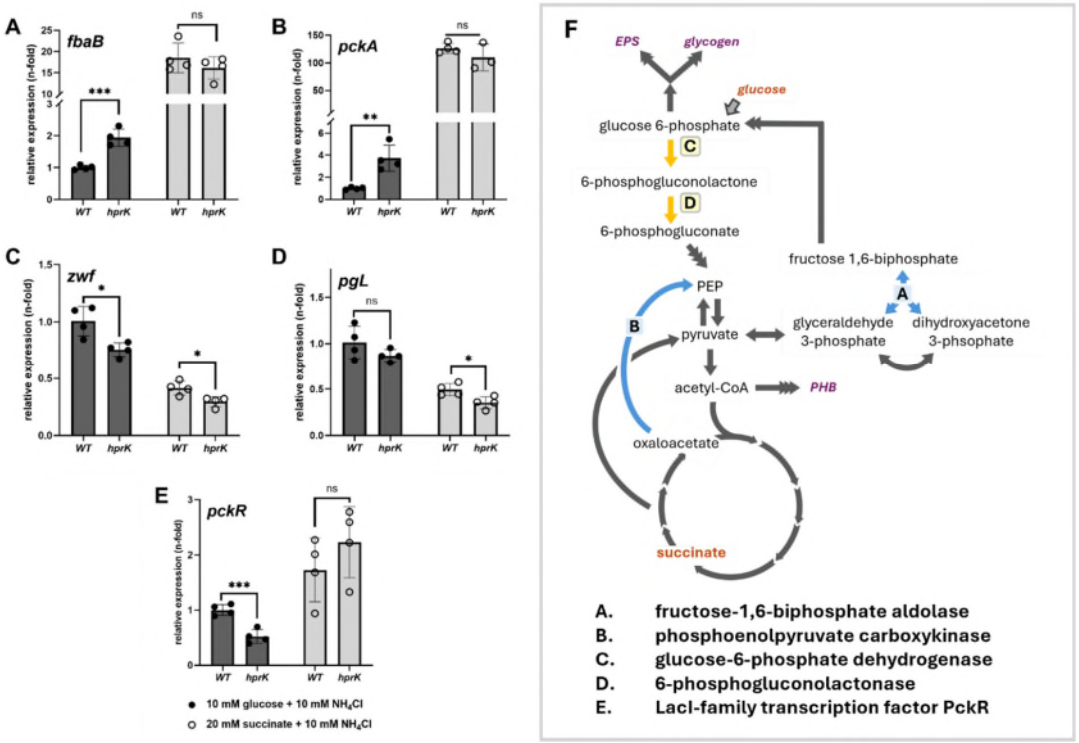

Figure 6. qPCR analysis of *pckR* and its target genes in the *hprK* mutant compared to wild-type. Relative transcript level of gluconeogenesis genes (A) *fbaB* and (B) *pckA*, the ED pathway genes (C) *zwf* and (D) *pgl*, and their transcriptional regulator (E) *pckR* are measured using quantitative PCR (qPCR). (F) Schematic representation of central carbon metabolism indicating the positions of the analysed enzymes within gluconeogenesis (A, B; blue) and glycolysis (C, D; yellow). Carbon storage compounds measured in this work are shown in purple, and carbon sources are marked in orange. Only selected intermediates are shown. The strains were grown in liquid UMS cultures supplemented with 10 mM NH_4Cl as the nitrogen source and either 10 mM glucose (dark grey bars) or 20 mM succinate (light grey bars) as the carbon source. Data are averages (±SEM) from at least three independent cultures. Statistical significances were assessed by Student's t-test, with asterisks indicating the following level of significance: *** $P \leq 0.001$, ** $P \leq 0.01$, * $P \leq 0.05$, and ns, not significant.

DISCUSSION

The regulation of carbon and nitrogen metabolism in symbiotic rhizobia is critically important for the success and efficiency of symbiotic nitrogen fixation (17). In Alphaproteobacteria, PTS^{Ntr} regulation ensures a balanced central metabolic activity and supply of energy based on nitrogen availability. Rhizobia are known to accumulate carbon polymers as energy reserves and as a mechanism to maintain redox balance during nitrogen starvation (41, 42). In line with this, we observed accumulation of two key internal polymers, PHB and glycogen, under such conditions in free-living *R. leguminosarum*. EPS production, which shares sugar biosynthetic precursors with glycogen, was also elevated. Additionally, a decreased level of pyrimidines was also detected, and this is consistent with data from *E. coli* and *S. cerevisiae*, where growth under nitrogen or carbon limitation similarly leads to diminished nucleotide abundance (38).

In *R. leguminosarum*, ManX and PtsN are the downstream effectors of the PTS^{Ntr} regulatory system, whose activity is modulated by the upstream sensor component PtsP and the relay protein NPr (17, 29). These regulators integrate environmental cues, particularly nitrogen and carbon availability, to control downstream metabolic outputs. In this study, we demonstrate that the absence of ManX leads to reduced activity of TCA cycle dehydrogenases, followed by the accumulation of key intracellular carbon-storage polymers (glycogen and PHB) and the extracellular carbon polymer EPS. The *manX* mutant also exhibited reduced levels of amides and pyrimidines, which resemble N-starved wild-type rhizobia (18).

394 The phenotype observed in the *manX* mutant when grown on sugar is likely caused by
395 overflow carbon metabolism. With the TCA cycle flux reduced, while sugar intake
396 remains relatively high, carbon is diverted into biosynthetic pathways for carbon
397 (glycogen and EPS) and energy (PHB) reserve polymers. Indeed, the accumulation of PHB
398 and lipids has been reported across diverse bacterial species as a mechanism to buffer
399 excess energy and reductants, which typically occurs under nutrient imbalance (43–45),
400 as observed in the N-starved wild-type strain.

401 The reduction in amides and pyrimidines observed in the *manX* mutant can be attributed
402 to similar underlying regulatory mechanisms. The overall slowdown of the TCA cycle
403 likely reduces the availability of intermediates such as 2-oxoglutarate, which is required
404 for glutamate synthesis and ammonia assimilation. The limited fumarate or oxaloacetate
405 availability contributes to less aspartate, which serves as a carbon backbone in *de novo*
406 pyrimidine synthesis. Overall, these results support previous conjectures (17, 29) that
407 ManX serves as the branch of the PTS^{Ntr} effector that is involved in carbon regulation.

408 The decrease in enzymatic activities observed in the *manX* mutant is restricted to
409 dehydrogenases linked to central metabolism. Because our enzymatic assays were done
410 *in vitro* under substrate-saturating conditions, the reduced dehydrogenase activities are
411 unlikely to result from substrate and cofactor limitation, or from differences in controlled
412 assay parameters such as pH and temperature. However, the observed differences may
413 arise from variations in enzyme abundance, post-translational regulation, or other
414 factors affecting enzyme function in cell extracts.

415 As a potential explanation for reduced TCA cycle dehydrogenases activities, we
416 assessed whether the expression of genes encoding TCA enzymes was altered.

417 However, transcript levels of malate and 2-oxoglutarate dehydrogenase components
418 remain unchanged in the *manX* mutant (17), further excluding transcriptional regulation
419 as the primary cause. A strain with a permanently non-phosphorylated ManX version
420 (ManX*H9A) restored growth, enzyme activities, and polymer accumulation to the wild-
421 type level, suggesting that ManX unlikely exerts its regulation through phosphorylation.
422 Taken together, these findings suggest that ManX predominantly influences
423 dehydrogenase activities at the post-translational level, potentially through protein-
424 protein interactions. This interpretation is consistent with prior evidence of ManX and α-
425 KDH (E1 component SucA) direct interaction in *B. melitensis* when assayed using Y2H
426 (19), and $EIIA^{Ntr}$ (PtsN homolog) with the E1 subunit of PDH in *P. putida* by co-
427 immunoprecipitation (18). However, our attempts to test these interactions by
428 expressing ManX protein from Rlv3841 and by using bacterial two-hybrid assays (BACTH)
429 in *E. coli* were inconclusive. ManX aggregated and precipitated during purification and
430 size-exclusion chromatography under all tested purification conditions. In addition,
431 BACTH assays did not detect an interaction between Rlv3841 ManX and MDH or between
432 ManX and SucA (**Figure S3**). Although negative BACTH results can have several
433 explanations (e.g. fusion geometry, absence of required cofactors, or expression level),
434 the strong tendency of ManX to aggregate suggests that misfolding or aggregation of the
435 ManX fusion protein in *E. coli* potentially limits the detection of this interaction.

436 The observed slowdown of the TCA cycle, accompanied by increased carbon allocation
437 toward storage compounds, despite unaltered amino acid transport in the *manX* mutant
438 (17), suggests that ManX may affect overall TCA cycle activity, and that the phenotypes
439 observed in the *manX* mutant cannot be explained just by the disturbances in one or

several TCA enzymatic steps. This interpretation is supported by comparison with the strain RU116 (32, 46), which carries a mutation in *sucD*, the gene for the β-subunit of succinyl-CoA synthetase. Although RU116 exhibited low growth rates, reduced succinyl-CoA synthase activity, and strong upregulation of MDH (46), it showed reduced amino acid uptake (46) and did not accumulate lipids (32) and glycogen (**Figure S4**). Therefore, when the TCA cycle is blocked due to direct enzyme impairment, cells avoid carbon and reductant buildups by redirecting the TCA intermediates and reducing cycle flux. In contrast, disruption of *manX* perturbs global carbon metabolism, allocating carbon overflow into storage.

It was established in previous work that the other PTS^{Ntr} effector, PtsN, regulates EPS biosynthesis through its interaction with the ChvG/I two-component system(17). We now show that the phosphorylated state of PtsN is essential for this function, as evidenced by differences in EPS accumulation between non-phosphorylatable (H66A) and phosphomimetic (H66D) PtsN variant strains. In the *ptsN**H66A mutant, EPS level is comparable to that of the original *ptsN* mutant, whereas in the ptsN*H66D strain, EPS accumulation is slightly higher than the Rlv3841 wild-type level. Other polymers are not altered in the *ptsN* mutant, suggesting that the role of PtsN in carbon metabolism is exclusively linked to the control of EPS biosynthesis or secretion. In the *hprK* mutant, the preferential accumulation of carbon into EPS, but not glycogen, is likely driven by the activity of PtsN~P, which is the predominant version in this mutant (19), leading to the upregulation of EPS production. This was further supported by EPS surface phenotypic assays on agar plates using NPr variants containing with substitutions at the Ser48 and

His17 phosphorylation sites, showing that the histidine phosphorylation is the dominant phosphorylation site (Fig. S5).

Similar to the regulation exerted by non-phosphorylated ManX, the regulatory role of HprK cannot be easily explained by a single target. The *hprK* mutant shows a severe growth defect on various carbon sources, including glucose or succinate (**Table S1**, **Figure S1**) (17, 22), along with a reduced O_2 consumption. Growth on succinate is slightly better (mean generation time, 5.48 ± 0.24 h) than on glucose (7.64 ± 0.17 h), although growth under both conditions remains markedly worse than that of Rlv3841 wild-type (3.42 ± 0.11 h on glucose; 3.44 ± 0.28 h on succinate) (17). The *hprK* mutant also shows EPS overproduction, elevated pyrimidine (nucleotide) levels, and increased MDH activity. Grown under N-limitation, the *hprK* mutant does not accumulate PHB when the carbon source is glucose, but it does when succinate is the carbon source. One potential explanation for these distinct phenotypes is that this *hprK* mutant biases carbon flow towards gluconeogenesis and TCA cycle activity under conditions that normally favour ED metabolism. MDH links the TCA cycle to gluconeogenesis by catalysing the conversion of malate to oxaloacetate (**Figure 1.B**). Increased MDH activity could therefore elevate oxaloacetate levels, leading to enhanced aspartate formation and subsequent nucleotide biosynthesis, which may account for the elevated pyrimidine levels observed in the *hprK* mutant. In addition, oxaloacetate may be converted to PEP via PEPCK, thereby directing carbon through gluconeogenesis toward glucose 6-phosphate, a central metabolic intermediate that supplies precursors for both glycogen and EPS biosynthesis.

Another piece of evidence for the relative shift toward the gluconeogenesis pathway in the *hprK* mutant is its PHB accumulation pattern. In rhizobia, glucose is normally processed primarily through the ED/PPP (pentose phosphate) pathways, and PHB synthesis requires a route from the carbon source to acetyl-CoA and a sufficient NADPH supply during nitrogen limitation (5, 47). Therefore, the lack of PHB accumulation by the *hprK* mutant during growth on glucose under nitrogen limitation, despite PHB accumulation on succinate, suggests a defect in ED/PPP-dependent PHB synthesis from glucose. It also indicates a potential carbon shift towards a more gluconeogenic state, rather than the typical ED-dominated metabolic state observed during growth on glucose.

In rhizobia, one well-characterised regulator for the decision between glycolysis/ED metabolism and TCA cycle/gluconeogenesis is PckR, a LacI-family transcriptional regulator that represses the ED pathway (*zwf–pgl–edd, eda2, mgsA*) and activates the gluconeogenic genes *pckA* and *fbaB* when bound to DNA (39, 40). Normally, elevated PEP causes the regulator PckR to dissociate from DNA, lifting repression of the ED pathway. However, strains carrying effector-insensitive missense alleles of *pckR* maintain ED repression even during growth on glucose. Measuring transcript levels of *pckR* and its target genes by qPCR under glucose and succinate conditions was therefore used to assess whether the misregulated central carbon control in the *hprK* mutant arises from altered PckR regulation.

The transcript level of *pckR* itself is reduced approximately twofold in the *hprK* mutant during growth on glucose and is unchanged on succinate. When PckR downstream targets were assessed on glucose, the *hprK* mutant showed higher *pckA* and *fbaB*

507 expression than wild-type and slightly reduced *zwf* expression. Grown on succinate,
508 *pckA*, *fbaB*, and *pckR* transcript levels are comparable to wild-type. This pattern
509 suggests that the mutant shifts central metabolism towards gluconeogenesis under
510 typically glycolytic conditions (e.g., glucose growth), while the transcriptional program
511 associated with succinate utilisation is largely intact. Altogether, these data are
512 consistent with PckR being a plausible participant in the misregulated central carbon
513 metabolic network caused by the *hprK* mutation. However, since *pckR* transcript
514 abundance changes only modestly, and only when cultures are grown on glucose but not
515 on succinate, these results do not demonstrate that HprK directly regulates *pckR*.
516 Instead, HprK likely influences how the PckR regulatory network responds to different
517 carbon sources, either indirectly by altering the cell's metabolic state or directly by
518 modulating *pckR* expression under certain conditions.

519 Loss of HprK was expected to relieve serine-dependent inhibition of NPr histidine
520 phosphorylation and thus favour phosphorylation of both downstream proteins ManX
521 and PtsN. The increased EPS production in the *hprK* background, along with the *npr*
522 complementation data, is consistent with enhanced His-phosphorylation through the
523 PtsN branch. However, the *hprK* mutant does not phenocopy the effects of ManX
524 perturbation. Although our study indicates that ManX is functionally active in its
525 nonphosphorylated form, the growth defect of the *hprK* mutant cannot be fully explained
526 by a simple reduction in the unphosphorylated ManX pool, as the *hprK* dehydrogenase
527 readouts do not match the *manX* mutant phenotype. This *hprK* phenotype might also
528 reflect the additional metabolic burden resulting from hyperphosphorylated PtsN, as
529 this state could lead to overactivation of ABC transport and misregulation of ion

530 homeostasis, among other effects, that may contribute to the growth defect. Thus, the
531 *hprK* mutation results in an overall regulatory imbalance between PtsN and ManX output
532 proteins, which in turn produces complex downstream effects that are more consistent
533 with differential regulation than with a uniform increase in phosphorylation of both ManX
534 and PtsN. Future studies will be needed to assign *hprK* mutant phenotypes to specific
535 downstream EIIA components and to determine whether HprK has additional regulatory
536 functions beyond those mediated by ManX or PtsN.

537 **CONCLUSION**

538 Our findings show that PTS^{Ntr} coordinates carbon metabolism and storage through
539 intricate metabolic interactions. Central to this role is ManX, whose activity is essential
540 for maintaining the activity of TCA cycle dehydrogenase enzymes. Loss of ManX disrupts
541 the flux throughout the TCA cycle, leading to the accumulation of all tested key polymers
542 (glycogen, PHB, and EPS), which mimic nitrogen starvation phenotypes even when
543 nitrogen is available. While the effect on internal polymers seems to be mediated by
544 ManX, analysis of PtsN variants further supports a role for phosphorylated PtsN in
545 promoting EPS production. This regulatory balance is mediated by Npr phosphorylation,
546 highlighting the importance of the control exerted via HprK. The metabolic phenotypes
547 of the *hprK* mutant suggest a bias toward the gluconeogenic state during growth on sugar
548 and confirm complex regulatory effects caused by increased phosphorylation of ManX
549 and PtsN. Collectively, our findings highlight the tight integration of both central
550 metabolism and the accumulation of carbon storage polymers. Imbalanced PTS^{Ntr}
551 regulation disrupts this coordination, leading to a slowed TCA cycle and atypical carbon

polymer accumulation patterns. This reinforces the role of PTS^{Ntr} as a key regulatory network of bacterial metabolic balance.

METHODS

Bacterial strains, plasmids, and culture conditions

This work was conducted using the laboratory reference strain *R.* leguminosarum bv. viciae 3841 or derivative mutants listed in **Table S2.** *R. leguminosarum* was grown on tryptone yeast (TY) nutrient-rich medium or the minimal medium Universal Minimal Salts (UMS) supplemented with 10 mM glucose and 10 mM ammonium chloride, unless otherwise stated (48, 49). *R. leguminosarum* was grown at 28˚C supplemented with antibiotics at the following concentrations (μg ml^{-1}): spectinomycin 100, streptomycin 500, tetracycline 1 (liquid cultures) or 5 (agar plates). *Escherichia coli* was grown on nutrient-rich Luria-Bertani (LB) medium at 37˚C unless otherwise stated (50). *E. coli* cultures were supplemented with antibiotics at concentrations (μg ml^{-1}) of ampicillin 100, kanamycin 20, spectinomycin 50, and streptomycin 25.

Reporter plasmids containing the *lacZ* (β-galactosidase) gene under control of the *mdh* or *sucA* promoter (pRU3037 and pRU3068, respectively) were conjugated into *R. leguminosarum* using the pRK2013 helper plasmid.

TCA cycle enzyme assays

R. leguminosarum strains were grown in 50 mL UMS supplemented with 10 mM glucose and 10 mM ammonia to mid-exponential growth at an OD_{600} of 0.4 – 0.6. Bacterial cells were then washed and resuspended in 20 mM phosphate buffer, pH 7.2, containing 1 mM dithiothreitol (DTT), and cytosolic fractions were obtained by breaking the cells with FastPrep-24 5G Ribolyzer (MP Biomedicals), followed by centrifugation at 13,000 rpm to remove membranes and debris. Enzyme activities were assayed with a spectrophotometer at 29°C by monitoring the rate of change in absorbance per second upon the addition of the cell lysate and respective substrates. The enzyme rate was standardised by measuring the protein concentration of whole cells using Qubit™ Protein Assay Kits following the manufacturer's instructions. The final compositions of the reaction mix and wavelength used for each enzyme assay were as follows: citrate synthase (200 mM Tris/HCl pH 8.1, 0.2 mM DTNB, 0.1 mM Acetyl-CoA, 0.5 mM Oxaloacetate; measured at 412 nm) (51), isocitrate dehydrogenase (20 mM Tris/HCl pH 7.4, 3.3 mM MgCl2, 0.5 mM NADP, 0.5 mM DL-Isocitric Acid, measured at 340 nm) (52), oxoglutarate dehydrogenase (100 mM Tris/HCl pH 8.4, 0.1 mM CoA, 7.8 mM Cysteine, 25 mM 2-oxoglutarate, 2 mM NAD; measured at 340 nm) (51), fumarase (50 mM Phosphate/NaOH pH 8, 50 mM L-malate, measured at 240 nm) (53), malate dehydrogenase (100 mM Phosphate/NaOH pH 7.5, 0.2 mM NADH, 0.5 mM Oxaloacetic acid; measured at 340 nm) (54), pyruvate dehydrogenase (50 mM pH Phosphate/NaOH 7.5, 3.5 mM NAD, 0.12 mM CoASNa, 4 mM Cysteine, 0.3 mM Thiamine pyrophosphate, 1.5 mM MgCl2, 2.5 mM Sodium pyruvate; measured at 340 mM) (54). All assays were performed from at least three independent biological replicates. Negative controls (lysates without substrate or cofactor) were included to account for background activity.

O_2 consumption assays

To measure oxygen (O_2) consumption, liquid cultures (25 mL) at the exponential phase were added to a glass universal with an OxyDot oxygen sensor and a magnetic stirrer, and quickly sealed. O_2 consumption was measured in real time every 15 seconds until the O_2 level decreased below 15% using a non-invasive O_2 electrode from the OxySense 325I System (Industrial Physics) and analysed with the OxySense GenIII program. The consumption rate was measured as the time taken for the bacterial population to reduce the O_2 level by 3% as previously described (17).

Promoter activity assays

The promoter activity of *mdh* or *sucA* was measured using the β-galactosidase method (55, 56). To do this, reporter plasmids containing the *lacZ* (β-galactosidase) gene under the control of the *mdh* or *sucA* promoter were conjugated into *R. leguminosarum* (17). A promoter-less plasmid containing only *lacZ* was included as an experimental control and baseline measure. Cultures were harvested during the exponential phase. Cells were lysed through the addition of 0.1% SDS and chloroform to a cell suspension in Z buffer (57). The β-galactosidase reaction was initiated by the addition of o-nitrophenyl-β-D-galactosidase with β-mercaptoethanol and stopped after the suspension turned yellow by adding 1 M Na_2CO_3. Centrifugation removed cell debris, and activity was quantified by measuring the absorbance at 420 nm. Transcriptional activity was converted into Miller's Units (56). Activity is reported as fold-change relative to strain-specific background rates. This adjusts for the overall lower transcriptional activity of slow-growing strains such as the *hprK* mutant.

PHB quantification

Cellular PHB content was determined by flow cytometry after staining cells with the fluorescent dye Nile Red (NR). The median fluorescence intensity, expressed in the arbitrary fluorescent unit (AFU), has been reported to correlate linearly well with the bacterial PHB content (58, 59). Briefly, *R. leguminosarum* was first grown in 10 mL UMS supplemented with 10 mM glucose as a carbon source and 10 mM ammonia (N-rich) or 0.5 mM ammonia (N-poor) to an OD_{600} of 0.8– 1. Bacterial cells were harvested and washed with PBS buffer and then permeabilised by treatment with 35% ethanol for 15 minutes. They were diluted in PBS to reach a concentration of 5×10^6 cells, stained with 0.01% (w/v) NR stock solution (20 µl for 1 mL sample) for 30 minutes under dark conditions, and then analysed on the flow cytometer (Amnis CellStream) with the excitation 488 nm wavelength of Argon Laser. Fluorescence was measured in channel F2, with a filter centred on a bandwidth of 585 nm. The data is analysed with CellStream™ software. Strain LMB816 (double mutant of *phaC1/phaC2*) was used as the negative control.

Glycogen quantification

Glycogen was extracted from *R. leguminosarum* cultures following the modified version of the previously described protocol (60) by boiling it with 30% KOH for 1.5 h. Dissolved glycogen was then precipitated with 70% EtOH, spun down, and dried. The glycogen amount for each sample was normalised with the total protein content of the cells. To quantify, pelleted glycogen was resuspended in 10 mM acetate buffer, pH 4.75 and digested with amyloglucosidase (4 units/assay) and amylase (8 units/assay) for 1.5 h at room temperature. Aliquots of the digested samples were then assayed by standard

638 hexokinase/glucose-6-phosphate dehydrogenase (G6P-DH/HK) assay coupled with
639 $NADP^+$ reduction [30]. The assay reaction mix contains 265 mM triethanolamine buffer
640 pH 7.6, 3.3 mM $MgCl_2$, 10 mM ATP, 10 mM NADP, 0.5 units of G6P-DH/HK, and the
641 sample. The increase in absorbance at 340 nm was read with the Omega FLUOstar plate
642 reader. Strain OPS2031 (*glgA* mutant), deficient in glycogen biosynthesis, was used as
643 the negative control, and glycogen content was calculated by comparing the absorbance
644 (340 nm) with that of the glycogen standards.

645 **EPS quantification**

646 EPS was quantified following the previously described protocol (17). *R. leguminosarum*
647 was grown in 50 mL UMS with 10 mM glucose and 10 mM NH_4Cl to reach an OD of 1. The
648 cultures were then centrifuged, and the pelleted cells were dried and weighed. The
649 supernatants were treated with twice the volume of ethanol (100 mL) and incubated at
650 4°C for 24h. The precipitated EPS was then collected, dried, and weighed. Strain LMB310
651 (*pssA* mutant) that did not produce EPS was used as the negative control.

652 **Raman spectroscopy and analysis**

653 Single-cell Raman spectra (SCRS) were acquired using a confocal Raman micro-
654 spectrometer (HR Evolution 800, Horiba, Japan) equipped with a continuous 532 nm
655 laser set to 80 mW. The laser beam was attenuated with a 10% neutral-density (ND) filter
656 and focused onto the sample through a 100× objective (NA 0.9; Olympus, Japan). Spectra
657 were recorded with a 300 lines/mm^{-1} grating, with the spectral centre set at 2000 cm^{-1}.
658 The Raman acquisition time was 12 s per cell. For each sample group, at least 30 SCRS
659 were randomly acquired.

Pre-processing of raw spectra comprised quality control to remove saturated high-intensity spectra, cosmic-ray spike removal, spectral trimming (retaining only the fingerprint region, 320–1,850 cm^{-1}), baseline fitting (third-order polynomial with 100 points) and baseline correction. The spectra were then normalised such that the sum of all integrated peak intensities was equal to one.

Principal component analysis (PCA) of SCRS: SCRS from all experimental groups were combined pairwise (wild-type vs wild-type N-limiting; wild-type vs *manX* mutant; wild-type vs *hprK* mutant), and PCA was performed on the fingerprint region for each pair. For each pairwise analysis, we examined combinations of the top ten principal components (e.g., Dim 1 vs Dim 2, Dim 3 vs Dim 6) to identify the projection that best separated the two groups (maximising inter-group distance on the score plots). Using the optimal Dim pair thus identified, we computed the loadings across Raman shifts for that projection and ranked the shifts by loading value (from +1 to -1), yielding an ordered list according to each shift's contribution to group discrimination. By cross-referencing our in-house Raman spectral database, we assigned the key biomolecular contributors underlying the separations observed for each pair of strains. PCA, computation of PCA loading matrices, and score-plot visualisation/analysis were carried out in R (version 4.4.2) using the base 'stats' package together with 'dplyr' and 'ggplot2'.

RNA extraction and real-time qPCR analysis

Rlv3841 cells were harvested by centrifugation at 4 °C, lysed using the FastPrep-24 5G instrument, and their cell debris was removed by another round of centrifugation. RNA was extracted from the lysate using the Qiagen RNAeasy extraction kit, and gDNA was depleted by treatment with Invitrogen Turbo DNAse according to the manufacturer's

683 recommendation. cDNAs are generated from 0.5 µg of purified RNA using an Invitrogen
684 SuperScript IV reverse transcriptase kit as per the manufacturer's recommendations.
685 Quantitative PCR reactions were prepared in 384-well qPCR plates containing 5 µL of
686 Applied Biosystems PowerUp SYBR Green master mix, 250 nM of each primer, and 5 ng
687 of RNA template, for a total volume of 10 µL per reaction. Reactions were run using the
688 StepOnePlus™ Real-Time PCR System. Four biological replicates were extracted for each
689 condition, each represented by two technical replicates and the average expression was
690 calculated. The primer pairs used in the real-time qRT-PCR are listed in **Table S3** and
691 were initially tested for amplification efficiency and target specificity by generating a
692 standard curve of amplification with the *rpoD* housekeeping gene. Relative expression of
693 each individual gene was calculated using the Pfaffl Method.

694 **Statistical analysis**

695 All statistical analyses were carried out using GraphPad Prism 10.5.0 (GraphPad
696 Software, 7825 Fay Avenue, Suite 230, La Jolla, CA 92037, USA). Student's T-tests and
697 analysis of variance were used to measure the significance of results. Where multiple
698 comparisons were necessary, the One-way ANOVA (Tukey-Kramer method) was used.
699 We took a *p-value* less than 0.05 to be statistically significant. All values are taken from
700 single colonies representing one biological replicate. Biological replicates were sampled
701 with two to three technical replicates each.

REFERENCES

1. Peoples MB, Brockwell J, Herridge DF, Rochester IJ, Alves BJR, Urquiaga S, Boddey RM, Dakora FD, Bhattarai S, Maskey SL, Sampet C, Rerkasem B, Khan DF, Hauggaard-Nielsen H, Jensen ES. 2009. The contributions of nitrogen-fixing crop legumes to the productivity of agricultural systems. Symbiosis 48:1–17. https://doi.org/10.1007/BF03179980

2. Reis Ely CR, Perakis SS, Cleveland CC, Menge DNL, Reed SC, Taylor BN, Batterman SA, Clark CM, Crews TE, Dynarski KA, Gei M, Gundale MJ, Herridge DF, Jovan SE, Kou-Giesbrecht S, Peoples MB, Piipponen J, Rodríguez-Caballero E, Salmon VG, Soper FM, Staccone AP, Weber B, Williams CA, Wurzburger N. 2025. Global terrestrial nitrogen fixation and its modification by agriculture. Nature 643:705–711. https://doi.org/10.1038/s41586-025-09201-w

3. Ledermann R, Schulte CCM, Poole PS. 2021. How Rhizobia Adapt to the Nodule Environment. J Bacteriol 203. https://doi.org/10.1128/JB.00539-20

4. Burghardt LT, diCenzo GC. 2023. The evolutionary ecology of rhizobia: multiple facets of competition before, during, and after symbiosis with legumes. Curr Opin Microbiol 72:102281. https://doi.org/10.1016/j.mib.2023.102281

5. Schulte CCM, Borah K, Wheatley RM, Terpolilli JJ, Saalbach G, Crang N, de Groot DH, Ratcliffe RG, Kruger NJ, Papachristodoulou A, Poole PS. 2021. Metabolic control of nitrogen fixation in rhizobium-legume symbioses. Sci Adv 7:eabh2433. https://doi.org/10.1126/sciadv.abh2433

6. Poole P, Ramachandran V, Terpolilli J. 2018. Rhizobia: From saprophytes to endosymbionts. Nat Rev Microbiol 16:291–303. https://doi.org/10.1038/nrmicro.2017.171

7. Engleman EG, Francis SH. 1978. Cascade control of *E. coli* glutamine synthetase. Arch Biochem Biophys 191:602–612. https://doi.org/10.1016/0003-9861(78)90398-3

8. Radchenko MV, Thornton J, Merrick M. 2010. Control of AmtB-GlnK Complex Formation by Intracellular Levels of ATP, ADP, and 2-Oxoglutarate. J Biol Chem 285:31037–31045. https://doi.org/10.1074/jbc.M110.153908

9. Huergo LF, Dixon R. 2015. The Emergence of 2-Oxoglutarate as a Master Regulator Metabolite. Microbiol Mol Biol Rev 79:419–435. https://doi.org/10.1128/MMBR.00038-15

10. Ninfa AJ, Atkinson MR. 2000. PII signal transduction proteins. Trends Microbiol 8:172–179. https://doi.org/10.1016/S0966-842X(00)01709-1

11. Noindorf L, Bonatto AC, Monteiro RA, Souza EM, Rigo LU, Pedrosa FO, Steffens MB, Chubatsu LS. 2011. Role of PII proteins in nitrogen fixation control of *Herbaspirillum seropedicae* strain SmR1. BMC Microbiol 11:8. https://doi.org/10.1186/1471-2180-11-8

12. Patriarca EJ, Taté R, Iaccarino M. 2002. Key Role of Bacterial $NH4^+$ Metabolism in Rhizobium-Plant Symbiosis. Microbiol Mol Biol Rev 66:203–222. https://doi.org/10.1128/MMBR.66.2.203-222.2002

13. Taté R, Riccio A, Merrick M, Patriarca EJ. 1998. The *Rhizobium etli amtB* Gene Coding for an NH_4^+ Transporter Is Down-Regulated Early During Bacteroid Differentiation. Mol Plant Microbe Interact 11:188–198. https://doi.org/10.1094/MPMI.1998.11.3.188

14. Deutscher J, Francke C, Postma PW. 2006. How Phosphotransferase System-Related Protein Phosphorylation Regulates Carbohydrate Metabolism in Bacteria. Microbiol Mol Biol Rev 70:939–1031. https://doi.org/10.1128/MMBR.00024-06

15. Powell BS, Court DL, Inada T, Nakamura Y, Michotey V, Cui X, Reizer A, Saier MH, Reizer J. 1995. Novel Proteins of the Phosphotransferase System Encoded within the rpoN Operon of *Escherichia coli*. J Biol Chem 270:4822–4839. https://doi.org/10.1074/jbc.270.9.4822

16. Merrick MJ, Edwards RA. 1995. Nitrogen control in bacteria. Microbiol Rev 59:604–622. https://doi.org/10.1128/mr.59.4.604-622.1995

17. Sánchez-Cañizares C, Prell J, Pini F, Rutten P, Kraxner K, Wynands B, Karunakaran R, Poole PS. 2020. Global control of bacterial nitrogen and carbon metabolism by a PTSNtr-regulated switch. Proc Natl Acad Sci U S A 117:10234–10245. https://doi.org/10.1073/pnas.1917471117

18. Pflüger-Grau K, Chavarría M, De Lorenzo V. 2011. The interplay of the $EIIA^{Ntr}$ component of the nitrogen-related phosphotransferase system (PTS^{Ntr}) of *Pseudomonas putida* with pyruvate dehydrogenase. Biochim Biophys Acta Gen Subj 1810:995–1005. https://doi.org/10.1016/j.bbagen.2011.01.002

19. Dozot M, Poncet S, Nicolas C, Copin R, Bouraoui H, Mazé A, Deutscher J, De Bolle X, Letesson J-J. 2010. Functional Characterization of the Incomplete Phosphotransferase System (PTS) of the Intracellular Pathogen *Brucella melitensis*. PLoS One 5:e12679. https://doi.org/10.1371/journal.pone.0012679

20. Bélanger L, Dimmick KA, Fleming JS, Charles TC. 2009. Null mutations in *Sinorhizobium meliloti exoS* and *chvI* demonstrate the importance of this two-component regulatory system for symbiosis. Mol Microbiol 74:1223–1237. https://doi.org/10.1111/j.1365-2958.2009.06931.x

21. Cheng H-P, Walker GC. 1998. Succinoglycan Production by *Rhizobium meliloti* Is Regulated through the ExoS-ChvI Two-Component Regulatory System. J Bacteriol 180:20–26. https://doi.org/10.1128/JB.180.1.20-26.1998

22. Pinedo CA, Gage DJ. 2009. HPrK Regulates Succinate-Mediated Catabolite Repression in the Gram-Negative Symbiont *Sinorhizobium meliloti*. J Bacteriol 191:298–309. https://doi.org/10.1128/JB.01115-08

23. Hu K-Y, Saier MH. 2002. Phylogeny of phosphoryl transfer proteins of the phosphoenolpyruvate-dependent sugar-transporting phosphotransferase system. Res Microbiol 153:405–415. https://doi.org/10.1016/S0923-2508(02)01368-4

24. Mijakovic I, Poncet S, Galinier A, Monedero V, Fieulaine S, Janin J, Nessler S, Marquez JA, Scheffzek K, Hasenbein S, Hengstenberg W, Deutscher J. 2002. Pyrophosphate-producing protein dephosphorylation by HPr kinase/phosphorylase: A relic of early life? Proc Natl Acad Sci U S A 99:13442–13447. https://doi.org/10.1073/pnas.202350199

25. Geddes BA, Oresnik IJ. 2014. Physiology, genetics, and biochemistry of carbon metabolism in the alphaproteobacterium *Sinorhizobium meliloti*. Can J Microbiol 60:491–507.

26. Dunn MF. 1998. Tricarboxylic acid cycle and anaplerotic enzymes in rhizobia. FEMS Microbiol Rev 22:105–123.

27. Noguez R, Segura D, Moreno S, Hernandez A, Juarez K, Espín G. 2008. Enzyme I Ntr, NPr, and IIA Ntr are involved in regulation of the poly-β-hydroxybutyrate biosynthetic genes in *Azotobacter vinelandii*. J Mol Microbiol Biotechnol 15:244–254. https://doi.org/10.1159/000108658

28. Velázquez F, Pflüger K, Cases I, De Eugenio LI, de Lorenzo V. 2007. The Phosphotransferase System Formed by PtsP, PtsO, and PtsN Proteins Controls Production of Polyhydroxyalkanoates in *Pseudomonas putida*. J Bacteriol 189:4529–4533. https://doi.org/10.1128/JB.00033-07

29. Pinedo CA, Bringhurst RM, Gage DJ. 2008. *Sinorhizobium meliloti* Mutants Lacking Phosphotransferase System Enzyme HPr or EIIA Are Altered in Diverse Processes, Including Carbon Metabolism, Cobalt Requirements, and Succinoglycan Production. J Bacteriol 190:2947–2956. https://doi.org/10.1128/JB.01917-07

30. Lagares A, Krol E, Müller T, Glatter T, Becker A. 2025. A systems-level insight into PHB-driven metabolic adaptation orchestrated by the PHB-binding transcriptional regulator AniA (PhaR). *mSystems* 0:e00760-25. https://doi.org/https://doi.org/10.1128/msystems.00760-25.

31. Udvardi M, Poole PS. 2013. Transport and Metabolism in Legume-Rhizobia Symbioses. Annu Rev Plant Biol 64:781–805. https://doi.org/10.1146/annurev-arplant-050312-120235

32. Terpolilli JJ, Masakapalli SK, Karunakaran R, Webb IUC, Green R, Watmough NJ, Kruger NJ, Ratcliffe RG, Poole PS. 2016. Lipogenesis and Redox Balance in Nitrogen-Fixing Pea Bacteroids. J Bacteriol 198:2864–2875. https://doi.org/10.1128/JB.00451-16

33. Huang WE, Griffiths RI, Thompson IP, Bailey MJ, Whiteley AS. 2004. Raman Microscopic Analysis of Single Microbial Cells. Anal Chem 76:4452–4458. https://doi.org/10.1021/ac049753k

34. Xu J, Webb I, Poole P, Huang WE. 2017. Label-Free Discrimination of Rhizobial Bacteroids and Mutants by Single-Cell Raman Microspectroscopy. Anal Chem 89:6336–6340. https://doi.org/10.1021/acs.analchem.7b01160

35. De Gelder J, De Gussem K, Vandenabeele P, Moens L. 2007. Reference database of Raman spectra of biological molecules. J Raman Spectrosc 38:1133–1147. https://doi.org/10.1002/jrs.1734

36. Movasaghi Z, Rehman S, Rehman IU. 2007. Raman Spectroscopy of Biological Tissues. Appl Spectrosc Rev 42:493–541. https://doi.org/10.1080/05704920701551530

37. Zhu G, Zhu X, Fan Q, Wan X. 2011. Raman spectra of amino acids and their aqueous solutions. Spectrochim Acta A Mol Biomol Spectrosc 78:1187–1195. https://doi.org/10.1016/j.saa.2010.12.079

38. Brauer MJ, Yuan J, Bennett BD, Lu W, Kimball E, Botstein D, Rabinowitz JD. 2006. Conservation of the metabolomic response to starvation across two divergent microbes. Proc Natl Acad Sci U S A 103:19302–19307. https://doi.org/10.1073/pnas.0609508103

39. Østerås M, O'Brien SAP, Finan TM. 1997. Genetic Analysis of Mutations Affecting *pckA* Regulation in *Rhizobium* (*Sinorhizobium*) *meliloti*. Genetics 147:1521–1531. https://doi.org/10.1093/genetics/147.4.1521

40. diCenzo GC, Muhammed Z, Østerås M, O'Brien SAP, Finan TM. 2017. A Key Regulator of the Glycolytic and Gluconeogenic Central Metabolic Pathways in *Sinorhizobium meliloti*. Genetics 207:961–974. https://doi.org/10.1534/genetics.117.300212

41. Zevenhuizen LPTM. 1981. Cellular glycogen, β-1,2-glucan, poly-β-hydroxybutyric acid and extracellular polysaccharides in fast-growing species of Rhizobium. Antonie Van Leeuwenhoek 47:481–497. https://doi.org/10.1007/BF00443236

42. Skorupska A, Janczarek M, Marczak M, Mazur A, Król J. 2006. Rhizobial exopolysaccharides: genetic control and symbiotic functions. Microb Cell Fact 5:7. https://doi.org/10.1186/1475-2859-5-7

43. De Philippis R, Sili C, Vincenzini M. Glycogen and poly-hydroxybutyrate synthesis in *Spirulina maxima*. J Gen Microbiol. 1992;138:1623–1628. doi:https://doi.org/10.1099/00221287-138-8-1623

44. Zaldívar Carrillo JA, Stein LY, Sauvageau D. Defining nutrient combinations for optimal growth and polyhydroxybutyrate production by *Methylosinus trichosporium* OB3b using response surface methodology. Front Microbiol. 2018;9:1513. doi:https://doi.org/10.3389/fmicb.2018.01513

45. Higuchi-Takeuchi M, Morisaki K, Toyooka K, Numata K. Synthesis of high-molecular-weight polyhydroxyalkanoates by marine photosynthetic purple bacteria. PLoS One. 2016;11:e0160981. doi:https://doi.org/10.1371/journal.pone.0160981

46. Walshaw DL, Wilkinson A, Mundy M, Smith M, Poole PS. 1997. Regulation of the TCA cycle and the general amino acid permease by overflow metabolism in *Rhizobium leguminosarum*. Microbiology 143:2209–2221. https://doi.org/10.1099/00221287-143-7-2209

47. Chohan SN, Copeland L. 1998. Acetoacetyl Coenzyme A Reductase and Polyhydroxybutyrate Synthesis in *Rhizobium (Cicer) sp*. Strain CC 1192. Appl Environ Microbiol 64:2859–2863. https://doi.org/10.1128/AEM.64.8.2859-2863.1998

48. Beringer JE. 1974. R factor transfer in *Rhizobium leguminosarum*. J Gen Microbiol 84:188–198. https://doi.org/10.1099/00221287-84-1-188

49. Wheatley RM, Ramachandran VK, Geddes BA, Perry BJ, Yost CK, Poole PS. 2016. Role of O2 in the Growth of *Rhizobium leguminosarum* bv. *viciae* 3841 on Glucose and Succinate. J Bacteriol 199. https://doi.org/10.1128/JB.00572-16

50. Sambrook J, Russell W. 2001. Molecular Cloning: A Laboratory Manual. Cold Spring Harbor Laboratory Press.

51. Reeves, H. C., Rabin, R., Wegener, W. S., & Ajl, S. J. 1971. Assays of enzymes of the tricarboxylic acid and glyoxylate cycles. In S. J. Ajl (Ed.), *Methods in Microbiology* (Vol. 6A, pp. 425–462). Academic Press.

52. Karr DB, Waters JK, Suzuki F, Emerich DW. 1984. Enzymes of the Poly-β-Hydroxybutyrate and Citric Acid Cycles of *Rhizobium japonicum* Bacteroids. Plant Physiol 75:1158–1162. https://doi.org/10.1104/pp.75.4.1158

53. Hill, R. L., & Bradshaw, R. A. (1969). Fumarase. In J. M. Lowenstein (Ed.), *Methods in Enzymology* (Vol. 13, pp. 91–99). Academic Press. https://doi.org/10.1016/0076-6879(69)13019-3

54. Saroso S, Dilworth MJ, Glenn AR. 1986. The Use of Activities of Carbon Catabolic Enzymes as a Probe for the Carbon Nutrition of Snakebean Nodule Bacteroids. Microbiology 132:243–249. https://doi.org/10.1099/00221287-132-2-243

55. Smale ST. 2010. β-Galactosidase Assay. Cold Spring Harb Protoc 2010:pdb.prot5423. https://doi.org/10.1101/pdb.prot5423

56. Miller JH. 1972. Assay of β-galactosidase. Experiments in molecular genetics 352–355.

57. Poole PS, Schofield NA, Reid CJ, Drew EM, Walshaw DL. 1994. Identification of chromosomal genes located downstream of *dctD* that affect the requirement for calcium and the lipopolysaccharide layer of *Rhizobium leguminosarum*. Microbiology (Reading) 140 (Pt 10):2797–2809. https://doi.org/10.1099/00221287-140-10-2797

58. Alves LPS, Almeida AT, Cruz LM, Pedrosa FO, de Souza EM, Chubatsu LS, Müller-Santos M, Valdameri G. 2017. A simple and efficient method for poly-3-hydroxybutyrate quantification in diazotrophic bacteria within 5 minutes using flow cytometry. Braz J Med Biol Res 50:e5492. https://doi.org/10.1590/1414-431X20165492

59. Lagares Jr. A, Valverde C. 2017. Quantification of Bacterial Polyhydroxybutyrate Content by Flow Cytometry. *Bio-Protocol* 7(23):e2638. https://doi.org/10.21769/BioProtoc.2638

60. Herbert, D., Phipps, P. J., & Strange, R. E. 1971. Chemical analysis of microbial cells. In J. R. Norris & D. W. Ribbons (Ed.), *Methods in Microbiology* (Vol. 5B, pp. 209–344). Academic Press.

DATA AVAILABILITY

All data supporting the findings of this study are available within the article and its Supplementary Information.

ACKNOWLEDGEMENT

We are grateful to Professor Antonis Papachristodoulou for his critical reading of the manuscript and helpful suggestions, and to Andrea Crespo Barreiro for technical support in qPCR analysis. This work was supported by funding from the Biotechnology and Biological Sciences Research Council (UKRI-BBSRC) [grant numbers BB/T008784/1, BB/K006134/1, BB/N003608/1], The Leverhulme Trust grant (RPG-2019-246) to PSP, and The Royal Society University Research Fellowship (URF\R1\221030) to CSC. O.T. is supported by the Indonesia Endowment Fund for Education Agency (LPDP) Scholarship. We thank MRC (OPP371) for research fund and EPSRC (EP/M02833X/1) for instrument support.

AUTHOR CONTRIBUTIONS

Conceptualisation: OT, CSC, PSP

Investigation: OT, JW, ET

Formal analysis: OT, JW

Visualisation: OT, JW

Supervision: CSC, PSP, WH

Writing – original draft: OT

Writing – review & editing: OT, CSC, ET, PSP, JW, WH

CHAPTER 3

Regulation of central carbon metabolism and storage polymers by PTS^{Ntr} in *Rhizobium leguminosarum*

Supplementary Information

Olivia Tjahjono, Jingkai Wang, Evan Turner, Jürgen Prell, Wei E. Huang, Philip Poole, Carmen Sánchez-Cañizares

Table S1. Mean generation time for PTS^{Ntr} mutants grown in Universal Minimal Salt (UMS) supplemented with ammonia (NH_4Cl 10 mM) as the nitrogen source and glucose or succinate as the carbon source, reproduced from (1). Strains shown in bold indicate those examined in this study. Mean generation times slower than the wild-type are highlighted in red, with increasing intensity indicating the magnitude of the difference (light red ~1h slower; medium red ~2h slower; dark red >3h slower).

Description	Strain	Mean Generation Time	
		Glucose 10 mM	Succinate 10 mM
wild-type	**3841**	3.42± 0.11	3.44 ± 0.28
ptsP	ptsP107	4.44 ± 0.16	5.65 ± 0.32
npr	AA031	4.43 ± 0.09	4.04 ± 0.43
ptsN1N2	**AA047**	3.33 ± 0.16	4.34 ± 0.35
***ptsN1N2**H66A**	**OPS1102**	3.42 ± 0.09	3.51 ± 0.11
***ptsN1N2**H66D**	**OPS1104**	4.48 ± 0.50	4.41 ± 0.08
manX	**LMB692**	6.13 ± 0.12	6.15 ± 0.21
***manX**H9A**	**OPS1012**	3.39 ± 0.11	3.46 ± 0.10
hprK	**AA081**	7.64 ± 0.17	5.48 ± 0.24

17 **Table S2**. List of strains and plasmids

Strains	Description	Reference
Escherichia coli		
DH5a	*supE44*, *hsdR17*, *recA*, *thi-1*, *ΔlacU169*(f801acZΔM15) *endA1*, *gyrA96*, *relA1*	(2)
Rhizobium leguminosarum		
Rlv3841	*R. leguminosarum* bv. *viciae*; Str^R derivative of strain 300	(3)
AA047	Rlv3841 *ptsN2* in-frame deletion in *ptsN1*::ΩSpec background or *ptsN1*(RL0425)/*ptsN2*(pRL110376) double mutant	(1)
LMB310	Rlv3841 *pssA*::Tn5 transductant or *pssA* (RL1532) mutant	(4)
LMB692	Rlv3841 *manX* (RL0033) in-frame deletion mutant	(1)
LMB816	Rlv3841 *phaC1* (RL2098)/*phaC2*(pRL100105) double mutant	(1)
OPS0374	Rlv3841 transduction *ptsN1*::Ωspec mutation transduced into LMB692 or *manX/ptsN1* double mutant	(1)
OPS1012	Rlv3841 with non-phosphorylatable ManX made by a single amino acid substitution at H9A	(1)
OPS1102	Rlv3841 *ptsN2* with non-phosphorylatable PtsN1 made by single amino acid substitution at H66A	(1)
OPS1104	Rlv3841 *ptsN2* with PtsN1 phosphomimetic made by single amino acid substitution at H66D	(1)
RU1448	Rlv3841 *glgA* in-frame deletion mutant	(5)
AA081	Rlv3841 *hprK*::ΩSpec	(1)
AA031	Rlv3841 npr::ΩSpec	(6)
PtsP107	Rlv3841 Tn5::*ptsP*	(4)
Plasmids		
pRK2013	Self-transmissible helper plasmid, Km^R	(7, 8)
pK18mobsacB	Wide range suicide vector, oriT (mobilisable), *sacB*; Kan^R	(9)
pRU3070	*mdh::lacZ*	(10)
pRU3068	*sucA::lacZ*	(10)
pOPS0186	*ptsN1* PCR-amplified from Rlv3841 genomic DNA using primers oxp516/517 and cloned into the BACTH vector pUT18C via BamHI/KpnI restriction sites.	(1)
pOPS0174	C-terminal region of *kdpD* PCR-amplified from Rlv 3841 using primers oxp520/521 and cloned into pKNT25 via BamHI/KpnI.	(1)
pOPS0179	*manX* PCR-amplified from Rlv3841 using primers oxp529/530 and cloned into pKNT25 via BamHI/KpnI.	this work
pOPS0193	*manX* PCR-amplified from Rlv3841 using primers oxp529/530 and cloned into pUT18C via BamHI/KpnI.	this work
pOPS0289	*mdh* PCR-amplified from Rlv3841 using primers oxp634/635 and cloned into pKNT25 via BamHI/KpnI.	this work
pOPS0291	*sucA* PCR-amplified from Rlv3841 using primers oxp632/633 and cloned into pKNT25via BamHI/KpnI.	this work
pOPS0292	*mdh* PCR-amplified from Rlv3841 using primers oxp634/635 and cloned into pUT18C via XbaI/KpnI	this work

pOPS0295	*sucA* PCR-amplified from Rlv3841 using primers oxp632/633 and cloned into pUT18C via XbaI/KpnI	this work
pKNT25	BACTH vector for fusions to the N-terminus of fragment T25	this work
pUT18C	BACTH vector for fusions to the C-terminus of fragment T18	this work
pOPS0741	*mdh* (Rlv3841) cloned into pOPINF with an N-terminal 3×FLAG and His-tag by BD (In-Fusion) cloning	this work
pOPS0114	*manX* (Rlv3841) cloned into pOPINF with an N-terminal 3×FLAG and His-tag by BD (In-Fusion) cloning	this work
pOPS1067	*manX* His9Ala cloned into pOPINF with an N-terminal 3×FLAG and His-tag by BD (In-Fusion) cloning;	this work
pOPINF	bacterial expression vector from the pOPIN for high-throughput cloning and expression	(11)
pAA039	pRK415 with *npr* containing a single amino acid substitution at H17A	(6)
pAA040	pRK415 with *npr* containing a single amino acid substitution at S48A	this work
pAA041	pRK415 with *npr* containing amino acid substitutions at H17A and S48A	this work
pRK415	IncP stable broad-host-range cloning vector	(12)

18

Table S3. List of primers

Primers	Description	Sequence
oxp6980	RT-qPCR primer for *rpoD*	GATGAAGTCGATCGGCAATCTG
oxp6981	RT-qPCR primer for *rpoD*	GCTTCGACCATTTCCTTCTTGG
oxp7570	RT-qPCR primer for *zwf*	TACTACGTCTCGGTCGATGC
oxp7571	RT-qPCR primer for *zwf*	GCTTGTGGTCGTGGATCTTC
oxp7572	RT-qPCR primer for *pgl*	CTTGCAACCGAGAAGACCAG
oxp7573	RT-qPCR primer for *pgl*	TCCGCTTCCATGGTGATGAT
oxp7592	RT-qPCR primer for *pckA*	GGTTCGACGACACCCTTTTC
oxp7593	RT-qPCR primer for *pckA*	GACTTCATCCCGAACGCTTC
oxp7594	RT-qPCR primer for *fbaB*	ATATCTCCGGCGTCATCCTC
oxp7595	RT-qPCR primer for *fbaB*	CGACCTTGATGCCTGGAATG
oxp7596	RT-qPCR primer for *pckR*	ATCGCTACCAGGGCTATGTC
oxp7597	RT-qPCR primer for *pckR*	CAGCGAAAGGAAATGCACTG
oxp529	PCR amplification of *manX* for cloning into BATCH vectors	TTTGGTACCCGGCGCCCGATATCCGGCACTT
oxp530	PCR amplification of *manX* for cloning into BATCH vectors	TTTGGATCCCATGATCGGACTTGTGCTTGT
oxp632	PCR amplification of *sucA* for cloning into BATCH vectors	ATGCGCCGCGGACAGGCGGC
oxp633	PCR amplification of *sucA* for cloning into BATCH vectors	ACCGCCCAATGCATCCTCGA
oxp634	PCR amplification of *mdh* for cloning into BATCH vectors	ATGGCGCGTAACAAGATCGC
oxp635	PCR amplification of *mdh* for cloning into BATCH vectors	CTTGAGGGCAGGCGCGATGT

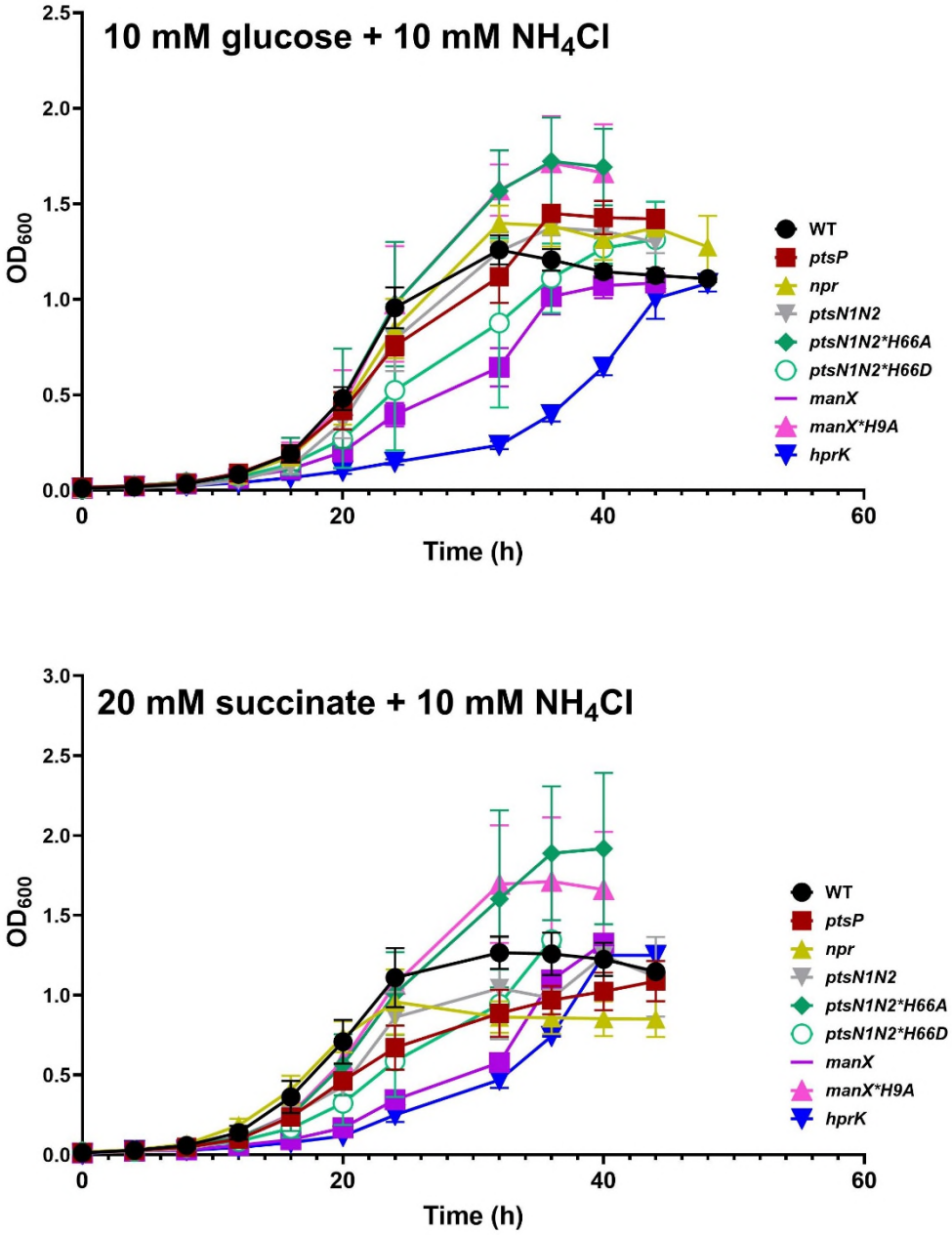

Figure S1. Growth curves of Rlv3841 strains grown in UMS supplemented with 10 mM NH_4Cl and (A) 10 mM glucose or (B) 20 mM succinate. Strains shown are wild-type Rlv3841, *ptsP*, *npr*, *ptsN1N2*, *ptsN1N2**H66A, *ptsN1N2**H66D, *manX*, *manX**H9A and *hprK* (1).

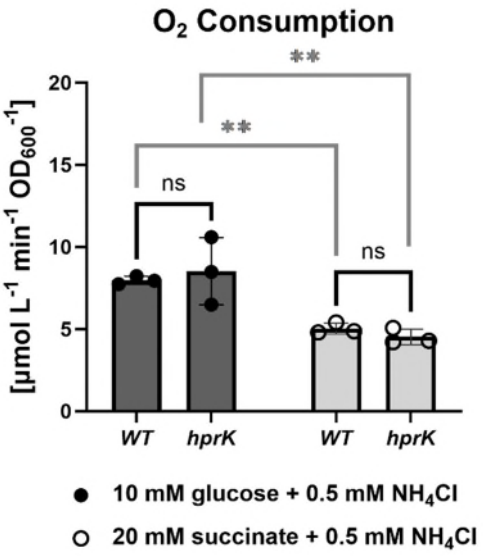

Figure S2. The O_2 consumption rates of *the hprK* mutant compared to wild-type under N-limiting conditions. The strains were grown in liquid UMS cultures supplemented with 0.5 mM NH_4Cl as nitrogen source and either 10 mM glucose (dark grey bars) or 20 mM succinate as carbon source (light grey bars). Data are averages (±SEM) from 3 replicates. Statistical significances were assessed by Student's t-test, with asterisks indicating the following level of significance: ** $P \leq 0.01$, and ns, not significant.

Figure S3. Bacterial two-hybrid assay (B2H) to study potential interaction between Rlv3841 ManX and TCA cycle dehydrogenase enzymes, MDH and α-KDH. 1. Positive control (KdpD-T25/T18-PtsN1), 2. Negative control (empty vector pKNT25/pUT18C), 3. Mdh-T25/T18-ManX, 4. ManX-T25/T18-Mdh, 5. Mdh-T25/T18-ManX, 6. ManX-T25/T18-SucA, 7. SucA-T25/T18-ManX, 8. SucA-T25/T18-ManX, 9. ManX-T25/T18-Mdh. Tested combinations did not yield detectable B2H signals.

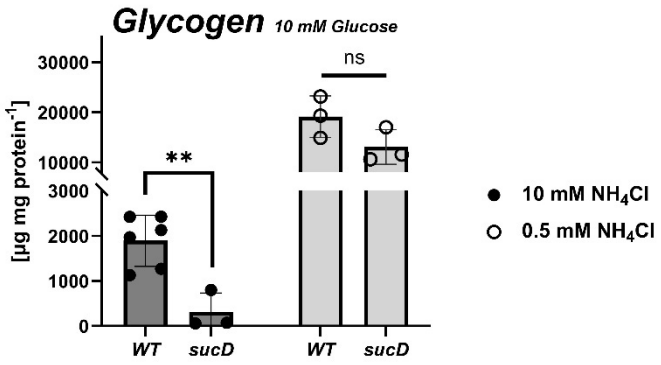

Figure S4. Glycogen quantification in the strain RU116 (*sucD* mutant) compared to wild-type. The strains were grown in liquid UMS cultures supplemented with 10 mM glucose as a carbon source and either 10 mM NH_4Cl (dark grey bars) or 0.5 mM NH_4Cl (light grey bars). Data are averages (±SEM) from 3 replicates. Statistical significances were assessed by Student's t-test, with asterisks indicating the following level of significance: ** $P \leq 0.01$, and ns, not significant.

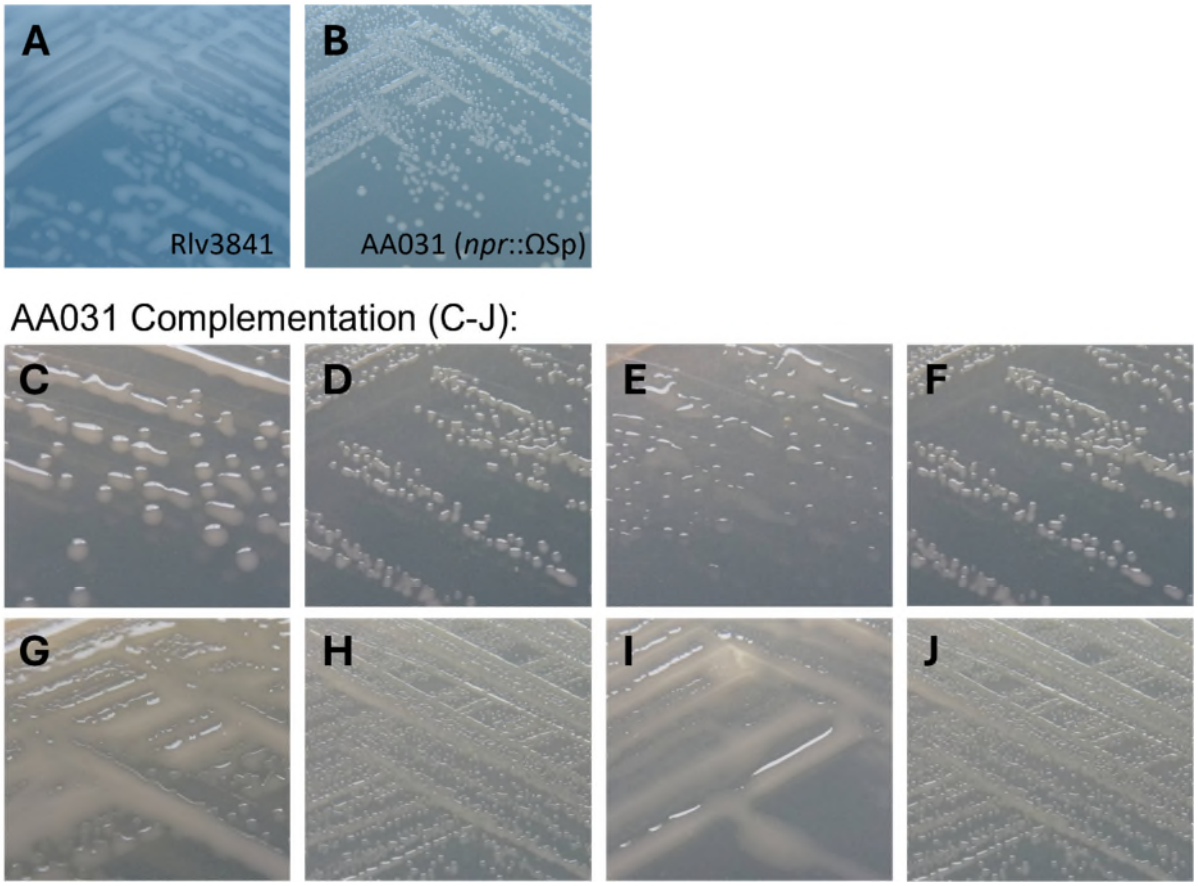

Figure S5. Colony morphology of the *R. leguminosarum npr* mutant and complemented strains on TY agar plates. Surface phenotypes are as follows: (A) Rlv3841 wild-type, mucoid; (B) AA031 (*npr*::ΩSpec), dry; (C, G) AA031(pRK415-*npr*), mucoid; (D, H) AA031(pRK415-*npr* H17A), dry; (E, I) AA031(pRK415-*npr* S48A), very wet; (F, J) AA031(pRK415-*npr* H17A,S48A), dry. Panels (A) and (B) are reproduced from (1). Panels (C-F) are magnified images of colonies grown in panels (G-J) to better appreciate colony morphology and surface mucoidity.

REFERENCES

1. Sánchez-Cañizares C, Prell J, Pini F, Rutten P, Kraxner K, Wynands B, Karunakaran R, Poole PS. 2020. Global control of bacterial nitrogen and carbon metabolism by a PTS^{Ntr}-regulated switch. Proc Natl Acad Sci U S A 117:10234–10245. https://doi.org/10.1073/pnas.1917471117.

2. Hanahan D. 1983. Studies on transformation of *Escherichia coli* with plasmids. J Mol Biol 166:557–580. https://doi.org/10.1016/S0022-2836(83)80284-8.

3. Johnston AWB, Beringer JE. 1975. Identification of the *Rhizobium* strains in pea root nodules using genetic markers. J Gen Microbiol 87:343–350. https://doi.org/10.1099/00221287-87-2-343.

4. Prell J, Mulley G, Haufe F, White JP, Williams A, Karunakaran R, Downie JA, Poole PS. 2012. The PTS^{Ntr} system globally regulates ATP-dependent transporters in *Rhizobium leguminosarum*. Mol Microbiol 84:117–129. https://doi.org/10.1111/j.1365-2958.2012.08014.x.

5. Lodwig EM, Leonard M, Marroqui S, Wheeler TR, Findlay K, Downie JA, Poole PS. 2005. Role of polyhydroxybutyrate and glycogen as carbon storage compounds in pea and bean bacteroids. Mol Plant Microbe Interact 18:67–74. https://doi.org/10.1094/MPMI-18-0067.

6. Untiet V, Karunakaran R, Krämer M, Poole P, Priefer U, Prell J. 2013. ABC transport is inactivated by the PTS^Ntr under potassium limitation in *Rhizobium leguminosarum* 3841. *PLoS One* 8(5):e64682. https://doi.org/10.1371/journal.pone.0064682

7. Knauf VC, Nester EW. 1982. Wide host range cloning vectors: a cosmid clone bank of an *Agrobacterium* Ti plasmid. Plasmid 8:45–54. https://doi.org/10.1016/0147-619X(82)90040-3.

8. Figurski DH, Helinski DR. 1979. Replication of an origin-containing derivative of plasmid RK2 dependent on a plasmid function provided in trans. Proc Natl Acad Sci U S A 76:1648–1652. https://doi.org/10.1073/pnas.76.4.1648.

9. Schäfer A, Tauch A, Jäger W, Kalinowski J, Thierbach G, Pühler A. 1994. Small mobilizable multi-purpose cloning vectors derived from the *Escherichia coli* plasmids pK18 and pK19: selection of defined deletions in the chromosome of *Corynebacterium glutamicum*. Gene 145:69–73. https://doi.org/10.1016/0378-1119(94)90324-7.

10. Poole P, Reid C, East AK, Allaway D, Day M, Leonard M. 1999. Regulation of the *mdh-sucCDAB* operon in *Rhizobium leguminosarum*. FEMS Microbiol Lett 176:247–255. https://doi.org/10.1016/S0378-1097(99)00243-8.

11. Berrow NS, Alderton D, Sainsbury S, Nettleship J, Assenberg R, Rahman N, Stuart DI, Owens RJ. 2007. A versatile ligation-independent cloning method suitable for high-throughput expression screening applications. Nucleic Acids Res 35:e45–e45.

12. Maeda H, Hirata Y, Takahashi H, Watanabe K, Aki T, Okamura Y. 2023. Development of a Transformation System for Nitratireductor sp. Marine Biotechnology 25:644–651.

Statement of Authorship for joint/multi-authored papers for PGR thesis

To appear at the end of each thesis chapter submitted as an article/paper

The statement shall describe the candidate's and co-authors' independent research contributions in the thesis publications. For each publication there should exist a complete statement that is to be filled out and signed by the candidate and supervisor **(only required where there isn't already a statement of contribution within the paper itself).**

Title of Paper	Regulation of central carbon metabolism and storage polymers by PTS^{Ntr} in *Rhizobium leguminosarum*
Publication Status	□Published □ Accepted for Publication □Submitted for Publication ✓ Unpublished and unsubmitted work written in a manuscript style
Publication Details	**Tjahjono, O.**, Wang, J., Turner, E., , Jürgen Prell, Huang, W., Poole, P., Sánchez-Cañizares, C. Regulation of central carbon metabolism and storage polymers by PTS^{Ntr} in *Rhizobium leguminosarum*. In preparation.

Student Confirmation

Student Name:	Olivia Tjahjono		
Contribution to the Paper	I performed the TCA cycle enzyme activity assays and polymer quantification experiments, analysed the data, created figures, and wrote the manuscript.		
Signature		Date	07 October 2025

Supervisor Confirmation

By signing the Statement of Authorship, you are certifying that the candidate made a substantial contribution to the publication, and that the description described above is accurate.

Supervisor name and title: Professor Philip Poole		
Supervisor comments The above statement by Olivia about authorship is a true reflection of the work and authorship.		
Signature 	Date	8th October 2025

This completed form should be included in the thesis, at the end of the relevant chapter.

List of figures constituting my work:

Figure 1: My own work.

Figure 2: My own work.

Figure 3: Panels 3.A-B were performed in collaboration with Evan Turner. Panel 3.C was performed by Evan Turner.

Figure 4: My own work.

Figure 5: I prepared the cultures; Raman analysis was performed by Jingkai Wang.

Figure 6: My own work.

Supplementary Figure S2: Performed in collaboration with Evan Turner.

Supplementary Figure S4: My own work.

CHAPTER 4

PTS^{Ntr} regulates the stringent response to control translation of transport systems in *Rhizobium leguminosarum*

Olivia Tjahjono[1], Alicia Uceda-Heras[1], Denis Shutin[1], Andrzej Tkacz[1], María Palomero-Gómez[1], Sylvie Citerne[2], Francesco Pini[1], Isidro Abreu[1], Jay Mulley[3], Ramakrishnan Karunakaran[3], Raphael Ledermann, Jürgen Prell[3], Ben Field[4], Jani Reddy Bolla[1], Philip Poole[1,3#], Carmen Sánchez-Cañizares[1#]

[1] Department of Biology, University of Oxford, Oxford, UK

[2] Institut Jean-Pierre Bourgin, UMR1318 INRA-AgroParisTech, INRAE Centre de Versailles-Grignon, Université Paris-Saclay, Versailles, France

[3] Department of Molecular Microbiology, John Innes Centre, Norwich Research Park, Norwich, UK

[4]Aix-Marseille University, CEA, CNRS, BIAM, LGBP Team, Marseille, France

Running title: PTS^{Ntr}–RelA nitrogen signalling in *R. leguminosarum*

correspondence to philip.poole@biology.ox.ac.uk and carmen.sanchez-canizares@biology.ox.ac.uk

ABSTRACT (172 words)

The nitrogen phosphotransferase system in *R. leguminosarum* (PTS^{Ntr}) balances carbon and nitrogen metabolism by utilising the output proteins PtsN and ManX, while the master regulator RelA synthesises the alarmone (p)ppGpp in response to stress such as amino acid starvation. Suppressors of a transposon mutant of PtsP, the first component of PTS^{Ntr}, mapped to different domains of RelA. This bifunctional (p)ppGpp synthase/hydrolase acts on cellular processes controlled by PtsN, with RelA being required for free-living activities and a fully functional legume-*Rhizobium* symbiosis. Bacterial two-hybrid and native mass spectrometry revealed that PtsN and RelA physically interact, confirming crosstalk between PTS^{Ntr} and RelA. This interaction alters (p)ppGpp levels, which modulate transcription of the small RNAs AbcR1 and AbcR2 and control translation of the Aap general amino acid transporter. Thus, PTS^{Ntr} signals the intracellular nitrogen balance to RelA, which, via (p)ppGpp synthesis, controls multiple aspects of transcription and translation. These results reinforce the importance of crosstalk between PTS^{Ntr}, RelA and AbcR1/R2 sRNAs, allowing bacteria to respond transcriptionally and post-transcriptionally according to the magnitude of nitrogen stress.

IMPORTANCE (146 words)

Bacteria constantly adapt to fluctuations in their environment to survive. Optimal resource allocation upon nutritional starvation requires efficient control of metabolism to adjust growth by modulating gene expression. We show that the stringent response modulates cell physiology at the transcriptional level in *R. leguminosarum* by sensing the carbon and nitrogen status of central metabolism via interaction with the nitrogen phosphotransferase system (PTS^{Ntr}). The multidomain bifunctional (p)ppGpp synthetase/hydrolase RelA interacts with PtsN~P to enable activation of RelA under nitrogen starvation. Furthermore, RelA is also required for an efficient symbiosis between rhizobia and legumes. The interaction between these regulatory pathways is highly conserved, highlighting the importance of these connections in various bacterial species that inhabit nutrient-limited or highly fluctuating environments like the soil and root environments. This PTS^{Ntr}-RelA-AbcR1/R2 crosstalk allows the cell to grade an adaptive response and maintain fitness depending on the severity of the stress.

KEY WORDS: plant-microbe interactions, bacterial metabolism, regulatory network, nitrogen, stringent response, small RNAs, amino acid transport

INTRODUCTION

Maintaining proper intracellular carbon (C) and nitrogen (N) levels is crucial in cell physiology to maximise nutrient utilisation and cell growth. Equally important for the survival of the cell is the ability to adapt itself to environmental stress. To this aim, bacteria have evolved intricate regulatory networks that coordinate their physiology based on a plethora of internal and external signals of their status. These regulatory networks are typically signal transduction pathways that sense chemical stimuli and drive cellular decision-making in processes such as nutrient uptake, central metabolism, motility and chemotaxis, and the production of surface and internal polymers. These regulatory networks have traditionally been characterised independently, but recent studies have shown the existence of crosstalk [1-4].

Rhizobia are soil-dwelling α-proteobacteria that induce the formation of nodules in legume plants under nitrogen limitation. As free-living cells in soil, they are confronted with diverse and stressful conditions, such as non-optimal temperatures and pH levels, near-starvation conditions, and competition with other microbial populations [5-7]. When they invade root nodules, rhizobia differentiate into specialised forms called bacteroids, which reduce atmospheric dinitrogen to biologically available ammonia and, in exchange, are provided with carbon and energy by the host plant [8, 9]. Therefore, these two lifestyles involve complex microbe-microbe and plant-microbe interactions, requiring signalling pathways and tight metabolic regulation between the host and the bacterium [10, 11]. We have previously shown that PTS^{Ntr} is an essential bacterial regulatory mechanism composed of an initial sensor protein PtsP, a phosphotransfer protein NPr, and two output regulatory proteins, PtsN and ManX [4, 12]. This system is a

77 phosphorylation cascade that is linked to nitrogen metabolism. Glutamine, which
78 signals high intracellular nitrogen, binds to an N-terminal GAF domain in PtsP, thereby
79 inhibiting PTS^{Ntr} autophosphorylation by phosphoenolpyruvate (PEP) [4, 13, 14]. This
80 inhibition downregulates amino acid uptake and upregulates TCA cycle activity,
81 respectively, increasing carbon catabolism to match the nitrogen status of the cell
82 through a carbon and nitrogen switch [4, 12, 15]. In contrast, under nitrogen-limiting
83 conditions, PtsP is phosphorylated (PtsP~P), the phosphate is transferred to the small
84 carrier protein NPr (NPr~P), and subsequently to a conserved histidine residue on the
85 output regulators PtsN (PtsN~P) and ManX (ManX~P). Interacting at the protein:protein
86 level, PtsN and ManX control essential processes for cell survival by modifying enzyme
87 activity or the binding affinity of target proteins, which, in the case of transcriptional
88 regulators, leads to changes in gene expression [2, 16].

89 Another global regulatory system is the stringent response that allows bacteria to
90 respond to amino acid and/or carbon deprivation through the synthesis of the alarmone
91 (p)ppGpp (guanosine penta- or tetra-phosphate). During nutrient stress, (p)ppGpp levels
92 increase significantly, leading to the repression of genes associated with rapid growth.
93 The accumulation of the alarmone arrests growth and helps in reallocating cellular
94 resources by reprogramming transcription and increasing the expression of stress-
95 responsive genes to ensure a timely cell adaptation and survival to nutrient downshift
96 [17-19]. In bacteria, (p)ppGpp also regulates translation, lowering ribosome abundance
97 and global translation [20]. Intracellular concentrations of (p)ppGpp are determined by
98 a highly conserved and widely distributed family of proteins called RelA-SpoT Homologs
99 (RSH). Whereas in *E. coli* the (p)ppGpp level is determined by the activities of two

paralogous enzymes: RelA, which synthesises (p)ppGpp in response to amino acid starvation (EC:2.7.6.5), and SpoT, responsible for the hydrolysis of this nucleotide (EC:3.1.7.2), α-proteobacteria involved in host-microbe interactions mainly harbour a single long bifunctional RelA-like protein that produces and degrades (p)ppGpp [21, 22]. A crosstalk between PTS^{Ntr} and RelA was found in *Caulobacter crescentus* and *Ralstonia eutropha*. In *C. crescentus,* low glutamine levels relieve glutamine-binding to PtsP, resulting in increased PtsN~P , and stimulating (p)ppGpp accumulation by modulating the synthetase and hydrolase activities of the RSH homolog (SpoT) [3, 18]. Whereas PtsN~P inhibits the hydrolase activity of SpoT in *C. crescentus* by binding to its ACT (Aspartokinase, Chorismate mutase and TyrA) domain [18], in the β-proteobacteria *R. eutropha,* non-phosphorylated PtsN interacts with the (p)ppGpp hydrolase SpoT1, which gets activated and triggers intermediate levels of ppGpp when nitrogen becomes available, integrating the nutritional status into the stringent response via PTS^{Ntr} [23].

ATP-binding cassette (ABC) transporters have been found among the targets controlled by PTS^{Ntr} [4, 12, 24, 25] and are also known to be upregulated under nitrogen limitation through a stringent response-dependent mechanism [17-19]. In *R. leguminosarum* and the related α-proteobacteria *Agrobacterium tumefaciens and Sinorhizobium meliloti*, mutations in the RNA chaperone *hfq* led to the misregulation of many ABC transporters [26-28]. The best-characterised Hfq-mediated small RNAs (sRNAs) in this role are the AbcR1-family sRNA (AbcR1/2), which uses conserved anti-Shine–Dalgarno motifs to silence the mRNAs of periplasmic binding proteins (PBPs) and permease subunits of ABC transporters [29, 30]. AbcR1, but not AbcR2, downregulates the expression of the periplasmic substrate-binding protein Atu2422 [27] in *A. tumefaciens,* and LivK in *S.*

meliloti [30]. Both proteins are orthologs of the branched-chain amino acid binding protein BraC (RL3745) in *R. leguminosarum*. Another study confirmed that the overexpression of AbcR1 or AbcR2 reduces *aapQ* transcript levels in *S. meliloti* [29], and hundreds of other potential targets were identified through MS2 affinity purification coupled with RNA sequencing (MAPS). Furthermore, the same study demonstrated that expression of AbcR1 and AbcR2 requires transcriptional factors LsrB and RpoH1, respectively. In mutants lacking these proteins, the expression of AbcR1 or AbcR2 was undetectable by Northern blot analysis.

Altogether, these findings suggested the existence of a global crosstalk acting through different regulatory mechanisms and modulated by nitrogen availability. Given the importance of metabolic control in the *Rhizobium*-legume symbiosis, we investigate in this work how the regulatory crosstalk between PTS^{Ntr}, RelA and the sRNAs AbcR1/AbcR2 allows the cells to orchestrate a comprehensive response to nutrient deprivation in *Rhizobium leguminosarum* bv. *viciae* 3841 (Rlv3841). We confirm RelA as an interacting component of PTS^{Ntr}, and show how this crosstalk occurs by RelA directly binding to PtsN~P. We also characterise the effects caused by a mutation in the *R. leguminosarum relA* gene, which is required for free-living adaptation to amino acid starvation and for establishing a functional symbiosis. Finally, (p)ppGpp measurements suggest a hierarchical signalling cascade from PTS^{Ntr}, RelA, and downstream amino acid transporters mediated by the small RNAs AbcR1 and AbcR2. Overall, this is the first study to simultaneously characterise all the molecular components underlying this regulatory crosstalk. The convergence of PTS^{Ntr}, RelA and AbcR1/2 sRNAs to signal the intracellular

nitrogen balance in *R. leguminosarum* illustrates the plasticity of the regulatory network controlling α-proteobacterial metabolism.

RESULTS

ptsP suppressor mutants appear when growing the *ptsP* mutant on aspartate

The ability of PtsN and ManX to interact with their partner proteins is regulated by their phosphorylation state. We previously showed that disruption of PTS^{Ntr} phosphorylation has pleiotropic effects, affecting cellular processes such as central metabolism, nutrient uptake and cell surface polymers [4, 12]. When grown on agar plates, PTS^{Ntr} mutants *ptsP, npr*, or *ptsN1N2* have a dry surface phenotype compared to wildtype, which is linked to a lower EPS production [4, 12]. When analysing the effect of PTS^{Ntr} mutations on growth, we observed that the *ptsP* Tn5 insertion mutant (PtsP107) can use aspartate as its sole nitrogen source only when dicarboxylates are absent. This is because aspartate uptake occurs via two routes:the dicarboxylate transport system (Dct), which is competitively blocked by the carbon source succinate [31], and via the ABC-type amino acid permeases Aap and Bra, whose activity is inhibited by the absence of PtsN~P [4, 12]. However, when PtsP107 was forced to grow by prolonged incubation on agar plates with UMS minimal medium supplemented with 20 mM succinate as the carbon source and 10 mM aspartate as the sole nitrogen source, several colonies with wild-type mucoid phenotype arose. This restrictive condition blocks Dct-mediated transport by succinate, forcing growth to depend solely on Aap-mediated aspartate uptake (**Supplementary Fig. S1**). These colonies retained the original Tn5 insertion, indicating the presence of a second-site suppressor mutation that presumably restores aspartate transport by compensating for the PtsN-dependent, Aap-mediated transport

in the PtsP107 background. Crucially, when these suppressor mutants were tested for amino acid transport using ^{14}C-radiolabelled α-aminoisobutyric acid (AIB), they recovered transport rates to similar levels to the wildtype (**Fig. 1**). Additionally, these suppressors also recovered the wildtype surface phenotype (**Supplementary Fig. S2**). Thus, this secondary mutation appears to have a global effect, altering uptake, growth and surface mucoidy, suggesting increased EPS production and amino acid transport.

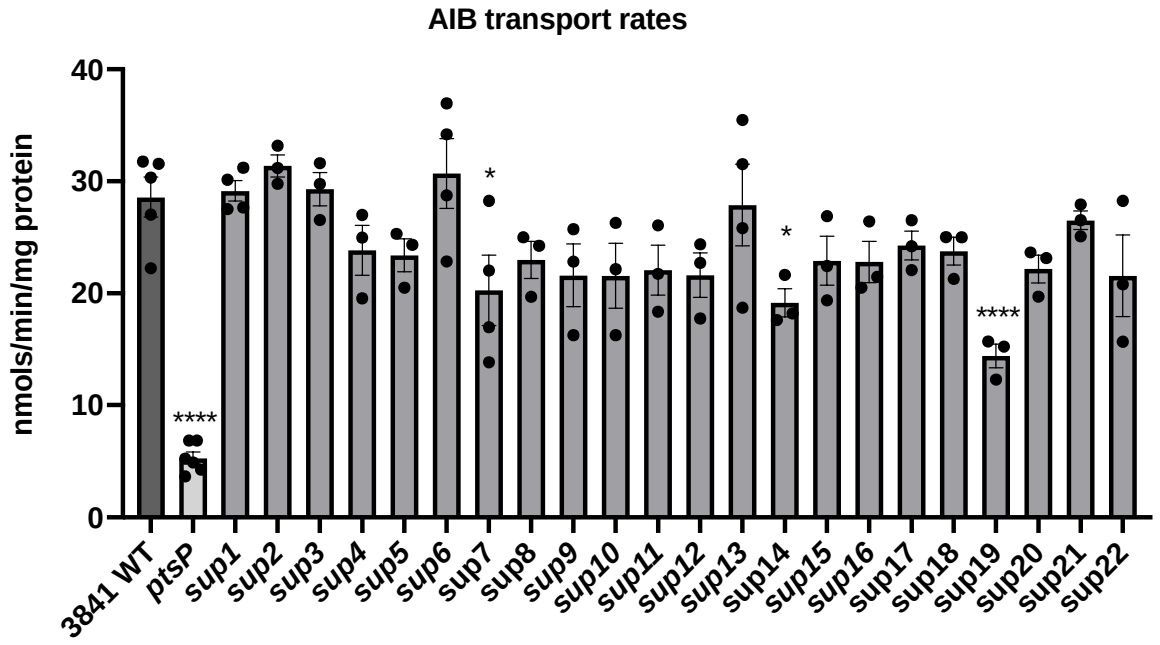

Figure 1. Amino acid transport rates. Standard rates obtained from cultures grown on UMS with 10 mM glucose and 10 mM NH_4Cl. Rlv3841 wildtype, *ptsP* (PtsP107), and the different *ptsP* suppressor isolates (1-22). AIB, α-aminoisobutyric acid. All rates are expressed in nmol min^{-1} mg protein^{-1}. Data are averages (±SEM) from biologically independent cultures (n = 5 for 3841 WT, n=6 for *ptsP*, n=4 for sup1, and n=3 for sup 2-22). Statistical significance was analysed by 1-way ANOVA with Dunnett's post-test for multiple comparisons with (****) $p < 0.0001$, (*) $p < 0.1$, and no asterisks denoting not significant.

RelA was identified as an interacting partner of PTS^{Ntr} in *R. leguminosarum*

Whole-genome sequencing of 20 *ptsP* suppressor mutants revealed SNPs (Single Nucleotide Polymorphisms) mutations exclusively restricted to the gene encoding RelA (RL1506), listed in **Table 1**. All SNPs in the *relA* gene were confirmed by Sanger sequencing, with the genomes of the wildtype strain Rlv3841 and the *ptsP* original mutant (PtsP107) being also sequenced as experimental controls (see **Supplementary Table 1** for sequencing data and statistics).

Table 1. SNPs identified in *ptsP* suppressor mutants. All SNPs map to *relA*.

Residue positions[a]	NCBI Rlv3841 RelA sequence	Mutation found	Suppressor genome sequence ID	Suppressor isolate number[b]
37	Q (CAA)	L (CTA)	3566 & 3579	9 and 22
101	T (ACC)	I (ATC)	3578	21
115	Q (CAG)	P (CCG)	3562	5
119	L (CTG)	P (CCG)	3573	16
142	H (CAC)	R (CGC)	3564	**7**
143	N (AAT)	S (AGT)	3561	4
162	T (ACG)	A (GCG)	3576	19
216	I (ATC)	M (ATG)	3570	13
294	D (GAC)	N (AAC)	3577	**20**
318	R (CGC)	H (CAC)	3575	18
368	I (ATC)	N (AAC)	3563	6
379	E (GAA)	K (AAA)	3567	10
381	L (CTC)	R (CGC)	3574	17
406	P (CCG)	L (CTG)	3566 & 3579	9 & 22
428	G (GGC)	D (GAC)	3568	11
445	G (GGC)	R (CGC)	3560	**2**
471	A (GCG)	V (GTG)	3569	12
563	W (TGG)	STOP (TGA)	3572	15
741	R (CGC)	L (CTC)	3571	14

(a) Colour code denotes the different domains of RelA as indicated in Fig. 2, with residues in black found in interdomain regions. (b) Suppressors selected for follow-up work are marked in bold.

194 α-Proteobacteria encode a single bi-functional synthetase/hydrolase RSH (RelA/SpoT
195 homologue) enzyme [21]. This is the case for *R. leguminosarum,* in which the long RSH
196 protein contains an N-terminal enzymatic domain and a C-terminal regulatory domain
197 [32]. The Rlv3841 *relA* gene encodes a protein of 744 amino acids and contains five
198 different domains (**Fig. 2A**): the hydrolase domain (HD, 26-176 aa, indicated in red) with
199 3'-pyrophosphatase activity that degrades (p)ppGpp to GDP/GTP and a RelA_SpoT-like
200 (p)ppGpp synthetase domain (SYNTH, 236-347 aa, shown in green), both located
201 towards the N-terminus; a RelA/SpoT_AH_RIS binding domain between the C-terminal
202 region and the ribosome (463-652 aa, shown in dark blue), and the nucleotide-binding
203 region TGS (ThrRS, GTPase and SpoT, 393-452 aa, shown in yellow) and ACT regulatory
204 domain (Aspartokinase, Chorismate mutase and TyrA, 663-741 aa, in light blue) at the C-
205 terminal end. We mapped the SNP mutations onto the RelA sequence and used
206 Alphafold to predict RelA structure (**Fig. 2A, B**) [33]. Interestingly, the SNPs identified
207 covered all the domains of the protein, with the highest number of changes found in the
208 HD, SYNTH and TGS domains and the lowest in the RIS and ACT domains, with the ACT
209 domain shown to interact directly with the phosphorylated version of (PtsN∼P), inhibiting
210 the hydrolase activity of RelA in *C. crescentus* [18].

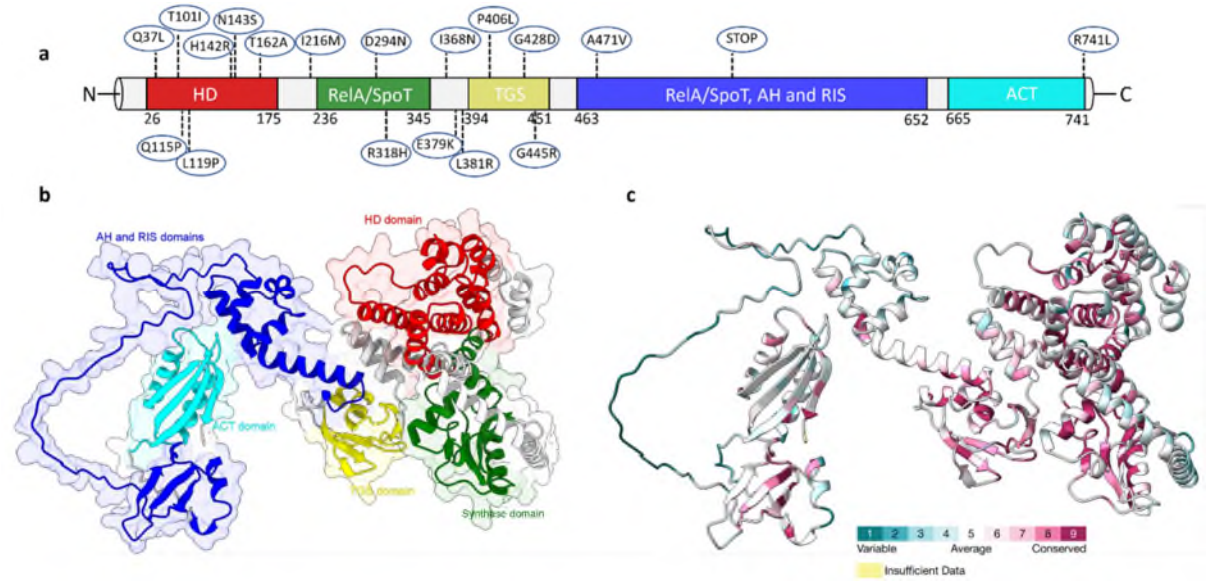

211

212 **Figure 2. Sequence and structural analysis of *R. leguminosarum* RelA. (a)** Sequence-
213 level domain organisation of Rlv3841 RelA. Domain arrangement identification based on
214 Pfam database model prediction: RelA/SpoT (SYNTH): ppGpp synthetase (EC:2.7.6.5);
215 HD: ppGpp phosphohydrolase (EC:3.1.7.2); TGS (PF02824) is a nucleotide-binding
216 region; AH/RIS: Alpha Helical and Ribosome-Inter Subunit, and the ACT regulatory
217 domain (PF01842). SNPs identified are indicated with the amino acid substitution and
218 position in the protein. **(b)** Cartoon representation of Alphafold predicted structure of
219 Rlv3841 RelA with different domains highlighted in different colours. **(c)** Alphafold
220 predicted structure of Rlv3841 RelA with residues coloured according to their degree of
221 conservation, using the colour-coded conservation scale: cyan (variable) to magenta
222 (fully conserved).

223 To further understand the nature of these suppressor mutants, we performed sequence
224 conservation analysis on *R. leguminosarum* RelA between different RelA sequences
225 across bacteria with 25-95% seq. ID to Rlv3841 RelA. Conservation analysis shows that
226 several residues, identified as suppressor mutants, are highly conserved, in particular
227 the Q37, T101, Q115, H142, N143, D294, E379, P406, G428, G445, A471, and R741,
228 suggesting that mutations may occur with comparably low frequency (**Fig. 2C** and
229 **Supplementary Fig. S3**).

relA secondary mutations are gain-of-function

To further confirm our results and test whether these point mutations resulted in a phenotypic gain or loss of function, three different versions of RelA were chosen, harbouring mutations in the main functional domains of the protein: suppressor 2 (TGS domain, G445R), 7 (HD domain, H142R) and 20 (SYNTH domain, D294N). These modified RelA versions and the wildtype gene were cloned into mTn7 vectors and integrated into the wildtype strain and the original *ptsP* Tn5 insertion mutant (PtsP107) as a single copy. All the RelA variants tested complemented PtsP107 as predicted by the protein model. PtsP107 retained the original dry phenotype and small colonies when the wildtype copy of *relA* was introduced as a control (**Supplementary Fig. S4**). We carried out the same mini-Tn7 complementation assay in Rlv3841, but no change was observed. This assay confirmed that the SNPs mutations were gain-of-function, and these suppressor mutants recovered the wildtype phenotype for amino acid transport and EPS production.

relA mutant phenocopies *ptsP* in free-living and symbiotic conditions

To determine the physiological role of the *R. leguminosarum* RelA, an ΩSpec marker was introduced with a *sacB* suicide vector into the *R. leguminosarum relA* gene to generate a stable *relA* mutant (OPS1097). OPS1097 exhibited a dry surface phenotype, resembling PtsP107 [4, 12], which was fully restored upon *relA* complementation (**Fig. 3A**), indicative of lower EPS production (**Fig. 3B**; p=0.0412 for *relA*, p=0.0024 for *ptsP*). Overall, *ptsP* and *relA* mutants displayed highly similar phenotypes across multiple PTS^{Ntr}-regulated functions linked to central metabolism [34], including reduced swimming motility on agar plates (**Fig. 3C**), growth (**Supplementary Fig. S5**) and oxygen consumption rates (**Fig. 3D**). Both mutants also showed a collapse in amino acid transport rates (**Fig. 3E**),

253 and this was also restored by single copy complementation by *relA* (RL1506 gene
254 sequence) integrated with Tn7 (strain OPS3331) into the original *relA* mutant (OPS1097).
255 The ability to restore both the mucoid Rlv3841 surface phenotype and transport rates
256 indicated that only the RelA protein was implicated in these phenotypes (**Fig. 3A, E**). The
257 (p)ppGpp alarmone has also been shown to be required for an effective symbiosis in *R.*
258 *etli* [35, 36], and this was also true for *R. leguminosarum*. Despite having similar nodule
259 numbers, the *relA* mutant showed reduced acetylene reduction (ARA) activity, indicating
260 impaired nitrogen fixation ability (**Fig. 3F**), as observed in the *ptsP* mutant.

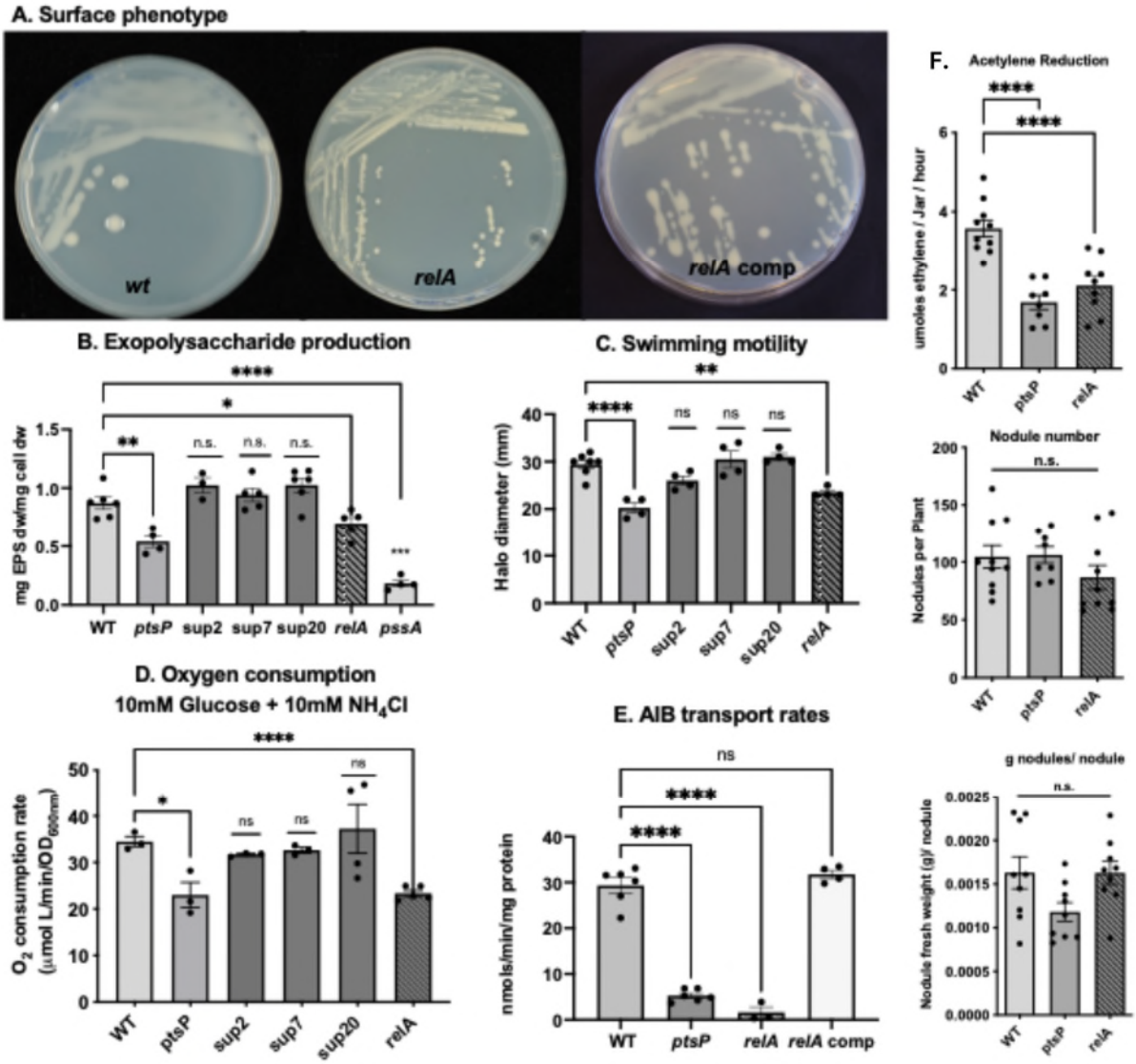

Figure 3. *relA* mutant phenotype in free-living conditions. (**A**) Surface phenotype on representative agar plates for wildtype, *relA* mutant and *relA* complemented strains. (**B**) EPS production measurements for Rlv3841 wildtype, *ptsP* (PtsP107), *ptsP* suppressors 2, 7 and 20 (LMB163-S2; G445R, ptsP107-S4; H142R, pstP107-S17; D294N), *relA* (OPS1097), and *pssA* (LMB310) EPS mutant as control. Data are averages (±SEM) from at least 4 independent cultures analysed by 1-way ANOVA with Dunnett's post-test for multiple comparisons (*) $P < 0.01$, (**) $P < 0.01$ and n.s., not significant. All rates are expressed in mg EPS dry weight mg^{-1} cell dry weight. **(C)** Swimming motility on UMS 0.22% agar plates (**D**) O_2 consumption assay on UMS supplemented with 10 mM glucose + 10 mM NH_4Cl for Rlv3841 wildtype, *ptsP* (ptsP107), suppressors 2, 7 and 20 and *relA* (OPS1097). O_2 consumption rates are expressed in µmol L^{-1} min^{-1} OD_{600nm}^{-1}. Data are averages (±SEM) from at least three independent cultures; 2-way ANOVA with Dunnett's

post-test for multiple comparisons (**E**) Membrane transport of AIB in wildtype cells (3841 WT), *ptsP* mutant (PtsP107), *relA* mutant (OPS1097) and *relA* complemented (OPS3331) grown on UMS with 10 mM glucose as the carbon source and 10 mM NH_4Cl. Data are averages (±SEM, n=3 independent cultures). **(F)** Symbiotic phenotype: acetylene reduction assay, nodule number and weight measured at 21 days post-inoculation (dpi) for Rlv3841 wildtype, *ptsP* (PtsP107), and *relA* (OPS1097) mutants. Data are averages (±SEM) from at least 8 plants inoculated with independent cultures. Statistical analyses are indicated following the level of significance, (*) $P < 0.05$, (**) $P < 0.01$, (***) $P < 0.001$, (****) $P < 0.0001$, and (n.s.) not significant.

One of the reasons that could explain the defective symbiotic phenotype could be that RelA is required for growth at low oxygen, as predicted in a whole genome InSeq mutagenesis screen carried out previously in UMS with 10 mM glucose or 20 mM succinate as carbon sources and 10 mM NH_4Cl as nitrogen source [37]. The response to oxygen limitation is crucial in rhizobia because microoxic conditions prevail inside root nodules, where symbiotic nitrogen fixation occurs [38]. Thus, RelA may be involved in regulating the stress response to oxygen limitation in Rlv3841. We looked first for the presence of the anaerobox sequence TTGAT-N_4-ATCAA [39, 40], corresponding to the binding site of the oxygen-responsive transcriptional factor FnrN-, upstream of the *relA* or the PTS^{Ntr} genes, but we found no anaeroboxes in these promoter regions. To assess the requirement for RelA under microaerobic conditions, we monitored bacterial growth at 1% oxygen compared with 21%. Both *ptsP* and *relA* mutants showed reduced growth at 21% and were also impaired in low oxygen when grown in glucose (**Supplementary Fig. S6**), being able to reach the same levels as wildtype after 48h, thus suggesting delayed growth rather than complete inability to grow. This growth defect was rescued when the *relA* mutant was complemented. These data therefore suggest that RelA and

PtsP contribute to optimal bacterial growth under both aerobic and microaerobic conditions, particularly during the early stages of growth. The lack of an anaerobox suggests that the oxygen-related growth defect for *relA* and *ptsP* is not due to a classical anaerobic gene regulation mechanism but instead to a more general metabolic response.

RelA interacts directly with PtsN~P

As the phenotypes restored in the suppressor mutants were linked to the role of PtsN (i.e. nutrient uptake, surface mucoidity or motility), we tested whether RelA was directly interacting with this regulatory protein. Initially, using Bacterial Two-Hybrid (BACTH) assays, we saw that $PtsN_1$ was able to bind to RelA – which is presumably phosphorylated in *E. coli* under these conditions (**Fig. 4A**). We then tested the two different versions of $PtsN_1$ that replaced the conserved histidine residue where NPr phosphorylation occurs with either a permanent phosphorylation mimic (H66D) or a non-phosphorylatable substitution (H66A). Although the $PtsN_1$-H66A mutant retains the ability to interact with RelA, the interaction seemed stronger with the phosphorylated mimic $PtsN_1$-H66D (**Fig. 4A**).

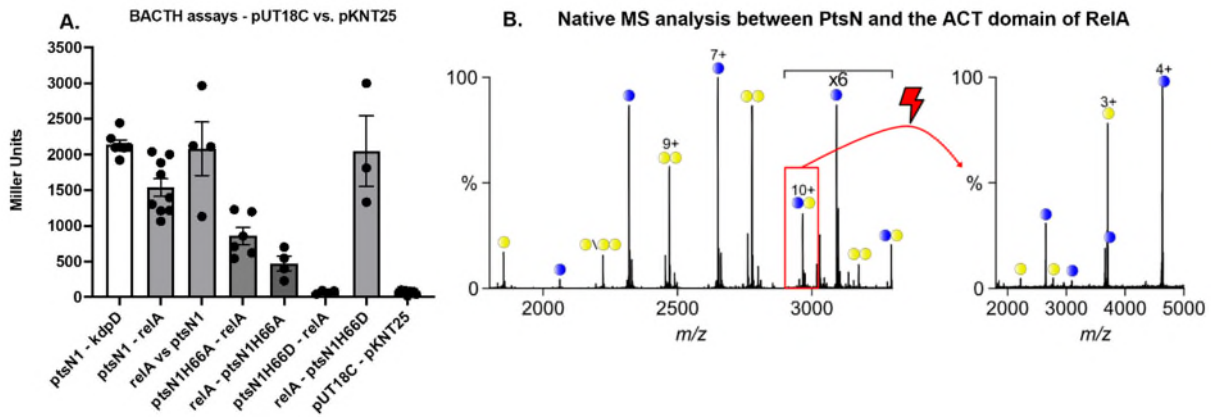

Figure 4. Protein-protein interaction shown between $PtsN_1$ and RelA. (A) Bacterial Two-Hybrid (BACTH) assays of the interaction of $PtsN_1$ with RelA. Interactions expressed in Miller units of LacZ activity. $PtsN_1$-KdpD is the positive control, and pUT18C-pKNT25 is

318 the empty vector negative control. Data are averages (±SEM) from at least 3 independent
319 cultures. **(B)** Native mass spectrum (left) of a complex between $PtsN_1$ (blue) and the ACT
320 domain of RelA (yellow). The region containing the complex is magnified 6 times as
321 indicated. Dissociation (right) of the 10+ charge state of the complex confirmed its
322 composition.

323 To further confirm that PtsN interacts directly with RelA, both Rlv3841 $PtsN_1$ and the ACT
324 domain of RelA were expressed in *E. coli*, as attempts to obtain the full-length protein
325 were unsuccessful due to precipitation. The interaction between them was then studied
326 using native mass spectrometry (**Fig. 4B**). The formation of a complex between $PtsN_1$ and
327 the ACT domain was observed and confirmed by tandem mass spectrometry, although
328 a large fraction of both proteins remained unbound. $PtsN_1$~P was also present, indicating
329 that the PTS systems in *E. coli* are able to phosphorylate *Rhizobium* PtsN; a similar
330 phenomenon was previously observed for *Caulobacter* PtsN in *E. coli* [3]. Consistently,
331 the ACT domain interactions were also tested with the different mutant versions of $PtsN_1$
332 (H66D and H66A), and binding of both $PtsN_1$-H66D and $PtsN_1$-H66A to the ACT domain
333 was observed (**Supplementary Fig. S7A, S7B**), regardless of the $PtsN_1$ phosphorylation
334 status. This differs from observations in *C. crescentus*, where the ACT binding is
335 dependent on phosphorylation [18]. Analysis of the isolated ACT domain may alter
336 protein conformation or accessibility, leading to a reduction in the phosphorylation
337 specificity observed in the full-length RelA protein.

(p)ppGpp measurements correlate with amino acid transport rates in *R. leguminosarum*

Given the role of RelA as the key enzyme in the synthesis of (p)ppGpp and its signalling interaction with PtsN, we next sought to determine whether nitrogen availability also modulates the intracellular levels of (p)ppGpp and if this regulation is mediated by PTS^{Ntr}. The mutants of *relA, ptsP* and its suppressors (*ptsP* sup 2, 7, and 20), *ptsN$_1$N$_2$*, *ptsN$_1$* H66D, and *ptsN$_1$* H66A were evaluated for their ability to produce (p)ppGpp in free-living cultures, measured with HPLC–MS/MS as described previously [41]. We observed no detectable signal for the *relA* mutant and a 2.5x increased production under nitrogen starvation (0.5mM NH_4Cl) in Rlv3841 wildtype (**Fig. 5A**), consistent with previous studies on other species [3, 42]. Whereas *ptsP* exhibited an approximately 75% reduction of (p)ppGpp levels compared to the wildtype, all three suppressors recovered wildtype levels. (p)ppGpp was not detected in *ptsN,* but it was present at lower levels (about 43% of the wildtype) in its unphosphorylated version ($ptsN_1$H66A) and increased to 154% in its phosphorylated version ($ptsN_1$H66D). These findings suggest that the phosphorylation of $PtsN_1$ favours a functionally productive interaction with RelA and increases(p)ppGpp levels. This aligns with previous findings in *C. crescentus*, where strains with mutated PtsN or other conditions that prevent PtsN phosphorylation (e.g. *ptsP* mutant) exhibited increased (p)ppGpp hydrolysis [3]. Further comparison of (p)ppGpp levels with the transport rates of AIB (**Fig. 5B**) shows that both measurements follow the same trend, indicating a crosstalk and shared regulatory mechanisms.

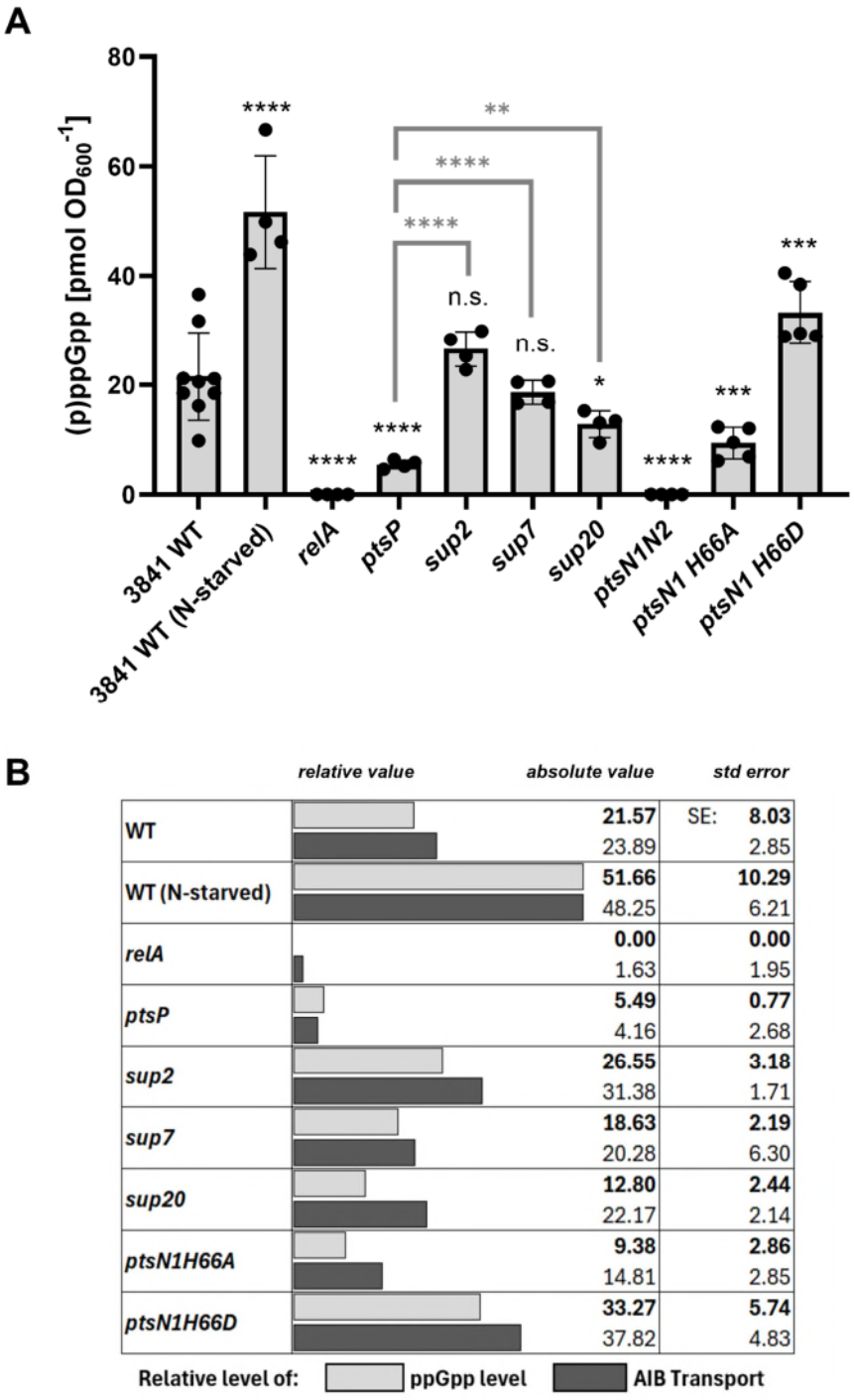

Figure 5. (p)ppGpp levels in *relA* and PTS^{Ntr} mutants compared to AIB transport rates. **(A)** Guanosine tetraphosphate ((p)ppGpp) levels in *relA* (OPS1097), *ptsP* (ptsP107), *ptsP* suppressors 2, 7, and 20 (LMB163-S2; G445R, ptsP107-S4; H142R, and pstP107-S17; D294N), *ptsN$_1$N$_2$* (AA047), *ptsN1*H66A (OPS1102), and *ptsN$_1$*H66D (OPS1104) wer quantified using 13-(p)ppGpp internal standards. Cultures were grown to the exponential phase on UMS supplemented with 10 mM glucose and 10 mM NH_4Cl, except WT (N-

starved) with 0.5 mM NH_4Cl. All values are expressed in pmol OD_{600nm}^{-1}. Data are averages (±SEM) from at least four independent cultures. Statistical significances were assessed by two independent one-way ANOVA, with asterisks indicating the following level of significance, (*) P < 0.05, (**) P < 0.01, (***) P < 0.001, (****) P < 0.0001, and (n.s.) not significant. Black asterisks indicate comparisons to the wild type, whereas grey asterisks represent comparisons to the *ptsP* mutant. These comparisons were calculated separately. **(B)** Comparison table of (p)ppGpp levels and AIB transport rates in various strains. AIB transport values for *ptsN₁N₂*, *ptsN1* H66A, and *ptsN₁* H66D were obtained from [4]. Absolute values for (p)ppGpp are expressed in pmol OD_{600nm}^{-1} and transports in nmol min^{-1} mg^{-1} protein. Bars indicate the relative values.

RelA orchestrates cellular adaptation by acting at different regulatory levels

To further characterise the PTS^{Ntr} - RelA transcriptional crosstalk, we tested the expression profile of genes previously reported to be regulated by (p)ppGpp as downstream targets of RelA. A *R. etli relA* mutant that prevented (p)ppGpp accumulation showed reduced nodulation ability due to deregulation of Nod factor production, demonstrated by a *nodA::lacZ* fusion [36]. *nodA* expression in this *relA* mutant was constitutive, as opposed to the wildtype, where it was expressed only after induction by naringenin, a flavonoid required to activate nodulation (*nod)* genes. In Rlv3841, a *nodA::lux* fusion (pLMB712) showed that the absence of *relA* significantly increases the expression of *nodA* after induction by naringenin (**Fig. 6A**), whereas no constitutive expression was observed without naringerin (**Supplementary Fig. S8**). Stress is also known to regulate quorum sensing in rhizobia. (p)ppGpp accumulation starts immediately after a shift to carbon or nitrogen starvation. In these conditions, the regulatory gene *sinR* was induced in a RelA-dependent manner in *S. meliloti* [43]. In *R. etli, N*-acyl homoserine lactone (AHL) accumulation and expression of the quorum-

390 sensing signal synthase genes *cinI* and *raiI* were reduced in a *relA* mutant [35].
391 Accordingly, the expression of a *cinI::lux* fusion (pOPS2016) in the Rlv3841 *relA* mutant
392 was also reduced (**Fig. 6B**). This reduction was also seen for the *ptsP* mutant, whereas
393 there was no transcriptional effect in the suppressor mutants. Finally, as mutants with a
394 disrupted PTS^{Ntr} phosphorylation cascade have a dry surface compared to wildtype, and
395 the Rlv3841 *relA* mutant also showed this phenotype on agar plates [4, 12], we also
396 measured the expression of *pssA*, a gene essential for exopolysaccharide biosynthesis.
397 A *pssA::lux* fusion (pOPS1000) showed reduced expression for both the *relA* and the *ptsP*
398 mutants, but no transcriptional effect in the *ptsP* suppressor mutants (**Fig. 6C**). These
399 results confirm that RelA (RL1506) alters transcription in *R. leguminosarum*.

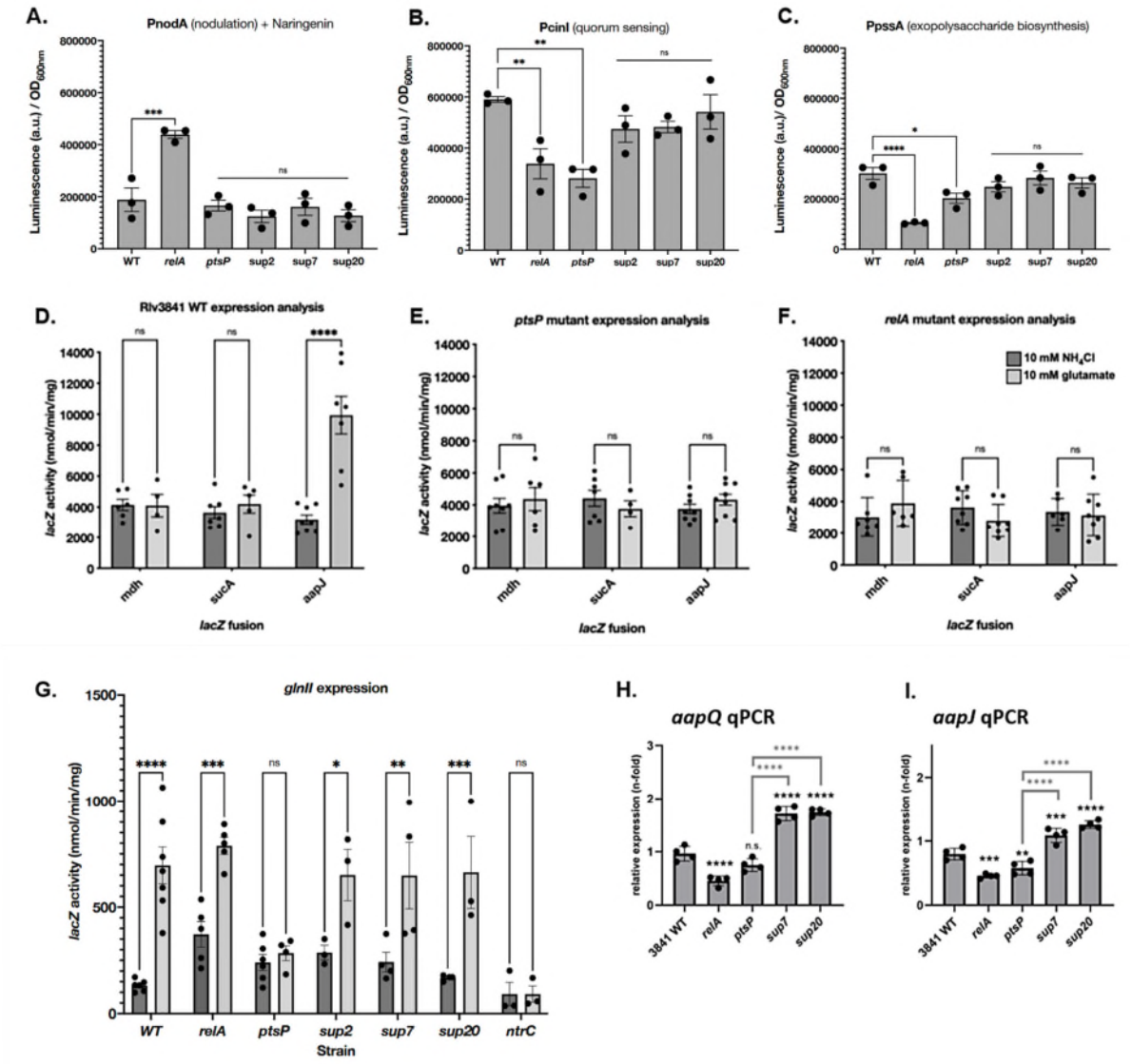

400

401 **Figure 6. Expression analysis of key genes. (A-C)** Quantification of promoter activity for
402 *nodA*, *cinI* and *pssA* measured by *lux* activity in Rlv3841 wildtype, *ptsP* (PtsP107), *relA*
403 (OPS1097), and *ptsP* suppressors 2, 7, and 20 (LMB163-S2; G445R, ptsP107-S4; H142R,
404 and pstP107-S17; D294N). All rates are expressed in luminescence arbitrary units
405 relative to OD_{600nm}. Cultures are grown in UMS supplemented with 10 mM glucose and 10
406 mM NH_4Cl. Data are averages (±SEM) from 3 independent cultures. **(D-F)** Quantification
407 of promoter activity for *mdh*, *sucA* and *aapJ* measured by *lacZ* activity in cosmids
408 introduced in Rlv3841 wildtype, *ptsP* (PtsP107), and *relA* (OPS1097) in 10 mM NH_4Cl (N-
409 rich, dark grey) and 10 mM glutamate (N-poor, light grey). All rates are expressed in
410 nmol/min/mg. Data are averages (±SEM) from at least 5 independent cultures. **(G)**
411 Quantification of promoter activity for *glnII* cloned in pMP220 expression vector and
412 introduced into Rlv3841 wildtype, *ptsP* (PtsP107), *relA* (OPS1097), *ptsP* suppressors 2, 7,

and 20 (LMB163-S2, ptsP107-S4, ptsP107-S17), and *ntrC* mutant. For each strain, bars compare growth under N-rich (dark grey) and N-poor (light grey) conditions. **(H-I)** qPCR done for *aapQ* and *aapJ* in Rlv3841 wildtype, *ptsP* (PtsP107), *relA* (OPS1097), and *ptsP* suppressors 2, 7, and 20 (LMB163-S2, ptsP107-S4, ptsP107-S17). Statistical analyses are indicated following the level of significance, with (****) as p-value <0.0001, (***) as p-value <0.001 and n.s., not significant.

The pleiotropic phenotypes of both *ptsP* and *relA* mutants indicated that PTS^{Ntr} and RelA act on common cellular processes and control similar genes involved in essential metabolic processes and stress adaptation through different regulatory mechanisms. We carried out different transcriptional assays using promoter-reporter fusions in the *ptsP* and *relA* mutant backgrounds to assess the expression of the genes encoding the TCA cycle enzymes *mdh::lacZ* (pRU3070) and *sucA::lacZ* (pRU3068), and the amino acid transporter *aapJ::lacZ* (pRU3028), in different nitrogen conditions (10 mM NH_4Cl, as N-rich with unphosphorylated PTS^{Ntr}, and 10 mM glutamate as N-limiting with phosphorylated PTS^{Ntr}). As expected, transcriptional upregulation of the TCA enzymes was independent of PTS^{Ntr}, with no changes observed in the *ptsP* mutant (**Fig. 6E**). Despite a severe decrease in amino acid transport observed in the ptsP mutant, the *aapJ* transcript level remains unchanged compared with WT under N-rich conditions. In N-poor conditions, *aapJ* transcription is not upregulated in the *ptsP* mutant. Notably, the transcriptional response observed in the *relA* mutant for any of the three genes under study matches the trend observed in the *ptsP* mutant (**Fig. 6F**). The *ptsP* suppressor mutants also showed the same *aapJ, mdh or sucA* expression profiles as the original *ptsP* mutant, indicating that their phenotypic differences might be the result of post-

436 transcriptional interactions rather than changes in the promoter activity
437 (**Supplementary Fig. S8**).

438 The only promoter-dependent upregulation observed in wild-type cells grown under N-
439 poor conditions was *aapJ* (Fig. 6D), suggesting regulatory control by another major
440 nitrogen metabolism regulator, potentially the Ntr system. Ntr is a candidate regulator
441 because it is activated under nitrogen limitation and has previously been shown to
442 control expression of amino acid transport genes, including the *aap* system, in response
443 to nitrogen availability [44]. To examine this possibility, we examined *glnII* promoter
444 activity, the gene encoding glutamine synthase II (GSII), a direct transcriptional target of
445 phosphorylated NtrC, and included the *ntrC* mutant as a control. We observed that *glnII*
446 expression was not altered in the *relA* or suppressor mutants, as transcription increased
447 under N-limiting conditions (**Fig. 6G**). However, this response was absent in the *ptsP*
448 mutant, suggesting a link to the Ntr system, which may become important under
449 nitrogen-limiting conditions. We then performed qPCR analysis on the *aapQ* and *aapJ*
450 genes under N-rich conditions, and this resulted in lower relative expression in the *relA*
451 mutant and higher levels in suppressors 7 and 20 (**Fig. 6H, I**). This suggested different
452 transcript levels despite wildtype level promoter activity, pointing again to post-
453 transcriptional regulation. Overall, whereas RelA alters transcription initiation at the
454 promoter level presumably via (p)ppGpp, the collapse of AIB transport under N-rich
455 conditions (**Fig. 1, 3E**) did not correlate with *aapJ* transcriptional control in the *relA*
456 mutant (**Fig. 6F**). All this pointed towards an alternative regulatory mechanism acting on
457 ABC transporters, potentially affecting translation.

AbcR1/2 post-translationally downregulate amino acid transport in *R. leguminosarum*

The tandemly encoded sRNAs AbcR1 and AbcR2 had been previously identified by a series of genome-wide screens conducted in *S. meliloti* [45] and were shown to act on different ABC uptake systems at the post-transcriptional level in an Hfq-dependent manner [29, 46]. These sRNAs belong to the αr15 family, whose members always exist in multiple copies in the genomes of bacteria of the Rhizobiaceae and Brucellaceae families of the order Rhizobiales [30, 47]. While (p)ppGpp measurements indicate a correlation between transport activity (i.e. protein levels) and (p)ppGpp levels (**Fig. 5B**), the collapse in transport rates for the *ptsP* and *relA* mutants (**Fig. 3E**) was not linked to transcriptional control (**Fig. 6E, F**). Taken together, these results suggest that ABC transport regulation by RelA occurs at the translational level. We therefore tested whether AbcR1 and AbcR2 are controlled by PTS^{Ntr} and RelA to mediate this effect.

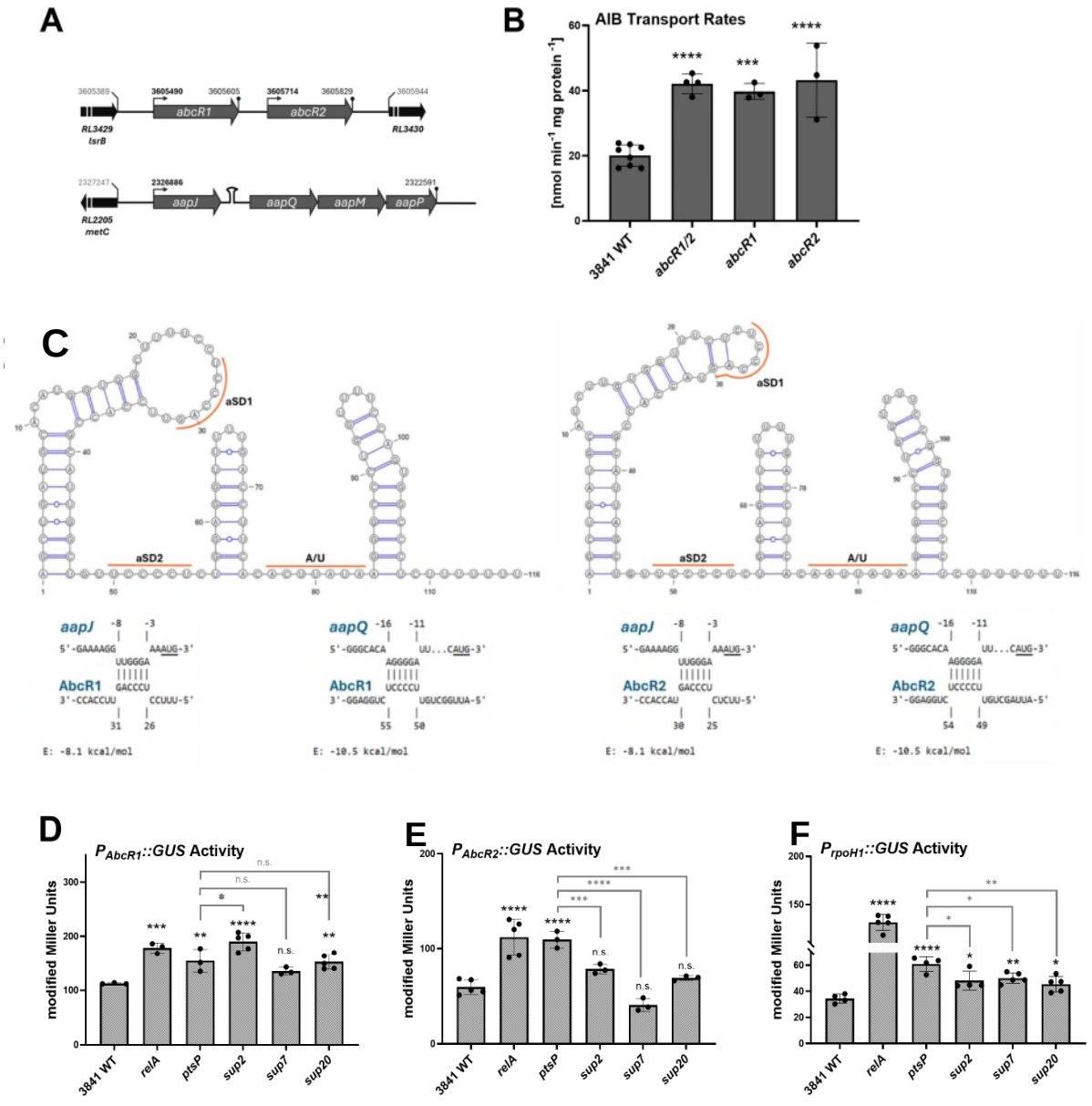

Figure 7. PTS^{Ntr}-RelA crosstalk with sRNAs AbcR1/2. (A) The genomic region of AbcR1 and AbcR2 sRNA in the *R. leguminosarum* bv. *viciae* 3841 chromosome, flanked by the genes *lsrB* (LysR family transcriptional regulator; RL3429) and ArsR-type transcriptional regulation (RL3430). **(B)** AIB transport rates of sRNA mutants *abcR1* (OPS3802), *abcR2* (OPS3803), and *abcR1/2* (OPS3804). Strains were grown to the exponential phase on UMS supplemented with 10 mM glucose + 10 mM NH_4Cl. All values are expressed in nmol min^{-1} mg^{-1} protein, and data are averages (±SEM) from at least three independent cultures. **(C)** Predicted secondary structures of *R. leguminosarum* sRNAs AbcR1 (left) and AbcR2 (right) and their base-pairing interactions with target mRNAs *aapJ* and *aapQ*. The anti-Shine-Dalgarno (aSD) and A/U-rich regions are highlighted in orange. Predicted base-

pairing sites between sRNAs and target mRNAs are shown, with numbers indicating nucleotide positions relative to the AUG start codon. The hybridisation energy [E, kcal/mol] is provided for each interaction. **(D-F)** Promoter activity of P_{abcR1}, P_{abcR2} and P_{rpoH1} measured with the GUS reporter system. Strains tested are *relA* (OPS1097), *ptsP* (ptsP107), *ptsP* suppressors 2, 7, and 20 (LMB163-S2; G445R, ptsP107-S4; H142R, and pstP107-S17; D294N), grown either in UMS media with 10 mM glucose + 10 mM NH_4Cl. Values are expressed as modified Miller units. Data are averages (±SEM) from at least four independent cultures. Statistical analyses are indicated following the level of significance, with (****) as p-value <0.0001, (***) as p-value <0.001, (**) as p-value <0.01, (*) as p-value <0.05 and n.s., not significant.

As in *S. meliloti*, AbcR1 and AbcR2 of *R. leguminosarum* are also tandemly encoded in the intergenic region between the transcriptional regulatory genes *lsrB* (RL3429) and *arsR* (RL3430) (**Fig. 7A**). The predicted secondary structure of AbcR1 and AbcR2 reveals a potential Hfq binding site [48, 49] and two anti-SD motifs, which can form base pairings with the translation initiation region of mRNAs of AapJ and AapQ (**Fig. 7C**). We then confirmed the effect of AbcR1/2 by generating single and double mutant strains and testing their amino acid uptake rates (**Fig. 7B**). The absence of AbcR1, AbcR2, or both leads to higher AIB transport rates, consistent with observations in *S. meliloti*, where overexpression of AbcR1/2 reduces *aapQ* transcript levels [29] and AbcR1 downregulates the solute-binding protein LivK (homolog of BraC in Rlv3841) [30].

To investigate the crosstalk between PTS^{Ntr}-RelA and sRNAs AbcR1/2, promoter-GUS fusions of AbcR1 and AbcR2 were generated and introduced into different mutant strains. The *relA*, *ptsP*, and *ptsN₁N₂* mutants showed upregulation of both the AbcR1 and AbcR2 promoters (**Fig. 7D, E**). In AbcR2 particularly, *ptsP* suppressors 2, 7, and 20 had significantly lower promoter activities than *ptsP*, closer to Rlv3841 wildtype levels. This

suggests that the PTS^{Ntr}-RelA interaction, presumably resulting in the production of (p)ppGpp, negatively regulates the AbcR2 promoter under high nitrogen conditions. On the other hand, while promoter activities of AbcR1 increased in *relA*, *ptsP*, and *ptsN$_1$N$_2$*, the *ptsP* suppressors did not show such a clear trend as seen for AbcR2. RT-qPCR analysis of transcriptional regulators involved in the expression of AbcR1 and AbcR2 in *S. meliloti*, namely *lsrB* and *rpoH1* [29], also showed that only *rpoH1* is upregulated in the *relA* mutant, but not *lsrB* in Rlv3841 (**Supplementary Fig. S9**). Additionally, the promoter activity of *rpoH1* has a similar trend to that of *abcR2* in the *relA, ptsP,* and *ptsP* suppressors. Specifically, *rpoH1* promoter activity was upregulated in the *relA* and *ptsP* backgrounds, and returned closer to wildtype levels in the *ptsP* suppressors, supporting the regulatory link between *rpoH1* and AbcR2. Indeed, in *S. meliloti*, it has been previously shown that the absence of RpoH1 is enough to render AbcR2 undetectable under standard and nutrient stress conditions [29]. Remarkably, while *ptsP* suppressor strains significantly reduced *rpoH1* transcription compared to *ptsP*, their expression remained higher than that of the wildtype. Given that *rpoH1* is a sigma factor that globally alters transcription in response to stress, even subtle changes may be sufficient to influence the AbcR2 and downstream transports. Altogether, these results connect PTS^{Ntr}-RelA regulation with AbcR2 sRNA expression, in which its transcription is dependent on the sigma factor RpoH1. Meanwhile, the effects observed in AbcR1 might be an indirect result of the misregulation of AbcR2.

DISCUSSION

The stringent response, mediated by accumulation of the alarmone (p)ppGpp, is one of the main homeostatic systems that rebalance bacterial physiology during nutrient

limitation and other stresses by globally reprogramming gene expression and resource allocation. Here, we present an integrated nitrogen-stress response pathway, from initial sensing to cellular response. We show how nitrogen availability is sensed by the PTS^{Ntr} system and transmitted to RelA, which induces (p)ppGpp production and thereby activates the stringent response to coordinate cell-wide adaptation. Within this pathway, enhanced amino acid uptake via the ABC transporters is fine-tuned by the sRNAs AbcR1 and AbcR2. Notably, our results indicate that *abcR2* transcription requires the sigma factor RpoH1, whose own transcription is dependent on PtsP and RelA, thereby establishing a regulatory cascade that links PTS^{Ntr} to the stringent response and, downstream, to amino acid transport.

The interaction between PTS^{Ntr} and RelA first became evident after we isolated *ptsP* suppressors. The original *ptsP* mutant of *R. leguminosarum* 3841 has a longer mean generation time, 5.65 hours, compared to 3.44 hours for the wildtype [4]. A previous InSeq screen done in our laboratory also showed that the *ptsP* mutant of *R. leguminosarum* 3841 is growth-defective in minimal medium with 10 mM NH_4Cl and 20 mM succinate as carbon source at 21% O_2 [37]. It was also unable to grow using glutamate as a nitrogen source because the Tn5 mutation inactivated the PTS^{Ntr} phosphorylation cascade to NPr and PtsN. The absence of PtsN~P results in post-translational repression of uptake by Aap and Bra, which are the sole transport systems for glutamate uptake. This inactivation blocked not only glutamate uptake but also transport of a broad range of amino acids, including aspartate [12, 50], which is itself a low-affinity solute for the Dct dicarboxylate transport system [31]. Thus, the use of aspartate as an organic carbon source readily selects for suppressor mutations in this

552 background, as it provides selection pressure while unphosphorylated PtsN weakly
553 activates ABC transporters, enabling survival. The ability of these *ptsP* suppressor
554 mutants to recover both EPS production and AIB uptake indicated that an unidentified
555 regulatory component was interacting with PTS^{Ntr}, and genome sequencing followed by
556 SNP analyses corroborated that the interacting partner was RelA.

557 Indeed, crosstalk with the stringent response has also been reported in *C. crescentus*
558 and *S. meliloti*, where the phosphorylated version of PtsN binds the ACT domain of RelA,
559 inhibiting the hydrolase activity and driving (p)ppGpp accumulation during nitrogen
560 starvation [18]. In this work, we utilised Alphafold to predict the protein structure of
561 Rlv3841 RelA and subsequently used mass spectrometry to show that the interaction
562 between PtsN and RelA is conserved in *R. leguminosarum*. As in most α-proteobacteria
563 [21, 22], this enzyme exists as a single long protein with dual function, containing the HD,
564 SYNTH, TGS, AH/RIS, and ACT domains. *R. leguminosarum* RelA interacts with PtsN via
565 its ACT domain and preferentially binds phosphorylated PtsN, as observed in *C.*
566 *crescentus* [18]. The ACT domain also controls the activity of the RelA protein in
567 *Rhodobacter capsulatus* by binding branched-chain amino acids (valine and isoleucine),
568 which subsequently increases (p)ppGpp hydrolase activity [51]. Depletion of branched-
569 chain amino acids inhibits (p)ppGpp hydrolysis, triggering the stringent response.

570 RelA exerts its regulation via the alarmone (p)ppGpp, which modulates transcription
571 primarily by binding to RNA polymerase and reprogramming promoter activity during
572 stress conditions. The pleiotropic effects of the *relA* mutant in Rlv3841 agree with
573 previous work, where RelA was shown to be acting in broader biological processes,
574 including quorum sensing, EPS production, and nodulation [17-19]. Consistent with this,

we find that transcription of *cinI*, *pssA*, and *nodA* is altered in the *relA* mutant. Both *cinI* and *pssA* promoter activities decrease in the *relA* and *ptsP* mutants, placing PTS^{Ntr} upstream of *relA*. Suppressor *ptsP* strains with gain-of-function mutations in *relA* restore *cinI* promoter activity to wildtype levels and increase the promoter activity of *pssA* towards wildtype, reinforcing this model. A regulatory connection between the stringent response and quorum sensing had been observed in other bacterial species [52, 53], including the endosymbionts *R. etli* and *S. meliloti*, where the expression of the synthases *cinI* and *rail*, or the regulator *sinR,* respectively, is RelA-dependent [35, 43]. In *S. meliloti*, a *rsh* mutant is defective in nodulation of *Medicago sativa* and overproduces the exopolysaccharide succinoglycan, which is crucial for root infection [54]. On the other hand, P_{nodA} is upregulated in the Rlv3841 *relA* mutant but not in the *ptsP* mutant background, suggesting that RelA also influences the activity of another regulator or responds to a signal independent of PTS^{Ntr}. A similar effect was already observed in *R. etli*, where Nod factor production was constitutively upregulated in a *relA* mutant [35, 36], and in *S. meliloti,* this mutant displayed strikingly different nodulation efficiencies depending on the host species [55]. (p)ppGpp has been shown to accumulate in symbiotic bacteria as a result of amino acid starvation [54, 56] and to be required for an effective symbiosis [35, 36]. Similarly, an *rsh* mutant in *Bradyrhizobium diazoefficiens* was defective in inducing the type 3 secretion system, elicited a stronger plant defence response at early root infection, and showed impaired competitiveness for nodulation in soybean plants [57]. Notably, plant-produced (p)ppGpp has been detected during plant-microbe interactions, and it is essential to fully understand the evolutionary interplay between (p)ppGpp in plants and pathogens or symbionts [58, 59].

598 Despite the growth defect and downregulation of amino acid transport in the *ptsP* and
599 *relA* mutants, no transcriptional response was observed in promoter fusions to the *mdh*
600 and *sucA* genes, encoding the TCA cycle enzymes, nor to *aapJ*, the substrate-binding
601 protein (SBP) component of the AapJQMP amino acid transporter under N-rich
602 conditions. Regardless, the correlation observed between (p)ppGpp levels and AIB
603 transport rates measured across PTS^{Ntr} strains and the *relA* mutant suggested a
604 (p)ppGpp-dependent regulation. The decrease in *aapJ* mRNA levels shown in the *ptsP*
605 and *relA* mutants, despite its unchanged promoter activity, pointed towards an
606 additional post-transcriptional mechanism acting on transport regulation. Indeed, a
607 GOGAT (*gltB*) mutant that prevents glutamine cycling via the glutamine synthase (GS)-
608 GOGAT pathway and has impaired N and C metabolism already suggested the
609 occurrence of post-transcriptional regulation of amino acid transport. While the
610 resuspension of Rlv3841 wildtype in glucose/glutamate resulted in an increased rate of
611 amino acid uptake via the Aap and Bra systems, the GOGAT mutant became starved of
612 amino acids due to the post-transcriptional shutdown of amino acid uptake [28].

613 Based on our results and previous work on *A. tumefaciens* and *S. meliloti* [27, 29], we
614 propose that (p)ppGpp negatively regulates the transcription of two small sRNAs, AbcR1
615 and AbcR2, which have been shown to repress the expression of ABC transporters,
616 including the AapJQMP system of rhizobia [29, 30] (**Figure 8**). Using *abcR1*, *abcR2*, and
617 *abcR1/2* double mutants, we demonstrated that the absence of these sRNAs results in
618 upregulation of AIB transport. We further showed that AbcR2 promoter activity increases
619 in the *ptsP* and *relA* mutants and reverts to wildtype levels in the *ptsP* suppressor strains.

This pattern of regulation is likely mediated by the sigma factor RpoH1, as the activity of the *rpoH1* promoter mirrors that of *abcR2*.

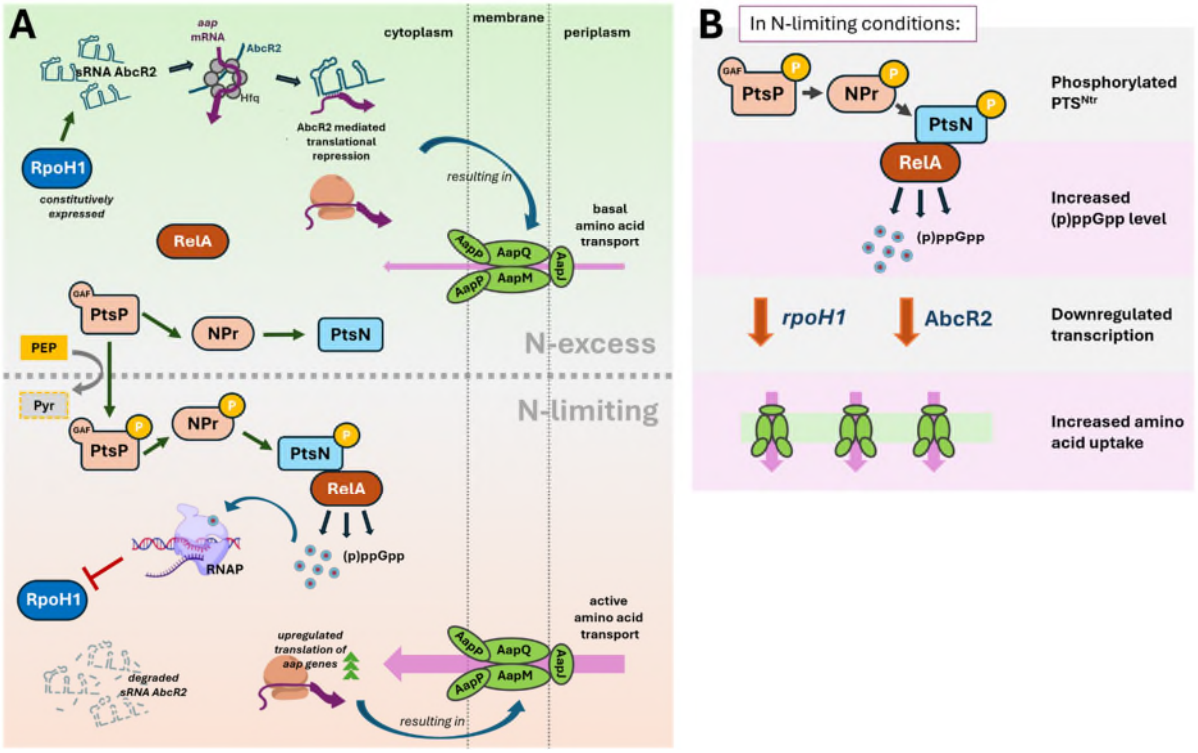

Figure 8. Nitrogen-dependent signalling via PTS^{Ntr} - RelA modulates AbcR2 control of amino acid transport via AapJQMP. (A) Under N-excess conditions (upper panel), PTS^{Ntr} is unphosphorylated, the interaction with RelA is minimal, and the transcription factor *rpoH1* is expressed. This maintains a steady level of the sRNA AbcR2, which represses translation of its target mRNAs *aapJ* and *aapQ,* resulting in basal amino acid uptake. Under N-limiting conditions (lower panel), PTS^{Ntr} becomes phosphorylated, leading to PtsN~P interaction with RelA. Activated RelA induces the synthesis of (p)ppGpp, which modulates the cell's global transcriptome, including suppression of *rpoH1* expression. The decline in *rpoH1* expression lowers AbcR2 sRNA abundance, relieving repression of the *aapJ* and *aapQ* mRNAs. These genes are translated at elevated levels, driving hyperactive amino acid transport. **(B)** Simplified diagram for the regulatory cascade PTS^{Ntr} → RelA → RpoH1 →AbcR2 → AapJQMP in nitrogen-limiting conditions.

635 Taken together, we conclude that the crosstalk between PTS^{Ntr}, RelA and AbcR1/R2
636 reprograms cell physiology during amino acid starvation mediated by a combined
637 response at different regulatory levels. PTS^{Ntr} controls the normal function of the cell by
638 protein-protein interactions upon sensing glutamine as an internal signal and reporting
639 to RelA on the carbon and nitrogen (C/N) balance **(Figure 8)**. Under nitrogen starvation,
640 autophosphorylated PtsP signals via PtsN~P to bind to the ACT domain of RelA, allowing
641 (p)ppGpp accumulation. This alarmone affects global transcription, including that of
642 *rpoH1* and consequently expression of the sRNAs *abcR1* and *abcR2*, thus adjusting
643 rhizobial physiology to ensure cell survival in their ever-changing surroundings. This
644 crosstalk indicates that the response of RelA to nitrogen starvation is graded, responding
645 quickly to C/N balance through protein:protein interactions mediated by PTS^{Ntr} but
646 subsequently stimulated by other signals, such as severe nitrogen starvation that causes
647 ribosome stalling [51]. To achieve optimal resource allocation in response to shifts in
648 nutrient availability, metabolic pathways must be precisely and timely tuned. RelA
649 activity may be dialled up in successive stages depending on the severity of the
650 starvation [32]. Efficient control of metabolism senses stress, adjusts growth
651 accordingly, and controls gene expression to ultimately provide a fitness advantage [60].
652 The crosstalk between PTS^{Ntr}-RelA-AbcR1/R2 can accomplish all of this.

653 This work is therefore the first to describe the comprehensive signalling crosstalk related
654 to nitrogen sensing in α-proteobacteria, revealing how different regulatory networks
655 operate at multiple levels to coordinate amino acid uptake and metabolism. The
656 elucidation of this intricate crosstalk is a crucial step toward understanding how bacteria

coordinate central metabolic adaptation and stress responses, ultimately informing future engineering strategies to modulate and control these processes.

METHODS

Bacterial strains and growth conditions. The bacterial strains and plasmids used in this study are listed in the SI Appendix, **Table S2**. *E. coli* strains were grown in liquid or solid Luria–Bertani (LB) medium [61] at 37°C supplemented with appropriate antibiotics (μg ml^{-1}): ampicillin, 100; tetracycline, 10; and kanamycin, 20. *R. leguminosarum* strains were grown at 28°C in Tryptone-Yeast (TY) extract [62] or Universal Minimal Salts (UMS) [37] with appropriate carbon and nitrogen sources at 10 mM unless otherwise stated. Antibiotics were used at the following concentrations (μg ml^{-1}) unless otherwise stated: gentamicin, 20; kanamycin, 20; neomycin, 40; spectinomycin, 50; streptomycin, 500; tetracycline (2 in UMS, 5 in TY). Mean generation times for Rlv3841-derived strains were obtained from cells grown in 50 mL UMS with the corresponding carbon and nitrogen sources at an initial optical density (OD_{600nm}) of 0.01. OD_{600nm} measurements were taken at 4-hour time intervals until growth reached the stationary phase from at least three biological replicates. Mean generation time (MGT) was calculated as the number of hours it takes the population to double while in the exponential growth phase.

Mutant and plasmid construction. All routine DNA analyses were done using standard protocols [61]. PCR reactions for cloning were carried out according to the manufacturer's instructions with Phusion High-Fidelity DNA Polymerase (ThermoFischer) and for mapping, with MangoTaq™ DNA Polymerase (Bioline). Restriction enzymes (New England Biolabs) were used according to the manufacturer's instructions. Sanger sequencing was carried out by Eurofins Genomics. All primers used

680 in this work are listed in the SI Appendix, **Table S3**. Conjugations were done as previously
681 described [63]. Transductions with bacteriophage RL38 were performed as described
682 [64]. The cloning details are described in the SI Appendix.

683 **Next-generation sequencing and SNP analysis.** We have sequenced genomes of the *R.*
684 *leguminosarum* bv. *viciae* 3841 WT, *ptsP* mutant and of 20 suppressor strains derived
685 from this mutant. The genomes were sequenced using Illumina MiSeq. For each strain,
686 the initial sequencing data were assembled into genomic contigs by MicrobeNG. For
687 further data analysis and SNP location identification, and core genome alignments, the
688 GitHub tool SNIPPY was used [65]. Knowing the locations of the SNPs of each suppressor,
689 we identified their positions in *relA*. We extracted the sequence of this gene for the *R.*
690 *leguminosarum* bv. *viciae* 3841 wildtype genome from the NCBI GenBank database and
691 BLAST-aligned it against the suppressor genomic contigs, yielding a single nucleotide
692 mismatch for each suppressor genome. Each suppressor had a single mismatch in their
693 *relA* gene; however, its exact location was strain specific. For each strain, we have
694 amplified the *relA* gene using PCR and used Sanger's sequencing to confirm the exact
695 SNP location.

696 **Protein conservation analysis and bioinformatics.** The degree of sequence
697 conservation in Rlv3841 RelA (UniProt Ref.: Q1MJ59_RHIL3) was obtained using the
698 Consurf server [66]. ConSurf defines a conservation score by analysing the evolutionary
699 rate of a specific position through alignment and phylogenetic analysis of homologous
700 sequences. A total of 300 sequences from the UniRef90 database were selected using
701 the HMMER package with an E-value of 0.01 and reporting threshold. The sequence
702 similarity search results have been further filtered by applying maximum and minimum

703 sequence identity cutoffs of 95% and 25%, respectively, and used to derive normalised
704 conservation scores. The conservation scores were plotted on the Alphafold-predicted
705 RelA structure using Chimera software [67]. Protein structures with desired mutations
706 were predicted using Alphafold [68], and the CB-Dock2 [59] web server was used for
707 protein-ligand docking (using PDB code: 6S2T as the template).

708 **Transport assays.** Uptake assays were performed with 25 μM (4.625kBq) of ^{14}C-labelled
709 solute [69, 70], using cultures grown in UMS with 10 mM glucose and 10 mM NH_4Cl
710 unless otherwise specified. α-aminoisobutyric acid (AIB) was used to measure amino
711 acid transport because it is transported exclusively by Aap and Bra permeases but
712 cannot be metabolised by the cell.

713 **Exopolysaccharide measurements.** 250 mL cultures were grown up to mid-
714 exponential phase. Cells were spun down, dried and weighed. The supernatant was
715 treated with two volumes (500 mL) of cold isopropanol. After precipitation, the EPS was
716 spun down, and the pellet was dried at 37°C. Values are expressed in mg/mg dry weight
717 of cells.

718 **Swimming test.** To study swimming activity, UMS plates containing 0.22% agar, 20 mM
719 succinate, and 10 mM NH4Cl were spot-inoculated with cultures in the exponential
720 phase and incubated at 28°C. The swimming halo diameter was measured after 5 days.

721 **Oxygen consumption assays.** Oxygen consumption rates were obtained from UMS
722 cultures grown with 10 mM glucose and 10 mM NH_4Cl, unless otherwise specified, to the
723 early exponential phase as described in Sánchez-Cañizares et al. [4] with the OxySense
724 325I system. The data was analysed with the OxySense Gen III software, and oxygen

consumption rates were calculated as the time it takes the population to decrease the oxygen concentration by 3%.

Microaerobic induction measurements in cultured cells. Rlv3841 strains were first grown on TY slopes with appropriate antibiotics for three days. Cells were resuspended and washed with UMS (no carbon nor nitrogen added) three times by centrifugation at 5,000 RCF for 10 minutes. Washed cells were diluted to an initial OD_{600nm} of 0.05 in 10 mL liquid UMS cultures supplied with 10mM NH_4Cl as the sole nitrogen source and either 10mM glucose or 20 mM succinate as the carbon source. Cultures were shaken at 28 °C and 200 rpm in an orbital shaker either in atmospheric conditions (21% O_2) or within a glove box (Belle Technology, UK) set at 1% O_2. OD_{600nm} readings were taken at 24 and 48 hours post-inoculation.

Promoter analysis and translational fusions. Promoter analysis with *lux* fusions was done by growing rhizobial strains on UMS 1.5% agar slopes (with appropriate antibiotics), following the protocol by Pini et al [71]. The sensitivity of each promoter fusion was measured using either the NightOWL in vivo Imaging System (Berthold Technologies) with agar plates or the Promega GloMax Microplate Reader with liquid cultures. β-Galactosidase fusions were assayed according to Miller [72], with modifications as described by Poole et al. [73]. Similarly, rhizobial strains for promoter analysis with ß-glucuronidase (GUS) fusions were grown in liquid UMS supplemented with corresponding carbon and nitrogen sources to an OD_{600nm} of 0.4 to 0.6. Cells were lysed and incubated with p-nitrophenyl-β-D-glucuronide (PNPG) until a light yellow colour appeared, and absorbance was measured at 405. The β-Glucuronidase activity was

747 measured using a modified Miller Unit [72] = (OD_{405} x 1000)/(OD_{600}-normalised cell
748 amount x incubation time in minutes).

749 **(p)ppGpp extraction and quantification.** Cultures were grown to the exponential phase
750 in UMS medium supplemented with 10 mM glucose as a carbon source and 10 mM NH_4Cl
751 or 0.5 mM NH_4Cl as a nitrogen source. Harvested cell pellets were then washed twice in
752 1 volume of TBS, OD adjusted to 2, and frozen at -80 °C before nucleotide extraction in 2
753 M formic acid. Quantification was done by HPLC–MS/MS at IJPB Paris using a ^{13}C-
754 labelled stable isotope as internal standard, as described previously [41].

755 **Bacterial two-hybrid (BACTH) assays**. Interacting partners on the high-copy pUT18C
756 vectors were transformed into MAE01 (Δ*cyaA*::Apra^R) cells, and BACTH interactions were
757 tested as in [4]. These colonies were grown overnight at 28 °C in 10 mL LB with ampicillin
758 and kanamycin at standard concentrations. A standard β-galactosidase assay [72] was
759 used to quantify the interaction between proteins. The KdpD/PtsN1 pair was used as a
760 positive control [12], whilst empty vectors were used as a negative control.

761 **Protein expression and native mass spectrometry analysis**. Geneblocks for Rlv3841
762 wildtype PtsN, PtsNH66A and PtsNH66D mutants, and the ACT domain of RelA (amino
763 acids 663-741) were inserted into a modified pET-15b expression vector between NdeI
764 and NheI cloning sites (C-terminal 6-His-tag) using In-Fusion snap-assembly master mix
765 (Takara Bio). The plasmids were transformed into Stellar cells for amplification, and the
766 insertion of the correct gene was verified by Sanger sequencing. The plasmid for each
767 protein was transformed into BL21 (DE3) competent cells (Agilent). Primary cultures (100
768 mL LB, 100 µg/mL ampicillin) were inoculated with 3-5 colonies from agar plates and
769 shaken at 37 °C and 200 rpm overnight. 20 ml of each primary culture was used to

inoculate 2x1 L LB (100 µg/ml ampicillin) and grown (37 °C, 200 rpm) until OD of 0.6-0.8. Protein expression was induced by adding IPTG at a final concentration of 0.2 mM, and the cultures were shaken at 20 °C and 200 rpm overnight. The cells were harvested by centrifugation (4000 g, 10 min) and resuspended in lysis buffer (20 mM Tris (pH 7.6), 150 mM NaCl, 10% glycerol) supplemented with 1 EDTA-free protease inhibitor cocktail tablet (Roche). The cells were lysed by several passes through a Microfluidiser (20,000 psi, 4 °C). The lysates were clarified by centrifugation (20,000 g, 20 min, 4 °C), and the supernatants were purified by IMAC at 4 °C. Empty gravity-flow chromatography columns (Bio-Rad) were supplemented with 3-5 ml of Ni-NTA agarose beads (Qiagen) and washed with 5 column volumes (CV) of water. Three IMAC buffers were prepared, varying in imidazole concentration (20 mM Tris (pH 7.6), 250 mM NaCl, 10% glycerol, and either 20 mM (IMAC buffer A), 80 mM (IMAC buffer B), or 300 mM (IMAC buffer C) imidazole). The columns were equilibrated in 5 CV of buffer A before the supernatants were loaded. Then, they were washed with 5 CV of buffer A and 5 CV of buffer B. The proteins were eluted with 5 CV of buffer C and then dialysed overnight at 4°C into 4 L of dialysis buffer (20 mM Tris (pH 7.6), 250 mM NaCl, 10% glycerol) using a 3.5 MWCO dialysis cassette (Thermo Scientific). The dialysed proteins were concentrated, flash-frozen, and stored at -80 °C. For native mass spectrometry analysis, the proteins were thawed and then desalted and buffer exchanged into 0.2 M ammonium acetate buffer using 2 micro-biospin P6 columns (Bio-Rad). Native mass spectrometry experiments were performed using an Orbitrap Q-Exactive UHMR instrument (Thermo Scientific). Proteins were diluted to a concentration of 10 µM. For the binding experiments, the two proteins were mixed together and incubated on ice for at least 2 hours before being introduced into the mass spectrometer. 3 µL of sample were loaded into gold-coated

794 borosilicate electrospray capillaries prepared in-house. The instrument was operated at
795 gentle activation conditions to promote desolvation while preserving the non-covalent
796 interactions: 1.2 kV capillary voltage, 30 °C capillary temperature, 20V HCD collision
797 energy, in-source trapping set to Off.

798 **Plant growth and acetylene reduction.** *Pisum sativum* cv. Avola seeds were surface
799 sterilised using 95% ethanol and 2% sodium hypochlorite at the time of sowing. Plants
800 were inoculated with 1×10^7 cells of the appropriate rhizobial strain and grown in 1 L
801 beakers filled with sterile medium-grade vermiculite and nitrogen-free nutrient solution
802 as previously described [73] in a growth room (16h light /8h dark). They were harvested
803 at pea flowering (3 weeks), and acetylene reduction was determined as previously
804 described [74].

805 **RNA extraction and real-time qPCR analysis.** Rlv3841 cultures are grown in 10 mM
806 glucose and 10 mM NH_4Cl as described above. Cells were harvested by centrifugation at
807 4 °C, lysed using the FastPrep-24 5G instrument, and their cell debris was removed by
808 another round of centrifugation. RNA was extracted from the lysate using the Qiagen
809 RNAeasy extraction kit, and gDNA was depleted by treatment with Invitrogen Turbo
810 DNAse according to the manufacturer's recommendation. cDNAs are generated from
811 0.5 µg of purified RNA using an Invitrogen SuperScript IV reverse transcriptase kit as per
812 the manufacturer's recommendations. Quantitative PCR reactions were prepared in
813 384-well qPCR plates containing 5 µL of Applied Biosystems PowerUp SYBR Green
814 master mix, 250 nM of each primer, and 5 ng of RNA template, for a total volume of 10 µL
815 per reaction. Reactions were run using the StepOnePlus™ Real-Time PCR System. Four
816 biological replicates were extracted for each condition, each represented by two

technical replicates and the average expression was calculated. The primer pairs used in the real-time qRT-PCR are listed in **Table S3** and were initially tested for amplification efficiency and target specificity by generating a standard curve of amplification with the *rpoD* housekeeping gene. Relative expression of each individual gene was calculated using the Plaffl Method.

Bioinformatics and statistical analysis. The IntaRNA 2.0 website (http://www.rnainter.org/IntaRNA/) was used to predict sRNA-mRNA base-pairing interactions [75], and VARNA ver. 3.93 was used to visualise the secondary structure of the sRNAs [76]. All statistical analyses were performed using GraphPad Prism 8 (GraphPad Software, 7825 Fay Avenue, Suite 230, La Jolla, CA 92037 USA). Significant differences between pairs of parameters were determined by Student's t-tests. Comparisons among more than two groups were performed using ANOVA followed by multiple comparisons post hoc corrections, as indicated in each figure legend. A p-value less than 0.05 was considered statistically significant.

DATA AVAILABILITY. The data supporting the findings of the study are available in this article and its SI Appendix.

AUTHOR CONTRIBUTIONS

PSP and CSC conceived the study, designed experiments and supervised the project; CSC, OT, AUH, DS, MPG, FP, IA, JM, RK and JP performed the experiments, and CSC and OT analysed the data. AT performed the SNPs bioinformatic analysis, DS conducted protein expression and native mass spectrometry analysis with the assistance of JRB, and JRB performed protein modelling and conservation analysis. BF and SC performed the (p)ppGpp extraction and quantification. CSC, OT, and PSP wrote the manuscript. All authors read and authorised the manuscript.

ACKNOWLEDGEMENTS

This work was supported by the Biotechnology and Biological Sciences Research Council (grant numbers BB/K006134/1, BB/N003608/1, BB/R017859/1, BB/T006722/1, BB/K001868/1, BB/K001868/2, BB/F013159/1, BB/T008784/1), The Leverhulme Trust grant (RPG-2019-246) to PSP, The Royal Society University Research Fellowship (URF\R1\221030) to CSC and (URF\R1\211567) to JRB, and the Agence Nationale de la Recherche (ANR-CE20-0033) to BF. OT is supported by the Indonesia Endowment Fund for Education Agency (LPDP) Scholarship. AUH and MPG got studentships by The Society of Spanish Researchers in the United Kingdom (SRUK/CERU) in collaboration with Universidad Autónoma de Madrid (Spain) funded by the Erasmus+ programme, and Universidad de Zaragoza (Spain) funded by the UNIVERSA programme, respectively. We thank Alison East for the critical reading of this manuscript and Julia Bartoli for supplying isotope-labelled (p)ppGpp. Nucleotide measurements were performed on the IJPB Plant Observatory technological platform.

REFERENCES

1. Brown, D.R., et al., *Nitrogen stress response and stringent response are coupled in Escherichia coli*. Nat Commun, 2014. **5**: p. 4115.
2. Chavarria, M., et al., *Regulatory tasks of the phosphoenolpyruvate-phosphotransferase system of Pseudomonas putida in central carbon metabolism*. MBio, 2012. **3**(2).
3. Ronneau, S., et al., *Phosphotransferase-dependent accumulation of (p)ppGpp in response to glutamine deprivation in Caulobacter crescentus*. Nat Commun, 2016. **7**: p. 11423.
4. Sanchez-Canizares, C., et al., *Global control of bacterial nitrogen and carbon metabolism by a PTS(Ntr)-regulated switch*. Proc Natl Acad Sci U S A, 2020. **117**(19): p. 10234–10245.
5. Mendoza-Suarez, M., et al., *Competition, Nodule Occupancy, and Persistence of Inoculant Strains: Key Factors in the Rhizobium-Legume Symbioses*. Frontiers in Plant Science, 2021. **12**.
6. Llorens, J.M.N., A. Tormo, and E. Martinez-Garcia, *Stationary phase in gram-negative bacteria*. Fems Microbiology Reviews, 2010. **34**(4): p. 476–495.
7. Ling, N., T.T. Wang, and Y. Kuzyakov, *Rhizosphere bacteriome structure and functions*. Nature Communications, 2022. **13**(1).
8. Ledermann, R., C.C.M. Schulte, and P.S. Poole, *How Rhizobia Adapt to the Nodule Environment*. Journal of Bacteriology, 2021. **203**(12).
9. Poole, P., V. Ramachandran, and J. Terpolilli, *Rhizobia: from saprophytes to endosymbionts*. Nat Rev Microbiol, 2018. **16**(5): p. 291–303.
10. Zipfel, C. and G.E.D. Oldroyd, *Plant signalling in symbiosis and immunity*. Nature, 2017. **543**(7645): p. 328–336.
11. Prell, J. and P. Poole, *Metabolic changes of rhizobia in legume nodules*. Trends Microbiol, 2006. **14**(4): p. 161–8.
12. Prell, J., et al., *The PTS(Ntr) system globally regulates ATP-dependent transporters in Rhizobium leguminosarum*. Mol Microbiol, 2012. **84**(1): p. 117–29.
13. Aravind, L. and C.P. Ponting, *The GAF domain: an evolutionary link between diverse phototransducing proteins*. Trends Biochem Sci, 1997. **22**(12): p. 458–9.
14. Lee, C.R., et al., *Reciprocal regulation of the autophosphorylation of enzyme INtr by glutamine and alpha-ketoglutarate in Escherichia coli*. Mol Microbiol, 2013. **88**(3): p. 473–85.
15. Deutscher, J., C. Francke, and P.W. Postma, *How phosphotransferase system-related protein phosphorylation regulates carbohydrate metabolism in bacteria*. Microbiol Mol Biol Rev, 2006. **70**(4): p. 939–1031.
16. Zimmer, D.P., et al., *Nitrogen regulatory protein C-controlled genes of Escherichia coli: scavenging as a defense against nitrogen limitation*. Proc Natl Acad Sci U S A, 2000. **97**(26): p. 14674–9.
17. Irving, S.E., N.R. Choudhury, and R.M. Corrigan, *The stringent response and physiological roles of (pp)pGpp in bacteria*. Nature Reviews Microbiology, 2021. **19**(4): p. 256–271.
18. Ronneau, S., et al., *Regulation of (p)ppGpp hydrolysis by a conserved archetypal regulatory domain*. Nucleic Acids Res, 2019. **47**(2): p. 843–854.

19. Zhu, M. and X. Dai, *Stringent response ensures the timely adaptation of bacterial growth to nutrient downshift*. Nat Commun, 2023. **14**(1): p. 467.
20. Diez, S., et al., *The alarmones (p) ppGpp directly regulate translation initiation during entry into quiescence*. Proceedings of the National Academy of Sciences, 2020. **117**(27): p. 15565–15572.
21. Atkinson, G.C., T. Tenson, and V. Hauryliuk, *The RelA/SpoT homolog (RSH) superfamily: distribution and functional evolution of ppGpp synthetases and hydrolases across the tree of life*. PLoS One, 2011. **6**(8): p. e23479.
22. Mittenhuber, G., *Comparative genomics and evolution of genes encoding bacterial (p)ppGpp synthetases/hydrolases (the Rel, RelA and SpoT proteins)*. J Mol Microbiol Biotechnol, 2001. **3**(4): p. 585–600.
23. Karstens, K., et al., *Phosphotransferase protein EIIANtr interacts with SpoT, a key enzyme of the stringent response, in Ralstonia eutropha H16*. Microbiology, 2014. **160**(Pt 4): p. 711–722.
24. Lee, C.R., et al., *Escherichia coli enzyme IIANtr regulates the K+ transporter TrkA*. Proc Natl Acad Sci U S A, 2007. **104**(10): p. 4124–9.
25. Luttmann, D., et al., *Stimulation of the potassium sensor KdpD kinase activity by interaction with the phosphotransferase protein IIA(Ntr) in Escherichia coli*. Mol Microbiol, 2009. **72**(4): p. 978–94.
26. Torres-Quesada, O., et al., *The Sinorhizobium meliloti RNA chaperone Hfq influences central carbon metabolism and the symbiotic interaction with alfalfa*. BMC microbiology, 2010. **10**(1): p. 71.
27. Wilms, I., et al., *Hfq influences multiple transport systems and virulence in the plant pathogen Agrobacterium tumefaciens*. J Bacteriol, 2012. **194**(19): p. 5209–17.
28. Mulley, G., et al., *Mutation of GOGAT prevents pea bacteroid formation and N2 fixation by globally downregulating transport of organic nitrogen sources*. Mol Microbiol, 2011. **80**(1): p. 149–67.
29. Garcia-Tomsig, N.I., et al., *Pervasive RNA Regulation of Metabolism Enhances the Root Colonization Ability of Nitrogen-Fixing Symbiotic alpha-Rhizobia*. mBio, 2021. **13**(1): p. e0357621.
30. Torres-Quesada, O., et al., *Independent activity of the homologous small regulatory RNAs AbcR1 and AbcR2 in the legume symbiont Sinorhizobium meliloti*. PLoS One, 2013. **8**(7): p. e68147.
31. Reid, C.J., D.L. Walshaw, and P.S. Poole, *Aspartate transport by the Dct system in Rhizobium leguminosarum negatively affects nitrogen-regulated operons*. Microbiology-Uk, 1996. **142**: p. 2603–2612.
32. Dworkin, J., *Understanding the Stringent Response: Experimental Context Matters*. mBio, 2023. **14**(1): p. e0340422.
33. Varadi, M., et al., *AlphaFold Protein Structure Database: massively expanding the structural coverage of protein-sequence space with high-accuracy models*. Nucleic Acids Res, 2022. **50**(D1): p. D439–D444.
34. Aroney, S.T.N., et al., *The motility and chemosensory systems of Rhizobium leguminosarum, their role in symbiosis, and link to PTSNtr regulation*. Environmental Microbiology, 2024. **26**(2): p. e16570.

35. Moris, M., et al., *Effective symbiosis between Rhizobium etli and Phaseolus vulgatis requires the alarmone ppGpp*. Journal of Bacteriology, 2005. **187**(15): p. 5460–5469.
36. Calderon-Flores, A., et al., *The stringent response is required for amino acid and nitrate utilization, nod factor regulation, nodulation, and nitrogen fixation in Rhizobium etli*. Journal of Bacteriology, 2005. **187**(15): p. 5075–5083.
37. Wheatley, R.M., et al., *Role of O2 in the Growth of Rhizobium leguminosarum bv. viciae 3841 on Glucose and Succinate*. J Bacteriol, 2017. **199**(1).
38. Rutten, P.J. and P.S. Poole, *Chapter Nine - Oxygen regulatory mechanisms of nitrogen fixation in rhizobia*, in *Advances in Microbial Physiology*, R.K. Poole, Editor. 2019, Academic Press. p. 325–389.
39. Colombo, M.V., et al., *A novel autoregulation mechanism of fnrN expression in Rhizobium leguminosarum bv viciae*. Mol Microbiol, 2000. **36**(2): p. 477–86.
40. Rutten, P.J., et al., *Multiple sensors provide spatiotemporal oxygen regulation of gene expression in a Rhizobium-legume symbiosis*. PLoS Genet, 2021. **17**(2): p. e1009099.
41. Bartoli, J., et al., *Quantification of guanosine triphosphate and tetraphosphate in plants and algae using stable isotope-labelled internal standards*. Talanta, 2020. **219**: p. 121261.
42. Friga, G.M., G. Borbely, and G.L. Farkas, *Accumulation of guanosine tetraphosphate (ppGpp) under nitrogen starvation in Anacystis nidulans, a cyanobacterium*. Arch Microbiol, 1981. **129**(5): p. 341–3.
43. Krol, E. and A. Becker, *ppGpp in Sinorhizobium meliloti: biosynthesis in response to sudden nutritional downshifts and modulation of the transcriptome*. Mol Microbiol, 2011. **81**(5): p. 1233–54.
44. Walshaw, D.L., et al., *Regulation of the TCA cycle and the general amino acid permease by overflow metabolism in Rhizobium leguminosarum*. Microbiology, 1997. **143**(7): p. 2209–2221.
45. del Val, C., et al., *A survey of sRNA families in alpha-proteobacteria*. RNA Biol, 2012. **9**(2): p. 119–29.
46. Torres-Quesada, O., et al., *Genome-wide profiling of Hfq-binding RNAs uncovers extensive post-transcriptional rewiring of major stress response and symbiotic regulons in Sinorhizobium meliloti*. RNA Biol, 2014. **11**(5): p. 563–79.
47. Sheehan, L.M. and C.C. Caswell, *An account of evolutionary specialization: the AbcR small RNAs in the Rhizobiales*. Mol Microbiol, 2018. **107**(1): p. 24–33.
48. Sauer, E. and O. Weichenrieder, *Structural basis for RNA 3'-end recognition by Hfq*. Proc Natl Acad Sci U S A, 2011. **108**(32): p. 13065–70.
49. Ishikawa, H., et al., *The functional Hfq-binding module of bacterial sRNAs consists of a double or single hairpin preceded by a U-rich sequence and followed by a 3' poly(U) tail*. RNA, 2012. **18**(5): p. 1062–74.
50. Untiet, V., et al., *ABC transport is inactivated by the PTS(Ntr) under potassium limitation in Rhizobium leguminosarum 3841*. PLoS One, 2013. **8**(5): p. e64682.
51. Fang, M. and C.E. Bauer, *Regulation of stringent factor by branched-chain amino acids*. Proc Natl Acad Sci U S A, 2018. **115**(25): p. 6446–6451.
52. Gan, H.M., et al., *Identification of an rsh gene from a Novosphingobium sp. necessary for quorum-sensing signal accumulation*. J Bacteriol, 2009. **191**(8): p. 2551–60.

53. van Delden, C., R. Comte, and A.M. Bally, *Stringent response activates quorum sensing and modulates cell density-dependent gene expression in Pseudomonas aeruginosa*. J Bacteriol, 2001. **183**(18): p. 5376–84.
54. Wells, D.H. and S.R. Long, *The Sinorhizobium meliloti stringent response affects multiple aspects of symbiosis*. Molecular Microbiology, 2002. **43**(5): p. 1115–1127.
55. Wippel, K. and S.R. Long, *Symbiotic Performance of Sinorhizobium meliloti Lacking ppGpp Depends on the Medicago Host Species*. Molecular Plant-Microbe Interactions, 2019. **32**(6): p. 717–728.
56. Howorth, S.M. and R.R. England, *Accumulation of ppGpp in symbiotic and free-living nitrogen-fixing bacteria following amino acid starvation*. Arch Microbiol, 1999. **171**(2): p. 131–4.
57. Perez-Gimenez, J., et al., *A Stringent-Response-Defective Bradyrhizobium diazoefficiens Strain Does Not Activate the Type 3 Secretion System, Elicits an Early Plant Defense Response, and Circumvents NH(4)NO(3)-Induced Inhibition of Nodulation*. Appl Environ Microbiol, 2021. **87**(9).
58. Qiu, D., et al., *Bacterial Pathogen Infection Triggers Magic Spot Nucleotide Signaling in Arabidopsis thaliana Chloroplasts through Specific RelA/SpoT Homologues*. J Am Chem Soc, 2023. **145**(29): p. 16081–16089.
59. Abdelkefi, H., et al., *Guanosine tetraphosphate modulates salicylic acid signalling and the resistance of Arabidopsis thaliana to Turnip mosaic virus*. Mol Plant Pathol, 2018. **19**(3): p. 634–646.
60. Steinchen, W., V. Zegarra, and G. Bange, *(p)ppGpp: Magic Modulators of Bacterial Physiology and Metabolism*. Frontiers in Microbiology, 2020. **11**.
61. Sambrook, J. and D.W. Russell, *Molecular Cloning: A Laboratory Manual*. 2001: Cold Spring Harbor Laboratory Press.
62. Beringer, J.E., *R factor transfer in Rhizobium leguminosarum*. J. Gen. Microbiol., 1974. **84**: p. 188–198.
63. Poole, P.S., et al., *Identification of chromosomal genes located downstream of dctD that affect the requirement for calcium and the lipopolysaccharide layer of Rhizobium leguminosarum*. Microbiology, 1994. **140 (Pt 10)**: p. 2797–809.
64. Buchanan-Wollaston, V., *Generalized transduction in Rhizobium leguminosarum*. Journal of General Microbiology, 1979. **112**(May): p. 135–142.
65. Seemann, T., *SNIPPY: fast bacterial variant calling from NGS reads* 2015: https://github.com/tseemann/snippy.
66. Ashkenazy, H., et al., *ConSurf 2016: an improved methodology to estimate and visualize evolutionary conservation in macromolecules*. Nucleic Acids Res, 2016. **44**(W1): p. W344–50.
67. Pettersen, E.F., et al., *UCSF ChimeraX: Structure visualization for researchers, educators, and developers*. Protein Sci, 2021. **30**(1): p. 70–82.
68. Jumper, J., et al., *Highly accurate protein structure prediction with AlphaFold*. Nature, 2021. **596**(7873): p. 583–589.
69. Poole, P.S., et al., *The transport of L-glutamate by Rhizobium-leguminosarum Involves a common amino-acid carrier*. Journal of General Microbiology, 1985. **131**(Jun): p. 1441–1448.
70. Hosie, A.H., et al., *Rhizobium leguminosarum has a second general amino acid permease with unusually broad substrate specificity and high similarity to*

branched-chain amino acid transporters (Bra/LIV) of the ABC family. J Bacteriol, 2002. **184**(15): p. 4071–80.
71. Pini, F., et al., *Bacterial Biosensors for in Vivo Spatiotemporal Mapping of Root Secretion*. Plant Physiol, 2017. **174**(3): p. 1289–1306.
72. Miller, J.H., *Experiments in molecular genetics*. 1972: Cold Spring Harbor Laboratory.
73. Poole, P.S., et al., *Myoinositol catabolism and catabolite regulation in Rhizobium-leguminosarum bv viciae*. Microbiology-Uk, 1994. **140**: p. 2787–2795.
74. Allaway, D., et al., *Identification of alanine dehydrogenase and its role in mixed secretion of ammonium and alanine by pea bacteroids*. Mol Microbiol, 2000. **36**(2): p. 508–15.
75. Mann, M., P.R. Wright, and R. Backofen, *IntaRNA 2.0: enhanced and customizable prediction of RNA-RNA interactions*. (1362-4962 (Electronic)).
76. Darty, K., A. Denise, and Y. Ponty, *VARNA: Interactive drawing and editing of the RNA secondary structure*. Bioinformatics, 2009. **25**(15): p. 1974–1975.

CHAPTER 4

PTS^{Ntr} regulates the stringent response to control translation of transport systems in *Rhizobium leguminosarum*

Supplementary Information

Olivia Tjahjono, Alicia Uceda-Heras, Denis Shutin, Andrzej Tkacz, María Palomero-Gómez, Sylvie Citerne, Francesco Pini, Isidro Abreu, Jay Mulley, Ramakrishnan Karunakaran, Raphael Ledermann, Jürgen Prell, Ben Field, Jani Reddy Bolla, Philip Poole, Carmen Sánchez-Cañizares

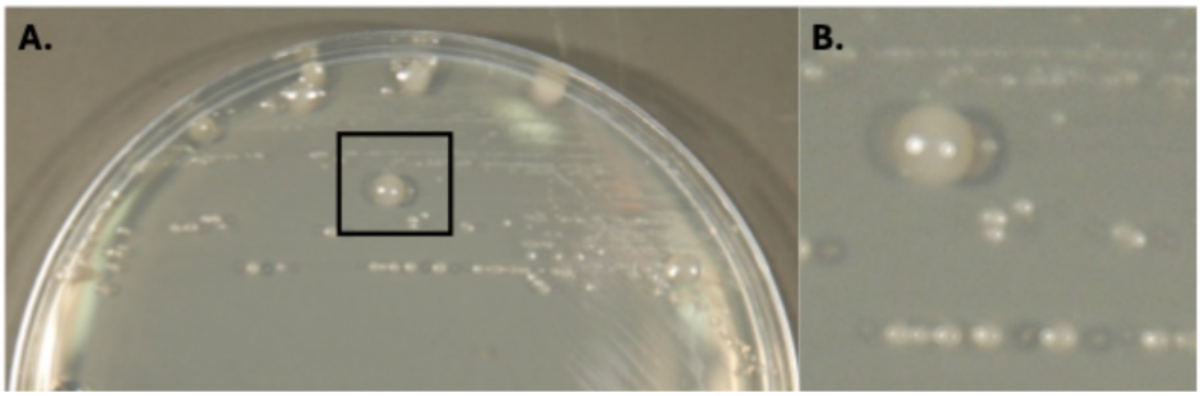

Supplementary Figure S1. PtsP suppressor isolates. (A) When the *ptsP* mutant was forced to grow for 7-14 days on UMS with 20 mM succinate and 10 mM aspartate, second-site suppressor mutants were recovered, showing large, mucoid colonies. (B) Detail of the surface phenotype of the *ptsP* suppressor colony marked with a black square in A and grown as above.

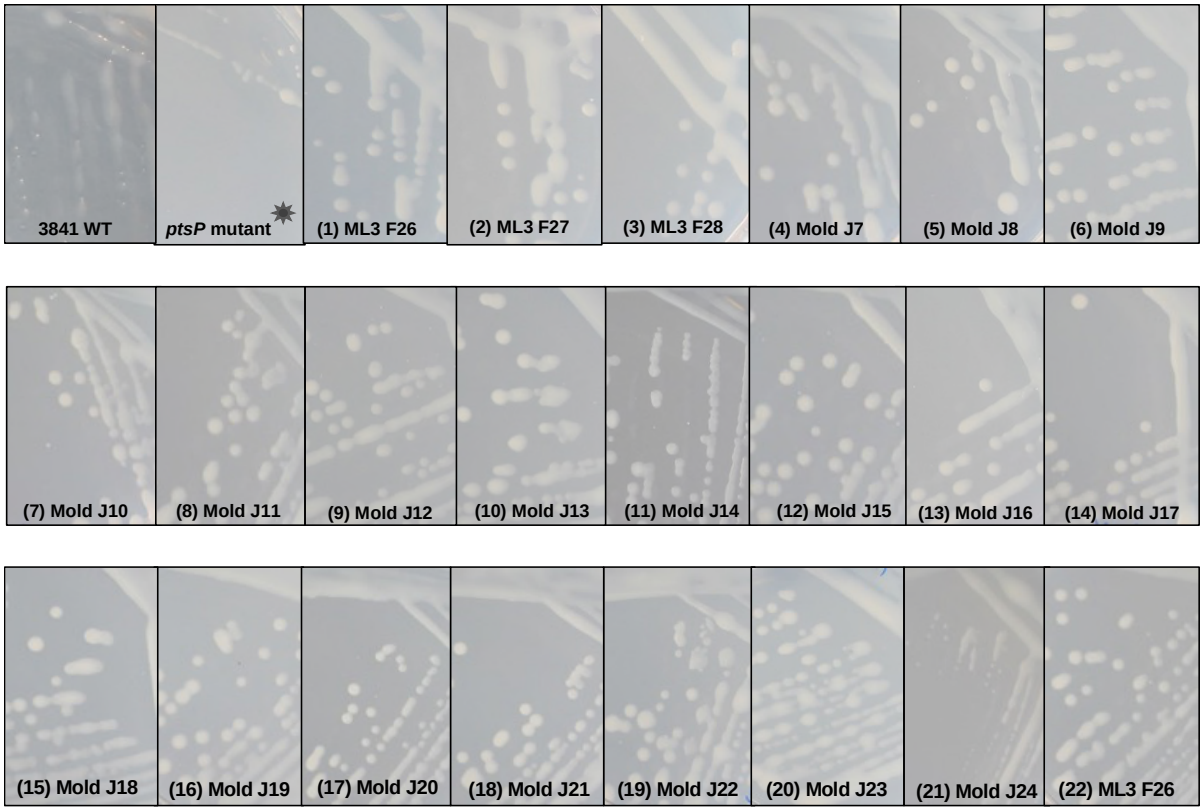

Supplementary Figure S2. Confirmation of suppressor isolates. Surface phenotype (mucoid) for suppressors 1 to 22 on representative agar plates with UMS 20mM succinate and 10mM aspartate compared to Rlv3841 wildtype (WT, mucoid) and *ptsP* original mutant (dry).

Supplementary Table S1. Genome sequencing results and statistics

Sample id	# contigs (>= 0 bp)	# contigs (>= 1000 bp)	Total length (>= 0 bp)	Total length (>= 1000 bp)	# contigs	Largest contig	Total length	GC (%)	N50	N75	L50	L75	# N's / 100 kbp
3558-3841 WT	138	73	7722016	7691049	88	598283	7701792	60.87	296051	163937	9	17	0
3559-ptsP107	151	77	7959610	7925075	96	651850	7937856	60.9	306369	180921	9	17	0
3560-sup2	112	73	7714267	7694288	87	642146	7704444	60.87	306369	180921	8	16	0
3561-sup4	171	79	7735989	7692137	103	598354	7708440	60.87	306369	180921	9	17	0
3562-sup5	130	81	7717510	7693732	96	651866	7704295	60.87	289482	180921	10	18	0
3563-sup6	143	77	7728788	7698401	93	1250173	7708800	60.88	306369	180924	6	14	0
3564-sup7	170	114	7712089	7683207	137	519018	7699033	60.87	152953	93712	16	33	0
3565-sup8	129	82	7721235	7699035	95	598314	7707717	60.87	301749	161435	10	18	0
3566-sup9	142	88	7717781	7691276	104	699160	7703174	60.87	254251	143605	10	20	0
3567-sup10	131	78	7721603	7695422	95	731175	7707169	60.87	290366	163937	9	18	0
3568-sup11	128	85	7713440	7692975	101	598421	7704148	60.88	289493	161435	10	19	0
3569-sup12	122	75	7717121	7692845	94	699160	7705951	60.87	364991	197343	7	14	0
3570-sup13	107	73	7693954	7677344	82	1157934	7683866	60.88	294171	180921	7	15	0
3571-sup14	120	71	8129655	8106896	80	1016698	8113919	60.91	364991	167214	7	15	0
3572-sup15	133	99	7715145	7697331	113	598421	7707310	60.87	270234	112082	10	22	0
3573-sup16	114	73	7716647	7696327	85	899071	7705384	60.88	296199	163937	8	17	0
3574-sup17	124	76	7718836	7695738	93	1250173	7706829	60.87	364991	180921	7	14	0
3575-sup18	134	76	7721985	7694519	93	1250173	7705882	60.87	364991	197343	7	14	0
3576-sup19	122	79	7717286	7696942	91	803760	7705688	60.87	307482	163937	8	17	0
3577-sup20	147	79	7721751	7690237	93	803662	7699819	60.87	307661	169507	8	17	0
3578-sup21	137	89	7719391	7696186	105	560931	7707073	60.87	259614	157027	12	21	0
3579-sup22	127	74	7720177	7695729	88	1157934	7705378	60.87	306369	168993	7	15	0

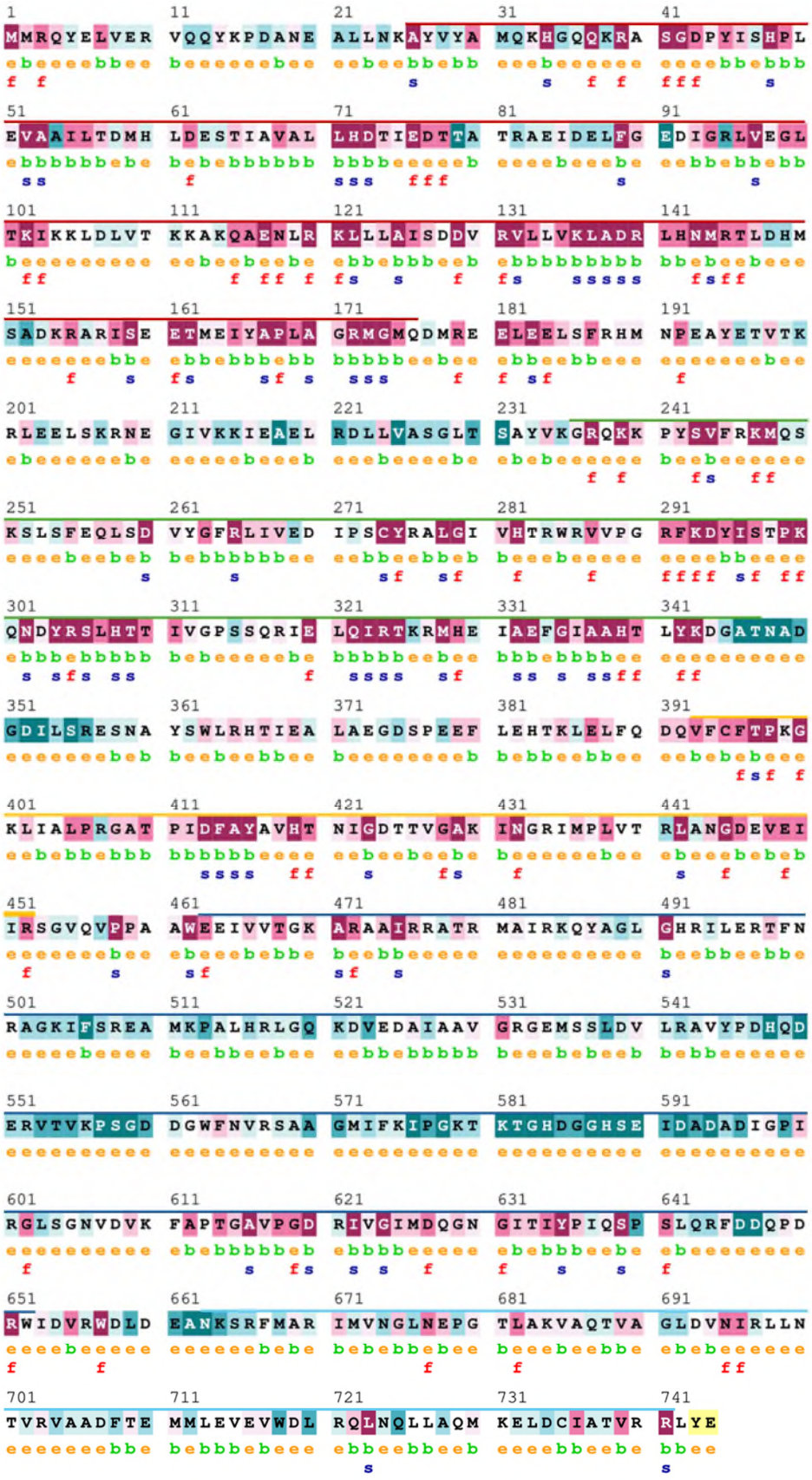

The conservation scale:

1 2 3 4 5 6 7 8 9

Variable Average Conserved

Supplementary Figure S3: **Consurf analysis of the RelA protein**. Evolutionary conservation of the residues in RelA between RelA sequences (with 25-95% seq. ID to *R. leguminosarum* RelA) across bacteria as obtained by ConSurf. e (orange): an exposed residue according to the NACSES algorithm, b (green): a buried residue according to the NACSES algorithm, f (red): a predicted functional residue (highly conserved and exposed), s (dark blue): a predicted structural residue (highly conserved and buried). Regions for which insufficient data were found are marked in yellow. RelA domains are indicated as lines above the sequences: HD (red), SYNTH (green), TGS (yellow), AH and RIS (dark blue), ACT (light blue).

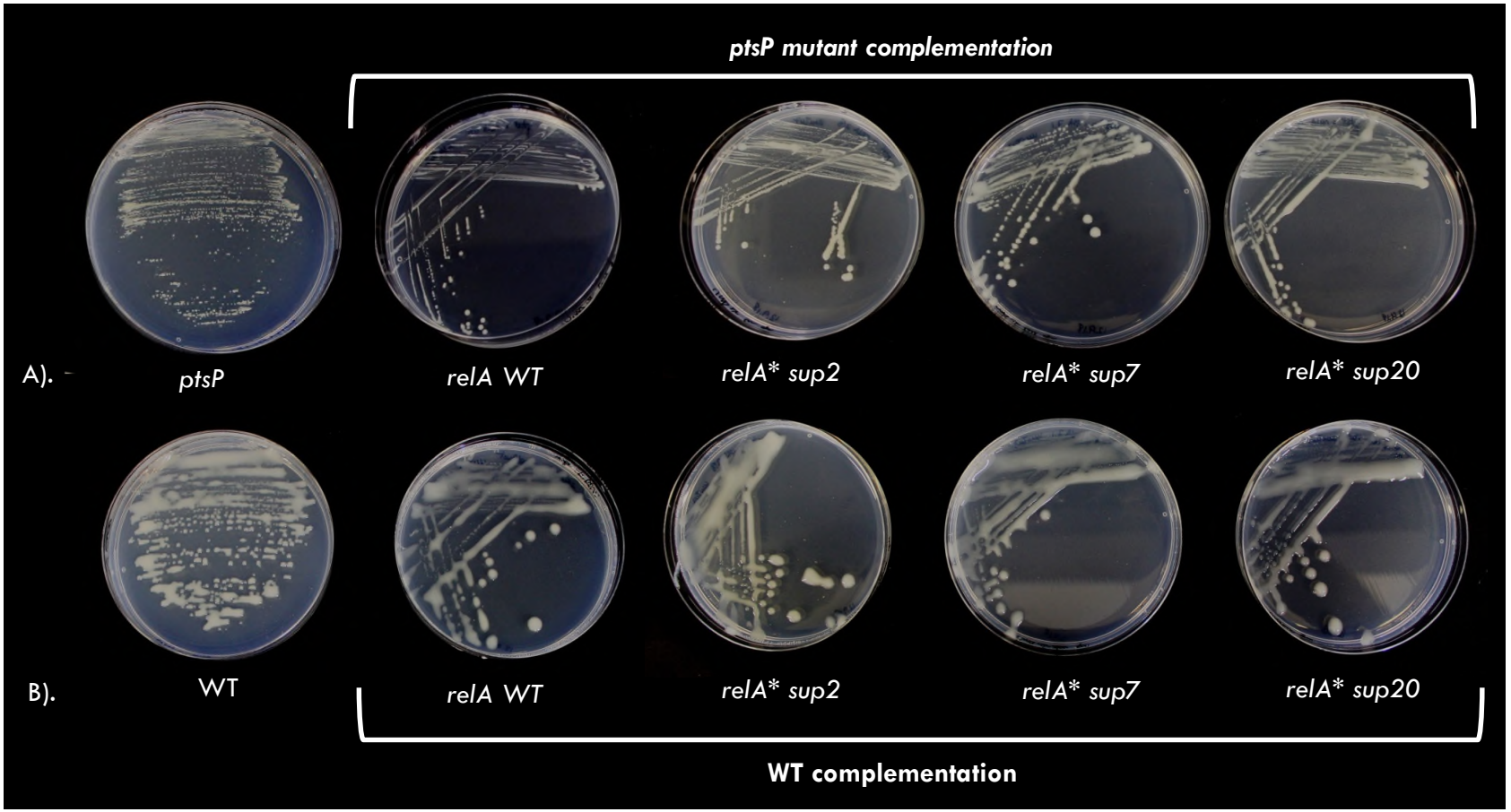

Supplementary Figure S4. RelA complementation assay. Different versions of *relA* were introduced by Tn7 chromosome integration into PtsP107 (ptsP mutant) and Rlv3841 WT: *relA* wildtype copy (*relA* WT), and the *relA* mutated versions of three different suppressors (sup2, sup7 and sup20). The surface phenotype was compared to wildtype Rlv3841 (WT) and the original *ptsP* mutant grown in the same conditions.

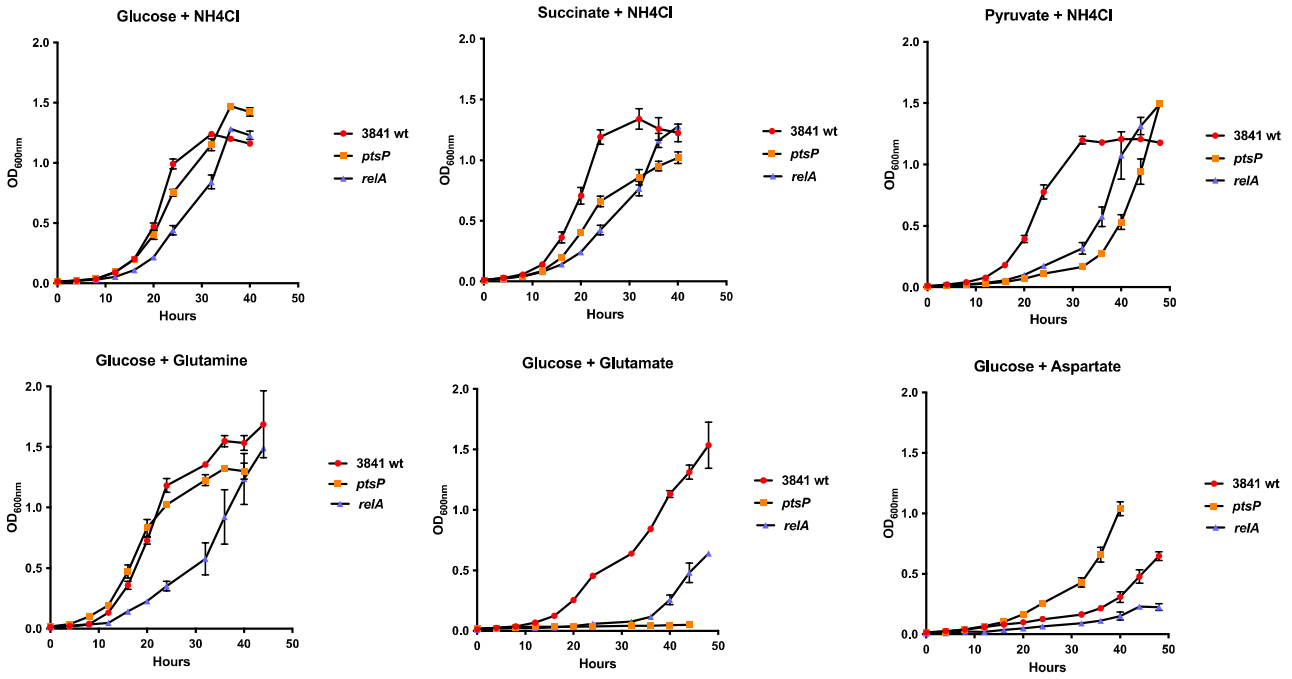

Mean Generation Time

Strain	Glucose 10mM UMS Glc+NH4Cl	Succinate 20mM UMS Succ+NH4Cl	Pyruvate 30mM UMS Pyr+NH4Cl	Glutamine 10mM UMS Glc+glutamine	Glutamate 10mM UMS Glc+glutamate	Aspartate 10mM UMS Glc+aspartate
WT	3.44 ±0.17 (n=4)	3.54 ±0.35 (n=4)	4.27 ±0.19 (n=4)	3.74 ±0.32 (n=3)	4.26 ±0.12 (n=4)	11.41 ±0.21 (n=4)
ptsP	4.19 ±0.16 (n=3)	6.02 ± 0.32 (n=3)	7.83 ± 0.03 (n=3)	3.65 ± 0.13 (n=3)	0 (n=3)	7.83 ± 0.44 (n=3)*
relA	3.94 ±0.07 (n=3)	5.18 ±0.32 (n=3)	4.98 ±0.12 (n=3)	4.25 ±0.19 (n=3)	extended lag phase	12.03 ±0.97 (n=3)

Supplementary Figure S5. Growth phenotype of Rlv3841 *relA* mutant (OPS1097) compared to *ptsP* (ptsP107) and WT strains. Growth curves on UMS supplemented with different carbon and nitrogen sources and MGT calculations (mean generation time) for each condition tested. Glc: glucose, Succ: succinate, Arab: arabinose, Pyr: pyruvate, Gln: glutamine, Glut: Glutamate, Asp: aspartate. Data are averages (± SEM) from at least 3 independent cultures. *Conditions leading to suppressor mutations.

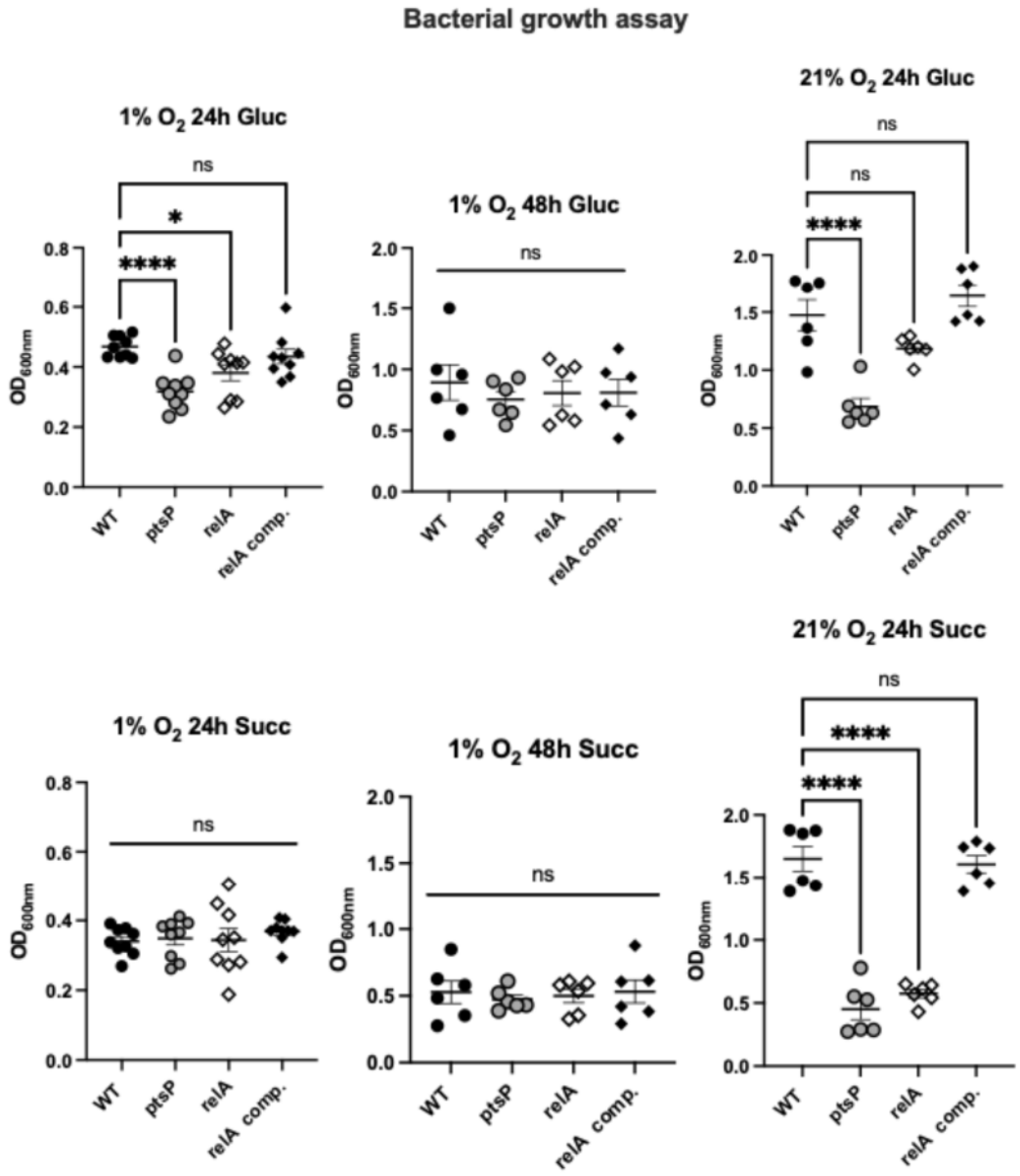

Supplementary Figure S6. Bacterial growth assay at different oxygen concentrations. Cells were grown in UMS liquid cultures with 10 mM glucose or 20 mM succinate and 10 mM NH_4Cl as nitrogen source at 1% oxygen inside a glove box or 21% in an orbital shaker. 1 mL samples were taken at 24 h and 48 h to measure OD_{600nm} and monitor their growth. The strains used were wildtype Rlv3841 (black dots), *ptsP* (PtsP107, grey dots), *relA* mutant (OPS1097, white diamonds) and the complemented *relA* (OPS3331, black diamonds). Statistical analyses are indicated following the level of significance, (*) $P < 0.05$, (**) $P < 0.01$, (***) $P < 0.001$, (****) $P < 0.0001$ and ns, not significant.

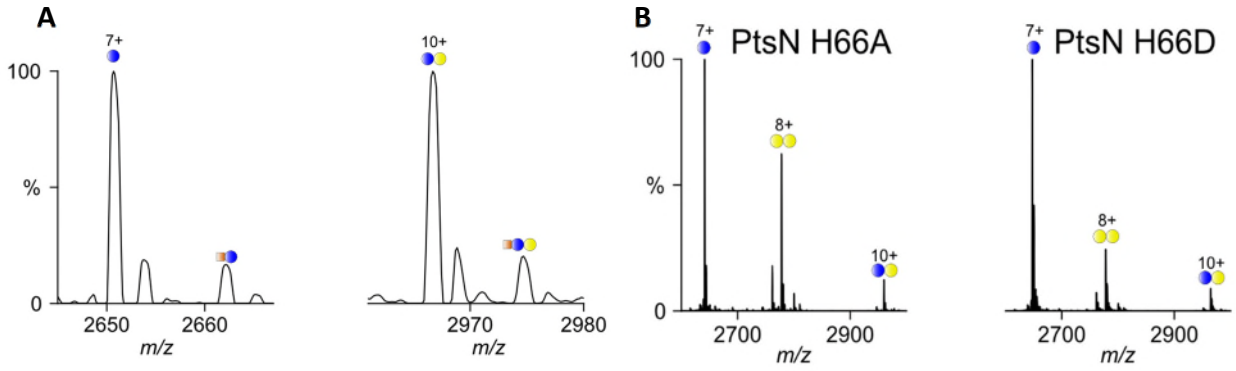

55

56 **Supplementary Figure S7.** (A) Relative amount of phosphorylation (orange square) for
57 PtsN (blue dot) and for its complex with the ACT domain of RelA (yellow dot). Each panel
58 is normalised to have the unphosphorylated peak at 100%. The unlabelled peaks
59 correspond to Na^+ adducts. (B) Native mass spectra of RelA ACT bound to PtsN mutant
60 variants H66A (permanent non-phosphorylated) and H66D (phosphomimic).

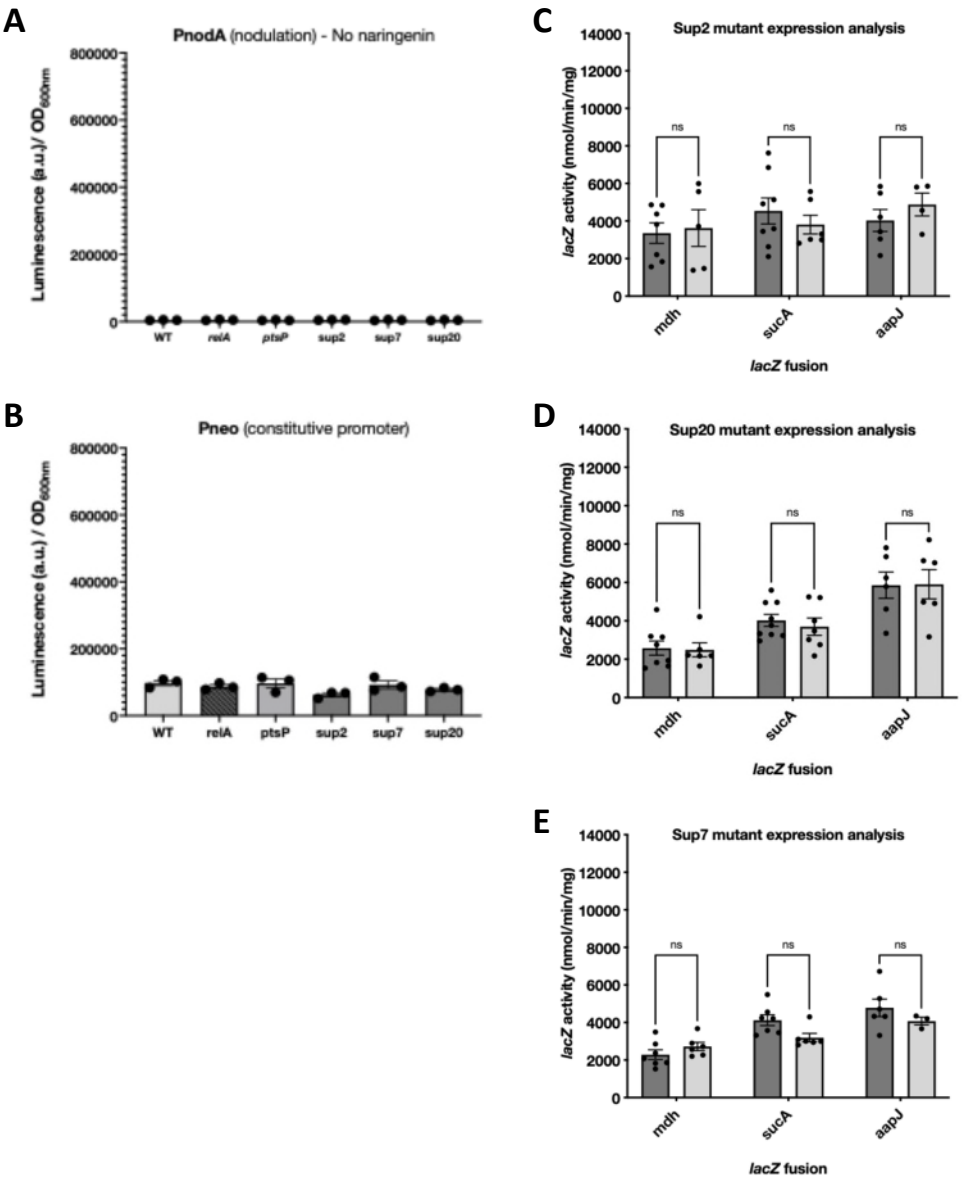

Supplementary Figure S8. Quantification of promoter activity by *lux* and *lacZ* fusions. (A) *nodA* without narigenin addition and (B) constitutive promoter Pneo, measured by *lux* activity in Rlv3841 wildtype, *ptsP* (PtsP107), *relA* (OPS1097), and *ptsP* suppressors 2, 7, and 20 (LMB163-S2, ptsP107-S4, ptsP107-S17). All rates are expressed in luminescence arbitrary units relative to OD_{600nm}; data are averages (±SEM) from 3 independent cultures. (C-D) Quantification of promoter activity for *mdh*, *sucA* and *aapJ* measured by *lacZ* activity in cosmids introduced in *ptsP* suppressors 2, 7, and 20 in 10 mM NH_4Cl (N-rich, dark grey) and 10 mM glutamate (N-poor, light grey). (A-E) Glucose 10 mM was used as a carbon source. All rates are expressed in nmol/min/mg. Data are averages (± SEM) from at least 5 independent cultures; n.s., not significant.

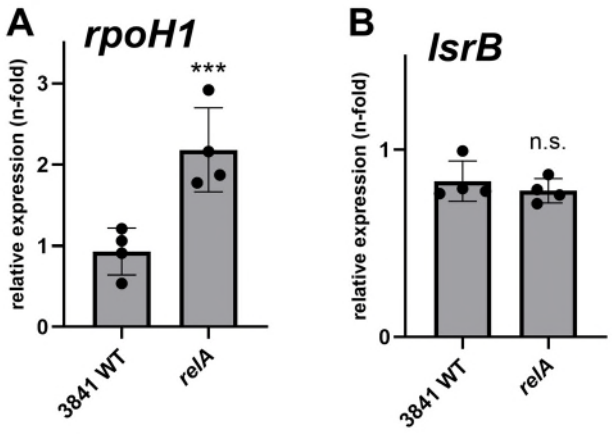

Supplementary Figure S9. qPCR analysis for *rpoH1* and *lsrB*. Rlv3841 wildtype and *relA* (OPS1097) cultures were grown in UMS supplemented with 10 mM glucose + 10 mM NH_4Cl. Data are averages (± SEM) from 4 independent cultures. Statistical analyses are indicated following the level of significance, with (***) as p-value <0.001 and n.s., not significant.

Supplementary Information Text

Materials and Methods.

Cloning details. PCR reactions for cloning were carried out according to the manufacturer's instructions using Phusion High-Fidelity DNA Polymerase (ThermoFischer) and for mapping, with MangoTaq™ DNA Polymerase (Bioline) or GoTaq™ (Promega). Restriction enzymes (New England Biolabs) were used according to the manufacturer's instructions. Sanger sequencing was carried out by Eurofins Genomics.

sRNAs mutant strains of *ΔabcR1*, *ΔabcR2*, and *ΔabcR1/2* were generated by exchanging the chromosomal loci with ΩSpec cassette from pHP45, adapting strategies used in *Sinorhizobium* [1]. A 2580 bp fragment encompassing *abcR1*, *abcR2*, and flanking sequences (1061 bp upstream of *abcR1* 5' region and 1143 bp downstream of *abcR2* 3' region) was amplified using primers oxp7151/7152, and cloned into pUC18 vector, resulting in plasmid pOPS2210. This plasmid was then used as the template for inverse PCR to incorporate the BamHI sites at the end of amplified fragments flanking *abcR1* (oxp7153/7154), *abcR2* (oxp7157/7158), and *abcR1/2* (oxp7153/oxp7158). PCR products were assembled with ΩSpec cassette, resulting in plasmids carrying *abcR1::ΩSpec* (pOPS2211), *abcr2::ΩSpec* (pOPS2212), and *abcR1/2::ΩSpec* (pOPS2213) mutations. After the amplification step by PCR, each of the products was ligated to pK18mobsacB vector digested by SmaI, followed by conjugation of plasmids into Rlv3841 and sucrose selection to produce OPS3802, OPS3803, and OPS3804, respectively.

For GUS reporter expression analysis, plasmid pOPS1850 was first generated by cloning promoterless *gusA* into mTn7 delivery plasmid pUC18T-mini-Tn7T-Gm. The promoter region of each of the candidate genes was amplified using primers listed in the SI

Appendix, **Table S3**. The fragments are cloned into pOPS1850 after digestion with PstI, and four-parental matings with prk2013 and ptNS3 were done to integrate the transposases into *Rhizobium*.

Supplementary Table S2. List of strains and plasmids.

Strains	Description	Reference
Escherichia coli		
DH5α	*supE44, hsdR17, recA1 thi-1, ΔlacU169(ϕ801acZΔM15) endA1 gyrA96 relA1*	[2]
MAE01	F^- λ^- *ilvG⁻ rfb-50 rph-1, ΔcyaA*::$Apra^R$ (host strain for BACTH assays)	[3]
Rhizobium leguminosarum		
Rlv3841	*R. leguminosarum* bv. viciae; Str^r derivative of strain 300	[4]
PtsP107	Rlv3841 Tn5::*ptsP*	[5]
OPS1097	Rlv3841 *relA* (RL1507) ΩSpec mutant	This work
LMB163-1	*ptsP* suppressor 1 mutant of PtsP107 isolated for rapid growth and large 'gloopy' colony morphology after 7 days on 20mM succinate/10mM aspartate	This work
LMB163-2	*ptsP* suppressor 2 mutant (G445R) of PtsP107 isolated for rapid growth and large 'gloopy' colony morphology after 7 days on 20mM succinate/10mM aspartate	This work
LMB163-3	*ptsP* suppressor 3 mutant of PtsP107 isolated for rapid growth and large 'gloopy' colony morphology after 7 days on 20mM succinate/10mM aspartate	This work
ptsP107-S1	*ptsP* suppressor 4 mutant (N143S) of PtsP107 isolated for rapid growth and large 'gloopy' colony morphology after 14 days on 20mM succinate/10mM aspartate	This work
ptsP107-S2	*ptsP* suppressor 5 mutant (Q115P) of PtsP107 isolated for rapid growth and large 'gloopy' colony morphology after 14 days growth on 20mM succinate/10mM aspartate	This work
ptsP107-S3	*ptsP* suppressor 6 mutant (I368N) of PtsP107 isolated for rapid growth and large 'gloopy' colony morphology after 14 days growth on 20mM succinate/10mM aspartate	This work
ptsP107-S4	*ptsP* suppressor 7 mutant (H142R) of PtsP107 isolated for rapid growth and large 'gloopy' colony morphology after 14 days on 20mM succinate/10mM aspartate	This work
ptsP107-S5	*ptsP* suppressor 8 mutant (no SNPs) of PtsP107 isolated for rapid growth and large 'gloopy' colony morphology after 14 days on 20mM succinate/10mM aspartate	This work

ptsP107-S6	*ptsP* suppressor 9 mutant (Q37L & P406L) of PtsP107 isolated for rapid growth and large 'gloopy' colony morphology after 14 days on 20mM succinate/10mM aspartate	This work
ptsP107-S7	*ptsP* suppressor 10 mutant (E379K) of PtsP107 isolated for rapid growth and large 'gloopy' colony morphology after 14 days on 20mM succinate/10mM aspartate	This work
ptsP107-S8	*ptsP* suppressor 11 mutant (G428D) of PtsP107 isolated for rapid growth and large 'gloopy' colony morphology after 14 days on 20mM succinate/10mM aspartate	This work
ptsP107-S9	*ptsP* suppressor 12 mutant (A471V) of PtsP107 isolated for rapid growth and large 'gloopy' colony morphology after 14 days on 20mM succinate/10mM aspartate	This work
ptsP107-S10	*ptsP* suppressor 13 mutant (I216M) of PtsP107 isolated for rapid growth and large 'gloopy' colony morphology after 14 days on 20mM succinate/10mM aspartate	This work
ptsP107-S11	*ptsP* suppressor 14 mutant (R741L) of PtsP107 isolated for rapid growth and large 'gloopy' colony morphology after 14 days on 20mM succinate/10mM aspartate	This work
ptsP107-S12	*ptsP* suppressor 15 mutant (W563*) of PtsP107 isolated for rapid growth and large 'gloopy' colony morphology after 14 days on 20mM succinate/10mM aspartate	This work
ptsP107-S13	*ptsP* suppressor 16 mutant (L119P) of PtsP107 isolated for rapid growth and large 'gloopy' colony morphology after 14 days on 20mM succinate/10mM aspartate	This work
ptsP107-S14	*ptsP* suppressor 17 mutant (L381R) of PtsP107 isolated for rapid growth and large 'gloopy' colony morphology after 14 days on 20mM succinate/10mM aspartate	This work
ptsP107-S15	*ptsP* suppressor 18 mutant (R318H) of PtsP107 isolated for rapid growth and large 'gloopy' colony morphology after 14 days on 20mM succinate/10mM aspartate	This work
ptsP107-S16	*ptsP* suppressor 19 mutant (T162A) of PtsP107 isolated for rapid growth and large 'gloopy' colony morphology after 14 days on 20mM succinate/10mM aspartate	This work
ptsP107-S17	*ptsP* suppressor 20 mutant (L381R) of PtsP107 isolated for rapid growth and large 'gloopy' colony morphology after 14 days on 20mM succinate/10mM aspartate	This work
ptsP107-S18	*ptsP* suppressor 21 mutant (T101I) of PtsP107 isolated for rapid growth and large 'gloopy' colony morphology after 14 days on 20mM succinate/10mM aspartate	This work
ptsP107-S19	*ptsP* suppressor 22 mutant (Q37L & P406L) of PtsP107 isolated for rapid growth and large 'gloopy' colony morphology after 14 days on 20mM succinate/10mM aspartate	This work

OPS3319	Rlv3841 Tn7 complemented with relA wiltype	This work
OPS3320	Rlv3841 Tn7 complemented with relA from suppressor 2	This work
OPS3321	Rlv3841 Tn7 complemented with relA from suppressor 7	This work
OPS3322	Rlv3841 Tn7 complemented with relA from suppressor 20	This work
OPS3323	*ptsP* mutant Tn7 complemented with relA wiltype	This work
OPS3324	*ptsP* mutant Tn7 complemented with relA from suppressor 2	This work
OPS3325	*ptsP* mutant Tn7 complemented with relA from suppressor 7	This work
OPS3326	*ptsP* mutant Tn7 complemented with relA from suppressor 20	This work
OPS3331	*relA* mutant OPS1097 Tn7 complemented with relA wildtype	This work
LMB310	*pssA1* Tn5::spec transductant into Rlv3841	[5]
LMB275	*ptsN1*:: ΩSPec; *ptsN2*:: ΩTet; *ptsP*::Tn5 Rlv3841 triple mutant	This work
AA047	Rlv3841 *ptsN2* (markerless mutation) in *ptsN1*::ΩSpec background (Rlv3841 *ptsN1/N2* double mutant)	[6]
OPS1102	*ptsN1* H66A (Rlv3841 *ptsN2* mutant with non-phosphorylatable PtsN1)	[6]
OPS1104	*ptsN1* H66D (Rlv3841 *ptsN2* mutant with PtsN1 phosphomimic)	[6]
OPS3802	Rlv3841 *abcR1::*ΩSpec mutant	This work
OPS3803	Rlv3841 *abcR2::*ΩSpec mutant	This work
OPS3804	Rlv3841 *abcR1/2::*ΩSpec mutant	This work
Plasmids		
pJET1.2/blunt	*E. coli* cloning vector	Thermo Fisher Scientific
pHP45ΩSpec	pBR322 derivative carrying ΩSpec interposon, pHP45 replicon; Amp^R, $Spec^R$	[7]
pIJ11268	Transcriptional bioreporter; *luxCDABE* cassette with upstream cloning site for driving Lux expression	[8]
pIJ11282	pIJ11268 with promoter region of *nptII* promoter cloned upstream of *luxCDABE, positive control for Lux expression studies*	[8]
pJQ200SK	Suicide vector, *pACYC* derivative, P15A origin of replication; Gm^R, *lacZ sacB traJ*	[9]
pKNT25	BACTH vector for fusions to the N-terminus of fragment T25; $Kana^R$	Euromedex
pUT18C	BACTH vector for fusions to the C-terminus of fragment T18; Amp^R	Euromedex
pRK415	IncP stable broad-host-range cloning vector; Tet^R	[10]
pBBRMCS5	Broad-host-range cloning vector; Gm^R	[11]

pOPS0984	*relA* amplified from wild type Rlv3841 with primers oxp1939/1940 and cloned into pUC18T-Tn7T for Tn7 integration	This work
pOPS0985	relA amplified from ptsP suppressor 2 with primers oxp1939/1940 and cloned into pUC18T-Tn7T for Tn7 integration (clon 2.8)	This work
pOPS0986	relA amplified from ptsP suppressor 7 with primers oxp1939/1940 and cloned into pUC18T-Tn7T for Tn7 integration (clon 7.1)	This work
pOPS0987	relA amplified from ptsP suppressor 20 with primers oxp1939/1940 and cloned into pUC18T-Tn7T for Tn7 integration (clon 13.5)	This work
pRU2204	*relA* PCR-amplified from Rlv3841 with primers p1628/p1629 and cloned into pCR2.1	This work
pRU2205	Inverse PCR from pRU2204 to generate *relA* deletion with primers p1712/p1713 and ΩSpec blunt-end ligated	This work
pRU2216	*relA*::ΩSpec digested ApaI/XbaI and cloned into pJQ200SK, used to generate *relA*::ΩSpec mutant	This work
pOPS0174	C-terminus of *kdpD* PCR-amplified from Rlv3841 with primers oxp0520/0521 and cloned into BACTH vector pKNT25 with BamHI/KpnI	This work
pOPS0357	*relA* PCR amplified with oxp0516/0517 in BACTH vector pKNT25 cloned via BamHI/KpnI	This work
pOPS0182	*ptsN1-H66A* PCR-amplified from Rlv3841 with primers oxp0516/0517 and cloned into BACTH vector pKNT25 with BamHI/KpnI	This work
pOPS0989	*ptsN1-H66D* PCR-amplified from Rlv3841 with primers oxp0516/0517 and cloned into BACTH vector pKNT25 with BamHI/KpnI	This work
pOPS0172	*ptsN1* PCR-amplified from Rlv3841 with primers oxp0516/0517 and cloned into BACTH vector pKNT25 with BamHI/KpnI	This work
pOPS0188	C-terminus of *kdpD* PCR-amplified from Rlv3841 with primers oxp0520/0521 and cloned into BACTH vector pUT18C with BamHI/KpnI	This work
pOPS0713	*relA* PCR-amplified from Rlv3841 with primers oxp0516/0517 and cloned into BACTH vector pUT18C with BamHI/KpnI	This work
pOPS0196	*ptsN1-H66A* PCR-amplified from Rlv3841 with primers oxp0516/0517 and cloned into BACTH vector pUT18C with BamHI/KpnI	This work
pOPS0994	*ptsN1-H66D* PCR-amplified from Rlv3841 with primers oxp0516/0517 and cloned into BACTH vector pUT18C with BamHI/KpnI	This work

pOPS0186	*ptsN1* PCR-amplified from Rlv3841 with primers oxp0516/0517 and cloned into BACTH vector pUT18C with BamHI/KpnI	This work
pUC18T-mini-Tn7T-Gm	Amp^R Gm^R oriT oriV(ColE1) Tn7 delivery vector	[12]
poPS1850	promoterless *gusA* in mTn7 delivery plasmid for promoter fusions	This work
pOPS1854	pOPS1850 derivative expressing the transcriptional fusion of *relA* promoter to *gusA*; Gm^R	This work
pOPS2248	pOPS1850 derivative expressing the transcriptional fusion of *abcR1* promoter to *gusA*; Gm^R	This work
pOPS2249	pOPS1850 derivative expressing the transcriptional fusion of *abcR2* promoter to *gusA*; Gm^R	This work
pUC18	pUC cloning vector; Amp^R	[13]
pOPS2210	pUC18 carrying Rlv3841 *abcR1/2* and its upstream and downstream regions for *abcR1/2* deletion; AmpR, $Spec^R$	This work
pOPS2211	pOPS2210 derivative where *abcR1* region is replaced with ΩSpec interposon; Amp^R, $Spec^R$	This work
pOPS2212	pOPS2210 derivative where *abcR2* region is replaced with ΩSpec interposon; Amp^R, $Spec^R$	This work
pOPS2213	pOPS2210 derivative where *abcR1/2* region is replaced with ΩSpec interposon; Amp^R, $Spec^R$	This work
pK18mobsacB	wide range suicide vector, oriT (mobilizable), sacB; Kan^R	[14]
pOPS2214	Suicide plasmid for *abcR1* deletion; Amp^R, $Spec^R$	This work
pOPS2215	Suicide plasmid for *abcR2* deletion; Amp^R, $Spec^R$	This work
pOPS2216	Suicide plasmid for *abcR1/2* deletion; Amp^R, $Spec^R$	This work

105 **Supplementary Table S3. List of primers.**

Primers	**Description**	**Sequence**
oxp5245	Forward for PCR *gusA* into pUC18T-mini-Tn7T-Gm with HindIII/KpnI site	GCTGCAGGAATTCCTCGAGATAGACTGAGGTAATCATGGTC
oxp5246	Reverse for PCR *gusA* into pUC18T-mini-Tn7T-Gm with HindIII/KpnI site	GCAAGGCCTTCGCGAGGTACTCATTGTTTGCCTCCCTG
oxp5253	Forward for PCR of the promoter of *relA* with PstI site	TTCGATCATGCATGAGCTCAACCAGATGTCGGAAGAAG
oxp5254	Reverse for PCR of the promoter of *relA* with PstI site	TATCTCGAGGAATTCCTGCAATAAAAATAAAAGCGCGCC

oxp7159	Forward for PCR of the promoter of *abcR1* with PstI site	CGATCATGCATGAGCTCACTGCAGATCAACAGCCAG
oxp7160	Reverse for PCR of the promoter of *abcR1*with PstI site	TCTCGAGGAATTCCTGCAATGAGCGATATGGTGGTTTATTG
oxp7161	Forward for PCR of the promoter of *abcR2* with PstI site	CGATCATGCATGAGCTCACTTTTCCTCCCAGTTCCAC
oxp7162	Reverse for PCR of the promoter of *abcR2* with PstI site	TCTCGAGGAATTCCTGCAGAGAGGGATATGGTGCTTC
oxp0721	Tn7 integration mapping primer	TTTTGAAGACAACATCTCCGAACTCACGAC
oxp0092	Tn7 integration mapping primer	CCACAGTTTTCGCGATCCAG
oxp7151	Forward for PCR to generate *abcR1/2* region with BamHI	TGCAGGTCGACTCTAGAGTATCTGACGGGCCACATG
oxp7152	Reverse for PCR to generate *abcR1/2* region with BamHI	TCGAGCTCGGTACCCGGGCCGATCAGGAACAGCGTC
oxp7153	Inverse PCR of *abcR1* with BamHI site added	TTTTTTGGATCCATGAGCGATATGGTGGTT
oxp7154	Inverse PCR of *abcR1* with BamHI site added	TTTTTTGGATCCGCCTTTCTTCCTCAG
oxp7155	Forward for PCR *abcR1/2* region with SmaI site	GACTCTAGAGGATCCCCTATCTGACGGGCCACATG
oxp7156	Reverse for PCR *abcR1/2* region with SmaI site	ATTCGAGCTCGGTACCCCCGATCAGGAACAGCGTC
oxp7157	Inverse PCR of *abcR2* with BamHI site added	TTTTTTGGATCCAGAGGGATATGGTGCT
oxp7158	Inverse PCR of *abcR2* with BamHI site added	TTTTTTGGATCCGCCCAAAATTTGCGCAT
oxp7177	*abcR1/2* region mapping primer	GATGGTGATCGATGGCGTCT
oxp7178	*abcR1/2* region mapping primer	AAGCTTGCCATTGCCCAAAG
oxp0584	ΩSpec interposon mapping for *abcR1/2* mutant check	TCACAAAACGGTTTACAAGC
oxp2326	pUC18 mapping for *abcR1* and *abcR2* mutant check	CGTTCGGTCAAGGTTCTGGA
oxp6980	RT-qPCR primer for *rpoD*	GATGAAGTCGATCGGCAATCTG
oxp6981	RT-qPCR primer for *rpoD*	GCTTCGACCATTTCCTTCTTGG

oxp7207	RT-qPCR primer for *rpoH1*	AAGCGCCTGTTCTTCAACC
oxp7208	RT-qPCR primer for *rpoH1*	ATGACCTCCTCCTCCGAGAC
oxp7029	RT-qPCR primer for *lsrB*	TGTGCACCGTGAAGAGCTT
oxp7030	RT-qPCR primer for *lsrB*	TGCAGATCCAGCTCATCCTC
oxp6439	RT-qPCR primer for *aapJ*	CGGCATTGATCAGCGCATAA
oxp6440	RT-qPCR primer for *aapJ*	TCCCGACGAACACATCATCC
oxp6441	RT-qPCR primer for *aapQ*	TATCATGCCCGTGTCGAAGA
oxp6442	RT-qPCR primer for *aapQ*	TCTGGTATCTCGGCGTTCTC
oxp6248	RT-qPCR primer for *pssA*	ACTTCCAAATTCGGCGCG
oxp6249	RT-qPCR primer for *pssA*	TGAAACGGGCAAGGCGAA

106

REFERENCES

1. Torres-Quesada O, et al. Independent activity of the homologous small regulatory RNAs AbcR1 and AbcR2 in the legume symbiont *Sinorhizobium meliloti*. *PLoS One*. 2013;8(7):e68147.
2. Hanahan D. Studies on transformation of *Escherichia coli* with plasmids. *J Mol Biol*. 1983;166(4):557–80.
3. Albareda M, Buchanan G, Sargent F. Identification of a stable complex between a [NiFe]-hydrogenase catalytic subunit and its maturation protease. *FEBS Lett*. 2017;591(2):338–47.
4. Johnston AW, Beringer JE. Identification of the rhizobium strains in pea root nodules using genetic markers. *J Gen Microbiol*. 1975;87(2):343–50.
5. Prell J, et al. The PTS(Ntr) system globally regulates ATP-dependent transporters in *Rhizobium leguminosarum*. *Mol Microbiol*. 2012;84(1):117–29.
6. Sanchez-Canizares C, et al. Global control of bacterial nitrogen and carbon metabolism by a PTS(Ntr)-regulated switch. *Proc Natl Acad Sci U S A*. 2020;117(19):10234–45.
7. Fellay R, Frey J, Krisch H. Interposon mutagenesis of soil and water bacteria: a family of DNA fragments designed for *in vitro* insertional mutagenesis of gram-negative bacteria. *Gene*. 1987;52(2–3):147–54.
8. Frederix M, et al. Mutation of *praR* in *Rhizobium leguminosarum* enhances root biofilms, improving nodulation competitiveness by increased expression of attachment proteins. *Mol Microbiol*. 2014;93(3):464–78.
9. Quandt J, Hynes MF. Versatile suicide vectors which allow direct selection for gene replacement in gram-negative bacteria. *Gene*. 1993;127(1):15–21.
10. Keen NT, et al. Improved broad-host-range plasmids for DNA cloning in gram-negative bacteria. *Gene*. 1988;70(1):191–7.
11. Kovach ME, et al. Four new derivatives of the broad-host-range cloning vector pBBR1MCS, carrying different antibiotic-resistance cassettes. *Gene*. 1995;166(1):175–6.
12. Choi KH, et al. Genetic tools for select-agent-compliant manipulation of *Burkholderia pseudomallei*. *Appl Environ Microbiol*. 2008;74(4):1064–75.

13. Norrander J, Kempe T, Messing J. Construction of improved M13 vectors using oligodeoxynucleotide-directed mutagenesis. *Gene*. 1983;26(1):101–6.

14. Schäfer A, et al. Small mobilizable multi-purpose cloning vectors derived from the *Escherichia coli* plasmids pK18 and pK19: selection of defined deletions in the chromosome of *Corynebacterium glutamicum*. *Gene*. 1994;145(1):69–73.

Statement of Authorship for joint/multi-authored papers for PGR thesis

To appear at the end of each thesis chapter submitted as an article/paper

The statement shall describe the candidate's and co-authors' independent research contributions in the thesis publications. For each publication there should exist a complete statement that is to be filled out and signed by the candidate and supervisor **(only required where there isn't already a statement of contribution within the paper itself).**

Title of Paper	PTS^{Ntr} interacts with RelA to signal the intracellular nitrogen and carbon balance in *Rhizobium leguminosarum*
Publication Status	□Published □ Accepted for Publication □Submitted for Publication ✓ Unpublished and unsubmitted work written in a manuscript style
Publication Details	**Tjahjono, O.**, Uceda Heras, Shutin, D., Tkacz, A., Palomero, M., Citerne, S., Pini, F., Abreu, I., Mulley, J., Karunakaran, R., Ledermann, R., Prell, J., Field, B., Bolla, J., Poole, P., Sánchez-Cañizares, C. PTS^{Ntr} interacts with RelA to signal the intracellular nitrogen and carbon balance in *Rhizobium leguminosarum.* In preparation.

Student Confirmation

Student Name:	Olivia Tjahjono		
Contribution to the Paper	I contributed to the later stages of the project, mainly on the regulation exerted by sRNAs and their sigma factors. I performed experiments (generation of constructs and mutant strains, sRNA bioinformatics, promoter activity assays, AIB transport rate measurements, and RT-qPCR for sigma factors and transporter genes), analysed the data, created figures, and wrote the related Introduction/Methods/Results sections. I also prepared the samples for (p)ppGpp quantification and coordinated their shipment to collaborators, made the conclusion figures, and co-wrote the Discussion with CSC.		
Signature 		Date	07 October 2025

Supervisor Confirmation

By signing the Statement of Authorship, you are certifying that the candidate made a substantial contribution to the publication, and that the description described above is accurate.

Supervisor name and title: Professor Philip Poole		
Supervisor comments The above statement by Olivia about authorship is a true reflection of the work and authorship.		
Signature 	Date	8th October 2025

This completed form should be included in the thesis, at the end of the relevant chapter.

List of figures constituting my work:

Figure 3: Replicates for panel 3.B.

Figure 5: I prepared the samples; (p)ppGpp analysis was performed by Sylvie Citerne and Ben Field.

Figure 6: Panels 6.H and 6.I were generated by me.

Figure 7: My own work.

Figure 8: My own work.

Supplementary Figure S10: My own work.

CHAPTER 5

Characterisation of the SixA phosphatase in *Rhizobium leguminosarum*

5.1 Introduction

In *Escherichia coli*, the HPr kinase/phosphorylase (HPrK/P) is absent, and instead the phosphohistidine phosphatase SixA has been shown to act on PTS^{Ntr} by dephosphorylating NPr at its histidine residue, helping to modulate signal transduction and maintain proper control of central metabolism. A loss-of-function mutation in *sixA* exhibits phenotypes consistent with hyperphosphorylated NPr, including impaired growth in various carbon sources (acetate, maltose, and glucose), and reduced potassium levels (1). Although the role of SixA (1) and its crystal structure (2) have been characterised in *E. coli*, information about its role, conservation, and physiological functions in other species, including rhizobia, is lacking (**Figure 1**). Here, we investigate whether SixA affects any cellular function associated with the nitrogen-related phosphotransferase system PTS^{Ntr} in *R. leguminosarum* and find no functional role under the tested conditions. SixA is dispensable in this context and may act under specific conditions yet to be identified.

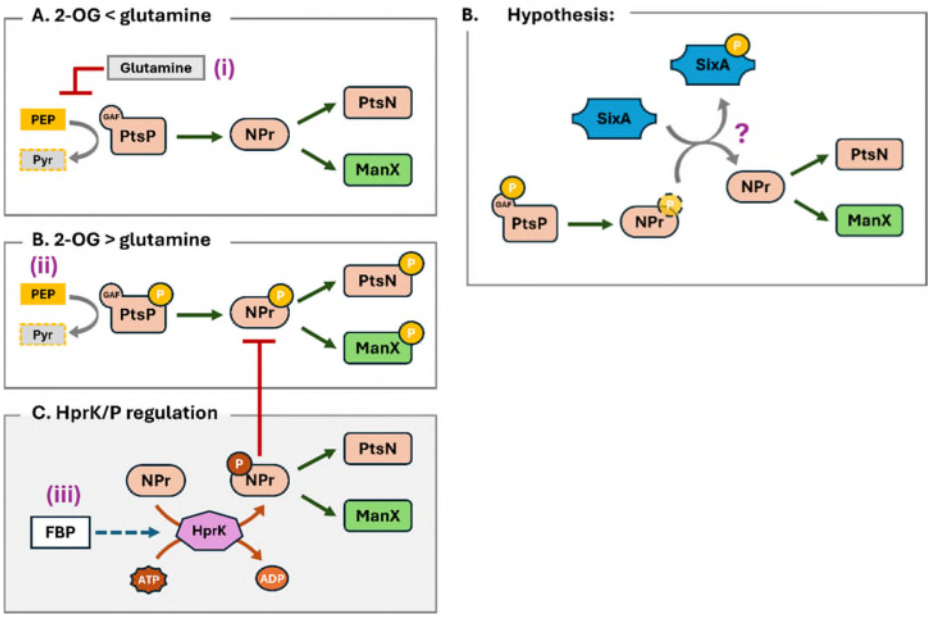

Figure 1. Schematic diagrams of (A) current phosphorylation model of PTS^{Ntr} regulated by different 2-OG/glutamine ratios and HprK/P. Points (i)–(iii) indicate key metabolic inputs: (i) glutamine; (ii) phosphoenolpyruvate (PEP), the phosphoryl donor that is converted into pyruvate (Pyr); and (iii) fructose-1,6-biphosphate (FBP). (B) working hypothesis for the role of SixA in *R. leguminosarum*. Yellow circles indicate histidine phosphorylation, while the red circles represent serine phosphorylation.

5.2 Materials and Methods

Sequence analysis and database search of the *sixA* gene

The *sixA* sequence of *E. coli* strain K12 (Taxonomy ID: 511145; Accession: NP_416842) was retrieved from the NCBI database. BLAST (4) and the Biocyc database (5) were used to find its homolog in *R. leguminosarum*.

Bacterial strains and culture conditions

E. coli strains were grown in Luria-Bertani (LB) (6) solid or liquid medium supplemented with appropriate antibiotics at 37 °C. *R. leguminosarum* strains were grown and maintained at 28 °C in the Tryptone Yeast (TY) extract with the appropriate antibiotics or transferred into universal minimum salts (UMS) (7) with various carbon and nitrogen

sources for the different assays. The bacterial strains and plasmids used in this study are shown in **Table 1**.

Table 1. List of strains and plasmids

Strains	Description	Reference
Escherichia coli		
DH5a	*sup*E44, *hsd*R17, *recA1 thi-1, ΔlacU169 (ϕ80lacZ*ΔM15*) endA1 gyrA96 relA1*	(8)
Rhizobium leguminosarum		
Rlv3841	*R. leguminosarum* bv. *viciae*; Str^R derivative of strain 300	(9)
LMB310	Rlv3841 *pssA*::Tn5 transductant or *pssA* (RL1532) mutant	(10)
AA081	Rlv3841 *hprK*::ΩSpec	(3)
OPS3278	Rlv3841 with MCS-sgfp with the promoter region of RL2644 (*sixA*) made from conjugation with pOPS1995	this work
OPS3279	Rlv3841 with MCS-sgfp with the promoter region of RL0036 (*chvI-chvG-hprK*) made from conjugation with pOPS1996	this work
OPS3280	Rlv3841 *ΔsixA* (RL2644) markerless deletion mutant generated with plasmid pOPS1997, mapped with oxp5738 and oxp5872	this work
OPS3282	Rlv3841 containing pOPS1916 (MCS-gfp empty vector) to use as negative control for expression analysis	this work
Plasmids		
pRK2013	Self-transmissible helper plasmid, Km^R	(11, 12)
pK18mobsacB	wide range suicide vector, oriT (mobilisable), *sacB*; Kan^R	(13)
pOPS1916	Golden Gate assembled plasmid (RK2 low-copy number backbone) with a multi-cloning site (MCS) upstream of a strong RBS, superolder GFP (sfGFP), and DT16 terminator	this work
pOPS1995	pOPS1916 (MCS-gfp) digested with SpeI to clone the promoter region of RL2644 (*sixA*); PCR amplified from Rlv3841 with oxp5818 and oxp5819 using HiFi	this work
pOPS1996	pOPS1916 (MCS-gfp) digested with SpeI to clone the promoter region of RL0036 (*chvI-chvG-hprK*) PCR amplified from Rlv3841 with oxp5820 and oxp5821 using HiFi assembly	this work
pOPS1997	pK19mobsacB digested with SmaI to clone the upstream/downstream region to make a deletion mutant of RL2644 (*sixA*) PCR amplified from Rlv3841 with oxp5734-oxp5735 and oxp5736-oxp5737 using HiFi assembly	this work

Bacteria growth curves and mean generation time

Single colonies of rhizobial strains were streaked and grown in 10 mL TY agar slopes at 28 °C for three days. The bacteria were then washed 3 times in UMS (without carbon and

nitrogen sources), and this cell suspension was used to inoculate 500 µL of UMS liquid media supplemented with the corresponding carbon and nitrogen sources in 24-well plates, adjusted to a starting OD_{600} value of 0.05. The bacteria were then grown for 48 hours to reach their stationary phase at 28 °C with shaking at 700 rpm inside the Omega FLUOstar plate reader, with their OD600 monitored every 30 minutes to obtain the growth curves. Mean generation times were calculated as the number of hours required for a population of a particular rhizobial strain to double in number.

Cloning and generation of mutants

Cloning was done following standard molecular biology protocols (6). PCR reactions were performed using Phusion High-Fidelity DNA Polymerase (Thermo Fisher) with primers listed in **Table 2**; restriction digests were conducted with enzymes from New England Biolabs, following the manufacturer's protocols. The cloning results were then confirmed using Sanger sequencing performed by Source Biosciences.

Table 2. List of primers

Primers	Description	Sequence
oxp5734	*sixA* upstream forward	GTCGACTCTAGAGGATCCCCGGTCCAGTTTCCATCCAG
oxp5735	*sixA* upstream reverse	GACTTCAGGCTACGGTCATGGGCAAATC
oxp5736	*sixA* downstream forward	CATGACCGTAGCCTGAAGTCTTTCTCGC
oxp5737	*sixA* downstream reverse	TGAATTCGAGCTCGGTACCCTTCCAGATCTTGCACGGC
oxp5738	*sixA* mapping forward	CTTTCCGATGCAGCGACAAG
oxp5872	*sixA* mapping reverse	TCCTTCACCAGCGCACGG
oxp5818	*sixA* promoter forward	CGAATTCGGATCCGGAGAAACGCGATTCTCCTGAAGAAC
oxp5819	*sixA* promoter reverse	AATTCTAGATGCGGCCGCTACATGGGCAAATCCAAGATC
oxp5820	*hprK* promoter forward	CGAATTCGGATCCGGAGAAAGGCGGAAAAGTTGTAGCG
oxp5821	*hprK* promoter reverse	AATTCTAGATGCGGCCGCTAATATCCTTCGGCCTCCAG

The *sixA* deletion mutant strain was constructed by first amplifying the 1kb upper and downstream regions of *sixA* (RL2644, 495bp) with the pair of primers oxp5734-oxp5735 and oxp5736-oxp5737 (**Table 2**). Amplified regions were subsequently integrated into the suicide plasmid pK19mobSacB, which had been cut with the SmaI restriction enzyme, and assembled using the Gibson assembly method. The resulting plasmid was conjugated into *R. leguminosarum* bv. viciae 3841 (Rlv3841), and the selection for single-crossover integration into the chromosomal region of interest was performed by plating cells on selective TY agar media containing 100 µg mL^{-1} kanamycin. The selected single-crossover mutants were then grown on TY agar supplemented with 10% (v/v) sucrose to select double-crossover deletions occurring at the target gene *sixA*, which was confirmed by antibiotic screening and PCR sequencing.

To study GFP expression, the promoter regions of the *sixA* and *hprK* genes were amplified with primers oxp5818-oxp5819 and oxp5820-oxp5821, respectively (**Table 2**). These fragments were then cloned into pOPS1916 by digestion with SpeI, followed by Gibson assembly. The resulting plasmids were transferred into Rlv3841 by conjugation.

Promoter activity assays

GFP reporter assays were used to study *sixA* and *hprK* promoter activity. Rhizobial colonies were prepared in TY agar slopes and washed twice in UMS, as described for the bacterial growth curves explained above. To study gene expression in different carbon and nitrogen sources, these bacterial suspensions were used to inoculate 500 µL of UMS with the corresponding carbon and nitrogen sources in 24-well plates with a starting OD_{600} value of 0.05. The bacteria were then grown for 48 hours to reach their stationary phase at 28 ˚C with shaking at 700 rpm inside the Omega FLUOstar plate reader. GFP

measurements were taken at time points 15h (log phase) with excitation 485 nm, emission 520 nm, and gain set at 750.

EPS quantification

EPS was quantified following the previously described protocol (3). *R. leguminosarum* liquid cultures were grown in 50 mL UMS with 10 mM glucose and 10 mM NH_4Cl to reach an OD_{600} of 1. The cultures were then centrifuged, and the pelleted cells were dried and weighed. The supernatants were treated with twice the volume of ethanol (100 mL) and incubated at 4°C for 24 hours. The precipitated EPS was then collected by centrifugation, dried, and weighed. The strain LMB310 (*pssA* mutant), which did not produce EPS, was used as the negative control.

Transport assays

Rhizobia strains were grown in 50 mL UMS liquid cultures with 10 mM glucose and 10 mM NH_4Cl overnight. After washing the cells with plain UMS twice, the cells were adjusted to an OD600 of 1 and starved for 2 hours (no carbon or nitrogen was added to the growth medium). Transport assays were performed with 25 µM (4.625 kBq) of ^{14}C-labelled solute of α-aminoisobutyric acid (AIB), following the protocols that have been previously described (14, 15).

Plant growth and acetylene reduction assays

Seeds of *Pisum sativum* cv. Avola were surface sterilised using 70% ethanol and 2% sodium hypochlorite. They were sown into 1 L beakers filled with sterile medium-grade vermiculite and N-free solution as described previously (16) and inoculated with appropriate rhizobial liquid cultures. Pea plants were grown under long-light conditions (16 h light/8 h dark, 24 °C) and harvested 3 weeks after sowing.

Acetylene reduction assays (ARA) were performed as described in (17). Pea plants were put inside Schott bottles, in which 2% of the total headspace atmosphere was replaced with acetylene using a 10 mL syringe and needles. After a 1 h interval, aliquots of the headspace atmosphere were collected using a 1 ml syringe. The conversion of acetylene gas to ethylene gas was measured using a gas chromatograph (PerkinElmer, Clarus 480, equipped with a HayeSep® N (80–100 MESH) 584 column).

Statistical analysis

All statistical analyses were carried out using GraphPad Prism 10.5.0 (GraphPad Software, 7825 Fay Avenue, Suite 230, La Jolla, CA 92037, USA). Student's t-tests and analysis of variance were used to measure the significance of results. Where multiple comparisons were necessary, the One-way ANOVA (Tukey-Kramer method) was used. We took a *p-value* less than 0.05 to be statistically significant. All values are derived from single colonies representing a single biological replicate. Biological replicates were sampled with two to three technical replicates each.

5.3 Results

The SixA phosphatase homolog was identified by sequence similarity in *R. leguminosarum*

To investigate the potential interplay between the HprK/P and the SixA phosphatase in regulating the phosphorylation state of NPr in *R. leguminosarum*, we first identified potential SixA candidates by performing a protein BLAST search against the *E. coli* SixA amino acid sequence (Taxonomy ID: 511145; Accession: NP_416842). The top hit RL2644 (RL_RS13650) was annotated as a putative histidine phosphatase family, sharing 36.05% (E-value $2e^{-09}$) amino acid identity with *E. coli sixA* (**Figure 2**). Despite its lower identity,

the *sixA* gene of Rlv3841 conserves the region corresponding to the phosphatase active site. RL2644 contains the histidine phosphatase active sites and two amino acid residues highly conserved in the *E. coli sixA* homolog (18). Additionally, Dali structural comparison (19) of the RL2644 revealed a highly significant match to proteins of the histidine phosphatase family with strong conservation of the overall folds (Z-score >20.0). Unlike in *R. leguminosarum*, in which only one homolog was identified, other rhizobia, such as *R. etli*, *Mesorhizobium loti*, and *Sinorhizobium meliloti*, seem to harbour two copies of *E. coli's sixA* homologs (18), although their functionality remains unknown.

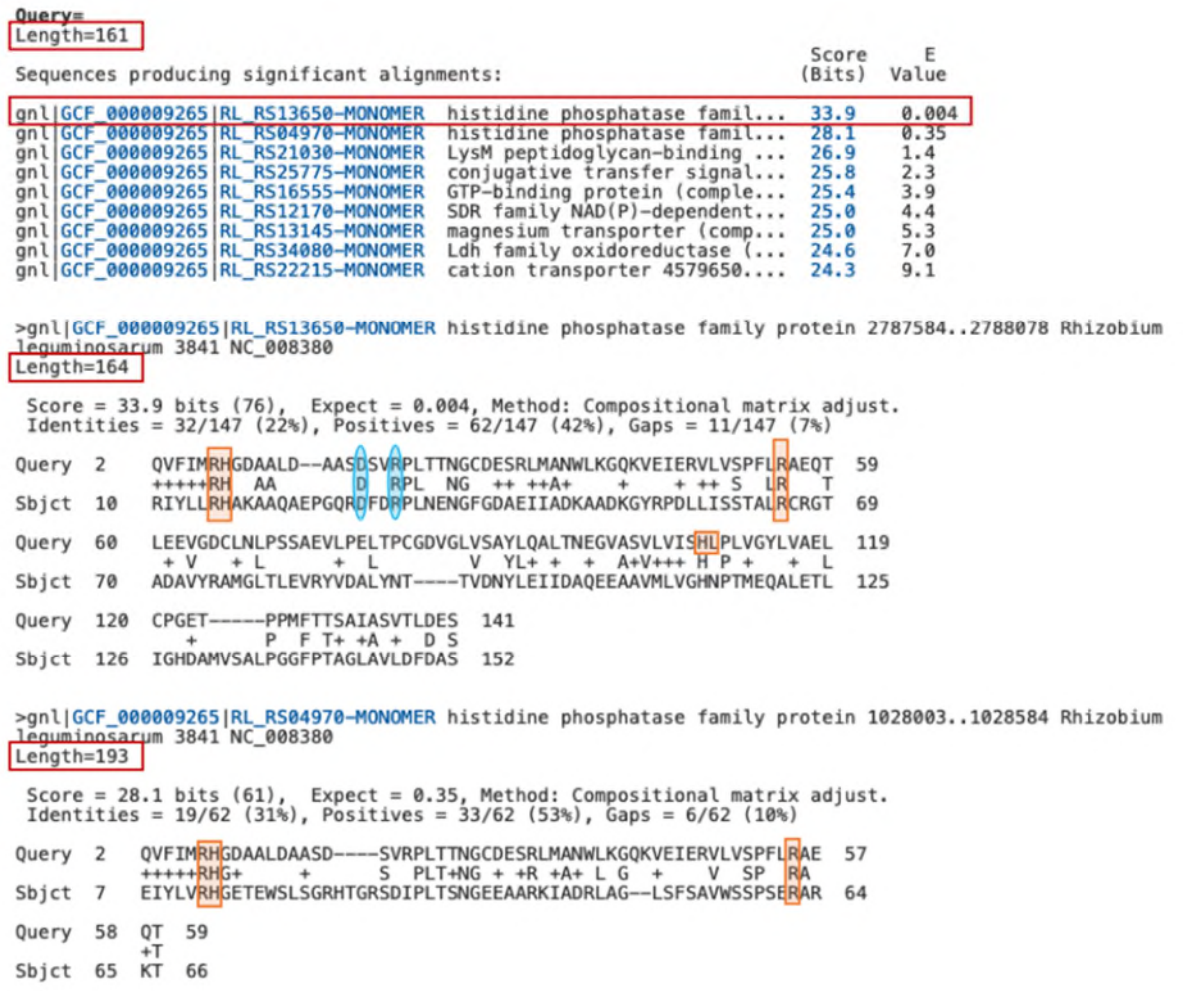

Figure 2. BLAST search result of *E. coli* SixA protein sequence in *R. leguminosarum*. The highest match obtained was RL2644 (RL_RS13650), followed by RL0954 (RL_RS04970). The residues highlighted in orange on the alignment correspond to the

phosphatase active site. On the other hand, the residues highlighted in blue are the residues which are considered to be highly conserved in the different sixA homologs across genera (18).

The existing INSeq library (20–22) (**Table 3**) and a Co-Expression database (23, 24) already available in our laboratory (**Table 4**) were used to narrow down the conditions under which SixA might be functional. The INSeq library data indicated that RL2644 mutant growth is defective during pea root attachment at pH 7.5 (22). Co-expression analysis (23, 24) shows the overlap of RL2644 expression with genes that function in carbon metabolism and transport (*aaC, glgB, xylA*), cell envelope biosynthesis (*murA, bamD*), and stress response (*dksA*, UbiH/UbiF family hydroxylase), among other genes (**Table 4**).

Table 3. INSeq Results for *sixA* (20–22). NE = Growth neutral; ***DE*** = Growth defective

Growth Condition	INSeq	Growth Condition	INSeq
Pea Root Attached Alkaline pH7.5	***DE***	21% Oxygen + 10mM Glucose	NE
Pea Root Attached Acid pH6.5	NE	21% Oxygen + 20mM Succinate	NE
Pea Root Attached Neutral pH7.0	NE	1% Oxygen + 10mM Glucose	NE
Bacteroid (pea)	NE	1% Oxygen + 20mM Succinate	NE
Rhizosphere (pea)	NE	TY media	NE
Colonisation (pea)	NE	Vincent's media	NE

Table 4. List of genes co-expressed with RL2644 (*sixA*). Community detection, Pajde Rank, and Edge Weight are 3 methods used to measure the degree of co-expression (23, 24). The smaller the value, the higher the chance that both genes are co-expressed. Genes which are counted as highly co-expressed with RL2644 by two or more detection methods (<50) are highlighted in blue.

Gene Code	Community detection	Padje rank	Edge weight	Gene	Description	Group
pRL120025	10	540	103		sugar phosphate isomerase/epimerase	carbon metabolism and transport
pRL120556	1148	5	516		sugar ABC transporter substrate-binding protein	

pRL120596	1394	2	696		phosphoenolpyruvate hydrolase family protein	
RL2088	146	305	6	***accC***	acetyl-CoA carboxylase biotin carboxylase subunit	
RL4115	19	233	8	***glgB***	1,4-alpha-glucan branching protein GlgB	
RL4176	186	150	2	***xylA***	xylose isomerase	
RL4621	41	170	9		acetyl-CoA C-acetyltransferase	
RL0611	2	120	4	***murA***	UDP-N-acetylglucosamine 1-carboxyvinyltransferase	cell envelope biosynthesis
RL3296	1082	9	245	***bamD***	outer membrane protein assembly factor BamD	
RL3463	4	241	48		prolipoprotein diacylglyceryl transferase	
RL3646	7	126	70		lipopolysaccharide biosynthesis protein	
RL2096	1650	4	867		LL-diaminopimelate aminotransferase	synthesis
RL0493	90	387	3		dihydroorotase	
RL2292	3	156	11		UbiH/UbiF family hydroxylase	stress response
RL2745	1457	1	602		aldehyde dehydrogenase family protein	
RL2643	1365	7	699	***dksA***	RNA polymerase-binding protein DksA	
pRL110545	9	231	10	***minD***	septum site-determining protein MinD	other
pRL90271	1150	10	487		prolyl-tRNA editing protein YbaK/EbsC family protein	
RL0196	25	90	45		BMP family ABC transporter substrate-binding protein	
pRL110618	34	337	1		hypothetical membrane protein	
RL1536	24	296	7		TIGR00730 family Rossman fold protein	
RL2697	162	220	5		DUF2059 domain-containing protein	
RL0961	1	64	12		hypothetical protein	
RL1608	8	194	41		hypothetical protein	
RL4074	6	115	17		hypothetical protein	
RL3480	5	292	49		hypothetical protein	
RL3891	1351	3	824		hypothetical protein	

154

R. leguminosarum SixA phosphatase does not affect PTS^{Ntr}-related functions

Because HprK and SixA are expected to act synergistically to promote the dephosphorylated state of NPr, the expression pattern of the *sixA* gene was studied together with *hprK* using their promoter regions fused to sfGFP and cloned in a RK2 low-copy-number plasmid background (pOPS1916). The bacterial cells harbouring these vectors were cultured with 10 mM glucose or 20 mM succinate as the carbon source. P_{sixA} was more strongly activated than P_{hprK} in the tested conditions, and both the expression of P_{sixA} and P_{hprK} were strongest when the strains were grown in 20 mM succinate (**Figure 3.A**). The expression patterns of P_{sixA} and P_{hprK} were also comparable when cells were grown under different pH levels supplemented with 10 mM glucose and 10 mM NH_4Cl (**Figure 3.B-C**). Both promoters were more active at a lower pH (pH 5.75).

Additionally, a stable *sixA* deletion mutant was also generated by double recombination and subjected to different phenotypic assays targeting the PTS^{Ntr}-regulated process (**Figure 4.A-D**). These include assessment of growth, O_2 consumption rates, EPS production, active nutrient uptake, and symbiosis capability. To measure nutrient uptake, α-aminoisobutyric acid (AIB) was used as substrate, as this amino acid cannot be metabolised but can be transported by the Aap and Bra ABC amino acid transport systems (15). Our results showed that the *sixA* mutant displayed no growth defect across the tested conditions (**Table 5**). The O_2 consumption, EPS production, and AIB transport rates were those of wild-type. The symbiotic capacity of the *sixA* mutant, measured by counting the nodule number and carrying out the acetylene reduction assay on the inoculated pea plants, with values also comparable to those of wild-type, indicating that the Rlv3841 SixA homolog has no impact on these PTS^{Ntr}-regulated processes. This is

unlike in *E. coli*, where the *sixA* mutant is less efficient in colonising the mouse gut than wild-type (1).

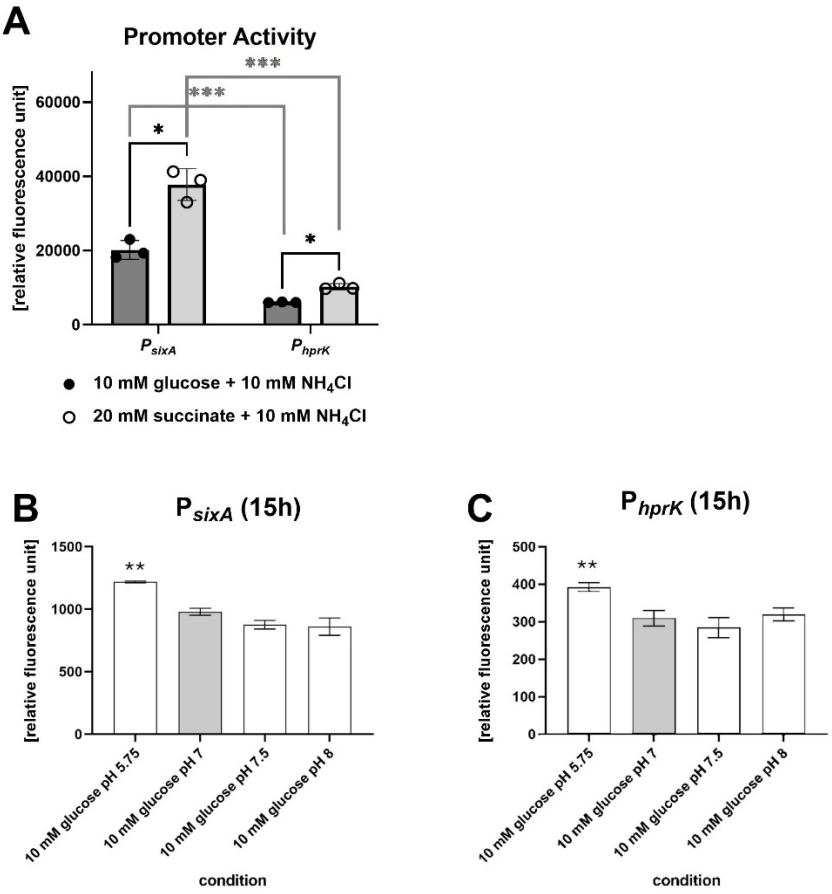

Figure 3. The *sixA* gene is transcribed in the same pattern as the *hprK* gene. (A) Promoter activities of the *sixA* and *hprK* genes of wild-type cells grown in UMS liquid culture supplemented with 10 mM NH4Cl and either 10 mM glucose (dark grey bars) or 10 mM succinate (light grey bars). Statistical significances were assessed by Student's t-test, with asterisks indicating the following level of significance: *** $P \leq 0.001$ and * $P \leq 0.05$. Expression of (B) P_{sixA} and (C) P_{hprK} at different pHs in media supplemented with 10 mM glucose and 10 mM NH_4Cl. Data are averages (±SEM) from at least three independent cultures. Statistical significances were assessed by one-way ANOVA against pH 7 (grey bar), with asterisks indicating the following level of significance: ** $P \leq 0.01$, and ns, not significant.

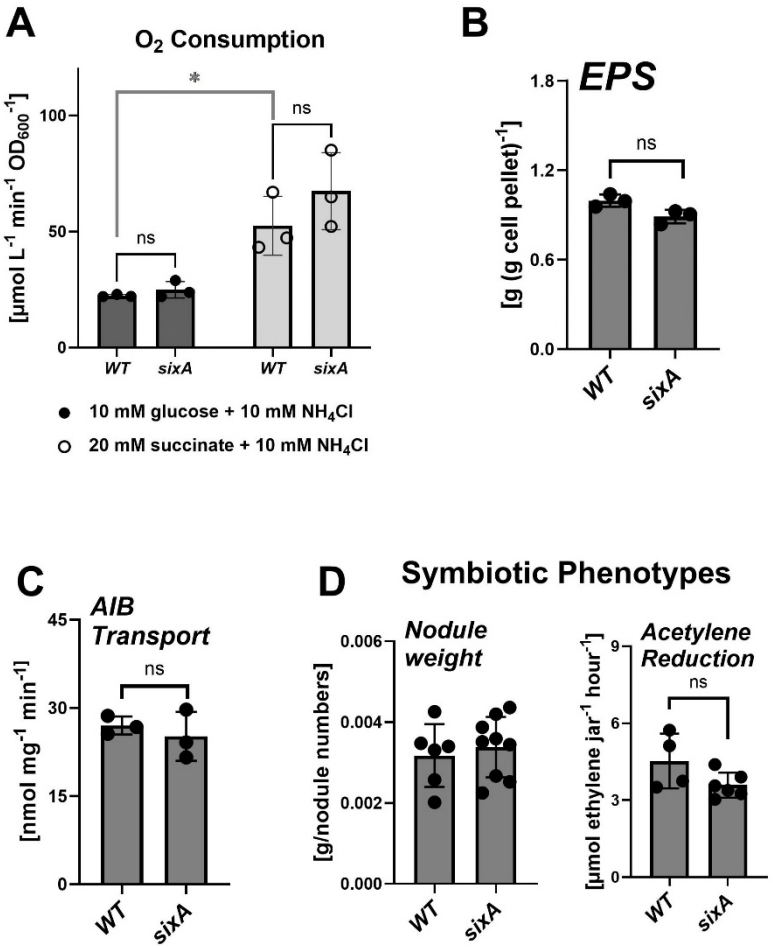

Figure 4. Deletion of *sixA* does not affect the tested phenotypes. Phenotypic assays comparing the *sixA* mutant to wild-type under identical conditions, with (B-C) done in free living cells in 10 mM glucose + 10 mM NH_4Cl; and (D) in pea plants inoculated with these strains. The oxygen consumption rate (A), EPS production (B), AIB transport (C), and symbiotic phenotypes (D) of the *sixA* mutant were comparable to those of the wild-type. Data are averages (±SEM) from at least three independent cultures. Statistical significances were assessed by Student's t-test, with asterisks indicating the following level of significance: * $P \leq 0.05$ and ns, not significant.

Table 5. Mean generation time of *sixA* mutants compared to Rlv3841 wild-type

Growth Condition	MEAN GENERATION TIME (hours)	
	wild-type	*ΔsixA*
10 mM glucose + 10 mM NH_4Cl	4.01 ± 0.93	4.27 ± 0.60
20 mM succinate + 10 mM NH_4Cl	3.75 ± 0.12	4.09 ± 0.67
10 mM glucose + 10 mM glutamine	3.04 ± 0.47	3.64 ± 0.77
10 mM glucose + 10 mM glutamate	7.43 ± 1.53	8.10 ± 2.83

Discussion

Because *E. coli* SixA functions as a phosphohistidine phosphatase that dephosphorylates NPr within the PTS^{Ntr} regulatory network (1), we therefore studied the role of its homologue in *R. leguminosarum*. Despite evidence from GFP promoter fusions suggesting that *sixA* and *hprK* share similar expression patterns, functional characterisation of the *sixA* mutant in *R. leguminosarum* showed no evidence that SixA affects known PTS^{Ntr} functions. Across all tested conditions, the *sixA* mutant phenotype is indistinguishable from wild-type. This contrasts with findings in *E. coli* (1), which notably lacks the *hprK* gene present in α-proteobacteria, suggesting that *R. leguminosarum* and *E. coli* may employ distinct regulatory mechanisms to control the phosphorylation state of NPr. It is also plausible that the regulatory function of SixA manifests only under environmental contexts not yet tested, such as carbon limitation or osmotic stress, as suggested by the co-expression databases (23, 24). Additionally, given the role of the PTS^{Ntr} in regulating carbon and nitrogen balance, future work should include analysis of this strain under nitrogen-limiting conditions.

Conclusion

R. leguminosarum, and possibly other Alphaproteobacteria, regulate NPr phosphorylation differently from *E. coli*. Given that HprK is present in this lineage, it likely serves as the dominant regulator which promotes the non-phosphorylated state of the NPr.

References

1. Schulte JE, Goulian M. 2018. The phosphohistidine phosphatase SixA targets a phosphotransferase system. mBio 9:e01666-18. https://doi.org/10.1128/mBio.01666-18.

2. Hamada K, Kato M, Shimizu T, Ihara K, Mizuno T, Hakoshima T. 2005. Crystal structure of the protein histidine phosphatase SixA in the multistep His–Asp phosphorelay. Genes Cells 10:1–11. https://doi.org/10.1111/j.1365-2443.2005.00817.x.

3. Sánchez-Cañizares C, Prell J, Pini F, Rutten P, Kraxner K, Wynands B, Karunakaran R, Poole PS. 2020. Global control of bacterial nitrogen and carbon metabolism by a PTS^{Ntr}-regulated switch. Proc Natl Acad Sci U S A 117:10234–10245. https://doi.org/10.1073/pnas.1917471117.

4. Altschul SF, Gish W, Miller W, Myers EW, Lipman DJ. 1990. Basic local alignment search tool. J Mol Biol 215:403–410. https://doi.org/10.1016/S0022-2836(05)80360-2.

5. Karp PD, Billington R, Caspi R, Fulcher CA, Latendresse M, Kothari A, Keseler IM, Krummenacker M, Midford PE, Ong Q, Ong WK, Paley SM, Subhraveti P. 2019. The BioCyc collection of microbial genomes and metabolic pathways. Brief Bioinform 20:1085–1093. https://doi.org/10.1093/bib/bbx085.

6. Green MR, Sambrook J. 2012. Molecular cloning: a laboratory manual, 4th ed. Cold Spring Harbor Laboratory Press, Cold Spring Harbor, NY.

7. Beringer JE. 1974. R factor transfer in *Rhizobium leguminosarum*. J Gen Microbiol 84:188–198. https://doi.org/10.1099/00221287-84-1-188.

8. Hanahan D. 1983. Studies on transformation of *Escherichia coli* with plasmids. J Mol Biol 166:557–580. https://doi.org/10.1016/S0022-2836(83)80284-8.

9. Johnston AWB, Beringer JE. 1975. Identification of the Rhizobium strains in pea root nodules using genetic markers. J Gen Microbiol 87:343–350. https://doi.org/10.1099/00221287-87-2-343.

10. Prell J, Mulley G, Haufe F, White JP, Williams A, Karunakaran R, Downie JA, Poole PS. 2012. The PTSNtr system globally regulates ATP-dependent transporters in Rhizobium leguminosarum. Mol Microbiol 84:117–129. https://doi.org/10.1111/j.1365-2958.2012.08014.x.

11. Knauf VC, Nester EW. 1982. Wide host range cloning vectors: a cosmid clone bank of an *Agrobacterium* Ti plasmid. Plasmid 8:45–54. https://doi.org/10.1016/0147-619X(82)90040-3.

12. Figurski DH, Helinski DR. 1979. Replication of an origin-containing derivative of plasmid RK2 dependent on a plasmid function provided in trans. Proc Natl Acad Sci U S A 76:1648–1652. https://doi.org/10.1073/pnas.76.4.1648.

13. Schäfer A, Tauch A, Jäger W, Kalinowski J, Thierbach G, Pühler A. 1994. Small mobilizable multi-purpose cloning vectors derived from the *Escherichia coli* plasmids pK18 and pK19: selection of defined deletions in the chromosome of *Corynebacterium glutamicum*. Gene 145:69–73. https://doi.org/10.1016/0378-1119(94)90324-7.

14. Poole PS, Franklin M, Glenn AR, Dilworth MJ. 1985. The transport of L-glutamate by *Rhizobium leguminosarum* involves a common amino acid carrier. J Gen Microbiol 131:1441–1448. https://doi.org/10.1099/00221287-131-6-1441.

15. Hosie AHF, Allaway D, Galloway CS, Dunsby HA, Poole PS. 2002. *Rhizobium leguminosarum* has a second general amino acid permease with unusually broad substrate specificity and high similarity to branched-chain amino acid transporters (Bra/LIV) of the ABC family. J Bacteriol 184:4071–4080. https://doi.org/10.1128/JB.184.15.4071-4080.2002.

16. Poole PS, Blyth A, Reid CJ, Walters K. 1994. myo-Inositol catabolism and catabolite regulation in *Rhizobium leguminosarum* bv. *viciae*. Microbiology 140:2787–2795. https://doi.org/10.1099/00221287-140-10-2787.

17. Haskett TL, Knights HE, Jorrin B, Mendes MD, Poole PS. 2021. A simple *in situ* assay to assess plant-associative bacterial nitrogenase activity. Front Microbiol 12:690439. https://doi.org/10.3389/fmicb.2021.690439.

18. Hakoshima T, Ichihara H. 2007. Structure of SixA, a histidine protein phosphatase of the ArcB histidine-containing phosphotransfer domain in *Escherichia coli*, p 288–304. In Simon MI, Crane BR (ed), Two-Component Signaling Systems, Part A. Methods in Enzymology, vol 422. Academic Press, San Diego, CA.

19. Holm L. 2022. Dali server: structural unification of protein families, *Nucleic Acids Research* 50: W210–W215. https://doi.org/10.1093/nar/gkac387.

20. Wheatley RM, Ford BL, Li L, Aroney STN, Knights HE, Ledermann R, East AK, Ramachandran VK, Poole PS. 2020. Lifestyle adaptations of *Rhizobium* from rhizosphere to symbiosis. Proc Natl Acad Sci U S A 117:23823–23834. https://doi.org/10.1073/pnas.2009094117.

21. Wheatley RM, Ramachandran VK, Geddes BA, Perry BJ, Yost CK, Poole PS. 2017. Role of O2 in the growth of *Rhizobium leguminosarum* bv. *viciae* 3841 on glucose and succinate. J Bacteriol 199:e00572-16. https://doi.org/10.1128/JB.00572-16.

22. Parsons JD, Cocker CR, East AK, Wheatley RM, Ramachandran VK, Kaschani F, Kaiser M, Poole PS. 2024. Factors governing attachment of *Rhizobium leguminosarum* to legume roots at acid, neutral, and alkaline pHs. mSystems 9:e00422-24. https://doi.org/10.1128/msystems.00422-24.

23. Bozhilova LV, Pardo-Diaz J, Reinert G, Deane CM. 2021. COGENT: evaluating the consistency of gene co-expression networks. Bioinformatics 37:1928–1929. https://doi.org/10.1093/bioinformatics/btaa787.

24. Pardo-Diaz J, Poole PS, Beguerisse-Díaz M, Deane CM, Reinert G. 2022. Generating weighted and thresholded gene co-expression networks using signed distance correlation. Network Science 10:131–145. https://doi.org/10.1017/nws.2022.13.

6. General discussion & future perspectives

First characterised in the 1990s (Powell et al., 1995), PTS^{Ntr} acts as a major sensor-actuator of the carbon and nitrogen status in Alphaproteobacteria and has been the subject of several studies. More recent work has begun to elucidate the molecular mechanism and direct targets, notably the non-phosphorylated PtsN ($EIIA^{Ntr}$) control of the KdpD-mediated potassium transport (Feng et al., 2022; Untiet et al., 2013) and PtsP~P binding to the ACT domain of long RSH protein (Ronneau, Petit, et al., 2016; Ronneau et al., 2019a). Nonetheless, dedicated PTS^{Ntr} reviews are sparse, with the last focused review on this system done by Pflüger-Grau and Görke (2010). Therefore, as the background for this thesis (**Chapter 2**), I review the most recent findings on PTS^{Ntr} with a focus on Alphaproteobacteria, discussing the general phosphorelay mechanism, each individual PTS^{Ntr} node, and its known regulatory targets. I also briefly cover some of the interaction partners identified in other clades but not yet confirmed in Alphaproteobacteria, as well as other key regulators that may act in concert with PTS^{Ntr}.

In **Chapter 3**, I sought to characterise the role of PTS^{Ntr} in shaping carbon metabolism. Enzyme activity assays and polymer quantification show that carbon flux is regulated by the carbon-nitrogen balance, and that mutations in *manX* or *hprK* disrupt this control. In its unphosphorylated state, ManX regulates the TCA cycle dehydrogenase enzymes. Mutating *manX*, in turn, results in reduced TCA activity under nitrogen excess conditions. This phenotype resembles that of the wild-type under nitrogen-limiting conditions, in which TCA activity is reduced and carbon is rerouted to PHB, glycogen, and EPS. Loss of HprK abolishes serine phosphorylation of NPr, which normally antagonises the NPr-His phosphorylation (Dozot et al., 2010; Pinedo & Gage, 2009). Consequently, PtsN is

hyperphosphorylated in the *hprK* mutant, and EPS accumulates in this strain. Pyrimidines likewise accumulate in the *hprK* mutant, consistent with increased MDH activity. The *hprK* mutant appears to shift toward gluconeogenesis under conditions that are typically glycolytic. Based on qPCR analysis, we observed that *pckR*, which encodes a transcriptional factor that differentially regulates glycolysis/ED versus gluconeogenesis/TCA genes, is affected in the *hprK* mutant. While the evidence remains indirect, our findings refine the functional roles of ManX and HprK, positioning them as components of PTS^{Ntr} involved in the regulation of carbon metabolism.

The interplay between the stringent response and PTS^{Ntr} under nitrogen starvation conditions was first established in the Alphaproteobacterium *Caulobacter crescentus* (Ronneau, Petit, et al., 2016). In **Chapter 4**, we confirmed that this regulation is indeed conserved in *R. leguminosarum*, as evidenced by epistasis between *ptsP* and *relA*, and a direct PtsN-RelA protein:protein interaction. We further demonstrated how the readout of the intracellular nitrogen status by PTS^{Ntr} engages with the stringent response, resulting in common downstream physiological shifts, including the upregulation of the AapJQMP amino acid uptake system. This regulation does not involve (p)ppGpp acting at the promoter of the *aapJQMP* operon; rather, it is mediated by the sRNAs AbcR1/2. These findings provide evidence that PTS^{Ntr}, acting via (p)ppGpp, coordinate a graded, hierarchical regulatory cascade that governs the nitrogen-stress response at transcription initiation. Downstream sRNAs then provide an additional post-transcriptional regulatory layer that scales the amplitude and timing of the response in proportion to the severity of starvation. The evidence for sRNA control obtained with the promoter activity reporters used in this study would be strengthened by direct

quantification of sRNA AbcR1 and AbcR2 abundance. Additionally, investigating whether NPr regulates RelA independently of PtsN in *R. leguminosarum*, as previously proposed for *C. crescentus* (Ronneau, Moussa, et al., 2016; Ronneau & Hallez, 2019b), is a potential direction for future study.

SixA is a phosphohistidine phosphatase originally characterised in *Escherichia coli* (Schulte & Goulian, 2018). Alphaproteobacteria encode SixA homologues that, despite their lower overall sequence similarity, retain the catalytic motif. In **Chapter 5**, we used a *sixA* mutant to study its PTS^{Ntr}-related function; however, the mutant was phenotypically indistinguishable from the wild-type under all conditions tested. Since *sixA* is predominantly co-expressed with genes involved in carbon metabolism, cell envelopes, and stress responses, future studies should investigate its role in these contexts.

Going forward, potential follow-up work includes identifying novel interacting partners of PtsN ($EIIA^{Ntr}$) and ManX ($EIIA^{Man}$) using affinity native pull-downs with cell extracts followed by mass spectrometry, or using *in vivo* screening platforms such as yeast two-hybrid (Y2H) or bacterial two-hybrid (B2H). A particularly attractive candidate to test this direct interaction is the phosphate stress signalling pair PhoR/PhoB, since direct binding between PtsN and PhoR has already been shown in *E. coli* (Hsieh & Wanner, 2010; Lüttmann et al., 2012), and well-characterised links between the Pho regulon and the nitrogen response in Alphaproteobacteria have been described (Al-Niemi et al., 1997; Hagberg et al., 2016). Additionally, phosphate is an essential element that serves as a structural component of nucleic acids, plays central roles in cellular energy metabolism, and mediates signalling via protein phosphorylation. Phosphate availability constrains both carbon and nitrogen utilisation, and the Pho regulon accordingly exerts broad

control over carbon and nitrogen metabolism. To better understand the PTS^{Ntr} system, it can be advantageous to consider it within a carbon–nitrogen–phosphorus context rather than only carbon and nitrogen.

A major challenge in studying the PTS^{Ntr} is disentangling the specific roles of its individual kinases, as well as in determining whether observed mutant phenotypes reflect direct or indirect effects of perturbing this globally acting signalling system. These difficulties are compounded because PTS^{Ntr} proteins have distinct targets and activities in different phosphorylation states. Consequently, simple loss-of-function mutants cannot unambiguously reveal whether a given defect is due to the phosphorylated form, the nonphosphorylated form, or both. This was particularly a challenge when we were studying the phenotype of the *hprK* mutant in **Chapter 3**. HprK regulates the phosphorylation states of NPr, PtsN, and ManX. Phenotypes attributed to an *hprK* mutation may result from hyperphosphorylated PtsN, ManX, or both, or from a direct activity of HprK that has not yet been identified. One important strategy for dissecting the PTS^{Ntr} function is therefore to use approaches that decouple protein presence from its phosphorylation state. This includes pairing phosphorylation-state mutants of one component with deletions of another (e.g. an *hprK* mutant combined with a non-phosphorylatable PtsN and ManX, or non-phosphorylatable PtsN in the *manX* mutant background). Such double-mutant approaches should help to clarify the contributions of individual PTS proteins and their phosphorylation states to the observed phenotypes.

Related to the signalling architecture of the PTS^{Ntr} regulatory system, it will also be informative to determine how phosphate is partitioned between the two PTS^{Ntr} branches, because asymmetric allocation of the phosphoryl groups will cause differential

regulation of downstream physiological programmes, with NPr acting as a control switch that sets the balance. It remains to be determined whether ManX and PtsN are phosphorylated at similar rates and whether, in the *manX* mutant, the absence of ManX as a phosphate sink results in hyperphosphorylation of PtsN, and conversely, whether loss of PtsN affects the phosphorylation state of ManX. Potential mechanisms that could shift this phosphate partitioning toward preferred regulatory output EIIA proteins include (i) partner abundance and affinity, which pull phosphate toward specific complexes and thereby shape the phosphorylation flow; (ii) the presence of multiple EIIA proteins (e.g., PtsN paralogues in rhizobia (Feng et al., 2022; Sánchez-Cañizares et al., 2020) that act as phosphate sinks; and (iii) serine phosphorylation of NPr by HprK/P competing with histidine phosphorylation. Indeed, the unequal distribution of phosphate observed in other clades is consistent with this view: in *Pseudomonas putida*, under fructose-utilising conditions, the PTS^{Ntr} branch dominates the phosphoryl flux, with most phosphate preferentially transferred to $EIIA^{Ntr}$ (PtsN) (Pflüger & de Lorenzo, 2008). Likewise, in *Ralstolnia eutropha*, HPr~P readily phosphorylates PtsN, but it transfers phosphate only very slowly to the ManX homolog, PtsM (Kraußе et al., 2009).

Overall, the work presented in this thesis extends current understanding of PTS^{Ntr}-mediated regulation in *R. leguminosarum* by elucidating roles for ManX and HprK in carbon metabolism and by describing how PTS^{Ntr} senses nitrogen and signals to the RSH (RelA) to trigger stringent response and promote amino-acid uptake during nitrogen stress. It also demonstrates that the *sixA* mutant displays no detectable phenotype in *R. leguminosarum* despite reported functions in *E. coli*, which refines our understanding of PTS^{Ntr} regulatory conservation across species.

BIBLIOGRAPHY

Al-Niemi, T. S., Summers, M. L., Elkins, J. G., Kahn, M. L., & McDermott, T. R. (1997). Regulation of the phosphate stress response in *Rhizobium meliloti* by PhoB. *Applied and Environmental Microbiology, 63*(12), 4978–4981. https://doi.org/10.1128/aem.63.12.4978-4981.1997

Burghardt, L. T., & diCenzo, G. C. (2023). The evolutionary ecology of rhizobia: Multiple facets of competition before, during, and after symbiosis with legumes. *Current Opinion in Microbiology, 72*, 102281. https://doi.org/10.1016/j.mib.2023.102281

Checcucci, A., diCenzo, G. C., Bazzicalupo, M., & Mengoni, A. (2017). Trade, diplomacy, and warfare: The quest for elite rhizobia inoculant strains. *Frontiers in Microbiology, 8*, 2207. https://doi.org/10.3389/fmicb.2017.02207

Dozot, M., Poncet, S., Nicolas, C., Copin, R., Bouraoui, H., Mazé, A., Deutscher, J., De Bolle, X., & Letesson, J.-J. (2010). Functional characterization of the incomplete phosphotransferase system (PTS) of the intracellular pathogen *Brucella melitensis*. *PLoS ONE, 5*(9), e12679. https://doi.org/10.1371/journal.pone.0012679

Feng, X.-Y., Tian, Y., Cui, W.-J., Li, Y.-Z., Wang, D., Liu, Y., Jiao, J., Chen, W.-X., & Tian, C.-F. (2022). The PTSNtr–KdpDE–KdpFABC pathway contributes to low potassium stress adaptation and competitive nodulation of *Sinorhizobium fredii*. *mBio, 13*(3), e03721-21. https://doi.org/10.1128/mbio.03721-21

Hagberg, K. L., Yurgel, S. N., Mulder, M., & Kahn, M. L. (2016). Interaction between nitrogen and phosphate stress responses in *Sinorhizobium meliloti*. *Frontiers in Microbiology, 7*, Article 1928. https://doi.org/10.3389/fmicb.2016.01928

Hsieh, Y.-J., & Wanner, B. L. (2010). Global regulation by the seven-component Pi signaling system. *Current Opinion in Microbiology, 13*(2), 198–203. https://doi.org/10.1016/j.mib.2010.01.014

Krauße, D., Hunold, K., Kusian, B., Lenz, O., Stülke, J., Bowien, B., & Deutscher, J. (2009). Essential role of the hprK gene in *Ralstonia eutropha* H16. *Journal of Molecular Microbiology and Biotechnology, 17*(3), 146–152. https://doi.org/10.1159/000233505

Ledermann, R., Schulte, C. C. M., & Poole, P. S. (2021). How rhizobia adapt to the nodule environment. *Journal of Bacteriology, 203*(12), e00539-20. https://doi.org/10.1128/JB.00539-20

Liu, J., Yu, X., Qin, Q., Dinkins, R. D., & Zhu, H. (2020). The impacts of domestication and breeding on nitrogen fixation symbiosis in legumes. *Frontiers in Genetics, 11*, 973. https://doi.org/10.3389/fgene.2020.00973

Lüttmann, D., Göpel, Y., & Görke, B. (2012). The phosphotransferase protein EIIANtr modulates the phosphate starvation response through interaction with histidine kinase PhoR in *Escherichia coli*. *Molecular Microbiology*. https://doi.org/10.1111/j.1365-2958.2012.08176.x

Mendoza-Suárez, M., Andersen, S. U., Poole, P. S., & Sánchez-Cañizares, C. (2021). Competition, nodule occupancy, and persistence of inoculant strains: Key factors in the rhizobium–legume symbioses. *Frontiers in Plant Science, 12*, 690567. https://doi.org/10.3389/fpls.2021.690567

Pflüger-Grau, K., & Görke, B. (2010). Regulatory roles of the bacterial nitrogen-related phosphotransferase system. *Trends in Microbiology, 18*(5), 205–214. https://doi.org/10.1016/j.tim.2010.02.003

Pflüger, K., & de Lorenzo, V. (2008). Evidence of in vivo cross talk between the nitrogen-related and fructose-related branches of the carbohydrate phosphotransferase system of *Pseudomonas putida*. *Journal of Bacteriology, 190*(9), 3374–3380. https://doi.org/10.1128/JB.02002-07

Pinedo, C. A., & Gage, D. J. (2009). HPrK regulates succinate-mediated catabolite repression in the Gram-negative symbiont *Sinorhizobium meliloti*. *Journal of Bacteriology, 191*(1), 298–309. https://doi.org/10.1128/JB.01115-08

Poole, P., Ramachandran, V., & Terpolilli, J. (2018). Rhizobia: From saprophytes to endosymbionts. *Nature Reviews Microbiology, 16*(5), 291–303. https://doi.org/10.1038/nrmicro.2017.171

Powell, B. S., Court, D. L., Inada, T., Nakamura, Y., Michotey, V., Cui, X., Reizer, A., Saier, M. H., & Reizer, J. (1995). Novel proteins of the phosphotransferase system encoded within the *rpoN* operon of *Escherichia coli*. *Journal of Biological Chemistry, 270*(9), 4822–4839. https://doi.org/10.1074/jbc.270.9.4822

Prell, J., Mulley, G., Haufe, F., White, J. P., Williams, A., Karunakaran, R., Downie, J. A., & Poole, P. S. (2012). The PTSNtr system globally regulates ATP-dependent transporters in *Rhizobium leguminosarum*. *Molecular Microbiology, 84*(1), 117–129. https://doi.org/10.1111/j.1365-2958.2012.08014.x

Reis Ely, C. R., Perakis, S. S., Cleveland, C. C., Menge, D. N. L., Reed, S. C., Taylor, B. N., Batterman, S. A., Clark, C. M., Crews, T. E., Dynarski, K. A., Gei, M., Gundale, M. J., Herridge, D. F., Jovan, S. E., Kou-Giesbrecht, S., Peoples, M. B., Piipponen, J., Rodríguez-Caballero, E., Salmon, V. G., … Wurzburger, N. (2025). Global terrestrial nitrogen fixation and its modification by agriculture. *Nature, 643*(8072), 705–711. https://doi.org/10.1038/s41586-025-09201-w

Ronneau, S., Moussa, S., Barbier, T., Conde-Álvarez, R., Zuniga-Ripa, A., Moriyon, I., & Letesson, J.-J. (2014). Brucella, nitrogen and virulence. *Critical Reviews in Microbiology, 42*(4), 507–525. https://doi.org/10.3109/1040841X.2014.962480

Ronneau, S., Petit, K., De Bolle, X., & Hallez, R. (2016). Phosphotransferase-dependent accumulation of (p)ppGpp in response to glutamine deprivation in *Caulobacter crescentus*. *Nature Communications, 7*, 11423. https://doi.org/10.1038/ncomms11423

Ronneau, S., Caballero-Montes, J., Coppine, J., Mayard, A., Garcia-Pino, A., & Hallez, R. (2019a). Regulation of (p)ppGpp hydrolysis by a conserved archetypal regulatory domain. *Nucleic Acids Research, 47*(2), 843–854. https://doi.org/10.1093/nar/gky1201

Ronneau, S., & Hallez, R. (2019b). Make and break the alarmone: Regulation of (p)ppGpp synthetase/hydrolase enzymes in bacteria. *FEMS Microbiology Reviews, 43*(4), 389–400. https://doi.org/10.1093/femsre/fuz009

Sánchez-Cañizares, C., Prell, J., Pini, F., Rutten, P., Kraxner, K., Wynands, B., Karunakaran, R., & Poole, P. S. (2020). Global control of bacterial nitrogen and carbon metabolism by a PTSNtr-regulated switch. *Proceedings of the National Academy of Sciences of the United States of America, 117*(19), 10234–10245. https://doi.org/10.1073/pnas.1917471117

Schulte, J. E., & Goulian, M. (2018). The phosphohistidine phosphatase SixA targets a phosphotransferase system. *mBio, 9*(6), e01666-18. https://doi.org/10.1128/mBio.01666-18

Schulte, J. E., Roggiani, M., Shi, H., Zhu, J., & Goulian, M. (2021). The phosphohistidine phosphatase SixA dephosphorylates the phosphocarrier NPr. *Journal of Biological Chemistry, 296*, 100090. https://doi.org/10.1074/jbc.RA120.015121

Untiet, V., Karunakaran, R., Krämer, M., Poole, P., Priefer, U., & Prell, J. (2013). ABC transport is inactivated by the PTSNtr under potassium limitation in *Rhizobium leguminosarum* 3841. *PLoS ONE, 8*(5), e64682. https://doi.org/10.1371/journal.pone.0064682

APPENDIX: Supplementary Data

A. Protein Purification

In **Chapter 3**, we demonstrated that the *manX* mutant shows reduced activity of TCA cycle dehydrogenases. To assess whether this effect is mediated by protein-protein interactions, we planned to perform pull-down assays, which require prior purification of the relevant protein. Here, we show two purification trials of (1) ManX, (2) ManX carrying a single amino acid substitution at His9 to Alanine (ManX*Ala), and (3) malate dehydrogenase (MDH).

The results of purification under non-reducing SDS-PAGE are shown in **Figure 1**. Proteins eluted in 300 mM imidazole were dialysed and then concentrated. MDH bands appeared as intense bands that corresponded to the expected molecular weight (~36.3 kDa). ManX and ManX*Ala appeared less abundant and appeared to be aggregated after dialysis, as shown by the shift of bands from the expected ~19 kDa to ~50 kDa post-dialysis. The presence of additional faint bands further suggested the presence of impurities in the sample.

Additional attempts were made to obtain non-aggregating ManX and ManX*Ala proteins by incorporating the reducing agent DTT (2 mM) and glycerol during purification (**Figure 2**). Under these conditions, aggregations appeared to be reduced.

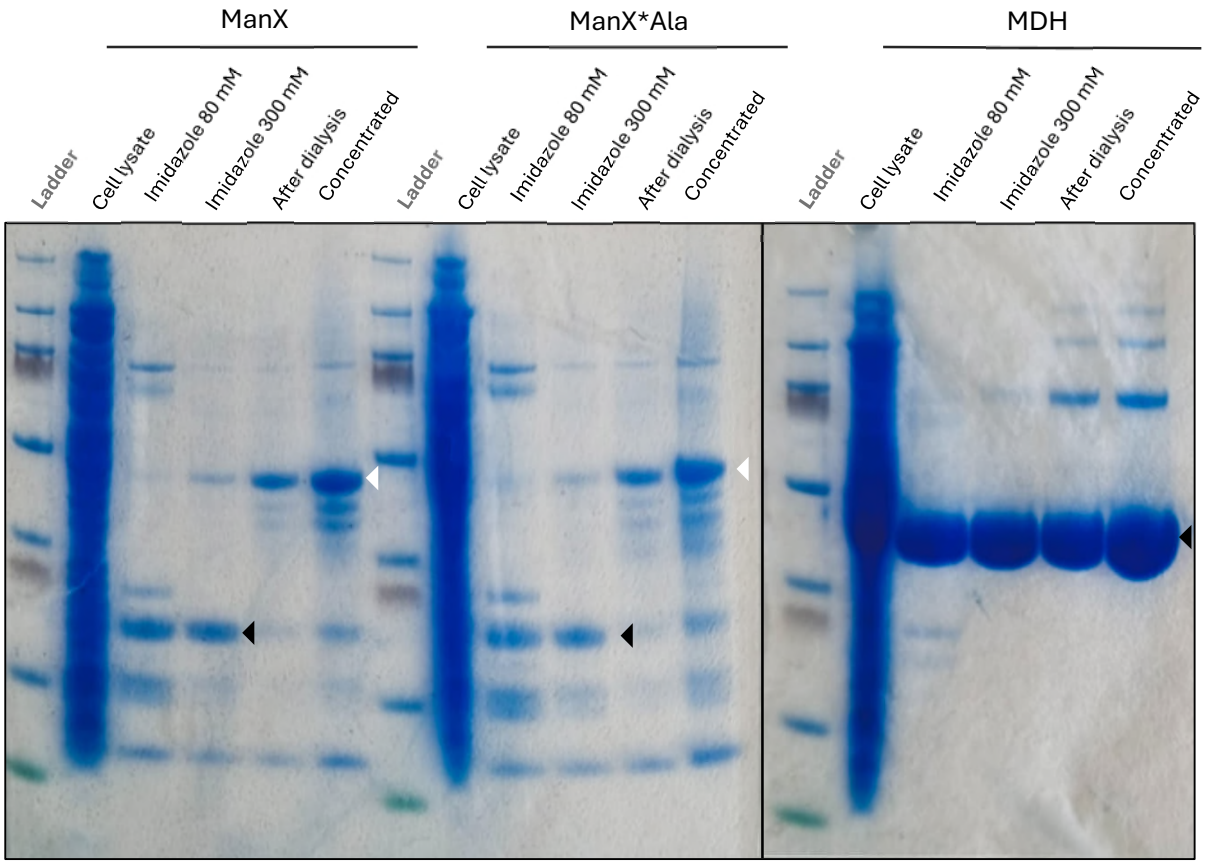

Figure 1. Purification results under non-reducing SDS-PAGE. Black arrows indicate the target protein based on the expected molecular weight, ~19 kDa for ManX and ManX*Ala, and ~36 kDa for MDH. White arrows show the aggregated ManX and ManX*Ala after overnight dialysis.

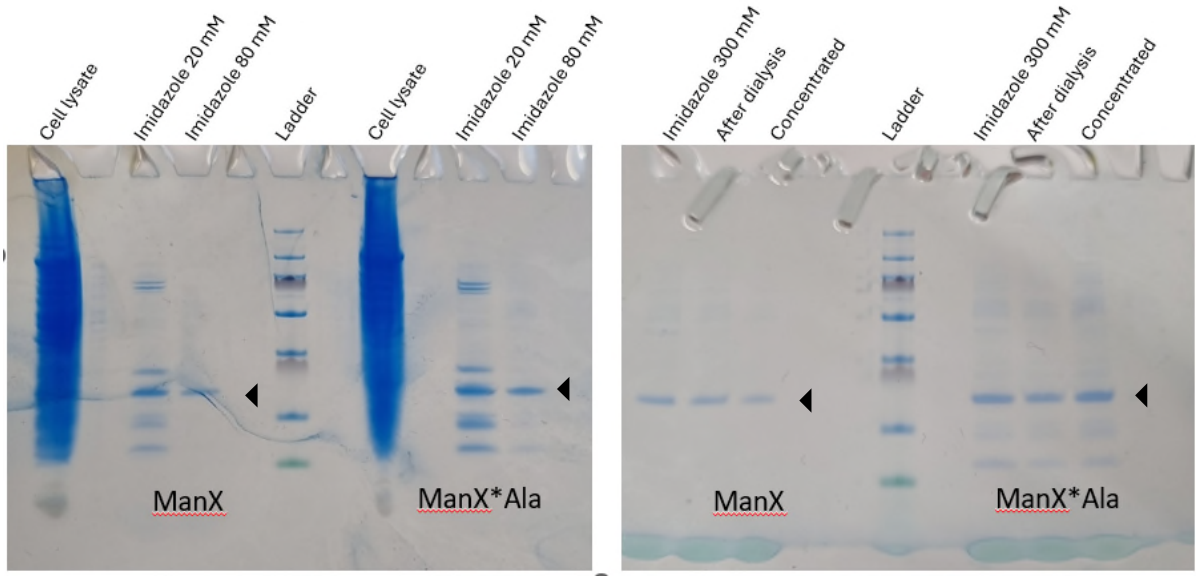

Figure 2. Purification of ManX and ManX*Ala proteins when reducing agent DTT (2 mM) and glycerol were added. Black arrows indicate the target protein based on the expected molecular weight (~19 kDa).

Methods

pOPINF plasmids [1] carrying 6xHis-tag fusion of *manX*, *manX* H9A, or *mdh* were transformed into competent cells BL21(DE3) [2]. *Escherichia coli* transformants were grown in Luria-Bertani (LB) [3] solid or liquid medium supplemented with appropriate antibiotics (50 μg ml^{-1} carbenicillin) at 37°C. 0.5 mM isopropyl β-D-thiogalactopyranoside (IPTG) was used to induce 6xHis-tagged fusion protein expression for 16 hours at 20°C. Protein extracts were then prepared and purified using Ni-NTA columns (Thermo Fisher) according to the manufacturer's recommendations. Purified proteins were recovered as soluble fractions, and their purity was assessed by SDS-PAGE stained with Coomassie Brilliant Blue.

References

1. Berrow, N. S., Alderton, D., Sainsbury, S., Nettleship, J., Assenberg, R., Rahman, N., Stuart, D. I., & Owens, R. J. (2007). A versatile ligation-independent cloning method suitable for high-throughput expression screening applications. Nucleic Acids Research, 35(6), e45. https://doi.org/10.1093/nar/gkm047

2. Studier, F. William., & Moffatt, B. A. (1986). Use of bacteriophage T7 RNA polymerase to direct selective high-level expression of cloned genes. Journal of Molecular Biology, 189(1), 113–130. https://doi.org/10.1016/0022-2836(86)90385-2

3. Green, M. R., & Sambrook, J. (2014). Molecular cloning: a laboratory manual. Cold Spring Harbor Laboratory Press.

B. Single-Nucleotide Polymorphism Analysis

Follow-up analysis of suppressor mutants identified in Muley [1]. Single-nucleotide polymorphisms (SNPs) detected in selected Δ*gltB* suppressor mutant strains isolated by selection of RU2307 (*gltB*::Ω - spec^{R}) for growth on AMS glucose–glutamate plates. These suppressor mutants exhibited elevated rates of amino acid uptake via the Aap and Bra transport systems; however, the genomic locations of the SNPs were not previously identified.

Table 1. Location of SNP detected in selected *ΔgltB* suppressor mutant strains.

STRAINS	CHROMOSOME	GENOMIC POSITION	TYPE	REF NT	ALT NT	EVIDENCE	FEATURE TYPE	STRAND	NT POSITION	AA POSITION	EFFECT	LOCUS TAG	GENE	PRODUCT
LMB88	pRL11	131216	snp	T	G	G:96 T:0								
LMB89	pRL7	84921	snp	G	A	A:50 G:4								
LMB89	Chromosome	2377579	snp	G	C	C:87 G:0	CDS	+	790/1452	264/483	missense_variant c.790G>C p.Gly264Arg	RL2257	ntrC	two-component sensor/regulator; nitrogen transcriptional regulator NtrC
LMB90	Chromosome	2058859	snp	A	C	C:64 A:0	CDS	-	348/435	116/144	synonymous_variant c.348T>G p.Gly116Gly	RL1952	RL1952	transmembrane protein
LMB90	Chromosome	2377579	snp	G	C	C:57 G:0	CDS	+	790/1452	264/483	missense_variant c.790G>C p.Gly264Arg	RL2257	ntrC	two-component sensor/regulator; nitrogen transcriptional regulator NtrC
LMB94	pRL12	551322	snp	T	A	A:66 T:0								
LMB94	Chromosome	2402322	snp	G	T	T:37 G:0	CDS	+	30/2271	10/756	synonymous_variant c.30G>T p.Ala10Ala	RL2281	ntrY	two-component sensor/regulator; nitrogen transcriptional regulator NtrY
LMB94	Chromosome	3610499	snp	C	T	T:44 C:0								
LMB94	Chromosome	4982059	snp	A	C	C:36 A:0	CDS	+	440/657	147/218	missense_variant c.440A>C p.Asp147Ala	RL4678	RL4678	acetyltransferase
LMB95	pRL12	551322	snp	T	A	A:42 T:0								
LMB95	Chromosome	2402322	snp	G	T	T:27 G:0	CDS	+	30/2271	10/756	synonymous_variant c.30G>T p.Ala10Ala	RL2281	ntrY	two-component sensor/regulator; nitrogen transcriptional regulator NtrY
LMB95	Chromosome	2406950	snp	A	G	G:30 A:0								
LMB95	Chromosome	2520244	snp	T	A	A:45 T:0	CDS	-	82/339	28/112	missense_variant c.82A>T p.Ile28Phe	RL2393	glnB*	nitrogen regulatory protein PII
LMB99	pRL12	551322	snp	T	A	A:93 T:1								
LMB99	Chromosome	2354431	snp	C	T	T:56 C:0	CDS	-	908/1290	303/429	missense_variant c.908G>A p.Gly303Asp	RL2234	gltA	bifunctional citrate synthase type II / type II citrate synthase
LMB99	Chromosome	2377849	snp	G	C	C:60 G:0	CDS	+	1060/1452	354/483	missense_variant c.1060G>C p.Val354Leu	RL2257	ntrC*	two-component sensor/regulator; nitrogen transcriptional regulator NtrC
LMB99	Chromosome	2402322	snp	G	T	T:49 G:0	CDS	+	30/2271	10/756	synonymous_variant c.30G>T p.Ala10Ala	RL2281	ntrY	two-component sensor/regulator; nitrogen transcriptional regulator NtrY
LMB99	Chromosome	3610499	snp	C	T	T:63 C:0								
LMB99	Chromosome	3867095	snp	C	A	A:65 C:0								

Methods

R. leguminosarum was grown on the minimal medium Universal Minimal Salts (UMS) supplemented with 10 mM glucose and 10 mM ammonium chloride to an OD_{600} of 0.7. Genomic DNA was then extracted using the GeneJET Genomic DNA Purification Kit (Thermo Fisher Scientific, K0721) according to the manufacturer's instructions. Purified DNA was submitted to MicrobesNG (Birmingham, UK) for whole-genome sequencing. Libraries were prepared and sequenced using Illumina short-read technology. Single nucleotide polymorphisms (SNPs) were identified using Snippy, a rapid haploid variant calling and core SNP phylogeny pipeline [2]. Snippy aligns Illumina reads to a reference genome, performs variant calling, and generates core SNP alignments for downstream phylogenetic analysis.

References

1. Mulley G, White JP, Karunakaran R, Prell J, Bourdes A, Bunnewell S, Hill L, Poole PS. 2011. Mutation of GOGAT prevents pea bacteroid formation and N_2 fixation by globally downregulating transport of organic nitrogen sources. *Molecular Microbiology* 80:149–167. https://doi.org/10.1111/j.1365-2958.2011.07565.x

2. Seemann T. *Snippy: rapid haploid variant calling and core SNP phylogeny*. Available at: https://github.com/tseemann/snippy